

# Annual Report 2008

**Association  
EURATOM / IPP.CR**

**INSTITUTE OF PLASMA PHYSICS, v.v.i.**  
ACADEMY OF SCIENCES OF THE CZECH REPUBLIC



## TABLE OF CONTENTS

PREFACE .....	6
<b>I. RESEARCH UNIT .....</b>	<b>8</b>
1. ASSOCIATION EURATOM/IPP.CR .....	8
2. MANPOWER AND BUDGET .....	9
<b>II. OVERVIEW OF ACTIVITIES .....</b>	<b>11</b>
<b>III. LIST OF PULICATIONS .....</b>	<b>32</b>
<b>IV. REPORTS .....</b>	<b>41</b>
1. PROVISIONOF SUPPORT TO THE ADVANCEMENT OF THE ITER PHYSICS BASIS .....	41
<i>Carbon impurity transport studies in TCV tokamak discharges.....</i>	<i>41</i>
<i>Determination of reflection properties of hydrocarbon radicals for ITER-like divertor</i> <i>conditions .....</i>	<i>43</i>
<i>Power loads into gaps during ELMs.....</i>	<i>45</i>
<i>On SOL Variations as a Function of LH Power.....</i>	<i>47</i>
<i>Experiments concerning fast particles emerging from LH antennas .....</i>	<i>49</i>
<i>Modeling of neutral beam (NB) and lower hybrid (LH) heating and current drive</i> <i>for COMPASS.....</i>	<i>51</i>
<i>Application of the Minimum Fisher Information inverse methods in the JET neutron cameras</i> <i>and compact spectrometers data analyses .....</i>	<i>53</i>
2. DEVELOPMENT OF PLASMA AUXILIARY SYSTEMS.....	55
<i>COMPASS NBI System Design.....</i>	<i>55</i>
<i>Direct measurements of the plasma potential and electron temperature in ELMy H-mode</i> <i>plasma with ball-pen probes on ASDEX Upgrade tokamak.....</i>	<i>57</i>
<i>Divertor probes on the COMPASS tokamak - commissioning and first results .....</i>	<i>59</i>
<i>Development of advanced probe for edge tokamak plasmas - emissive and tunnel probes .....</i>	<i>61</i>
<i>Development of millimeter-wave reflectometry methods for the measurement of edge pedestal</i> <i>plasma in tokamak COMPASS-D .....</i>	<i>63</i>
<i>Beam emission spectroscopy system for COMPASS.....</i>	<i>65</i>
<i>Design and construction of fast tomography systems based on fast bolometric and SXR arrays</i> <i>for COMPASS.....</i>	<i>67</i>

<i>Development of fast digital video camera system for machine control, plasma overview and turbulence measurements</i> .....	69
<i>Thomson scattering diagnostic development on COMPASS</i> .....	71
<i>Atomic Beam Probe system for COMPASS</i> .....	73
<b>3. DEVELOPMENT OF CONCEPT IMPROVEMENTS AND ADVANCES IN FUNDAMENTAL UNDERSTANDING OF FUSION PLASMAS</b> .....	<b>75</b>
<i>Contributions to study of interaction of magnetic perturbations with rotating plasmas</i> .....	75
<i>EBW Power Deposition and Current Drive in WEGA Comparison of Simulation with Experiment</i> .....	77
<i>Coupling of the AMR and the LUKE codes</i> .....	79
<i>Implementation of the induced currents model in efit++ code</i> .....	81
<i>Test electron and Landau damping calculations of the radial extent of lower hybrid power - edge plasma interaction</i> .....	83
<i>A 2D PIC code for tunnel probe simulation</i> .....	93
<b>4. MATERIALS &amp; TECHNOLOGY</b> .....	<b>95</b>
<i>Influence of neutron irradiation on the properties of candidate fusion materials</i> .....	95
<i>Static and dynamic fracture toughness of plates and weldments at the transition irradiated up to 2.5 dpa at 200°C – 250°C</i> .....	97
<i>EUROFER and Pb-Li melts testing under higher temperature irradiation conditions</i> .....	99
<i>Development and testing cold traps, high temperature flanges and circulation pump for the liquid metal Pb-Li loop</i> .....	101
<i>Compatibility of EUROFER samples coated by Al and Er<sub>2</sub>O<sub>3</sub> layers with Pb-Li melt under higher temperature conditions</i> .....	103
<i>The Facility for Thermal Fatigue Tests of Be Coated First Wall Qualification Mock-ups</i> .....	104
<i>Progress and results of thermal fatigue tests of Be coated First Wall Qualification Mock-ups</i> .....	106
<i>In-pile thermal fatigue testing device for Primary First Wall Mock-ups with Beryllium cladding</i> .....	108
<i>Experiments for the validation of Bi cross-sections up to 35 MeV in a quasi-monoenergetic neutron spectrum</i> .....	110
<i>Determination of reflection properties of hydrocarbon radicals for ITER-like divertor conditions</i> .....	112
<i>Transport and Deposition of First Wall Impurities SEWG Chemical Erosion and Material Transport</i> .....	115
<i>Study of the micro-mechanisms of cleavage fracture of 14% Cr and 18% Cr ODS ferritic steels</i> .....	117
<i>Development of functional gradient materials using powder laser deposition</i> .....	119
<b>5. TRAINING AND CAREER DEVELOPMENT</b> .....	<b>121</b>
<i>Collaboration of IPP Prague with Universities in fusion training</i> .....	121
<i>Training and education</i> .....	122
<b>6. OTHER ACTIVITIES CONTRIBUTING TO THE EURATOM FUSION PROGRAMME</b> .....	<b>123</b>
<i>Outreach and Public Information Activities</i> .....	123

7. COORDINATION, IN THE CONTEXT OF A KEEP-IN-TOUCH ACTIVITY, OF THE MEMBER STATE'S CIVIL RESEARCH ACTIVITIES ON INERTIAL FUSION ENERGY ..... 127

*Experiments on interaction of focused high-power laser beams*

*with multilayer high-Z targets* ..... 127

*Laser generated plasma jets for ICF and astrophysics*..... 129

## PREFACE

This report summarizes the main activities and achievements of the Association EURATOM/IPP.CR in 2008. The Association participates in the joint European effort in mastering controlled fusion by carrying out relevant plasma physics and technology R&D, including participation in JET and other European devices and activities related to the international fusion experiment ITER.

The Association was founded on December 22, 1999 through a contract between the European Atomic Energy Community (EURATOM) represented by the European Commission, and the Institute of Plasma Physics, v. v. i., Academy of Sciences of the Czech Republic (IPP). Several other institutions have been included in the Research Unit to contribute to the work programme in physics and technology research:

- Faculty of Mathematics and Physics, Charles University in Prague
- Institute of Physical Chemistry, v. v. i., Academy of Sciences of the Czech Republic
- Faculty of Nuclear Science and Physical Engineering, Czech Technical University
- Nuclear Physics Institute, v. v. i., Academy of Sciences of the Czech Republic
- Nuclear Research Institute in Rez, Plc
- Institute of Applied Mechanics, Brno, Ltd
- Institute of Physics of Materials, v. v. i., Academy of Sciences of the Czech Republic

Measured in person years, the effort expended on the Association's fusion research has slightly decreased, compared to the previous year, to about 48 py (from 52 py). This reflects the phasing out of the support of technology development by EFDA; however, the drop was partially compensated by a moderate increase of manpower in connection with the COMPASS project. The overall 2008 expenditure was about 1.7 M€.

With the tokamak COMPASS transferred from UKAEA in 2007, most of our efforts were invested this year into the re-installation of this unique facility. The tokamak was officially inaugurated in IPP on April 1<sup>st</sup>, 2008 and the first plasma was generated on December 9<sup>th</sup>, 2008 so that the tight schedule was fulfilled. In this respect we also experienced considerable increase in the interest of media and general public in our research, as well as calls for lectures and general collaboration from several Universities.

However, this Annual report demonstrates that our research scientists also pursued an important number of underlying fusion-relevant plasma research, oriented both to preparation of the scientific programme for the COMPASS tokamak and to our traditional topics, e.g. the study of phenomena at the plasma edge, wave-plasma interaction and diagnostics development. The research was performed in close collaboration with many of the other EURATOM Associations and EFDA JET (as mentioned in the reports).

In the technology area, most effort has been spent on finishing the running tasks of the "old" EFDA, though some of these will still continue into 2009. Under the label of "emerging technologies" supported by the "new" EFDA, several tasks in the area of fusion materials have been addressed. We hope that with a more massive support of technology work by Fusion for Energy (European Joint Undertaking for ITER and Development of Fusion Energy), we will be able to build upon the expertise acquired under EFDA and exploit the existing facilities (the cyclotron, the fission reactor, thermal fatigue testing facility etc.) to further contribute to the R&D in areas such as Vessel/In Vessel or Tritium Breeding and Materials.

Pavol Pavlo  
Head of Research Unit  
Association EURATOM/IPP.CR

## Composition of the Research Unit in 2008

- IPP Institute of Plasma Physics, v.v.i., Academy of Sciences of the CR**  
 Address: Za Slovankou 3,  
 182 00 Praha 8, Czech Republic  
 Tel: +420 286 890 450  
 Fax: +420 286 586 389  
 Contact Person: Jan Stöckel  
 e-mail: stockel@ipp.cas.cz
- FMP Faculty of Mathematics and Physics, Charles University**  
 Address: V Holešovičkách 2,  
 182 00 Praha 8, Czech Republic  
 Tel: +420 221 912 305  
 Fax: +420 221 912 332  
 Contact person: Milan Tichý  
 tichy@mbox.troja.mff.cuni.cz
- JHIPC J Heyrovský Institute of Physical Chemistry, v.v.i., Academy of Sciences of the CR**  
 Address: Dolejškova 3,  
 182 23 Praha 8, Czech Republic  
 Tel: +420 266 053 514  
 Fax: +420 286 582 307  
 Contact person: Zdeněk Herman  
 zdenek.herman@jh-inst.cas.cz
- FNSPE Faculty of Nuclear Science and Physical Engineering, Czech Technical University**  
 Address: Břehová 7,  
 115 19 Praha 1, Czech Republic  
 Tel: +420 224 358 296  
 Fax: +420 222 320 862  
 Contact person: Vojtěch Svoboda  
 svoboda@br.fjfi.cvut.cz
- NPI Institute of Nuclear Physics, v.v.i., Academy of Sciences of the CR**  
 Address: 250 68 Řež, Czech Republic  
 Tel: +420 266 172 105 (3506)  
 Fax: +420 220 941 130  
 Contact person: Pavel Bém  
 e-mail: bem@ujf.cas.cz
- NRI Nuclear Research Institute Plc., Řež**  
 Address: 250 68 Řež, Czech Republic  
 Tel: +420 266 172 453  
 Fax: +420 266 172 045  
 Contact person: Karel Šplíchal  
 e-mail: spl@ujv.cz
- IAM Institute of Applied Mechanics Brno, Ltd.**  
 Address: Veveří 85,  
 611 00 Brno, CR  
 Phone: +420 541 321 291  
 Fax: +420 541 211 189  
 Contact person: Lubomír Junek  
 e-mail: junekl@uam.cz
- IAM Institute of Physics of Materials, v.v.i., Academy of Sciences of the CR**  
 Address: Žitkova 22, 616 62 Brno,  
 Czech Republic  
 Tel: +420 5 322 90 379  
 Fax: +420 5 412 18 657  
 Contact person: Tomáš Kruml  
 e-mail: kruml@ipm.cz

## Steering Committee

### EURATOM

Yvan Capouet, Head Unit J4, DG RTD  
 Steven Booth, Unit J4, DG RTD  
 Carlos Dedeu Fontcuberta, Unit J3, DG RTD

### Head of Research Unit

Pavol Pavlo

### IPP.CR

Ivan Wilhelm (Ministry of Education, Youth and Sports)  
 Petr Křenek (Charles University)  
 Pavel Chráska (Institute of Plasma Physics)

### Secretary of the SC

Jan Mlynář

# I RESEARCH UNIT

---

## 1 Association EURATOM/IPP.CR

---

### International Board of Advisors of the Association EURATOM/IPP.CR

Prof. Hardo Bruhns	Chair
Dr. Carlos Hidalgo	CIEMAT, Madrid, Spain
Dr. Jochen Linke	Forschungszentrum Jülich GmbH, Jülich, Germany
Dr. Bernard Saoutic	CEA Cadarache, France
Prof. Fernando Serra	Centro de Fusao Nuclear, Lisboa, Portugal
Dr. Wolfgang Suttrop	Max-Planck-Institut für Plasmaphysik (IPP), Garching, Germany
Dr. Martin Valovič	UKAEA Fusion, Culham Science Centre, United Kingdom
Prof. Guido Van Oost	Ghent University, Gent, Belgium
Dr. Henri Weisen	EPFL, Lausanne, Switzerland
Dr. Sandor Zoletnik	RMKI KFKI, Budapest, Hungary

The Board was established to help with the formulation of scientific program, and to assess the scientific achievements of the Association EURATOM-IPP.CR.

### Representatives of the Association IPP.CR in Committees and Bodies

#### *Consultative Committee for the EURATOM Specific Programme on Nuclear Energy Research - Fusion*

Pavel Chráska	Institute of Plasma Physics, Academy of Sciences of the Czech Republic
Milan Tichý	Faculty of Mathematics and Physics, Charles University, Prague

#### *EFDA Scientific and Technical Advisory Committee*

Jan Stöckel	Institute of Plasma Physics, Academy of Sciences of the Czech Republic
-------------	--

#### *EFDA Steering Committee*

Pavol Pavlo	Institute of Plasma Physics, Academy of Sciences of the Czech Republic
Radomír Pánek	Institute of Plasma Physics, Academy of Sciences of the Czech Republic

#### *Governing Board of Fusion for Energy*

Pavol Pavlo	Institute of Plasma Physics, Academy of Sciences of the Czech Republic
Jan Kysela	Nuclear Research Institute pls., Řež

## 2 Manpower and Budget

### Manpower Analysis of the Association EURATOM/IPP.CR in 2008

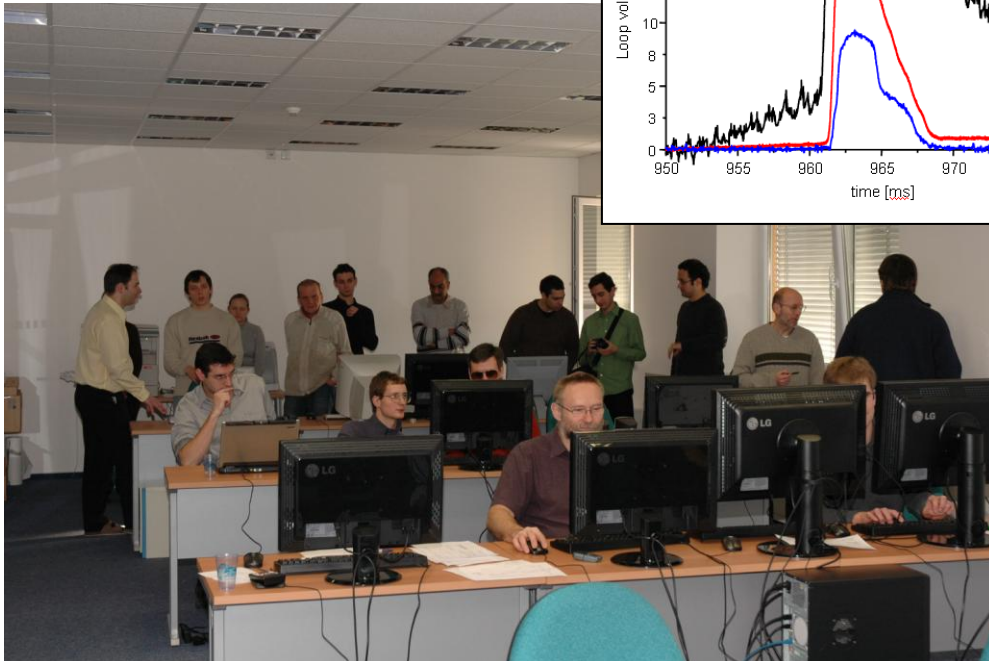
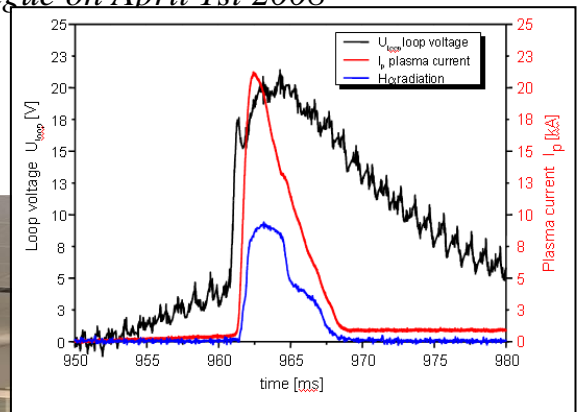
Institution	STAFF, PY			STAFF, Person					
	Physics	Technology	TOTAL	Female	Male	Prof.	Non-Prof.	TOTAL	Total, %
IPP	36.665	0.000	36.665	13	63	45	31	76	61.8
FMP	1.028	0.000	1.028	5	11	3	13	16	13.0
JHIPC	0.640	1.060	1.700	0	3	3	0	3	2.4
FNSPE	0.500	0.000	0.500	1	1	2	0	2	1.6
NRI	0.000	5.810	5.810	2	14	13	3	16	13.0
NPI	0.000	0.400	0.400	1	3	3	1	4	3.3
IPM	2.500	0.000	2.500	1	5	4	2	6	4.9
IAM	0.000	0.000	0.000	0	0	0	0	0	0.0
<b>TOTAL</b>	<b>41.333</b>	<b>7.270</b>	<b>48.603</b>	<b>23</b>	<b>100</b>	<b>73</b>	<b>50</b>	<b>123</b>	<b>100.0</b>
<b>Total, %</b>	<b>85.0</b>	<b>15.0</b>	<b>100.0</b>	<b>18.7</b>	<b>81.3</b>	<b>59.3</b>	<b>40.7</b>	<b>100.0</b>	

### Expenditures in 2008

	Euro
Physics	1 233 601
JET Notifications	0
Operational cost of major facilities	91 220
Coordination, in the context of a keep-in-touch activity, of the Member State's civil research activities on Inertial Fusion Energy	11 917
<b>Sub-total</b>	<b>1 336 738</b>
Large Devices	0
Specific Co-operative actions 8.2a	13 011
Specific Co-operative actions 8.2b	0
JET S/T Task (EFDA Art. 6.3)	16 533
Technology contracts (TCN-TCP) (Art 5.1a)	38 338
Technology contracts (Art 5.1b)	233 254
<b>Sub-total</b>	<b>301 136</b>
<b>Mobility Actions</b>	<b>83 966</b>
<b>TOTAL</b>	<b>1 721 840</b>



*Tokamak COMPASS was unveiled during its official inauguration in the Institute of Plasma Physics in Prague on April 1st 2008*



*The control room of tokamak COMPASS on December 9th 2008  
Inset: Parameters of the very first plasma achieved on this date*

# II

# OVERVIEW

The main areas of the research undertaken in the Association EURATOM/IPP.CR in 2008 were as follows:

1. Provision of Support to the Advancements of the ITER Physics Basis
2. Development of Plasma Auxiliary Systems
3. Development of Concept Improvements and Advances in Fundamental Understanding of Fusion Plasmas

Here, the most important results, activities and achievements are briefly summarized; details are given after the list of publications. Notice that the major part of the Association activities in Physics relies on broad collaboration with other EURATOM Associations.

## 1. Provision of support to the advancement of the ITER Physics Basis

### 1.1 Development of ITER candidate scenarios

#### **Study of carbon transport phenomena in reactor relevant regimes**

**Principal Investigator:** V.Piffli

**Collaboration:** H.Weisen, CRPP EPFL, Lausanne

Experimental study together with theoretical interpretation of the plasma and impurity radial profiles seems to be fundamental for the prediction of the reactor performance developed in the frame of the fusion program. Analyse of steady-state radial profiles with central or off-axis EC Heating in L-mode indicates that the flattening density profile is accompanied by peaked or hollow peaked profile of fully-ionized carbon.

The experimentally observed character of impurity density radial profile behaviour in tokamak, could be explained analogous to the particle plasma transport across the magnetic field, by microscopic instabilities and fluctuations of electric potential and magnetic field. One of the most important drift instabilities that results from passing particle dynamics is the ion temperature gradient (ITG) mode. The ITG mode is a drift wave driven by an ion pressure gradient and destabilized by the coupling with the parallel transit drift in the unfavourable magnetic curvature. The other under consideration are trapped electron modes (TEM), which are represent basically by drift waves that are destabilized by an electron temperature gradient in the presence of a population of trapped electrons.

#### **Statistical comparison of ELMing H-mode with advanced regimes on JET tokamak**

**PI & Co-workers:** I. Duran, M. Kubic

**Collaboration:** R. Pitts, CRPP EPFL, Lausanne

The development of discharge scenarios with weak and strong internal transport barriers (ITB) is one of the primary goals of research at JET. Such scenarios are the key to non-inductive, steady-state operation in future devices and are being developed as ITER candidate scenarios. Two types of study are possible: the detailed investigation of individual discharges (from S1 and S2), including numerical fluid code modeling and a statistical approach in which a large number of edge and core plasma quantities are compared across a large discharge database to assess the level of similarity in the edge plasma of each type of scenario. We have begun by following the latter, statistical approach, compiling a database of more than 80 relevant quantities which characterize plasma geometry, basic plasma

parameters including profiles of Te, ne, Ti, and all edge and SOL properties which are currently measured on JET.

In the end of 2007, the further extension of the database was practically paralyzed due to instability of JET data access through MDS+ in MATLAB. The problem was caused by upgrade of the operating system of the JET MDS+ computer and consequent incompatibility with MATLAB MDS+ interface. Because, the support for MATLAB on JET was stopped, we decided that the most effective solution will be to fully migrate the database to IDL platform. A new database creation IDL routine, following partly the MDB architecture, was created. This opportunity was also used to refine the data evaluation of some of the parameters included into the database and also to add additional ones. The migration of the database was finished and the work will continue along the originally envisaged path of further extension and database content evaluation.

#### 1.4 Power and particle exhaust, plasma-wall interaction

##### **Determination of reflection properties of hydrocarbon radicals for ITER-like divertor conditions**

**PI & Co-workers:** Z. Herman, J. Žabka, A. Pysanenko

**Collaboration:** Research Group of Prof. T. D. Märk, Association EURATOM-ÖAW, Institute for Ion and Applied Physics, University of Innsbruck, Innsbruck, Austria Dr. J. Roth, Dr. W. Schustereder, Association EURATOM-IPP, Max-Planck Institute for Plasma Physics, Garching, Germany

Transport and Deposition of First Wall Impurities. SEWG Chemical Erosion and Material Transport: Reactive Interaction of Molecular Ions with Surfaces

Interaction of slow ions  $C_3H_n^+$  and  $C_3D_n^+$  ( $n=2-8$ ) with room temperature carbon surfaces was investigated over the collision energy range 15 – 45 eV and surface-induced fragmentation pathways of the projectile ions were determined. A simple correlation between survival probability of the hydrocarbon ions ( $C_3$  measured here and earlier measured  $C_1$ ,  $C_2$ ,  $C_7$ ) and ionization energy of the species in question (instead of the unknown recombination energy) was found. It showed a decrease from more than 10% to less than 1% in between IE 8.5 - 9.5 eV and a further decrease at higher IE. A semi-logarithmic plot  $\log S_a - IE$  showed that the decrease of  $S_a$  in these coordinates was approximately linear over the entire range of IEs of the investigated species and the data could be fitted with an empirical relation  $\log S_a = (3.9 \pm 0.5) - (0.39 \pm 0.04) IE$ . [104]

Collisions of low energy  $C_2D_4^+$  and  $Ar^+$  ions with stainless steel, carbon (HOPG), and two different diamond surfaces were studied to find out, how different material of a surface at room-temperature, underlying a hydrocarbon coverage, influences surface processes, namely to compare the behaviour of hydrocarbon-covered H-terminated diamond (hydrophobic) and O-terminated diamond (hydrophilic) with two standard surfaces (carbon and stainless steel). The presence of hydrocarbons was observed on all the studied room-temperature surfaces. Fragmentation, chemical reactions, and energy transfer at surfaces were very similar for all surfaces. The only observed difference between the two diamond surfaces was the ratio of probabilities of reactive vs. reactive and dissociative processes,  $PR/(PR+PD)$ , as a function of incident energy. This ratio increased from a threshold at 6-7 eV to about 70% for the SS, HOPG, and DO surfaces, but only to about 45% for the DH surface. [105]

Ref.: [57, 58, 59, 60, 104, 105]

##### **Determination of power loads on gaps (PWI-08-TA-09/IPP.CR/ BS/01 & PS/01).**

**PI & Co-workers:** R. Dejarnac, M. Komm

Kinetic calculations of power fluxes to ITER's castellated plasma facing components during ELMs have been performed. Three species are followed (deuterium, tritium, carbon) and power flux profiles in a narrow gap between tiles are presented. The global penetration of the

two hydrogen species in the gap is in the order of the gap width ( $\sim 0.5$  mm) and their contribution on the total heat flux is estimated. The impurity carbon penetrates into the gap in between 50 to 70% of the total plasma deposition but with a power deposited less than 1% of the total deposited power.

### 1.5 Physics of plasma heating and current drive

#### **Theory&Modelling (EDGE2D) of relevant physical processes including the ITER SOL and long distance coupling B. Experiments concerning fast particles emerging from LH and ICRF antennas.**

**Principal Investigator:** V. Petrzilka

**Collaboration:** M. Goniche, J. Gunn, L. Colas (CEA Cadarache, Fr) J. Mailloux, M.L. Mayoral, G. Corrigan, V. Parail, K. Erents (Jet, UK), K. Rantamaki (TEKES, FI)

A. Numerical modeling was performed of the JET Scrape-off-Layer (SOL) time evolution with the fluid code EDGE2D. The code includes direct SOL ionization by the LH (lower hybrid) wave and effects of near LH grill limiters. The original contribution here is that we explore for the first time the SOL time evolution when switching on/off the LH and near grill gas puff. More far from the separatrix, where the LH parasitic dissipation and corresponding local SOL heating takes place, the computed plasma density increases with time at the onset of the local LH wave ionization with a short characteristic time of less than about 10 ms. Closer to the separatrix, the plasma density approaches the new equilibrium with a several times longer characteristic times. The values of the density and saturation currents in the outer mid-plane (OMP) and reciprocating probe (RCP) locations were compared. The results are relevant to JET LH coupling and modulated LH power experiments, and corresponding measurements of SOL temporal variations are being prepared.

B. In dedicated experiments, we determined, by using RFA (Retarding Field Analyzer), the radial – poloidal pattern of the fast particle flux profile in front of the Tore Supra grill. In these experiments, we obtained for the first time the energy distribution function of electrons in the fast beam at full r-theta scan. In a specially designed experiment, for the first time the whole radial extent of the fast beam was explored. The envisaged computations of the heat flux in the fast electron beam near to the in front of the grill were not performed because of problems with determination of the power flux slit transmission factor of the RFA. Ref.: [1, 2, 3, 4, 5, 6, 7, 13, 82]

#### **Modelling of neutral beam (NB) and lower hybrid (LH) heating and current drive for COMPASS.**

**PI & Co-workers:** V. Fuchs, R. Dejarnac, M. Komm, M. Stransky, J. Urban

**Collaboration:** I. Voitsekhovitch (UKAEA), Y. Peysson and V. Basiuk (CEA Cadarache)

Results of our Lower Hybrid Current Drive (LHCD) simulations with the ACCOME and C3PO/LUKE ray tracing and Fokker-Planck codes were reported at the 2008 EPS conference [103]. We concentrated on the planned COMPASS operational range  $B=1.2-2.1$  Tesla and  $I=170-250$  kA. Because of the relatively low LH source frequency (1.3 GHz), low magnetic field and high density, the study was of great interest to the understanding of LHCD under poor LH slow wave accessibility conditions. The LH antenna power spectrum is also non-typical having at 60 degree waveguide phasing a broad main peak situated at  $n//=2.1$  with a width of about 2. LH power deposition and current was determined in 9 iterations between the ACCOME equilibrium and LHCD modules, and was verified using the ray-tracing and 3-D Fokker-Planck package LUKE. The principal difference between the LH ACCOME and LUKE codes is in ray tracing: ACCOME uses multiple rays, LUKE just one ray. This was the first time that the ACCOME LH module, conceived for computational speed is tested against a module devised for determining an accurate distribution function suitable for interpreting

hard X-ray diagnostics. An important result was that even in the worst-accessibility regime the LH-driven current makes a considerable 25-30% of the 170 kA of feedback controlled plasma current with 110 kW of deposited LH power.

For the broad COMPASS LH spectrum problem we decided to apply stationary phase methods to investigate wave propagation in a inhomogeneous plasma. In the last quarter we started to work on this method in cooperation with R. Cairns.

Intensive simulations have been performed to simulate NBI behaviour on COMPASS using the FAFNER Monte-Carlo code. Results indicate that the orbit losses can be as high as 40 % for the counter-injection scenario, making it considerably less efficient than co-injection. The so-called beam-halo effect causes significant charge-exchange losses for the dual-beam setup. These losses can be decreased by increasing the plasma density. Simulations for alternative particle energies show that the nominal selected 40 keV is a rather good choice. Ref.: [81, 103]

## 1.6 Energetic particle physics

### **Application of the Minimum Fisher Information inverse methods in the JET neutron cameras and compact spectrometers data analyses**

**PI & Co-workers:** Mlynář J., Svoboda V.

**Collaboration:** Bonheure G., Association EURATOM-Etat Belge, ERM, Belgium Tsalas M., Association EURATOM-Hellenic state, NCSR "Demokritos", Greece Murari A., Association EURATOM-ENEA, Consorzio RFX, Padova, Italy Popovichev S., Association EURATOM-UKAEA, Culham Science Centre, UK

The inversion method based on Minimum Fisher Regularisation (MFR) contributed to data analyses and, in particular, to tritium transport studies at JET in 2008. This method - implemented at JET in collaboration with the Association EURATOM/IPP.CR in previous years - was validated as a robust and rapid tool to analyse sparse data. Works in 2008 concentrated on extension and exploitation of the algorithm in spatial analyses of plasma neutron emissivities measured by the JET profile monitor (MFR tomography). In particular, the reconstruction matrix was determined based on the actual widths of viewing chords [46] and, more importantly, transport coefficients (diffusivity and pinch velocity) of tritium fuel were derived using a novel ratio method applied on the MFR tomography results [47]. Some efforts were also invested into preparation of an automated tool that would systematically analyse spectra of neutrons detected by the NE213 compact spectrometer and unfolded by the MFR [49].

Ref.: [46, 47, 49]

## 2. Development of plasma auxiliary systems

### 2.1 Heating and current drive systems

#### **COMPASS-D NBI system design.**

**PI & Co-workers:** J. Urban, J. Stöckel, J. Mlynar, V. Piffel, M. Komm

**Collaboration:** I. Voitsekhovich, UKAEA

A complex design of the beam ducts is required to avoid beam blocking. The design has not been finalized yet; however, calculations for a realistic engineering project indicate that the risk of the beam blocking can be sufficiently minimized.

Intensive simulations have been performed to simulate NBI behaviour on COMPASS using the FAFNER Monte-Carlo code. They indicate that the orbit losses can be as high as 40 % for the counter-injection scenario, making it considerably less efficient than co-injection. The so-

called beam-halo effect causes significant charge-exchange losses for the dual-beam setup. These losses can be decreased by increasing the plasma density. Simulations for alternative particle energies show that the nominal selected 40 keV is a rather good choice.

Ref.: [81]

## 2.2 Plasma diagnostics

### **Design of the detection system for BES.**

**Principal investigator:** V. Weinzettl

**Collaboration:** G. Anda, D. Dunai, D. Nagy, M. Berta, S. Zoletnik, Association EURATOM – HAS

A conceptual design of the beam emission spectroscopy system for the COMPASS tokamak was clarified and finished. The BES system will be provided with an exchangeable ion source (Li, Na). Detailed calculations for beam penetration depth were done. Maximum energy of the beam will be 100 keV. The beam will be able to reach a confined region of COMPASS plasmas also in H-mode. An array of avalanche photodiodes is assumed as a detection system for BES in preliminary calculations considering their routine use on MAST and TEXTOR tokamaks.

### **Development of fast tomography systems based on fast bolometric and SXR arrays for COMPASS.**

**PI & co-workers:** V. Weinzettl, D. Naydenkova, D. Šesták, J. Vlček, R. Melich, D. Jareš, M. Vácha

**Collaboration:** V. Igochine, Association EURATOM-IPP, IPP Garching, Germany, D. Sarychev, NFI RRC "Kurchatov Institute", Moscow, Russia

Multi-channel spectroscopic diagnostics on the COMPASS tokamak comprising AXUV-based bolometers, soft X-ray (SXR) and visible light detectors will cover a wide spectral range of the core and edge plasma emission aiming to realize a fast tomography at microsecond time scales. The design of the special complex port plug combining all detection systems taken into account a strongly limited available space, a heat protection and a shielding during a cleaning glow discharge was finalized. All in-vessel components needed for bolometric and SXR measurements were manufactured, new electronic amplifiers were constructed and their connection with the data acquisition system was realized. The design of the visible light detection system was developed and chosen detectors were bought. [20, 21]

### **Development of fast digital video camera system for machine control, plasma overview and turbulence measurements.**

**PI & co-workers:** V. Weinzettl, M. Hron

**Collaboration:** M. Berta, G. Veres, T. Szilveszter, A. Szappanos, S. Zoletnik, Association EURATOM – HAS

A new visible range video diagnostic was developed and installed on the COMPASS tokamak. The system contains mechanical engineering parts like a port plug, a cooling, a camera holder and appropriate optics with variable scaling and focusing possibilities, and a fast visible range camera of the EDICAM (Event Detection Intelligent Camera – produced by the Hungarian Association) type with advanced features, adapted to locale conditions and requirements. The diagnostic system is equipped by a modular software package with graphical user interface and own database system for data storage.

### **Realization of Thomson scattering system for COMPASS.**

**PI & co-workers:** P. Bílková, M. Aftanas, P. Böhm, V. Weinzettl, R. Melich, D. Šesták, J. Stöckel

**Collaboration:** M. Walsh, R. Scannell, G. Naylor, M. Dunstan Association EURATOM-UKAEA Fusion, Culham Science Centre

The main outcome from the period of January-September 2008 has been preparation of a feasibility assessment and options for the design of the Thomson scattering (TS) system. Lack of knowhow with designing such a complex system led us to find help of expert in the field, Mike Walsh from UKAEA/EURATOM in Culham. Thanks to his kind help since February 2008 and namely during mobility stay (one month, Petra Bílková), our group could draw from the experience of him and move forward. Participation in a number of conferences, above all in the 17th Topical Conference High Temperature Plasma Diagnostics in Albuquerque, New Mexico in May 2008 (Petr Böhm, Petra Bílková) was also beneficial thanks to unique opportunity to meet a high number of experts in Thomson scattering diagnostic and discuss with them.

In contrary to our previous report, the priority was not given to detection system only. Instead, both laser and detection parts of the TS system have been investigated as a whole at high level. The main task was to determine minimum laser energy necessary to detect sufficient number of scattered photoelectrons and thus fulfill ultrahigh spatial resolution requirement for the edge plasma region. This has been done by scaling from old COMPASS-D data. To achieve an ultrahigh spatial resolution of 3mm at the plasma edge, 4J Nd:YAG laser is required. Considering a ruby laser, an energy estimate is higher (12 J) compared to Nd:YAG because of generally lower efficiency of the grating detection. As a next step, two basic options of TS design which can meet requirements have been identified – Nd:YAG at first harmonic followed by polychromators equipped with spectral filters and Avalanche photodiodes or Ruby followed by spectrometer and ICCD detection. Particular options have been compared, its risks evaluated and detailed cost estimates as well as timescale prepared. To reduce price of the TS system, a duplexing of polychromators as an alternative option has been considered. Advanced laser options (doublepulse and burst regimes) allowing to achieve temporal resolution have been supposed, too. One of laser options considered earlier, Nd:YAG at second harmonic, has been excluded since its energy would not allow to meet ultrahigh spatial resolution requirement.

Afterwards, main decisions have been made in the last quarter of 2008 year. We based our concept around the established Nd:YAG (1064 nm, 4J)/APD technology. Access to the tokamak has been studied and vertical direction of laser has been chosen. The technical proposal of laser beam path and mimic laser beam path have been prepared. In the detection part of TS diagnostic, use of polychromators with the design based on the design of MAST TS polychromators has been chosen. Spectral analysis of the scattered signal is done in polychromators by means of set of spectral filters. First proposal of spectral filter selection (the bandwidth, the central wavelength) has been done. Optimization of selection and relevant error calculations are under development. Design of collection optics as well as optical fibre arrangement are in progress.

Ref.: [21, 24, 25, 26, 33]

**Development of millimeter-wave reflectometry methods for the measurement of edge pedestal plasma in tokamak COMPASS-D.****PI & Co-workers:** J. Zajac, F. Zacek, J. Vlcek**Collaboration:** IST, Centro de Fusão Nuclear, Lisbon M. Manso, A. Silva, P. Varela and L. Cupido

The primary achievement in 2008 was the solving of financial support of the project. IPP and CFN/IST decided in 2008 to propose to the subvention in the frame of the EFDA task WP08-TGS-01-06. Realization of the reflectometry system in a close collaboration with IST/CFN is delayed due to limited manpower in IST/CFN. Development of the unique band-combiners and the quasi-optical antennas in the Institute of Radiophysics and Electronics, Kharkov, Ukraine, is technically possible and therefore the partnership was included in the proposal.

**Measurements of the plasma potential, the electron temperature and diffusion coefficient in the edge plasma using the Ball-pen probe on ASDEX-U tokamak.****PI & Co-workers:** J. Adánek, J. Brotánková, J. Stöckel**Collaboration:** V. Rohde, W. Mueller, A. Herrmann - ASDEX-u, EURATOM-IPP, Garching, Germany; R. Schrittwieser, C. Schrittwieser, F. Mehlmann - Leopold-Franzens University of Innsbruck, EURATOM-ÖAW, Innsbruck, Austria

The direct measurements of the plasma potential have been performed on ASDEX Upgrade in June 2008. The modified design of the Ball-pen probe (reduction of the exposition of the boron nitride part) has been used. The Ball-pen probe head has been mounted on the reciprocating manipulator located at the midplane. The probe was exposed in the edge plasma, maximum 20 millimeters outside the limiter shadow, for several times during the discharge. The measurements have been performed in the ELMy H-mode. Moreover, two standard Langmuir probes have been used for the floating potential measurements in order to simultaneously measure the plasma and floating potential during and in between the ELM events. This provides a unique information of about the difference of the plasma and floating potential and possibly also the electron temperature during the ELM events (it will be presented on 36th EPS in Sofia).

The next campaign on ASDEX Upgrade tokamak in November 2008 was focused on the direct measurements of the electron and ion saturation currents by the ball-pen probes in ELMy H-mode with different NBI power at the edge plasma. The raw data shows that the crucial ratio of these two currents,  $I_{sat-}/I_{sat+}$ , is in the range  $<1,2>$  even during ELM events. It indicates the probe behaviour is similar on small and large fusion devices during L-mode and ELMy H-mode.

Ref.: [23]

**Divertor probes on COMPASS.****PI & Co-workers:** J Stockel, J Adamek, R Dejarnac**Collaboration:** Tsv. Popov, Association EURATOM/INRNE, Bulgaria

The COMPASS tokamak is equipped with an array of Langmuir probes embedded to a divertor plate. In the year 2008, the probes were tested and equipped by corresponding measuring circuits. First measurements indicate a proper performance of the system. Furthermore, a new power supply unit is designed and tested in collaboration with Association EURATOM/INRNE [14]. The probe voltage is of a triangular shape, but it is applied in steps. This novel approach allows better treatment of plasma fluctuations in processing of the IV characteristics and more precise determination of the electron distribution function.

Ref.: [14]

**Emissive and tunnel probes.**

**PI & Co-workers:** M. Tichý, P. Kudrna, J. Havlíček, M. Komm, R. Hrach, Z. Pekárek, E. Havlíčková

**Collaboration:** R. Schrittwieser, Petru Balan, Association EURATOM-OAW, Innsbruck University, Austria J.P. Gunn, Association EURATOM-CEA, Cadarache, France E. Martines, Association EURATOM-ENEA, Consorzio RFX, Padova, Italy

In accord with the forecast in the recent report we decided to study the discharge plasma in the cylindrical magnetron in pulsed regime. For this purpose we constructed a high-voltage dc switch based on power IGBT transistors, and a capacitor bank that powered the discharge during the active pulse. Time-resolved radial dependences of discharge current, plasma density, electron temperature and floating and plasma potential measured both during the on time and in the afterglow phase were evaluated from cylindrical probe data. The pressure range was changed from 1 to 10 Pa while the homogeneous magnetic field strength was kept at 10 mT where the pulsed discharge is stable. Pulses with amplitude about 700 V, duty cycle of 100 and 200 microseconds and repetition period of 1 ms were applied.

Ref.: [74, 75, 76, 77]

**Multichannel interferometer.**

**Principal Investigator:** J. Urban

New 16 channel radiometer will be available on COMPASS for detecting electron cyclotron emission (ECE) from the first harmonic in the frequency range of 26 – 40 GHz and possibly from the second harmonic in the frequency range of 60 – 90 GHz, supposing scenario with low magnetic field. For the central density in the range of  $5 \times 10^{19} \text{ m}^{-3}$  the first harmonic is cutoff for O- and X-mode emission and therefore only electron Bernstein waves, converted to the electromagnetic waves in upper hybrid resonance region, can be responsible for ECE.

COMPASS magnetic equilibria, computed by ACCOME, were applied for EBW simulations using our AMR code. From our simulation it follows that the radiometer and antenna system are well-suited for the detection of EBW emission from the first harmonic. In a model situation we found the optimum angles for the proper antenna aiming. We plan to use our radiometer for detecting the central temperature with very high time resolution.

**Development of Edge current measurements (WP08-TGS-01a-02 (III-3-a))**

**PI & co-worker:** V. Weinzettl, J. Havlíček

**Collaboration:** M. Berta, A. Bencze, G. Veres, G. Anda, S. Zoletnik, EURATOM-HAS

A new method for the measurement of magnetic field fluctuations and the poloidal magnetic field in the outer regions of COMPASS tokamak plasmas is introduced as an extension of the Beam Emission Spectroscopy (BES) system by collecting the ions stemming from beam ionization. Therefore we call it Atomic Beam Probe diagnostic (ABP). The BES system is already being manufactured by KFKI RMKI and it is planned to be operated by Li and Na beams. The extension will require operating it with somewhat heavier ions and/or at higher energies.

### **3. Development of concept improvements and advances in fundamental understanding of fusion plasmas**

#### **3.1 Optimization of operational regimes for improved concepts**

**Modelling of plasma response to RMP perturbations on the COMPASS tokamak.**

**PI & Co-workers:** P. Cahyna, R. Panek

**Collaboration:** M. Becoulet, CEA Cadarache

The reduced MHD code by G. Huysmans, M. Becoulet and E. Nardon was transferred to IPP Prague and used with the predicted equilibria and perturbation field of the COMPASS tokamak. It was found that the perturbation field penetrates in the edge region and is screened by rotation in the inner region [106]. We also contributed to the application of the code for ITER [45,107]. Together with the MHD code we transferred a code for estimating the impact of the neoclassical toroidal viscosity (NTV) and performed initial calculations for COMPASS. During the development of the code we found that the analytic formula for the NTV in the ITER-relevant collisionality is divergent. This important result was published together with a corrected formula (derived by K.C.Shaing) [15, 17]. We improved the vacuum model of the COMPASS perturbation coil field and performed calculations of perturbation spectra for a broader range of COMPASS operating parameters. As a result we obtained the optimal positions of the adjustable perturbation coils for research of the ELM mitigation technique by resonant magnetic perturbations. The optimal coil positions are the same for all the equilibria considered [106]. This will simplify future experiments.  
Ref.: [15, 17, 19, 45, 106, 107]

### 3.3 Other experimental activities

#### **Đuran - 3.3-A1: Tests and exploitation of Hall probe based systems on tokamaks JET (EP2 project), Tore Supra, and on stellarator TJ-II.**

**PI & Co-workers:** I. Duran, M. Hron, K. Kovarik

**Collaboration:** I. Bolshakova, R. Holyaka, V. Erashok (MSL, Lviv Polytechnic National University, Ukraine); V. Coccoresse, Antonio Quercia (Ass. ENEA/CREATE, Italy); P.J. Moreau, F. Saint-Laurent (CEA Cadarache, France); C. Hidalgo, M.A. Pedrosa (Ass. CIEMAT, Spain)

1. In frame of JET EP2 project RHP, six 3D ex-vessel radiation hard Hall probes were delivered to JET by MSL, Ukraine. The commissioning of the system was delayed due to problems with design and manufacturing of the support structure for the probes. The project was extended to mid-2009. In 2008, IPP.CR participated on solution of cabling system for the probes on JET. Further, we estimated the required settings of integrators for each particular coil incorporated in triplets within each 3D Hall probe. The coils serve as an independent magnetic sensor for comparison with Hall probes and also as a source of calibration magnetic field allowing to measure and compensate possible long term drift of Hall probes in radiation environment.

2. The prototype high-temperature (200 degC) wide bandwidth (500 kHz) Hall probe developed by MSL, Ukraine was installed in-vessel on Tore Supra on the back surface of antenna protecting limiter (APL). Unfortunately, the probe was destroyed early in the Tore Supra campaign. According to post campaign analysis of the probe taken out from the Tore Supra vessel, the damage was caused by halo currents flowing through the APL structure or by problems in probe grounding. Repeating of the experiment with improved cabling and isolation is envisaged but it is at present hampered by lack of funding on MSL side.

3. The combined probe head of 6 coils, 2 Hall probes and 3 Langmuir probes, developed by IPP.CR, was installed on TJ-II and the first experimental campaign using this probe was performed. Unexpectedly high level of magnetic turbulence in the range 1-2 mT was measured. Complex picture of electrostatic and magnetic modes and their interaction was studied using advanced statistic tools. Initial results turned out to be promising and stimulating further exploitation of this new probe diagnostic on TJ-II.

Ref.: [51, 53, 55]

### **Edge tokamak turbulence modelling compared with experiments.**

**Principal Investigator:** Jan Horacek

**Collaboration:** R. A. Pitts (CRPP EPFL, Switzerland), A. H. Nielsen (Riso, Denmark)

The inconsistency of turbulence structure sizes in ESEL wrt. experiment, together with results from CASTOR, was presented already in November 2007 as [oral J. Horacek, APS'07]. We computed the plasma-wall interaction, using the ESEL model, presented in [44]. Simulations for the ITER configuration are, however, found not to be possible with current version of ESEL because ESEL is valid only for plasma with much higher collisionality than in ITER.

We focused in addition on other topics:

1. we successfully verified credibility of the TCV fast (120kHz) electron temperature measurement in LFS SOL. Unique data from this new diagnostic were compared with two models: ESEL and SOLPS5 (on ELMs), presented as [43,109].
2. with ESEL, we predict an external transport barrier generation in far SOL, presented as [44]. We found, however, that experimental verification is complicated in current tokamaks.
3. Limited collaboration with CRPP Switzerland yielded several other publications. We studied ELM-induced divertor heat loads on TCV tokamak using infra-red camera [8,10,108]. We also studied ELMs with both SOLPS5 modelling [11] and using divertor Langmuir probes. Publications [50], [92] and [93] are linked through usage of the TCV reciprocating Langmuir probe, ESEL turbulence modelling and plasma parallel flow measurements.
4. Modelling of Lévy walk kinetics of charged particles in edge electrostatic turbulence in tokamaks yielded publication [38]. We model a single particle cross-field anomalous diffusion of heavy ions and electrons in a realistic background electrostatic potential. In our model we found that whereas ions can diffuse anomalously, electrons are rather trapped. Since in ergodic divertors electrons diffuse very fast along the chaotic magnetic lines, the combination of both effects can influence this scenario. Moreover, the nonambipolar diffusion, which we found, can generate radial electric field.

Ref.: [8, 9, 10, 11, 38, 43, 44, 50, 92, 93, 108, 109, 111]

## **3.4 Theory and modelling**

### **Quasineutral 1-D particle-in-cell (QPIC) simulations of scrape-off layer (SOL) plasma.**

**Principal Investigator:** V Fuchs

**Collaboration:** J. P. Gunn (CEA Cadarache)

We analyzed the radial extent of interaction of tokamak edge plasma with the lower hybrid (LH) antenna electric field. The antenna field interacts with the plasma by means of electron Landau damping. The electron acceleration associated with the power absorption results in high power-flows along magnetic field lines toward tokamak vessel components causing their possible damage. It is therefore of some practical importance to understand the radial extent of the LH-generated fast electron population. The standard present understanding of the radial fast electron – grill electric field interaction zone is based on the self-consistent antenna calculations of Jacquet et al which include the LH-generated hot electrons, and on linear Landau damping results from 2-D simulations of Rantamäki et al. Their results indicate a radial interaction zone of the order of a few millimeters adjacent to the grill mouth. However, recent experimental results from RFA (retarding field analyzer) measurements on Tore Supra have shown the existence of fast electrons as far as few centimeters from the grill mouth [79]. The LH-generated fast electrons causing hot spots on tokamak edge components can be divided into two quite distinct classes. To the first class belong fast electrons generated very near the grill, so we refer to these as “near-field” electrons. The “near-field” population is characterized by electric probe signals, which persist for the duration of LH power. The

second class of electrons causing spots on target components stream along magnetic field lines further away from the grill mouth - of the order of cm. Importantly, this second class of electrons exhibits temporal intermittency at a rate comparable with the detachment rate of relatively hot and dense plasma “blobs” from the main body of the plasma [97]. In general, the probe measurements indicate the presence of two electron components: the “cold” background plus a “hot” contribution. Details aside, the two groups of fast electrons appear to form one single fast electron beam extending radially over a few cm from the grill mouth toward towards the separatrix. In the present contribution we explained the observed substantial width of the LH-generated fast electron beam on the basis of linear electron Landau damping, thereby extending the previous understanding of the interaction. Our test electron simulations (using an LH antenna electric field from the coupling code ALOHA) to determine the fast electron distribution functions, combined with electron Landau damping calculations, gave radial interaction regions up to about 5 cm, in agreement with Retarding Field Analyzer probe measurements on Tore Supra.

Jacquet, Y. Demers, V. Fuchs, et al. Phys. Plasmas 6 (1999) 214.

K. M. Rantämäki, T. G. H. Pättikangas, S. J. Karttunen, et al., Nucl. Fusion 40 (2000) 1477.

Ref.: [73, 97]

### **2D particle-in-cell modeling of the plasma sheath.**

**PI & Co-workers:** R. Dejarnac, M. Komm

**Collaboration:** J. P. Gunn (CEA Cadarache)

The 2D version of our in-house particle-in-cell code in cylindrical coordinates has been validated. We needed to work again on the injection module and density calculation. Due to the cylindrical geometry of the simulation box, cells at larger radii have larger volumes than cells closer to the axis. More particle are therefore needed in the outer cells. This is achieved by launching particle in a homogeneous way along the injection plane and by adding a geometrical weighting proportional to the radius of the launched particle. However, such a geometrical weighting generate errors in the interpolation scheme and corrections must be done. The density calculation has been validated in a first approach without electric field and with monoenergetic ions. With electric field, the profiles are flat and the electric potential match the analytic solution of the Poisson's equation in a simple box (square).

### **EBW simulations for WEGA.**

**PI & Co-workers:** J. Preinhaelter, J. Urban

**Collaboration:** H.P. Laqua, IPP Greifswald

Electrostatic electron Bernstein waves (EBW) are studied numerically and compared to experimental results on the WEGA stellarator. Using the WEGA antenna, the two O-/X-mode radiation lobes are modelled by sets of rays with intensity proportional to the measured radiation pattern. After projecting these rays onto the plasma periphery, a full wave adaptive mesh solver of the cold plasma equations determines the O-X-EBW mode conversion efficiency around the upper hybrid resonance. From the roots of the EBW dispersion relation, ray tracing is performed to determine the power absorption on the 1st or 2nd cyclotron harmonic and current drive, assuming the Fisch-Boozer mechanism. Detailed simulations are performed on specific WEGA equilibria and its antenna launch of 2.45 GHz waves, with excellent agreement with experiment. In particular, the off-axis power deposition and the outward shift of the absorption maximum produced by increasing the magnetic field can only be explained by the presence of a hot electron component, which permits wave absorption at the 2nd harmonic near the plasma periphery. Moreover, the simulations also reproduce the current density reversal at the plasma centre for low magnetic fields and that this reversal is destroyed when larger magnetic fields are employed.

Ref.: [27, 34, 86, 88, 89, 91]

### **MAST EBW studies.**

**PI & Co-workers:** J. Preinhaelter, J. Urban

**Collaboration:** M. Valovic, UKAEA V. Shevchenko, UKAEA

We have modified the AMR code for UKAEA computers. Particularly, we alternated IMSL library routines by public available or NAG routines and successfully tested the code compilation remotely on UKAEA computers. The AMR code is now prepared for running simulations for the MAST experiment on UKAEA computers. UKAEA scientists will therefore be able to run the code themselves.

### **Fokker-Planck EBW studies.**

**PI & Co-workers:** J. Urban, J. Preinhaelter

**Collaboration:** J. Decker, CEA Cadarache

Electron Bernstein wave (EBW) physics can be simulated with a linear code capable of ray-tracing and mode-conversion calculation as far as low power applications, i.e. emission or low-power heating and current drive, are concerned. AMR (antenna → mode-conversion → ray-tracing) has been created at our institute for these calculations. However; higher-power applications necessitate quasi-linear approach to solve the Fokker-Planck equation. For this reason, it was decided to couple AMR with the LUKE code to create a state-of-the-art EBW simulation suite. Presently, a basic coupling of the two codes is working. AMR can provide necessary inputs for LUKE (in data files), which LUKE can conveniently read. Test cases were successfully simulated validating the consistency of the transferred data and proving the functionality. More integrated interface is foreseen. LUKE is also running on IPP Prague computer systems.

### **EFIT2006 development.**

**Principal Investigator:** J. Havlicek

**Collaboration:** L.C. Appel, UKAEA Culham

The EFIT2006 code has changed the name to efit++; henceforth, we refer to it as efit++. The main work related to the efit++ development was performed during the visit of J. Havlíček to UKAEA Culham in September / October 2008. The main goal of this visit was to implement (within efit++) a computational model to represent the induced currents that are not measured in tokamaks. These may be present particularly in coil cases and in vessel or other structural elements. The modelling was restricted to axisymmetric currents as the efit++ code itself assumes the axisymmetry. The model was written entirely in C++ as a consistent set of objects utilising freeware scientific libraries, such as GSL.

The status of the implementation of the induced currents model into efit++ is as follows. All data structures necessary for actual computation of the induced currents (matrices of self and mutual inductances) are prepared, computed and tested on a simplified testing example. The coding of a C++ method "computeInducedCurrents" began but has not been finished. This method is still in a testing phase of development—induced currents were computed only for a testing example of 2 passive structures, one coil and a plasma current computational grid consisting of 4 points. It is supposed that the induced currents model implementation will be finished in 2009.

### **Preparation of modules for handling boundary conditions for edge codes (ITM-08-IMP3-T13).**

**Co-worker:** R. Dejarnac

**Collaboration:** D. Tskhakaya, Association Euratom ÖAW, Innsbruck (principal investigator), F. Subba, S. Kuhn, N. Jelic and D. Tskhakaya senior.

Boundary conditions for the stationary sheath and for the divertor sheath during ELMs have been reported. The potential drop and the particle and heat fluxes equations have been

developed for a quasi 2D model including ExB drifts and implemented in a running module. The first version of the code and the corresponding description were provided to EFDA.

## 4. Materials & Technology

### 4.1 Development of Materials science and advanced materials for DEMO

#### **Feasibility study of "metal Hall sensors" as radiation hard steady state magnetic field sensors.**

**PI & Co-workers:** I. Duran, IPP, L. Viererbl, NRI, J. Sentkerestiova, FNSPE

Several samples of thin layers (50 nm) of bismuth were obtained from AREPOC company, Slovakia to assess the perspectives of this material for use in Hall sensors for fusion reactors. Several methods of providing reliable electrical contacts to these thin layers were tested. First, it was found out that it is impossible to provide long term reliable electrical contacts directly to bismuth layers. As a result, sensors with copper layers at contact areas were prepared. Mechanical spring loaded contacts turned out to be unreliable, particularly at elevated temperatures above 150 °C. Further, ultrasonic bonding of 40 micrometer gold wires to the copper contact plates of the bismuth sensor was tried in collaboration with Poznan University of Technology, Poland. Following these preliminary experiments the collaboration with company MicrowaveLab, Kutna Hora, Czech Republic was established in order to provide bonding of the contacts to the samples [52,54,55].

Additional, optimization of parameters and design of a new Helmholtz coils pair for calibration of metal Hall sensors, usable in wide temperature range from room to 300 °C, was performed. It was found out that the maximum magnetic field of cca 200 mT can be achieved with coils winding made from KAPTON isolated copper wire with cross-section of cca 4mm<sup>2</sup>, respecting the constraints imposed by space and power sources available [54].

Finally, we have participated on preparations of irradiation tests of ITER candidate bolometers in SCK.CEN, Belgium.

Ref.: [52, 54, 55]

#### **Irradiation and characterization of fusion-relevant materials.**

**PI & Co-workers:** Jiri Matejcek, IPP, Karel Splichal, NRI, Ladislav Viererbl, NRI

**Collaboration:** Jochen Linke - Forschungszentrum Julich, Germany

Several samples of plasma sprayed layers of tungsten, copper, stainless steel, and corundum together with samples of bulk materials were prepared to test impact of neutron irradiation on their thermal and electrical properties. The thermal and electrical properties of these samples were characterized. Six irradiation containers were designed and manufactured. Their waterproofness was tested. The thermal calculations were done for containers with stainless steel samples where the required irradiation temperature is high. All six containers were installed inside the LVR-15 reactor and the irradiation campaign with the target neutron fluence of up to 1 dpa was started. One of the containers containing samples with lower target neutron fluence was extracted and the neutron fluence received was measured. The remaining capsules were rearranged in the irradiation channel, in order to approximately balance out the spatial variation of the neutron flux.

### **TW2-TTMS-001b, D3**

#### **Static and dynamic fracture toughness at the transition temperature: Neutron irradiation of plate end weldments after up to 2.5 dpa at 200°C – 250°C and PIE**

**Field:** Tritium Breeding and Materials, Area: Materials Development

**Principal Investigator:** P. Novosad, NRI Řež, plc

**Co-workers:** M. Falcnik M. Kytka, K. Splichal

Revised due date: 31.12.2009, status: in progress

EUROFER 97 specimens of base metal and weld metal irradiated at temperature 235°C on irradiation level of 2.51 dpa have been tested. For dynamic fracture toughness testing, the cells have been equipped with a Tinius Olsen Model 74, Zwick RKP450 and RKP50 impact test machines, instrumented with data acquisition and analysis system. Fracture toughness was measured with irradiated EUROFER sub size specimens 3.5 x 4 x 27 mm for both base and weld metals. Testing of dynamic and static fracture toughness were finished and the transition temperature curves of base and weld metals in as received state and after irradiation at the temperature of 235°C were evaluated. Final report will be prepared..

### **TW2-TTMS-003b,**

#### **In-pile corrosion testing of TBM's weldments up to 2dpa**

**Field:** Tritium Breeding and Materials, Area: Materials Development

**Principal Investigator:** K. Splichal, NRI Řež, plc

**Co-workers:** J. Berka, J. Burda, E. Keilová, Vl. Masarik, Z. Lahodová, L. Viererbl

Revised due date: 31. 12. 2009, status: in progress

Compatibility of martensitic steel EUROFER 97 was investigated with Pb-Li eutectic melt under at temperature 500°C under irradiation condition. Effect of irradiation on Pb-Li melts properties was investigated regarding microstructure, chemical composition and radioactivity. The irradiation of eutectic melts results in the production of tritium and polonium owing to transmutation reaction and bismuth from induced reaction. The post irradiation examinations did not show any noticeable attack of martensitic steel. Surface layers affected by corrosion attack were observed EDX. Metallographic investigations continue.

### **TW5-TTBC-005, D2**

#### **Development and testing cold traps, high temperature flanges and circulation pump for the liquid metal Pb-Li loop**

**Field:** Tritium Breeding and Materials, Area: Breeding Blanket

**Principal Investigator:** Vl. Masarik, NRI Řež, plc

**Co-workers:** L. Kosek, J. Berka, M. Ruzickova, K. Splichal M. Zmitko,

Revised due date: 31. 12. 2009, status: in progress

Operational parameters for PbLi loop were verified. Temperatures and flow speed required for purification experiments were in projected ranges. Two purification experiments with artificially added impurities were carried out. Design of sampling system was simplified from once shot to more flexible one. Efficiency of cold trap for removing corrosion products from circuit was investigated with these results: content of Fe was reduced by 30%, Mn 80%, Ni 70% and Cr showed no change. Simple evaluation of kinetics of precipitation process was also performed. High temperature flanges was manufactured and testing is ongoing. Special loop for measurement of circulation pump characteristic was designed and now is being manufactured.

**TW6-TTMS-003, D5****Compatibility of EUROFER samples coated by Al and Er<sub>2</sub>O<sub>3</sub> layers with Pb-Li melt under higher temperature conditions**

**Field:** Tritium Breeding and Materials, Area: Materials Development

**Principal Investigator:** K. Šplíchal, NRI, Řež, plc

**Co-workers:** L. Kosek, J. Berka, M. Zmitko

**In collaboration with:** Forschungszentrum Karlsruhe, IPP Garching

Revised due date: 31. 12. 2009, status: in progress

Under Test Blanket Module (TBM) operation conditions sufficient corrosion resistance and limitation of tritium penetration through EUROFER steel are required. Two types of anti-corrosion and/or tritium anti-permeation coatings on EUROFER steel will be used. The compatibility and corrosion resistance of Al coatings ( Forschungszentrum Karlsruhe) and erbium oxide coatings (IPP Garching) will be investigated with Pb-Li liquid eutectic alloy under TBM conditions. The investigations will evaluate kinetics of the coating thickness changes, mechanism of surface interaction of eutectic melt with coating layers, microstructure and chemical composition of layers and characterization coating - base metal bonding. The experiments will start after finishing of EFDA tasks with the Pb-Li loop and after verifications of prepared specimen holder.

**TW4-TVB-TFTEST2****Thermal Fatigue Tests of Be Coated Primary First Wall Mock-ups (equipment)**

**Field:** TV – Vessel / in Vessel, Area: TVB - Blanket

**Principal investigator:** T. Klabík, NRI Řež, plc

**Co-workers:** V. Masařík, O. Zlámal, P. Hájek,

**In collaboration with:** P.Lorenzetto, S. Wikman, F4E, Barcelona, Spain

Revised due date: 30.6.2009, status: in progress

In the frame of international project focused on material testing for ITER first wall the BESTH (**B**eryllium **S**ample **T**hermal **T**esting) device was constructed and operated in Nuclear Research Institute Rez, plc. Purpose for construction was based on need of having non-active testing device which is capable of providing required heat flux with data record and evaluation. The main goal of proposed tests is to validate Be-CuCrZr HIP joint endurance under high heat flux cycle load, which simulates thermal conditions in fusion reactor with respect to joint life-time. Tested mock-ups come from EU, USA, Japan, China, Korea and Russia. This paper describes realisation steps and progress in BESTH device operation.

**TW6-TVM-TFTEST****Thermal Fatigue Tests of Be Coated Primary First Wall Mock-ups (tests) – Test Campaigns of 110/80 Wide Mock-ups**

**Field:** TV – Vessel/in Vessel, Area: TVM - Materials

**Principal investigator:** T. Klabík, NRI Řež, plc

**Co-workers:** O. Zlámal, V. Masařík, P. Hájek,

**In collaboration with:** P. Lorenzetto, S. Wikman, F4E, Barcelona, Spain

Due date: 30.6.2010, status: in progress

The BESTH testing device operated by Reactor Services Division, NRI Řež,plc in Czech Republic, allows to carry out out-of-pile tests of Beryllium coated First Wall Qualification Mock-ups under conditions of cyclic heat load in order to evaluate soundness of Be/CuCrZr HIP joint for fusion reactors.

Testing of Aluminium and Copper samples for evaluation of heat flux distribution is successfully finished as well as testing of first two FWQ mock-ups, supplied by US and EU Domestic Agencies (DA). Obtained results were evaluated and testing of four more mock-ups from different DA is foreseen during year 2009.

### **TW3-TVB-INPILE**

#### **In-pile thermal fatigue testing device for Primary First Wall Mock-ups with Beryllium cladding**

**Field:** TV – Vessel / in Vessel, Area: TVB – Blanket

**Principal investigator:** T. Klabík, NRI Řež, plc

**Co-workers:** V. Masařík, O. Zlámal, P. Hájek

**In collaboration with:** P. Lorenzetto, S. Wikman, F4E, Barcelona, Spain

Revised due date: 31.12.2009, status: in progress

The objective of this task is to perform in-pile thermal fatigue testing of actively cooled Primary First Wall (PFW) mock-ups to check the effect of neutron irradiation on the Be/CuCrZr heterogeneous joints under representative PFW operation conditions. Two PFW mock-ups will be irradiated at 0.6 dpa with parallel thermal fatigue testing at 0.6 MW/m<sup>2</sup> for 20,000 cycles. Investigation is focused on design, manufacturing and verifications on thermal fatigue equipments and qualification testing without irradiation.

### **TW6-TTMN-002, D6**

#### **Experiments for the validation of Bi cross-sections up to 35 MeV in a quasi-monoenergetic neutron spectrum**

**Field/Area:** Tritium Breeding and Materials / Materials Development

**Principal Investigator:** P. Bém, Nuclear Physics Institute Řež

**Co-workers:** V. Burjan, M. Götz, M. Honusek, V. Kroha, J. Novák and E. Šimečková

**In collaboration with:** U. Fischer and S.P. Simakov, Association FZK-Euratom, Forschungszentrum Karlsruhe, Germany

Due date: (revised within F4E) October 2009, Status: **D6 completed**

The experimental investigation of  $^{209}\text{Bi}(n,3-5n)^{207-204}\text{Bi}$  reaction cross-sections was carried out utilizing the quasi-monoenergetic neutrons from the NPI p-<sup>7</sup>Li source in neutron energy range from 19 to 35 MeV (neutron peak energy). The spectral yield data were measured by TOF technique at proton energies of 20, 25, 30, 35 and 45 MeV. Measured data of specific activities of reaction products will be analyzed in terms of EASY-2007 system under close collaboration with the team of FZ Karlsruhe (TW6-TTMN-002B, D7).

### **TW6-TPP-CNDMSTICK**

#### **Determination of reflection properties of hydrocarbon radicals for ITER-like divertor conditions**

**Principal investigator:** Z. Herman, J. Heyrovsky Inst. of Physical Chemistry AS CR

**Co-workers:** J. Žabka, A. Pysanenko

**In collaboration with:** T. D. Märk et al, Association EURATOM-ÖAW, Austria

Collisions of selected hydrocarbon ions  $\text{CD}_4^+$ ,  $\text{CD}_5^{++}$ ,  $\text{C}_2\text{D}_4^+$  and  $\text{C}_2\text{H}_5^+$  with room-temperature and heated tungsten surfaces were investigated at incident energies of 15–45 eV. From the data, information on processes at surfaces, energy transfer at surfaces, and absolute ion survival probabilities of ions were determined. The ion survival probability of the investigated ions for both room-temperature and heated W-surfaces was in general 2-15 times smaller than on carbon (HOPG) surfaces and tended to be smaller for radical cations ( $\text{CD}_4^+$ ,  $\text{C}_2\text{D}_4^+$ ) than for even-electron ions ( $\text{CD}_5^{++}$ ,  $\text{C}_2\text{H}_5^+$ ). Mass spectra, translational energy distributions and angular distributions of product ions from collisions with W-surfaces were very similar to distributions measured earlier for carbon (HOPG) surfaces. On room-temperature surfaces of W, radical cations showed both direct surfaces-induced fragmentations of incident ion and chemical reactions with the surface material, while even-electron ions exhibited only fragmentation processes. On heated surfaces, only fragmentations of the incident projectile ions were observed.[58]

Scattering of the hydrocarbon radical cation  $C_2D_4^{++}$  from room-temperature carbon (highly oriented pyrolytic graphite, HOPG) surface was investigated at very low incident energies of 6- 12 eV [59,61]. The absolute survival probability of the ions for the incident angle of  $30^\circ$  (with respect to the surface) decreased from about 1.0 % (16 eV) towards zero at incident energies below 10 eV. Estimation of the effective surface mass involved in the collision process led to  $m(S)_{\text{eff}}$  of about 57 a.m.u. for inelastic non-dissociative collisions of  $C_2D_4^{++}$  and of about 115 a.m.u. for fragment ions ( $C_2D_3^+$ ,  $C_2D_2^{++}$ ) and ions formed in reactive surface collisions ( $C_2D_4H^+$ ,  $C_2D_2H^+$ ). This suggested a rather complex interaction between the projectile ion and the hydrocarbon-covered surface during the collision.[59,61,116]

Collisions of dications and cations  $SF_4^{2+/+}$  with hydrocarbon-covered steel surface were investigated and collision-energy resolved mass spectra (CERMS) curves were determined [60,115]. The results indicate that the likely major reaction sequence responsible for the observed CERMS curves of product ions from  $SF_4^{2+}$  collisions is charge exchange to form singly-charged projectile ions followed by subsequent unimolecular fragmentation to cations  $SF_3^+$ ,  $SF_2^+$  and  $SF^+$ , increasing with increasing incident energy. In addition, chemical reactions between projectile ions and hydrocarbon adsorbates were observed leading to  $SF_2CH_3^+$ ,  $SFCH_2^+$ , and  $SCH^+$  ions.[60,115]

#### **WP08-PWI-06, PWI-08-TA-06**

#### **Transport and Deposition of First Wall Impurities. SEWG Chemical Erosion and Material Transport: Reactive Interaction of Molecular Ions with Surfaces**

**Principal investigator:** Z. Herman, J. Heyrovsky Inst. of Physical Chemistry AS CR

**Co-workers:** J. Žabka, A. Pysanenko

**In collaboration with:** T. D. Märk et al, Association EURATOM-ÖAW, Austria

Interaction of slow ions  $C_3H_n^+$  and  $C_3D_n^+$  ( $n=2-8$ ) with room temperature carbon surfaces was investigated over the collision energy range 15 – 45 eV and surface-induced fragmentation pathways of the projectile ions were determined. A simple correlation between survival probability of the hydrocarbon ions ( $C_3$  measured here and earlier measured  $C_1$ ,  $C_2$ ,  $C_7$ ) and ionization energy of the species in question (instead of the unknown recombination energy) was found. It showed a decrease from more than 10% to less than 1% in between IE 8.5 - 9.5 eV and a further decrease at higher IE. A semi-logarithmic plot  $\log S_a - IE$  showed that the decrease of  $S_a$  in these coordinates was approximately linear over the entire range of IEs of the investigated species and the data could be fitted with an empirical relation  $\log S_a = (3.9 \pm 0.5) - (0.39 \pm 0.04 \text{ IE})$ . [1]

Collisions of low energy  $C_2D_4^+$  and  $Ar^+$  ions with stainless steel, carbon (HOPG), and two different diamond surfaces were studied to find out, how different material of a surface at room-temperature, underlying a hydrocarbon coverage, influences surface processes, namely to compare the behaviour of hydrocarbon-covered H-terminated diamond (hydrophobic) and O-terminated diamond (hydrophilic) with two standard surfaces (carbon and stainless steel). The presence of hydrocarbons was observed on all the studied room-temperature surfaces. Fragmentation, chemical reactions, and energy transfer at surfaces were very similar for all surfaces. The only observed difference between the two diamond surfaces was the ratio of probabilities of reactive vs. reactive and dissociative processes,  $P_R/(P_R+P_D)$ , as a function of incident energy. This ratio increased from a threshold at 6-7 eV to about 70% for the SS, HOPG, and DO surfaces, but only to about 45% for the DH surface.[2]

### **Study of the micro-mechanisms of cleavage fracture of 14% Cr and 18% Cr ODS ferritic steels**

**Principal investigator:** *H. Hadraba, Institute of Physics of materials AS CR, v.v.i.*

**In collaboration with:** *B. Fournier, CEA Saclay, France*

An impact testing of specimen prepared in the institute was conducted by means of instrumented pendulum impact tester. A bar and a plate were prepared by hot extrusion from mechanically alloyed powders. The powders were produced by atomisation of the prealloyed powder (Aubert & Duval) and subsequent mechanical alloying of the powder by  $Y_2O_3$  (Plansee). The observation of fracture surfaces for both materials highlighted the strong influence of morphological texture (elongated grains) on the brittle fracture process. Numerous secondary cracks were observed.

### **Development of functional gradient materials using powder laser deposition.**

**PI & co-worker:** *J. Matějček, H. Boldyryeva*

**In collaboration with:** *P. Ambrož, Czech Technical University in Prague*

Laser spraying (also called laser cladding or laser sintering) has potential advantages in comparison to other techniques of production of the tungsten-steel functionally graded materials (FGMs). Tungsten powder used for laser spraying in the experiments was pre-treated by water-stabilized plasma jet torch. During scanning, the powder was blown down from the bottom of the head onto the steel substrate while simultaneously melted by the laser beam. Two different speeds of scanning (200 mm/min and 400 mm/min) were employed, whereas the feed rate of tungsten powder and supplying Ar gas pressure (1 bar) were kept stable. Cross-sectional SEM image of samples produced were studied.

## **5. Training and career development**

### **5.1 Collaboration with the Universities in training in fusion research**

#### **Collaboration of IPP Prague with the Charles University and the Czech Technical University in Prague.**

J. Mlynar, J. Stockel, F. Zacek, I. Duran

Although the tokamak department of IPP had no experimental facility in 2008, it attracted increasing number students from Universities who got extended training support. Ten postgraduate (doctoral) students have been preparing their dissertation here. Number of undergraduate students looking for a fusion-oriented topic also increased. The tokamak department tried hard to find suitable research topics and an expert supervisor for all of them. In 2008 the tokamak department of IPP Prague led practical works of 7 MSc level students and 7 BSc level students from both Czech Technical University and Charles University. In total, 12 doctoral students and 18 undergraduate students were involved in the work of the IPP tokamak department in 2008. Research scientists from the institute also participated in teaching. In the summer term, our staff was responsible for 3 courses: Introduction to thermonuclear fusion, Technology of thermonuclear facilities and Topics from magnetic confinement fusion. In the winter term, our staff was responsible for the course Tokamak physics and for organising joint FNSPE – IPP seminars.

#### **Undergraduate training in Fusion science and technology.**

V. Svoboda, J. Mlynar, D. Bren

The MSc curriculum Physics and Technology of Thermonuclear Fusion started at FNSPE CTU in 2006. In 2008 first students entered their final year of the curriculum, while for the third time new students enrolled the curriculum. Several new subjects were opened in 2008

for the first time (e.g. Diagnostics of fusion plasmas, Technology of thermonuclear fusion, Modelling of fusion plasmas, Fusion seminars). Other members of the Association were considerably involved, in particular the Faculty of Mathematics and Physics, and the Institute of Plasma Physics AS CR. Importantly, on 17th November FNSPE CTU hosted international kick-off meeting of the FUSENET consortium, which is responsible for the EURATOM Coordination and Support Activity (CSA) in fusion education. The consortium will allow to our students and our teachers extend their keep-in-touch activities with other European Universities as well as with fusion laboratories. Faculty of Mathematics and Physics, who is in particular responsible for doctoral studies of Plasma physics (followed by most of the tokamak doctoral students) is also member of the consortium as well as the Institute of Plasma physics AS CR.

## **5.2 Training in laboratory experience, principles of data validation, analyses and interpretation, and presentation of results**

### **International summer training course (SUMTRAIC 2008).**

J. Stockel

The 6th Summer Training Course (SUMTRAIC 2008) was organized by the Association EURATOM/HAS in Budapest in the period 26.6.08 - 4.7.2008. The SUMTRAIC took place at Budapest University of Technology and Economics, Budapest. The Course was attended by 11 students from 6 countries, who were trained in measurement of Langmuir probe characteristics in a glow discharge, spectroscopy of different light sources and fluctuations in fluids. Before practical training, several lectures have been presented to participants.

## **6.3 EFTS (European Fusion Training Scheme)**

### **Conduct training of two young engineers within EODI and ENTICE projects.**

**PI & Co/workers:** I. Duran, J. Stockel, J. Zajac, J. Brotankova, A. Krivska, D. Sestak

**Collaboration:** J.-M. Noterdaeme, IPP Garching, Germany M. Nightingale, UKAEA, United Kingdom B. Beaumont, CEA Cadarache, France R. Koch, ERM-KMS, Belgium R. Maggiora, Polytechnico di Torino, Italy K. Numssen, Spinner GmbH, Germany W. Biel, FZJ Julich, Germany R. Jaspers, FOM, The Netherlands N.H. Balshaw UKAEA, United Kingdom R. Reichle, CEA Cadarache, France R. Konig, IPP Garching, Germany P.K. Michelsen, RISOE, Denmark

1. ENTICE: IPP.CR based ENTICE trainee Alena Krivska started in January 2008 her 15 months long secondment to IPP Garching, Germany. She was engaged there into the modeling of ASDEX-U ICRH antenna, contributing particularly to the definition of the proposed antenna enhancement project [71,72]. Generally, her training proceeds successfully along her carrier development plan.

2. EODI: In february 2008, IPP Prague concluded an employment contract, in frame of its EODI training project involvement, with David Sestak - fresh graduate of Czech Technical University. His carrier development plan was formulated and his training proceeded accordingly. In particular, he was involved in design of new optical diagnostics for COMPASS tokamak [20,21].

Ref.: [20, 21, 71, 72]

## **6. Other activities contributing to the EURATOM fusion programme**

### **6.1 Public information**

M. Ripa, J. Mlynar

Without any question the main event in public information last year was the official unveiling of the COMPASS tokamak in Prague on April 1st. The programme had been prepared well in advance and attracted many VIPs of Europe and Czech Republic: HM ambassador Ms Linda Joy Duffield, chairman of the Consultative Committee EURATOM-Fusion Sir Chris Llewellyn Smith, Director of EURATOM Mr Octavio Quintana Triaz, Minister of industry of the Czech republic Mr Martin Říman, President of the Czech Academy of Sciences prof Václav Pačes, chairman of International Board of Advisors of the Association EURATOM-IPP.CR prof Hardo Bruhns, Mr Vladimír Remek MEP, and others. The extraordinary interest of media was proved by 17 newspaper and magazine reports, 12 internet reports, four broadcastings and three Czech press office reports.

During 2008, tokamak COMPASS hosted well above 20 visits from schools, universities, governmental institutes and industries in 2008. Quite naturally, all these visits involved rather detailed information on the ITER project and its status. PI activities of Association were presented in the 8th Public Information Group meeting in Lisboa on May 8 to 10, 2008.

## **7. Coordination, in the context of a keep-in-touch activity, of the Member State's civil research activities on Inertial Fusion Energy**

### **8.1. Scientific developments**

#### **Experiments on interaction of focused high-power laser beams with multilayer high-Z targets.**

J. Ullschmied

The aim of the experiments performed in 2008 was to elucidate the relative role of two different mechanisms responsible for formation of plasma jets at interaction of a flat-profile pulsed high-power iodine laser beam with flat solid-state targets, namely the radiation cooling and the cumulative hydrodynamic effects. Our earlier experiments [63-66] have shown that well formed jets can be produced on high-Z targets only (Cu, Ta, Pb). Now we used double targets consisting of a massive high-Z substrate covered by a thin layer of a lighter material (Cu-plastic, Ta-plastic, Cu-Al, Ta-Al) and, on the contrary, Al and plastic targets covered with thin high-Z layers. It turned out that a thin layer of high-Z material makes it possible to generate plasma jets even on very low-Z materials such as plastic, and, vice versa, low-Z surface layer inhibits jet formation on high-Z targets [67, 98]. This result speaks in favour of the decisive role of cumulative effects caused by strong target irradiation inhomogeneities resulting from non-linear laser beam - plasma interaction at the very beginning of the laser pulse. This would open the way for producing plasma jets e.g. on IFE-relevant frozen D-T targets. Plasma motion in the reported experiments was watched by multi-frame laser interferometer, as well as the motion of a foil driven by the ablative plasma, on the base of which the amount of laser energy transferred to the latter was determined [62, 68]. In this context also new original methods of ablative laser acceleration of macroparticles were studied [101, 102]. Among them namely the reversed acceleration scheme [102] promises acceleration of macroparticles to ICF-relevant velocities.

Ref.: [62, 63, 64, 65, 66, 67, 68, 98, 101, 102]

## 8.2 Coordination Activities

### **Laser generated plasma jets for ICF and astrophysics.**

J. Ullschmied

Collimated plasma outflows - plasma jets - are a subject of interest both in ICF research and in astrophysics. Plasma jets are observed at contact surfaces of different materials at laser interaction with multi-shell targets, highly supersonic plasma jets may find its use in some impact fast ignition schemes. They can propagate over considerable distances, so that their interaction with surrounding media can be used for laboratory simulation of some astrophysical phenomena, such as Herbig-Haro objects. In the collaborative experiments performed at the PALS facility the jet like structures have been created in several ways by using a modest energy (~100 J) 250 ps laser beam at the 1st and 3rd harmonics of the iodine laser (1315 nm) [65-67]. The direct method of plasma jet generation consisted in irradiation of a massive planar target made of a relatively heavy material (atomic number at least 29) by a partly defocused laser beam [65]. For formation of a convergent narrow jet in that case an annular structure of the laser focal spot proved to be indispensable, however the annular target irradiation can be created spontaneously during the laser beam – plasma interaction providing that the focal point of a focusing lens is situated inside the target [63, 98]. The other two indirect methods employed either the impact of an ablatively accelerated flyer, or a cumulative compression of a conically shaped foil target [66].

The optimised directly generated highly supersonic plasma jets were used at detailed investigations of jet interaction with gas-puff plasmas [65]. By varying the gas pressure and composition, the nature of interaction zone changes from a quasiadiabatic outflow to a strongly radiation-cooled jet. The scale structures of the interaction zone were studied by means of optical and x-ray diagnostics [69] and interpreted by using a semi-analytical model in combination with 2D radiation hydrodynamic simulations [65, 99, 100].

Ref.: [63, 65, 66, 67, 69, 98, 99, 100]



## III

## LIST OF PUBLICATIONS

*For overview of Public Information activities in 2008 please refer to the report in Part IV, section 7.*

- [1] **J. P. Gunn, L. Colas, A. Ekedahl, E. Faudot, V. Fuchs, S. Heuraux, M. Goniche, M. Kočan, A. Ngadjeu, V. Petržílka, F. Saint-Laurent, K. Vulliez:** Extreme Scrape-off Layer Phenomena during RF Heating in Tore Supra. *To be presented at the 22nd IAEA Fusion Energy Conference, Geneva 2008, Switzerland.*
- [2] **M. Goniche, A. Ekedahl, K. Rantamäki, J. Mailloux, V. Petrzilka, G. Arnoux, Y. Baranov, L. Delpech, K. Erents, P. Jacquet, K. Kirov, M-L. Mayoral, J. Ongena, F. Piccolo, A. Sirinelli, M. Stamp, K-D. Zastrow and JET EFDA contributors:** Lower Hybrid Current Drive Experiments on JET in ITER-Relevant Coupling Conditions. *To be presented at the 22nd IAEA Fusion Energy Conference, Geneva 2008, Switzerland, on JET pinboard*
- [3] **J. Gunn, V. Petrzilka, A. Ekedahl, V. Fuchs, E. Gauthier, M. Goniche, M. Kocan, F. Saint-Laurent:** Measurement of LH hot spots using a retarding field analyzer in Tore Supra. *Oral paper O11, presented at the PSI-18 Plasma Surface Interactions in Controlled Fusion Devices, Toledo 2008, Spain*
- [4] **J. Ongena, Yu. Baranov, V. Bobkov, C.D. Challis, L. Colas, S. Conroy, F. Durodié, A. Ekedahl, G. Ericsson, L.-G. Eriksson, Ph. Jacquet, I. Jenkins, T. Johnson, L. Giacomelli, M. Goniche, G. Granucci, C. Hellesen, T. Hellsten, A. Hjalmarsson, K. Holmström, S. Huygen, J. Källne, V. Kiptily, K. Kirov, A. Krasilnikov, M. Laxåback, E. Lerche, J. Mailloux, M.L. Mayoral, I. Monakhov, M. Nave, M. Nightingale, J.M. Noterdaeme, M. Lennholm, V. Petrzilka, K. Rantamäki, A. Salmi, M. Santala, E. Solano, D. Van Eester, M. Vervier, M. Vrancken, A. Walden :** ITER-relevant Heating and Current Drive Studies on JET . *To be presented at the 22nd IAEA Fusion Energy Conference, Geneva 2008, Switzerland, on JET pinboard*
- [5] **A. Ekedahl, K. Rantamäki, M. Goniche, J. Mailloux, V. Petrzilka, G. Granucci, B. Alper, G. Arnoux, Y. Baranov, V. Basiuk, P. Beaumont, G. Calabrò, V. Cocilovo, G. Corrigan, L. Delpech, K. Erents, D. Frigione, N. Hawkes, J. Hobirk, F. Imbeaux, E. Joffrin, K. Kirov, T. Loarer, D. McDonald, F. Nave, I. Nunes, J. Ongena, V. Parail, F. Piccolo, E. Rachlew, C. Silva, A. Sirinelli, M. Stamp, K-D. Zastrow and JET EFDA contributors:** LH power coupling over ITER-like plasma-wall distances at JET. *Submitted to Plasma Physics and Controlled Fusion, on JET pinboard*
- [6] **M. Goniche, A. Ekedahl, J. Mailloux, V. Petržílka, K. Rantamäki, P. Belo, G. Corrigan, L. Delpech, K. Erents, P. Jacquet, K. Kirov, M.-L. Mayoral, J. Ongena, C. Portafaix, M. Stamp, K.-D. Zastrow and JET EFDA contributors:** SOL characterisation and LH coupling measurements on JET in ITER relevant conditions. *Submitted to Nuclear Fusion, on JET pinboard*
- [7] **V. Petrzilka, M. Goniche, F. Clairet, G. Corrigan, P. Belo, J. Ongena and JET EFDA contributors:** On SOL Variations as a Function of LH Power. *Presented at the 35th EPS Conf on Plasma Physics , Hersonissos 2008, Crete, Greece, paper P1.106, on JET pinboard*
- [8] **J. Marki, R. A. Pitts, J. Horacek, G. Turri, D. Tskhakaya and the TCV Team:** ELM induced divertor heat loads on TCV. *Annual meeting of the Swiss physical society, University of Geneva 26-27.3.2008*
- [9] **R. Tye, J. Horacek, R. A. Pitts:** ELM Filament Characteristics on TCV. *Annual meeting of the Swiss physical society, University of Geneva 26-27.3.2008*

- [10] **J. Marki, R. A. Pitts, J. Horacek, G. Turri, D. Tskhakaya and the TCV Team:** ELM induced divertor heat loads on TCV. *Proceedings of the International Conference on Plasma Surface Interactions, Toledo, Spain, 2008*
- [11] **B. Gulejová, R.A. Pitts, D. Coster, X. Bonnin, R. Behn, M. Beurskens, S. Jachmich, J. Horáček, A. Kallenbach:** SOLPS5 simulations of ELMing H-mode. *Oral presentation for the Annual meeting of the Swiss physical society, University of Geneva, 26-27.3.2008*
- [12] **J. Adamek, M. Kocan, R. Panek, J. P. Gunn, E. Martines, J. Stockel, C. Ionita, G. Popa, C. Costin, J. Brotankova, R. Schrittwieser, and G. Van Oost, , :** Simultaneous Measurements of Ion Temperature by Segmented Tunnel and Katsumata Probe. *Contribution to Plasma Physics* 48,(2008,395–399/DOI/10.1002/ctpp.200810000
- [13] **J. Gunn, V. Petrzilka, A. Ekedahl, V. Fuchs, E. Gauthier, M. Goniche, M. Kocan, F. Saint-Laurent:** Measurement of LH hot spots using a retarding field analyzer in Tore Supra. *Submitted to J. Nucl. Materials*
- [14] **Popov Tsv. K., Ivanova P., Benova E., Dias F. M., Stöckel J., Dejarnac R. :** On the Interpretation of the Electron Part of the Langmuir Probe Characteristics in Tokamak Edge Plasma . *35th EPS Conference on Plasma Physics, Hersinissos, Crete, June 9-13, 2008* Poster presentation, P-4.081
- [15] **Shaing K.C., Sabbagh S.A., Chu M.S., Becoulet M., Cahyna P.:** Effects of orbit squeezing on neoclassical toroidal plasma viscosity in tokamaks. *Physics of Plasmas* 15 (2008) 082505
- [17] **Shaing K.C., Cahyna P., Becoulet M., Park J.-K., Sabbagh S.A., Chu M.S.:** Collisional boundary layer analysis for neoclassical toroidal plasma viscosity in tokamaks. *Physics of Plasmas* 15 (2008) 082506
- [18] **Nardon E., Kirk A., Ben Ayed N., Bécoulet M., Huysmans G., Thomas P.R., Koslowski H.R., Liang Y., Cahyna P.:** ELM control by resonant magnetic perturbations on JET and MAST. *submitted to Journal of Nuclear Materials*
- [19] **Cahyna P., Bécoulet M., Pánek R., Fuchs V., Nardon E., Krilin L.:** Resonant Magnetic Perturbations and Edge Ergodization on the Compass Tokamak. *Plasma Physics Reports* 34 (2008) 746
- [20] **Naydenkova D.I., Weinzettl V., Stockel J., Šesták D., Aftanas M.:** Design of New Optical System for Visible Plasma Radiation Measurements at COMPASS Tokamak. *WDS 2008 - Proceedings of Contributed Papers Proceedings of the 17th Annual Conference of Doctoral Students - WDS 2008, Prague, 3th June - 6th June, 2008*
- [21] **Šesták D., Weinzettl V., Bílková P., Böhm P., Aftanas M., Naydenkova D.I., Stöckel J., Ďuran I., Walsh M.:** Design and engineering of optical diagnostics for COMPASS. *25th Symposium on Fusion Technology , Rostock, Germany, 15-19 September 2008* P2.20
- [22] **Brotankova J., Martines E., Adamek J., Stockel J., Popa G., Costin C., Ionita C., Schrittwieser R., Van Oost G.:** Novel Technique for Direct Measurement of the Plasma Diffusion Coefficient in Magnetized Plasma. *Contributions to Plasma Physics* 48, No. 5-7, 418 – 423 (2008) / DOI 10.1002/ctpp.200810067
- [23] **J. Adamek, V. Rohde, H. W. Müller, A. Herrmann, C. Ionita, R. Schrittwieser, F. Mehlmann, J. Stöckel, J. Horacek, J. Brotankova:** Direct measurements of the plasma potential in ELMy H-mode plasma with ball-pen probes on ASDEX Upgrade tokamak.. *Submitted to J. Nucl. Materials*
- [24] **M.Yu.Kantor, A.J.H.Donné, R.J.E.Jaspers, H.J.van der Meiden, P.Bilkova, P.Bohm and TEXTOR Team:** Laser Multipass Intracavity Probing System for Thomson scattering of TEXTOR Plasma. *20th Symposium Plasma Physics and Radiation Technology, Lunteren, Netherlands, March 4-5, 2008*
- [25] **Petra Bílková, Petr Böhm, Milan Aftanas, Vladimír Weinzettl, Jana Brotánková and Jan Stöckel:** High resolution Thomson scattering system for the reinstalled COMPASS tokamak. *17th Topical Conference High Temperature Plasma Diagnostics, Albuquerque, New Mexico, USA, May 11-15, 2008* Contribution No F36, Page 88
- [26] **M.Aftanas, P.Bohm, P. Bílková, V.Weinzettl and J.Stockel:** Estimation of Plasma Light in Thomson Scattering System Design for the COMPASS Tokamak. *17th Annual Student Conference Week of Doctoral Students 2008, Prague, June 2008* submitted

- [27] **H.P. Laqua, D. Andruczyk, S. Marsen, M. Otte, Y. Y. Podoba, J. Preinhaelter, J. Urban :** Experiments with Electron Bernstein Waves at the WEGA Stellarator . *15th Joint Workshop on Electron Cyclotron Emission and Electron Cyclotron Resonance Heating* 10-13 March 2008, Yosemite National Park, California, USA
- [28] **S.J. Diem, G. Taylor, P.C. Efthimion, H.W. Kugel, B.P. LeBlanc, C.K. Phillips, J.B. Caughman, J.B. Wilgen, R.W. Harvey, J. Preinhaelter, J. Urban, S.A. Sabbagh :** Investigation of EBW Thermal Emission and Mode Conversion Physics in H-mode Plasma on NSTX. *15th Joint Workshop on Electron Cyclotron Emission and Electron Cyclotron Resonance Heating* 10-13 March 2008, Yosemite National Park, California, USA
- [29] **G. TAYLOR, S.J. DIEM, R.A. ELLIS, E. FREDD, N. GREENOUGH, J.C. HOSEA, T.S. Bigelow J.B. Caughman, D.A. Rasmussen, P. Ryan, J.B. Wilgen, R.W. Harvey, A.P. Smirnov, J. Preinhaelter, J. Urban, A.K. Ram:** Modeling Results for Proposed NSTX 28 GHz ECH/EBWH System. *15th Joint Workshop on Electron Cyclotron Emission and Electron Cyclotron Resonance Heating* 10-13 March 2008, Yosemite National Park, California, USA
- [30] **Brotankova J., Stockel J., Hron M., Duran I., Horacek J., Van Oost G.:** Detailed measurements of poloidal velocity of density and floating potential fluctuations in the edge plasma of the CASTOR tokamak. *Proceedings of Contributed Papers Proceedings of the 17th Annual Conference of Doctoral Students - WDS 2008, Prague, 3th June - 6th June, 2008* to be published
- [31] **J. Preinhaelter , V. Fuchs, J. Urban, J. Zajac:** PLANS for ELECTRON BERNSTEIN WAVES EMISSION DETECTION in COMPASS. *35th EPS Conference on Plasma Phys. Hersonissos, 9 - 13 June 2008 ECA Vol.32, P-2.096 (2008)*
- [32] **S.J. Diem, G. Taylor, J.B. Caughman, P. Efthimion, H. Kugel, B.P. LeBlanc, J. Preinhaelter, S.A. Sabbagh, J. Urban, J. Wilgen:** Electron Bernstein Wave Emission and Mode Conversion Physics on NSTX. *17th High Temperature Plasma Diagnostic, Albuquerque, New Mexico May 11-15, 2008 (to be published in Rev. Sci. Insts.*
- [33] **P.Bohm, M.Yu.Kantor, P. Bílková:** Multi-pass Thomson Scattering Diagnostic System on TEXTOR Tokamak. *17th Annual Student Conference Week of Doctoral Students 2008, Prague, June 2008*
- [34] **J. Preinhaelter, H.P. Laqua, J. Urban, L. Vahala, G. Vahala:** Simulations of EBW Power Deposition and Current Drive in WEGA . *17th High Temperature Plasma Diagnostic, Albuquerque, New Mexico May 11-15, 2008*
- [35] **J. Havlicek, J. Horacek:** Modelling of Compass tokamak poloidal field coils magnetic fields. *35th EPS Conference on Plasma Phys. Hersonissos, 9 - 13 June 2008 ECA Vol.32, P-4.080 (2008)*
- [36] **F. Janky, J. Horacek:** Fast feedback control system for plasma shape and position for tokamak Compass. *Proceedings of Contributed Papers Proceedings of the 17th Annual Conference of Doctoral Students - WDS 2008, Prague, 3th June - 6th June, 2008* to be published
- [37] **I. Nanobashvili, P. Devynck, J. Horacek, S. Nanobashvili, J. Stöckel, G. Van Oost:** External Modification of Intermittent Burst Temporal Characteristics at the Edge of the CASTOR Tokamak. *Oral at EFTSOMP2008 - 11th Workshop on Electric Fields, Turbulence and Self-Organisation in Magnetized Plasmas, a satellite meeting of the 35th EPS Plasma Physics Conference, Crete, 2008.* Submitted to Plasma Physics Reports
- [38] **Krlín L., Papřok R., Svoboda V.:** Modelling of Lévy walk kinetics of charged particles in edge electrostatic turbulence in tokamaks . *European Physical Journal D* 48 (2008) 95
- [39] **Seidl J., Krlín L., Pánek R., Pavlo P., Stockel J., Svoboda V.:** Simulation of Anomalous Diffusion of Particles in Experimentally Measured Turbulent Potential. *European Physical Journal* submitted
- [40] **Seidl J., Krlín L., Pavlo P., Pánek R., Stockel J.:** Nonlinear Interaction of Localized LHW with Plasma Electrons . *Symposium on Plasma Physics and Technology, Prague 2008* poster

- [41] **R. Dejarnac, M. Komm, J. P. Gunn, R. Panek:** Power flux in the ITER divertor tile gaps during ELMs. *Proceedings of the 18th International Conference on Plasma Surface Interactions (to be published in Journal of Nuclear Materials) Toledo, Spain May 26 - 30, 2008.*
- [42] **R. Dejarnac, M. Komm, J. Stöckel, R. Panek:** Measurement of plasma flows into tile gaps. *Accepted for publication in Journal of Nuclear Materials (2008)*
- [43] **J. Horacek, J. Zajac, J. Seidl, B. Gulejova:** Fast temperature fluctuation measurements in SOL of tokamak TCV. *Poster presentation at 13th EU-US TTF workshop 2008 and 1st EFDA Transport Topical Group Meeting*
- [44] **J. Seidl, J. Horacek, L. Krlín:** Observation of spontaneous density gradient steepening in ESEL interchange turbulence in large SOL. *Poster presentation at 13th EU-US TTF workshop 2008 and 1st EFDA Transport Topical Group Meeting*
- [45] **Bécoulet M., Huysmans G., Nardon E., Schaffer M., Garofalo A., Cole A., Cahyna P. :** Report on the Task: TW7-TPO-ELMCONT “Evaluation of ELM control coil configuration in ITER, effects on plasma and power loads on PFCs” . *Association EURATOM-CEA internal report PHY/NTT-2008.007*
- [46] **Bonheure G., Mlynar J., Bertalot L., Popovichev S., Murari A. and JET-EFDA contributors:** A novel method for tritium transport studies and its validation at JET. *35th EPS Plasma Physics Conference, June 2008, Crete, Greece poster presentation P-4.084*
- [47] **Mlynar J., Bonheure G., Craciunescu T., Popovichev S., Weinzettl V. and JET-EFDA Contributors:** Upgrade of the Minimum Fisher Regularisation to Finite Width of Viewing Chords. *23rd Symposium on Plasma Physics and Technology, June 2008, Prague, Czech Republic poster presentation*
- [49] **Mlynar J.:** Unfolding of the NE213 data at JET via Minimum Fisher Regularisation. *TFD Technical Meeting on Unfolding and Tomographic Techniques for Fusion Applications, July 2008, EFDA JET, Culham oral contribution*
- [50] **A. Fasoli and the TCV Team with V.Piffl and J.Horacek:** Overview of TCV results. *Nuclear Fusion Vol.48,(2008),034001(10pp)*
- [51] **I. Ďuran, J. Sentkerestiová, J. Havlicek, O. Hronová, J. Stöckel:** Magnetic measurements using array of integrated Hall sensors on the CASTOR tokamak. *Review of Scientific Instruments 79 (2008)*
- [52] **P. Bystriansky, I. Ďuran, J. Sentkerestiová:** Magnetic diagnostics in the project “International Thermonuclear Experimental Reactor”. *Acta Technologica Agriculturae 10 (2007),p.11-14*
- [53] **M. Kočan, J. P. Gunn, J.-Y. Pascal, G. Bonhomme, P. Devynck, I. Ďuran, E. Gauthier, Y. Marandet, B. Pegourie, J.-C. Vallet:** Measurements of scrape-off layer ion-to-electron temperature ratio in ohmic plasma of Tore Supra tokamak. *submitted to Journal of Nuclear Materials within proceedings of 2008 PSI conference*
- [54] **I. Ďuran, J. Sentkerestiová, K. Kovařík, L. Viererbl:** Perspectives of metal Hall sensors for steady state magnetic field measurements in fusion devices. *poster presentation on 25th SOFT conference, Rostock, Germany*
- [55] **I. Ďuran:** Development of Hall sensors for magnetic measurements in nuclear fusion devices. *oral presentation at seminar of Poznan University of Technology. January 2008*
- [56] **Valcárcel D.F., Neto A., Sousa J., Carvalho B.B., Fernandes H., Fortunato J.C., Gouveia A.S., Batista A.J.N., Fernandes A.G., Correia M., Pereira T., Carvalho I.S., Duarte A.S., Varandas C.A.F., Hron M., Janky F., Pisačka J.:** An ATCA Embedded Data Acquisition and Control System for the Compass Tokamak. *Fusion Engineering and Design* submitted for publication
- [57] **Pysanenko A., Zabka J., Zappa F., Märk T.D., Herman Z.:** Scattering of very slow (3-10 eV) hydrocarbon ions CD<sub>3</sub><sup>+</sup>, CD<sub>4</sub><sup>+</sup>, and CD<sub>5</sub><sup>+</sup> from room-temperature carbon (HOPG) surfaces. *Int. J. Mass Spectrom. 273, 35-47 (2008)*
- [58] **Pysanenko A., Zabka J., Märk T.D., Herman Z.:** Collisions of slow hydrocarbon ions CD<sub>4</sub><sup>+</sup>, CD<sub>5</sub><sup>+</sup>, C<sub>2</sub>D<sub>4</sub><sup>+</sup>, and C<sub>2</sub>H<sub>5</sub><sup>+</sup> with room temperature and heated tungsten surfaces. *Int. J. Mass Spectrom. (accepted)*

- [59] **Pysanenko A., Zabka J., Herman Z.** : Scattering of low energy (5-12 eV) C<sub>2</sub>D<sub>4</sub><sup>+</sup> ions from room temperature carbon (HOPG) surfaces. *Collection Czech. Chem. Commun.* (accepted)
- [60] **Feketeova L., Grill V., Zappa F., Endstrasser N., Rsul B., Herman Z., Scheier P., Märk T.D.**: Charge exchange, surface-induced dissociation and reactions of doubly-charged molecular ions SF<sub>4</sub><sup>2+</sup> upon impact on a stainless steel surface: A comparison with surface-induced dissociation of singly-charged SF<sub>4</sub><sup>+</sup> molecular ions.. *Int. J. Mass Spectrom.* (accepted)
- [61] **Pysanenko A., Zabka J., Feketeova L., Märk T.D., Herman Z.**: Collisions of slow ions C<sub>3</sub>H<sub>n</sub><sup>+</sup> and C<sub>3</sub>D<sub>n</sub><sup>+</sup> (n=2-8) with room temperature carbon surfaces: Mass spectra of product ions and the ion survival probability. *Eur. J. Mass Spectrom.* (accepted)
- [62] **Kasperczuk A., Pisarczyk T., Gus'kov S.Yu., Ullschmied J., Krousky E., Masek K., Pfeifer M., Rohlena K., Skala J., Kalal M., Tikhonchuk V., Pisarczyk P.**: Laser energy transformation to shock waves in multi-layer flyers . *Radiation Effects and Defects in Solids* 163 (2008), No 4-6, 519-533
- [63] **Kasperczuk A., Pisarczyk T., Kalal M., Martinkova M., Ullschmied J., Krousky E., Masek K., Pfeifer M., Rohlena K., Skala J., Pisarczyk P.** : PALS laser energy transfer into solid targets and its dependence on the lens focal point position with respect to the target surface . *Laser and Particle Beams* 26(2) JUN 2008: 189-196
- [64] **Badziak, J., Kasperczuk, A., Parys, P., Pisarczyk, T., Rosinski, M., Ryc, L., Wolowski, J., Suchanska, R., Krasa, J., Krousky, E., Laska, L., Masek, K., Pfeifer M., Rohlena K., Skala J., Ullschmied J., Dhareshwar L.J., Foldes I.B., Suta T., Borrielli A., Mezzasalma A, Torrisi L., Pisarczyk P.** : The effect of high-Z dopant on laser-driven acceleration of a thin plastic target . *Applied Physics Letters* 92 (21): Art. No. 211502 MAY 26 2008
- [65] **Tikhonchuk V.T., Nicolai Ph., Ribeyre X., Stenz C., Schurtz G., Kasperczuk A., Pisarczyk T., Juha L., Krousky E., Masek K., Pfeifer M., Rohlena K., Skala J., Ullschmied J., Kalal M., Klir D., Kravarik J., Kubes P., Pisarczyk P.,** : Laboratory modeling of supersonic radiative jets propagation in plasmas and their scaling to astrophysical conditions . *25th EPS Conf. on Plasma Phys., Hersonissos, Greece, 9-13 June 2008*
- [66] **Kasperczuk A., Pisarczyk T., Kalal M., Ullschmied J., Krousky E., Masek K., Pfeifer M., Rohlena K., Skala J., Velarde P., González M., González C., Oliva E., Pisarczyk P.** : Direct and indirect methods of the plasma jet generation . *25th EPS Conf. on Plasma Phys., Hersonissos, Greece, 9-13 June 2008*
- [67] **Kasperczuk A., Pisarczyk T., Kalal M., Ullschmied J., Krousky E., Masek K., Pfeifer M., Rohlena K., Skala J., Pisarczyk P.** : Characteristics of the plasma jet generated from a joint of materials with different atomic number . *25th EPS Conf. on Plasma Phys., Hersonissos, Greece, 9-13 June 2008*
- [68] **Pisarczyk T., Kasperczuk A., Borodziuk S., Kalal M., Guskov S.Yu., Ullschmied J., Krousky E., Masek K., Pfeifer M., Rohlena K., Skala J., Pisarczyk P.**: Investigations of acceleration and collision of planar flyer targets with massive target on the PALS experiment . *30th Eu. Conf. on Laser Interaction with Matter (ECLIM), Darmstadt, Germany, Aug. 31 – Sep. 5, 2008*
- [69] **Kasperczuk A., Pisarczyk T., Nicolai Ph., Stenz Ch., Tikhonchuk V., Kalal M., Ullschmied J., Krousky E., Masek K., Pfeifer M., Rohlena K., Skala J., Klir D., Kravarik J., Kubes P., Pisarczyk P.**: Investigations of plasma jet interaction with ambient gases by the multi-frame interferometric and x-ray pinhole camera systems . *30th Eu. Conf. on Laser Interaction with Matter (ECLIM), Darmstadt, Germany, Aug. 31 – Sep. 5, 2008*
- [70] **Radek Beňo**: Modelování systému řízení polohy plazmatu v tokamaku Compass. Bakalářská práce, 2008, ČVUT FEL
- [71] **J. Zajac, R. Pánek, F. Žáček, J. Vlček, J. Kladrubský, A. Křivská, R. Hauptmann, M. Daněk, J. Šimek, J. Prosek**: Power supply system for the COMPASS tokamak re-installed in IPP Prague. *submitted to Fusion Engineering and Design (proceedings of 25th SOFT conference, P1.52)*
- [72] **I. Zammuto, A. Krivska, V. Bobkov, F. Braun, R. Bilato, J.-M. Noterdaeme, ASDEX Upgrade Team**: ICRF antennas optimized for operation with a metallic wall in ASDEX Upgrade. *submitted to Fusion Engineering and Design (proc. 25th SOFT conference, P2.12)*

- [73] **Gunn J.P., Fuchs V.:** Quasineutral kinetic simulation of the scrape-off layer. *35th EPS Plasma Physics Conference, June 2008, Crete, Greece*
- [74] **Stranak V., Quaas M., Wulff H., Hubicka Z., Wrehde S., Tichy M., Hippler R.:** Formation of TiOx films produced by high-power pulsed magnetron sputtering . *J. Phys. D: Appl. Phys* 41(2008)055202
- [75] **Kluson J., Kudrna P., Picková I., Tichý M.:** Langmuir Probe Diagnostic of Pulsed Cylindrical Magnetron. *Proc. 23rd Symposium on Plasma Physics and technology, June 16-19, 2008, Prague* ISBN 978-80-01-04030-0, page 155.
- [76] **Kudrna P., Kluson J., Pickova I., Tichy M.:** A Diagnostic Study Of Dc Discharge In Cylindrical Magnetron In Pulsed Regime. *Journal of Optoelectronic and Advanced Materials* (submitted)
- [77] **Marek A., Jílek M., Picková I., Kudrna P., Tichý M., Schrittwieser R., Ionita C.:** Emissive Probe Diagnostics in Low Temperature Plasma - Effect of the Space Charge and Variations of Electron Saturation Current. *Contrib. Plasma Phys. No 5-7* 48(2008)491-496
- [78] **Pekárek Z., Hrach R.:** Influence of Non-Axial Magnetic Field in a 3D3V Particle-In-Cell Plasma Model. *Vacuum* 82 (2008), 244-247
- [79] **Havlíčková E., Zagórski R., Pánek R.:** Numerical Investigations of Plasma Parameters in COMPASS Tokamak. *Plasma Phys. Rep.* (to be published)
- [80] **Havlíčková E., Bartoš P., Hrach R., Hrachová V. :** Study of Sheath Structure in Electronegative Gases at Various Pressures. *Proceedings of 35th EPS Conference on Plasma Physics, Hersonissos, Crete, Greece, 2008*
- [81] **Stránský M., Bilyková O., Fuchs V., Havlíčková E., Pánek R., Stöckel J., Urban J., Voitsekhovitch I., Valovič M.:** Transport simulations for the COMPASS tokamak with NBI and LH heating and current drive systems. *23rd Symposium on Plasma Physics and Technology, June 2008, Prague, Czech Republic* poster presentation
- [82] **K. K. Kirov, M L. Mayoral, J. Mailloux, Yu. Baranov, L. Colas, A. Ekedahl, K. Erents, M. Goniche, P. Jacquet, A. Korotkov, P. Morgan, V. Petržilka, J. Ongena, K. Rantamäki:** LH Wave Coupling And ICRF Induced Density Modifications At JET. *Submitted to Nucl. Fusion, on JET pinboard*
- [83] **Oliva, V. Materna, A. Vaclavík, J.:** Mechanical Testing of a PFW Panel Attachment system for ITER. Final report. [http://people.fjfi.cvut.cz/oliva/Final\\_report\\_EFDA-04-1137d.pdf](http://people.fjfi.cvut.cz/oliva/Final_report_EFDA-04-1137d.pdf) . *Research Report V-KMAT-706/07/ CTU in Prague – FNSPE, 2007, 153 p.*
- [84] **Oliva, V. Václavík, J. Materna, A. Lorenzetto, P. Furmanek, A. :** Mechanical Testing of a FW Panel attachment system for ITER.. *25th Symposium on Fusion Technology, 2008, Rostock, Germany* submitted
- [85] **Zacek F., Zajac J., Kryška L., Havlicek J.:** Test of Potential Interturn Faults of COMPASS-D Toroidal Field Coils. *a)Acta Technica CSAV, b) 23rd Symposium on Plasma Physics and Technology, June 16-19, 2008, Prague, Czech Republic, poster presentation, a) 53 (2008), 287-294, b) 2008, page 59*
- [86] **H.P. Laqua, D. Andruczyk , S. Marsen , M. Otte , Y. Y. Podoba , J. Preinhealter , J. Urban :** Fundamental Investigation of Electron Bernstein Wave Heating and Current Drive at the WEGA Stellarator . *22nd IAEA Fusion Energy Conference, 13-18 October 2008 Geneva, Switzerland* Book of Abstract, EX/P6-18, p 75 [http://www-pub.iaea.org/MTCDD/Meetings/PDFplus/2008/cn165/cn165\\_BookOfAbstracts.pdf](http://www-pub.iaea.org/MTCDD/Meetings/PDFplus/2008/cn165/cn165_BookOfAbstracts.pdf)
- [87] **S.J. Diem, G. Taylor, J.B. Caughman, P.C. Efthimion, H. Kugel, B.P. LeBlanc, C.K. Phillips, J. Preinhaelter, S.A. Sabbagh, J. Urban, J.B. Wilgen :** Investigation of Electron Bernstein Wave (EBW) Coupling and its Critical Dependence on EBW Collisional Loss in High b, H-Mode Spherical Tokamak Plasmas. *22nd IAEA Fusion Energy Conference, 13-18 October 2008 Geneva, Switzerland* Book of Abstract, EX/P6-17, p 75 [http://www-pub.iaea.org/MTCDD/Meetings/PDFplus/2008/cn165/cn165\\_BookOfAbstracts.pdf](http://www-pub.iaea.org/MTCDD/Meetings/PDFplus/2008/cn165/cn165_BookOfAbstracts.pdf)
- [88] **H.P. Laqua, D. Andruczyk, S. Marsen, M. Otte, J. Preinhealter, J. Urban, G.B. Warr, D. Zhang:** Fully Electron Bernstein Wave Sustained Overdense Plasma Operation with 28 GHz ECRH at the WEGA Stellarator. *22nd IAEA Fusion Energy Conference, 13-18 October 2008 Geneva, Switzerland* Accepted Post-Deadline papers, PD/P1-7

- [89] **J. Urban, J. Preinhaelter, S.J. Diem, H.P. Laqua, P. Pavlo, V. Shevchenko, G. Taylor, G. Vahala, L. Vahala and M. Valovič** ICCP200: EBW Simulations in an Experimental Context. *ICPP2008 (International Congress on Plasma Physics 2008), 8-12 September 2008, Fukuoka, Japan* Book of Abstract, to be published in *Journal of Plasma and Fusion Research Series*
- [90] **S.J. Diem, G. Taylor, P.C. Efthimion, H. Kugel, B.P. LeBlanc, C.K. Phillips, J.B. Caughman, J.B. Wilgen, J. Preinhaelter, J. Urban, S.A. Sabbagh**: Investigation of EBW Coupling and Propagation in H-Mode Plasmas in NSTX. *50th Annual Meeting of the Division of Plasma Physics, Dallas, Texas, November 17–21 2008* DDP08 Web Bulletin of the American Physical Society, Volume 53, Number 14
- [91] **Josef Preinhaelter, H. Laqua, Jakub Urban, L. Vahala, G. Vahala**: EBW Power Deposition and Fisch-Boozer Current Drive in the WEGA stellarator. *50th Annual Meeting of the Division of Plasma Physics, Dallas, Texas, November 17–21 2008*, DDP08 Web Bulletin of the American Physical Society, Volume 53, Number 14
- [92] **R. A. Pitts, A. Bencze, O. E. Garcia, B. Gulejova, J. Horacek, J. Marki, D. Tskhakaya, R. Tye, G. Veres**: SOL Transport in TCV. *Abstract and Poster, IAEA Fusion Energy Conference, Geneva 2008*
- [93] **A. Fasoli for the TCV Team (incl. J. Horacek, V. Piff)**: Overview of Physics Research on the TCV Tokamak. *Paper and overview talk OV/1-1 at IAEA FEC'08 Geneva*
- [94] **Havlicek J., Hronová O.**: Characterization of Magnetic Fields in the COMPASS Tokamak. *Poster on 17th Annual Student Conference: Week of Doctoral Students 2008 and paper in WDS'08 Proceedings of Contributed Papers: Part II - Physics of Plasmas and Ionized Media 2008*, 110-114.
- [95] **J. Brotankova, J. Adamek, E. Martinez, J. Stockel, M. Spolaore, R. Cavazzana, G. Serianni, N. Vianello, M. Zuin**: Measurements of plasma potential and electron temperature by Ball-pen probes in RFX-mod. *Problems of Atomic Science and Technology, 2-nd volume of the Journal of Conference proceedings* to be published in January (2009)
- [96] **J. Brotankova, J. Stockel, I. Duran, M. Hron, G. Van Oost**: Measurement of Sheared Flows at the Plasma Edge of the CASTOR Tokamak. *Proceedings of the 18th IAEA Technical Meeting on Research Using Small Fusion Devices* to be published
- [97] **J. P. Gunn, V. Petržílka, A. Ekedahl, V. Fuchs, E. Gauthier, M. Goniche, M. Kočan, J.-Y. Pascal, F. Saint-Laurent**: Measurement of lower hybrid hot spots using a retarding field analyzer in Tore Supra. *To appear in: Journal of Nuclear Materials*
- [98] **A. Kasperczuk, T. Pisarczyk, J. Badziak, R. Miklaszewski, P. Parys, J. Wolowski, E. Krouský, K. Mašek, M. Pfeifer, K. Rohlena, J. Skála, J. Ullschmied, P. Pisarczyk**: Influence of the focal point position of a focusing lens on a character of an ablative plasma expansion. *J. Phys.: Conf. Ser.* 112 (2008) 022047(1) - 022047(7).
- [99] **P. Velarde, M. Gonzalez, C. G. Fernandez, E. Oliva, A. Kasperczuk, T. Pisarczyk, J. Ullschmied, J.P. Colombier, A. Ciardi, Ch. Stehle, M. Busquet, B. Rus, D. G. Senz, A. Relano**: Simulations of jet formation and blast wave collision in laboratory plasmas. *J. Phys.: Conf. Ser.* 112 (2008) 042010(1) - 042010(4)
- [100] **Ph. Nicolaï, C. Stenz, A. Kasperczuk, T. Pisarczyk, D. Klir, L. Juha, E. Krousky, K. Masek, M. Pfeifer, K. Rohlena, J. Skala, V. Tikhonchuk, X. Ribeyre, S. Galera, G. Schurtz, J. Ullschmied, M. Kalal, J. Kravarik, P. Kubes, P. Pisarczyk, T. Schlegel**: Studies of supersonic, radiative plasma jet interaction with gases at the Prague Asterix Laser System facility. *Phys. Plasmas* 15, 082701 (2008)
- [101] **J. Wolowski, J. Badziak, A. Borrielli, L. Dareshwar, I. B. Foldes, A. Kasperczuk, E. Krouský, L. Lásková, K. Mašek, A. Mezzasalma, P. Parys, M. Pfeifer, T. Pisarczyk, M. Rosinski, L. Ryc, R. Suchanska, T. Suta, L. Torrissi, J. Ullschmied, P. Pisarczyk**: Application of laser-induced double ablation of plasma for enhanced macroparticle acceleration. *J. Phys.: Conf. Ser.* 112 (2008) 022072(1) - 022072(4)
- [102] **S. Borodziuk, A. Kasperczuk, T. Pisarczyk, J. Ullschmied, E. Krousky, K. Masek, M. Pfeifer, K. Rohlena, J. Skala, P. Pisarczyk**: Reversed scheme of thin foil acceleration. *Applied Physics Letters* 93, 101502 (2008)

- [103] **V. Fuchs, O. Bilyková, R. Pánek, M Stránský, J. Stöckel, J. Urban, F. Žáček, J. Decker, Y. Peysson, I. Voitsekhovitch, M. Valovič** : Heating and current drive modeling for the IPP Prague COMPASS tokamak . *Proceedings of the 35th EPS Conf. on Plasma Physics, Hersonissos, Crete, 2008*.
- [104] **A. Pysanenko, J. Žabka, L. Feketeová, T.D. Märk , Z. Herman**: Collisions of slow ions C3Hn+ and C3Dn+ (n = 2–8) with room temperature carbon surfaces: mass spectra of product ions and the ion survival probability. *Eur. J. Mass Spectrom.* 14 (2008) 335-343
- [105] **L. Feketeová, J. Žabka, F. Zappa, V. Grill, P. Scheier, T. D. Märk, Z. Herman**: Surface-Induced Dissociation and Chemical Reactions of C2D4+ on Stainless Steel, Carbon (HOPG), and Two Different Diamond Surfaces. *J. Am. Soc. Mass Spectrom.* (accepted)
- [106] **Cahyna P., Pánek R., Fuchs V., Krlín L., Bécoulet M., Huysmans G., Nardon E.**: Optimization of magnetic perturbation spectra for the COMPASS tokamak. *22nd IAEA Fusion Energy Conference, Geneva 2008, Switzerland* paper TH/P9-7, preprint at [http://www-pub.iaea.org/MTC/Meetings/FEC2008/th\\_p9-7.pdf](http://www-pub.iaea.org/MTC/Meetings/FEC2008/th_p9-7.pdf)
- [107] **Bécoulet M., Huysmans G., Garbet X., Nardon E., Schaffer M., Garofalo A., Shaing K., Cole A., Park J.-K., Cahyna P.**: Physics of penetration of resonant magnetic perturbations used for Type I edge localized modes suppression in tokamaks. *22nd IAEA Fusion Energy Conference, Geneva 2008, Switzerland* paper TH/2-1Ra, preprint at [http://www-pub.iaea.org/MTC/Meetings/FEC2008/th\\_2-1ra.pdf](http://www-pub.iaea.org/MTC/Meetings/FEC2008/th_2-1ra.pdf)
- [108] **J. Marki, R.A. Pitts, J. Horacek, D. Tskhakaya and The TCV Team**: ELM induced divertor heat loads on TCV . *Journal of Nuclear Materials* 390-391 (2009) 801-805 <http://dx.doi.org/10.1016/j.jnucmat.2009.01.212>
- [109] **J. Horacek, A.H. Nielsen, R. A. Pitts, J. Zajac, J. Seidl, O.E. Garcia, B. Gulejova** : Fast Temperature Fluctuation Measurements in SOL of Tokamak TCV. *11th Workshop on Electric Fields, Turbulence and Self-Organisation in Magnetized Plasmas, Crete, 2008* Abstract O2-4.4. [http://www.rmki.kfki.hu/~eftsomp2008/EFTSOMP2008\\_AbstractBooklet.pdf](http://www.rmki.kfki.hu/~eftsomp2008/EFTSOMP2008_AbstractBooklet.pdf)
- [110] **R. Dejarnac, M. Komm, J. P. Gunn, R. Panek**: Power flux in the ITER divertor tile gaps during ELMs. *Journal of Nuclear Materials* (2009)  
DOI: <http://dx.doi.org/10.1016/j.jnucmat.2009.01.216>
- [111] **J. Horacek**: What we (don't) know about blobs from modeling and experiment. . *Oral at the European Fusion Physics Workshop, Cork, Dublin, 1-3/12/2008*.
- [112] **Marmy P., Kruml T.**: Low cycle fatigue of Eurofer 97. *Journal of Nuclear Materials* 377 (2008) 52
- [113] **R.A. Forrest, J. Kopecky, M. Pillon, A. Klix, S.P.Simakov, J-Ch. Sublet, P. Bém, M. Honusek and E. Šimečková**: Validation of EASY-2007 using integral measurements. *UKAEA FUS 547* (2008) 563
- [114] **S.P. Simakov, P. Bém, V. Burjan, U. Fischer, R.A. Forrest , M. Götz, M. Honusek, H. Klein, V. Kroha, J. Novák, A. Sauer, E. Šimečková, R. Tiede**: Activation of the IFMIF prototype accelerator and beam dump by deuterons and protons. *Fusion Engineering and Design* 83 (2008) 1543
- [115] **B. Rasul, F. Zappa, N. Endstrasser, W. Schustereder, J. D. Skalny, Z. Herman, P. Scheier, T.D. Märk** Ion surface collisions with surfaces relevant for fusion devices *18th International Conference on Plasma-Surface Interactions, Toledo (E), 2008* (Abstract)
- [116] **A. Kendl, K. Becker, S. Denifl, O. Echt, N. Endstrasser, B. Farizon, M. Farizon, S. Feil, L. Feketeova, V. Grill, Z. Herman, T.D. Mark, S. Matejčík, S. Matt-Leubner, M. Probst, B. Rasul, P. Scheier, W. Schustereder, J.D. Skalny, P. Sulzer, M. Winkler, F. Zappa**: Hydrocarbon characteristics in fusion edge plasmas from electron-molecule and ion-surface collision experiments. *Proceedings of the 22nd IAEA Fusion Research Conference, Geneva, 2008* EX/P4-1

## 1. Provision of support to the advancement of the ITER Physics Basis

### Carbon impurity transport studies in TCV tokamak discharges

V.Piffel

In collaboration with:

*H. Weisen, A. Bortolon, B.P. Duval, A. Karpushov, M. Bernard, D. Wagner, A. Zabolotsky, Centre de Recherches en Physique des Plasmas, Association Euratom-Confédération Suisse, CH-1015 Lausanne, Switzerland*

*Experimental study together with theoretical interpretation of the particle and impurity radial profiles seems to be fundamental for the prediction of the reactor performance developed in the frame of the fusion program. Analyse of steady-state radial profiles with central or off-axis EC Heating in L-mode indicates that the flattening density profile is accompanied by peaked or hollow peaked profile of fully-ionized carbon. Neoclassical and anomalous transport is believed to lead to peaked profiles due to the presence of pinch mechanism characterized by an inward/outward convection velocity combining with diffusion. Anomalous convective process like turbulent equipartition (TEP) and ion temperature gradient (ITG) mode may contribute to the shaping of the particle and impurity density profiles in plasma L-mode.*

#### 1. Ohmic discharges

As already noticed in low current Ohmic discharges, the  $C^{6+}$  profiles are more peaked than the electron density profiles and for the high current discharges ( $q_{95} < 4$ ) the normalized gradients of  $C^{6+}$  and of  $n_e$  become similar. The region of  $\langle j \rangle / j_0 q_0$ , in which gradients of  $C^{6+}$  are higher than electron density gradients, is characterized by the absence of sawtooth activity. The scaling of normalized  $C^{6+}$  gradients does not depend on the absolute value of the electron density or temperature.

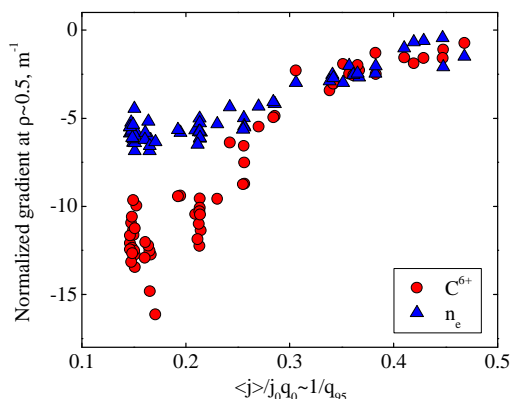
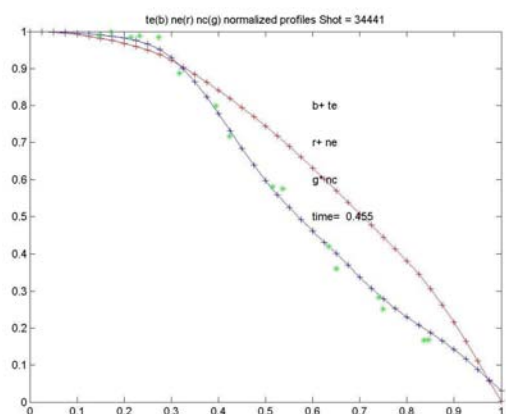


**Fig. 1** Normalized gradients  $\nabla n/n$  of  $C^{6+}$  measured by CXRS and of electron density profiles from TS at  $\rho_{pol} = 0.5$  in OH discharges. The parameter  $\langle j \rangle / j_0 q_0$  is known to provide a scaling for electron density gradient in TCV Ohmic plasmas.

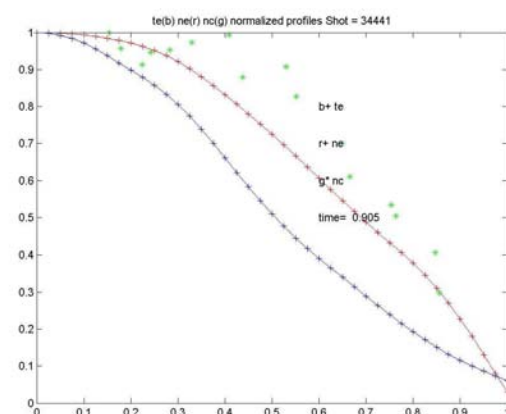
#### 2. L-mode ECRH discharges

Measurements of  $C^{6+}$ - fully-ionized carbon profiles were performed in low current ( $q_{95} > 5$ ) L-mode ECRH discharges. The addition of ECH (in this case 0.2MW) at high  $q_{95}$  leads to a reduction of both the electron and carbon density gradients. The behavior of electron density profiles has been documented previously Zabolotsky and TCV team.



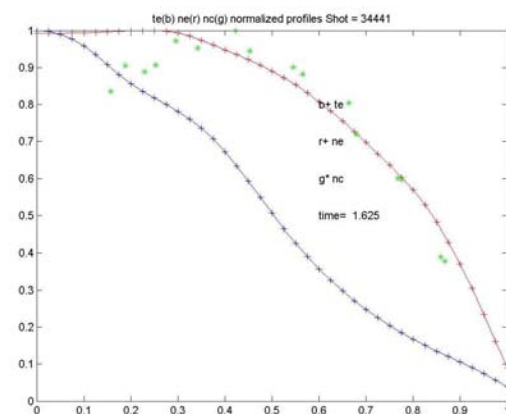
Now we concern our attention on carbon density profile behaviour in different discharge period and during the off-axis EC Heating. In the OH plasma phase (without adding EC Heating, shot 34441,  $I_p=140$  kA), the normalized carbon density profile  $nc$  (green +), in **Fig.1a**, is similar as normalized electron temperature profile  $te$  (blue +).

<= **Fig. 1a** Normalized  $ne, nc$  and  $te$  profiles in ohmic phase,  $t = 0.455$  sec



During the off-axis EC Heating (step like from 250kW to 400kW) in L-mode ( $I_p=140$ kA, shot=34441), the carbon profile seems much broader and flat than  $ne$  and  $te$  profiles. We notice, the measured profiles reflect the steady-state plasma conditions. For an interpretation of the processes, which influenced the particle and impurity transport, it seems the higher time resolution of used CXRS diagnostic system is needed.

<= **Fig. 1b** Normalized profiles in off-axis EC Heating (250kW) phase,  $t = 0.905$  sec



<= **Fig. 1c** Normalized hollow  $nc$  profile (green +) in off-axis EC Heating (450kW) phase,  $t = 1.625$  sec

During the OH plasma phase a core impurity enrichment is observed, and more, the normalized  $nc$  profile is almost the same as normalized  $te$  profile. Which of the mechanism plays a basic role in carbon density profile forming is unknown yet.

As well as the electron density profiles in TCV in the Ohmic phase are peaked too. The Ware

pinch and anomalous convective process like turbulent equipartition (TEP), turbulent thermo-diffusion (TTD) and ion temperature gradient (ITG) mode may contribute to the shaping of the electron density profiles.

The addition of EC Heating leads to a flattening and broadening of the electron density profile and more the electron density profile width is modified by an additional dependence on power deposition localisation.

In some discharges is observed, that the modest addition of EC Heating causes not only a broadening of electron density profile but consequently a peaked-hollow carbon density profile. Evidently, such examples provide the elements for validating comprehensive turbulent light-impurity transport models.

**Determination of reflection properties of hydrocarbon radicals  
for ITER-like divertor conditions**  
**Transport and Deposition of First Wall Impurities SEWG Chemical Erosion and  
Material Transport (WP08-PWI-06)**

**Reactive Interaction of Molecular Ions with Surfaces (PWI-08-TA-06)**

*Z. Herman, J. Žabka, A. Pysanenko*

*J. Heyrovsky Institute of Physical Chemistry, Academy of Sciences of the CR*

In collaboration with:

*T. D. Märk and his research group (Institute for Ion and Applied Physics, University of Innsbruck, Innsbruck), Association EURATOM-ÖAW, Austria*

*The aim of this research are dedicated ion-surface scattering experiments with low-energy beams of ions on carbon surfaces to determine energy transfer, surface processes and ion survival probability as a function of impact energy using special ion-surface beam machines.*

**1. Collisions of slow ions  $C_3H_n^+$  and  $C_3D_n^+$  ( $n=2-8$ ) with room temperature carbon surfaces: mass spectra of product ions and the ion survival probability. [1]**

Mass spectra of product ions from collisions of  $C_3H_n^+$  ( $n=2-8$ ) ions and some of their per-deuterated analogues with room temperature carbon (HOPG) surfaces (hydrocarbon-covered at room temperature) were measured at incident energies of 16, 31, and 46 eV and main fragmentation paths of the incident projectile ions, energized by the surface collision, were determined. The extent of fragmentation increased with increasing incident energy. Mass spectra of even-electron ions  $C_3H_7^+$  and  $C_3H_5^+$  showed only fragmentations of the incident projectile ions, mass spectra of radical cations  $C_3H_8^{*+}$  and  $C_3H_6^{*+}$  showed both simple fragmentations of the incident projectile and formation of products (protonated projectile and its fragmentation products) of a surface reaction of H-atom transfer between the projectile ion and hydrocarbons on the surface. No indication of carbon-chain build-up reactions (formation of C4 hydrocarbons) was detected.

The survival probability of the incident ions was found to be usually about 1 - 2% for radical cation projectile ions ( $C_3H_8^{*+}$ ,  $C_3H_6^{*+}$ ,  $C_3H_4^{*+}$ , and  $C_3H_2^{*+}$ ) and several % up to about 20% for even-electron C3 projectile ions ( $C_3H_7^+$ ,  $C_3H_5^+$ ,  $C_3H_3^+$ ). There was no systematic change with incident energy. The main process in ion-surface collisions is tralization of the incident ion projectile.

A simple correlation between survival probability of the hydrocarbon species C1, C2, C3, C7 and ionization energy of the species in question (instead of the unknown recombination energy) was found. It showed a decrease from more than 10% to less than 1% in between IE 8.5 - 9.5 eV (Fig. 1a) and a further decrease at higher IE. A semi-logarithmic plot  $\log S_a - IE$  showed that the decrease of  $S_a$  was approximately linear over the entire range of IEs of the investigated species (Fig. 1b) and the data could be fitted with an empirical relation  $\log S_a = (3.9 \pm 0.5) - (0.39 \pm 0.04) IE$ .

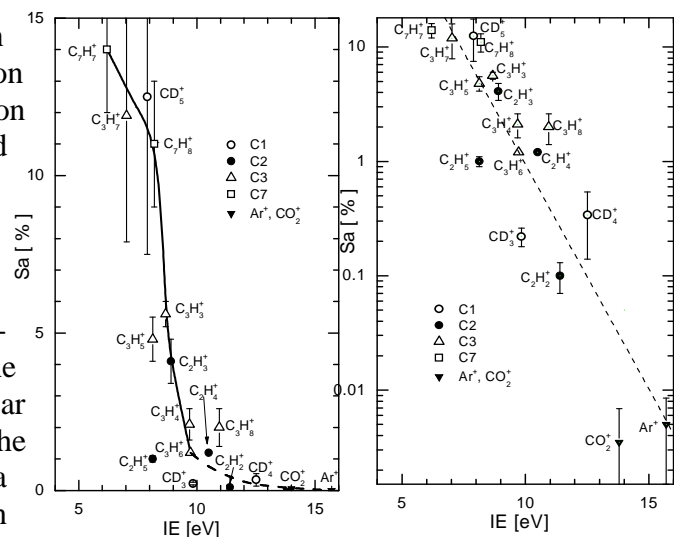


Fig 1a,b: Dependence of  $S_a$  on  $IE$ .

## 2. Collisions of low energy $C_2D_4^+$ and $Ar^+$ ions with stainless steel, carbon (HOPG), and two different diamond surfaces: Surface-induced dissociation and chemical reactions. [2]

The subject of this research was to find out, how different material of a surface at room-temperature, underlying a hydrocarbon coverage, influences surface processes, namely to compare the behaviour of hydrocarbon-covered H-terminated diamond (hydrophobic), O-terminated diamond (hydrophilic) with two standard surfaces (carbon and stainless steel).

Mass spectra of the product ions were measured over the range of incident energies from a few eV up to about 50 eV and the respective CERMS (collision-energy resolved mass spectra) curves of the product ions were determined. The product ions observed with projectile ions  $C_2D_4^+$  indicated both fragmentation of the projectile ion  $C_2D_4^+$ , chemical reactions of H-atom transfer with the surface hydrocarbons, chemical reactions of carbon chain build up (C3 hydrocarbon ion formation), and a small contribution of hydrocarbon ions sputtered from the surface. Sputtering by  $Ar^+$  ions showed the presence of hydrocarbons on all investigated surfaces.

The CERMS curves of the product ions were analyzed to provide the CERMS curves for product ions coming from direct surface-induced dissociation of the projectile ion and those coming from chemical reactions of H-atom transfer. The CERMS curves for direct dissociation of the projectile were (after a correction of the data for the DH surface) very similar for all studied surfaces and thus indicated a similar translational-to-internal energy transfer in the surface collisions. No substantial difference was found between the two room-temperature (hydrocarbon covered) substances of diamond (DO and DH). The product ion distributions over the studied incident energy range could be fitted by an energy transfer distribution function that included the initial internal energy of the projectile ion and assumed a conversion of 10% of the incident energy of the projectile ion in the surface translation-to-internal energy transfer. The CERMS curve for reactive processes (formation and fragmentation of  $C_2D_4H^+$ ) on DO and DH surfaces were very similar. The only observed difference between the two diamond surfaces at room temperature was the ratio of probabilities of reactive vs. reactive and dissociative processes,  $P_R/(P_R+P_D)$ , as a function of incident energy (Fig. 2). This ratio increased from a threshold at 6-7 eV to about 70% for the SS, HOPG, and DO surfaces, but only to about 45% for the DH surface.

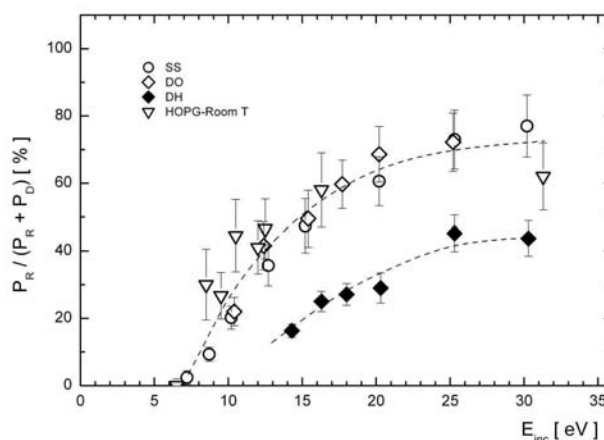


Fig. 2: The ratio  $P_R/(P_R+P_D)$  as a function of the incident energy of  $C_2D_4^+$ .

### References

1. A. Pysanenko, J. Žabka, L. Feketeová, T.D. Märk, Z. Herman, *Eur. J. Mass Spectrom.* **14**, 335-343 (2008).
2. L. Feketeová, J. Žabka, F. Zappa, V. Grill, P. Scheier, T. D. Märk, Z. Herman, *J. Am. Soc. Mass Spectrom.* (accepted)

## Power loads into gaps during ELMs

*R.Dejarnac, M. Komm*

*The aim of this project was to perform kinetic calculations of power fluxes to ITER's castellated plasma facing components during ELMs. Three species are followed (deuterium, tritium, carbon) and power flux profiles in a narrow gap between tiles are presented. The global penetration of the two hydrogen species in the gap is in the order of the gap width (~0.5 mm) and their contribution on the total heat flux is estimated. The impurity carbon penetrates into the gap in between 50 to 70% of the total plasma deposition but with a power deposited less than 1% of the total deposited power.*

We have performed kinetic calculations of plasma deposition in the gaps between tiles for ITER plasma facing components (PFCs) during ELMs. We have investigated hydrogen plasmas with a 50-50% mixture of deuterium/tritium and with 3% of carbon as a main impurity. The two basic orientations of the gap with respect to the magnetic field, poloidal (PG) and toroidal (TG), have been studied. The code used for this purpose, SPICE, has been developed at the IPP Prague and is adapted to such a tile gap geometry [1,2,3,4]. SPICE is a three velocity – two-dimensional kinetic code based on particle-in-cell (PIC) technique. The code is based on the resolution of the equations of motion and the integration of Poisson's equation to obtain the self-consistent electric field that accelerates the particles. The novelty of the code is its ability to inject arbitrary velocity distribution functions. For the ions, we use a non-Maxwellian distribution given by a one-dimensional quasineutral kinetic calculation of the scrape-off layer (SOL) [5,6] that satisfies the kinetic Bohm criterion at the sheath entrance. Therefore, we will be able to study the plasma heat loads to ITER PFCs taking into account the specific geometry of the components, the inclination of the magnetic field lines and the gyration of the incoming particles with realistic velocities. The gap simulated in this study corresponds to the ITER's divertor plates and has a width of 0.5 mm. The inclination angle of the magnetic field lines is taken at  $\alpha = 4^\circ$  with a magnitude for the magnetic field of  $B = 7 T$ . The plasma density and temperature of the different species are the results of kinetic simulations of the parallel transport in the ELMy SOL [7,8] with ITER conditions. The simulated ELM has an energy of 4 MJ with pedestal density and temperature  $n_{ped} = 6 \cdot 10^{19} m^{-3}$  and  $T_{ped} = 5 keV$ , respectively. The unperturbed perpendicular flux falling to the tile surface is  $q_{\perp} = 380 MW/m^2$ .

We observe that the deposition is strongly asymmetric. Only one side of the gap is wetted by the plasma in both PGs and TGs. In the case of PGs, the wetted side is the plasma facing side and in the case of TGs, the wetted side is the one favored by the  $E \times B$  drift. The total peak value at the entrance of the gap is ~3 times the incoming, unperturbed heat flux in PGs and ~2 times in TGs. The gap orientation affects the deposition length too by increasing by 20-25% the distance where the plasma is deposited in TGs compared to PGs. The total deposition of the plasma in the gaps is found to be of the same order than the gap width, i.e. ~0.5 mm.

Concerning the deposition of the different species, we observe that the D carries most of the flux. However, the deuterium and the tritium are deposited on the same distance which corresponds to the total deposition length. By integrating the particle fluxes along the gap we find that the tritium represents 45% of the deposited deuterium in the gap, i.e. ~30% of the total flux in the gap. We can note that the peak value of the tritium is below the total incoming flux by 30 to 50% whereas the deuterium peak value is higher within the same ratio for the 2 gap orientations.

Concerning the carbon deposition in the gap, we observe a smaller penetration (50% to 70% the total deposition length) but with very low power (see Figure 1). The (slow) carbon ions contribute to less than 1% to the total heat flux inside the gap in PGs and TGs. These

results are important for the next step that would consist of modeling the erosion of the gap sides knowing precise incoming fluxes in such a complex geometry and for estimating the amount of tritium trapped in a gap.

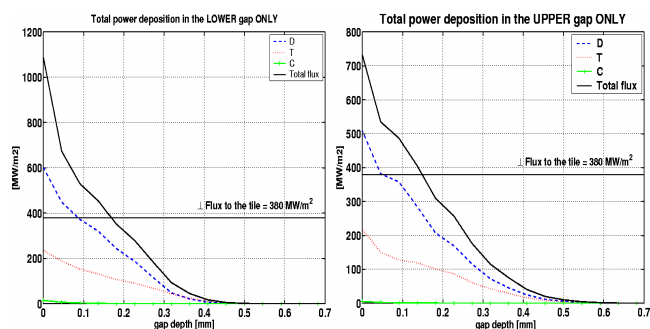


**Figure 1:** Power flux profiles of D, T and C along a PG (left) and a TG (right) during an ELM. The unperturbed perpendicular flux falling to the tile surface far from the gap is also represented.

## References:

- [1] R. Dejarnac and J.P. Gunn, *J. of Nucl. Mater.* **363-365** (2007) 560-564.
- [2] R. Dejarnac et al., TW6-TPP-DAMTRAN EFDA Task report (2008).
- [3] R. Dejarnac et al., '*Power flux in the ITER divertor tile gaps during ELMs*', *J. Nucl. Mater.* (2009), accepted for publication – Proceedings of the 18<sup>th</sup> PSI Conference, Toledo, Spain (May 28-30, 2008).
- [4] R. Dejarnac et al., *J. Nucl. Mater.* **382** (2008) 31-34.
- [5] V. Fuchs et al., 32<sup>nd</sup> EPS Plasma Physics Conference, Tarragona 2005.
- [6] J. P. Gunn, *J. Nucl. Mater.* **337-339**, 310 (2005).
- [7] D. Tskhakaya and R. Schneider, *J. of Comp. Phys.* **225** (1), 829-839 (2007).
- [8] D. Tskhakaya et al., '*PIC simulations of ELM particle and heat loads to the JET divertor targets*', *J. Nucl. Mater.* (2009), accepted for publication – Proceedings of the 18<sup>th</sup> PSI Conference, Toledo, Spain (May 28-30, 2008).

## On SOL Variations as a Function of LH Power

*V. Petržílka, V. Fuchs*

In collaboration with:

*M. Goniche, F. Clairet*, Assoc. EURATOM-CEA-Cadarache, DRFC, 13108 Saint Paul-lez-Durance, France

*G. Corrigan*, Assoc. EURATOM-UKAEA, Culham Science Centre, Abingdon, OXON OX14 3DB, UK

*P. Belo*, Association Euratom-IST, Centro de Fusao Nuclear, Lisboa, Portugal

*J. Ongena*, Plasma Physics Laboratory, RMA, Association EURATOM – Belgian State, Brussels

Numerical modeling was performed of the JET Scrape-off-Layer (SOL) time evolution with the fluid code EDGE2D. The code includes direct SOL ionization by the LH wave [1] and effects of near LH grill limiters [2]. In [1] and [2], a stationary state was modeled. In contrast, the original contribution here is that we also explore for the first time the SOL time evolution when switching on/off the LH and near grill gas puff. Our interest in this problem was originally motivated by recent Tore Supra measurements. Shorter (less than

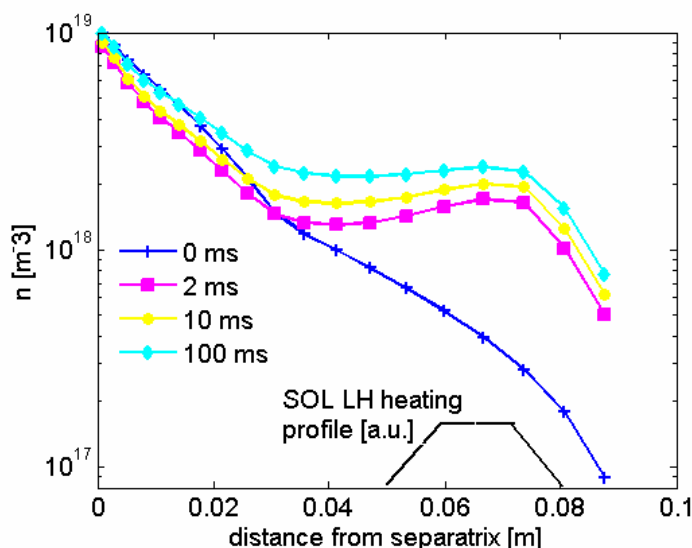


*Fig. 1. OMP plasma density at switching on the LH field  
50 kW dissipated in front of the grill, gas puff  $1e22 \text{ el/m}^3$ .*

about 10 ms) and longer (about 50 ms) characteristic times for the SOL plasma density evolution in locations magnetically connected and not-connected to the LH launcher are measured by frequency swept reflectometry on Tore Supra during LH power modulation. We realized that similar effects can be present also on JET. On Fig. 1 and 2, we can see the plasma density changes at the JET OMP (Outer mid-plane) and at the RCP (Reciprocating probe) locations at switching on the LH field. The grill mouth is assumed to be at 8 centimeters from the separatrix, 1 cm retracted behind the limiters. The SOL parasitic absorption takes place near the grill mouth [1,2], between 5 and 8 centimeters from the separatrix. At switching on/off the LH field or the gas puff, the plasma density reaches equilibrium after 50 -100 ms. More far from the separatrix, the equilibrium is reached more quickly (in about 10 ms) than more near to the separatrix.

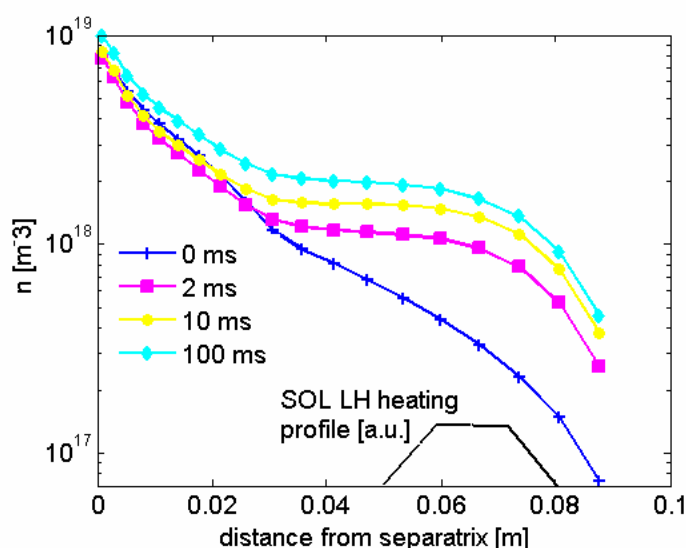


**Fig. 2.** RCP location plasma density at switching on the LH field  
50 kW dissipated in front of the grill, gas puff  $1e22 \text{ el/m}^3$ .

Similar temporal behavior is exhibited also by the H<sub>α</sub> radiation intensity. The density rises at LH switching on at a constant gas puff because of the direct LH ionization in the SOL. Similarly, we derived the temporal behavior of the plasma density at switching on/off the gas puff, when the LH is on. At switching off the LH/or gas puff at constant gas puff/or LH power, the plasma density is decreasing to its previous values, again more quickly far from the separatrix, where the parasitic LH absorption and corresponding direct LH SOL ionization are taking place. The plasma flows and their temporal behavior were computed, too.

**Conclusions:** More far from the separatrix, where the LH parasitic dissipation and corresponding local SOL heating takes place, the computed plasma density increases with time at the onset of the local LH wave ionization with a short characteristic time of less than about 10 ms. Closer to the separatrix, the plasma density approaches the new equilibrium with a several times longer characteristic times. Naturally, the SOL plasma variations at LH switching on/off are larger with a larger near grill gas puff and also with larger variations of the LH power. Evolution of the SOL neutral particles density and of other SOL parameters was also explored. The results are relevant to JET LH coupling and modulated LH power experiments, and corresponding measurements of SOL temporal variations are being prepared. It may be important to take into account the computed JET SOL relaxation times in evaluation of LH coupling, LH driven currents and other parameters.

#### References:

- [1] V. Petrzilka et al., 33rd EPS Rome 2006 Conference, paper P-1.067.
- [2] V. Petrzilka et al., 34th EPS Warsaw 2007 Conference, paper P-4.100.

## Experiments concerning fast particles emerging from LH antennas

*V. Petržílka, V. Fuchs*

In collaboration with:

*J. Gunn, A. Ekedahl, M. Kocan, M. Goniche, Assoc. EURATOM-CEA-Cadarache, DRFC, 13108 Saint Paul-lez-Durance, France*

In dedicated experiments, we determined by using RFA (Retarding Field Analyzer) the radial – poloidal pattern of the fast particle flux profile in front of the Tore Supra grill. Only 5 modules from 8 were working on C2, so that 1 MW launched power corresponded to the power density for 1.6 MW launched by all C2 modules. In the first part of experiment, we obtained for the first time the energy distribution function of electron in the fast beam at full r-theta scan, Fig. 1. In the 2<sup>nd</sup> part of the experiment, a Tore Supra discharge configuration with wide SOL was created. The C2 launcher was moved from the LCFS till the SOL was about 7 cm wide. Surprisingly, the intensity of the fast beam generation was higher at the lower density part of the wide SOL region, Fig. 2.

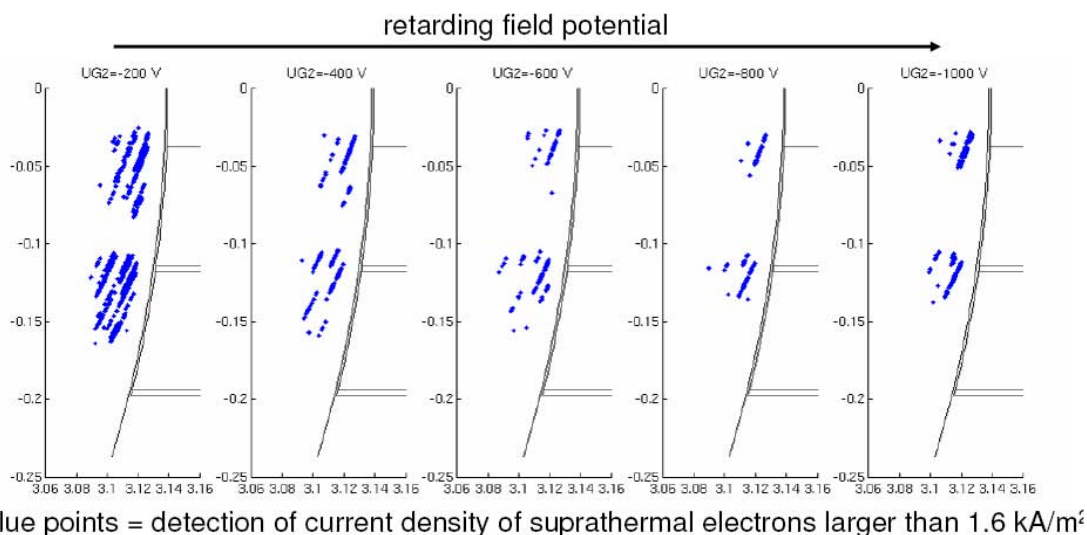


**Fig. 1.** Energy distribution of electrons in the fast beam.

For the wide SOL, the r-theta scan of the beam was again done for the grid voltage  $UG2 = -200V$ , by varying the q value. Because of the wide SOL, it was now possible to see for the first time the whole radial extent of the fast beam, Fig. 3. The results of the experiment are now being analyzed in details, and are prepared for publication [1]. The envisaged computations of power flux namely in the fast electron beam near to the in front of the grill, based on our RFA Tore Supra measurements from several last years, were not performed because of problems with determination the power flux slit transmission factor of the RFA.

### Reference:

[1] J. Gunn et al., to be submitted to the 2009 RF Topical Conference, Gent.

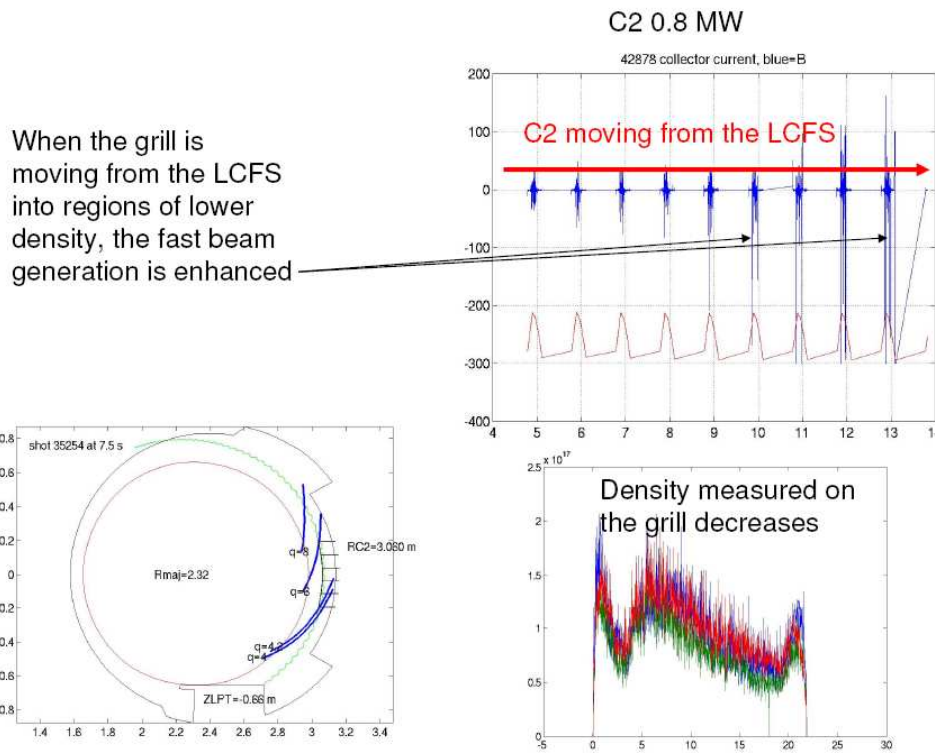


Fig. 2. Enhancement of the fast beam generation, when moving the launcher from the LCFS.

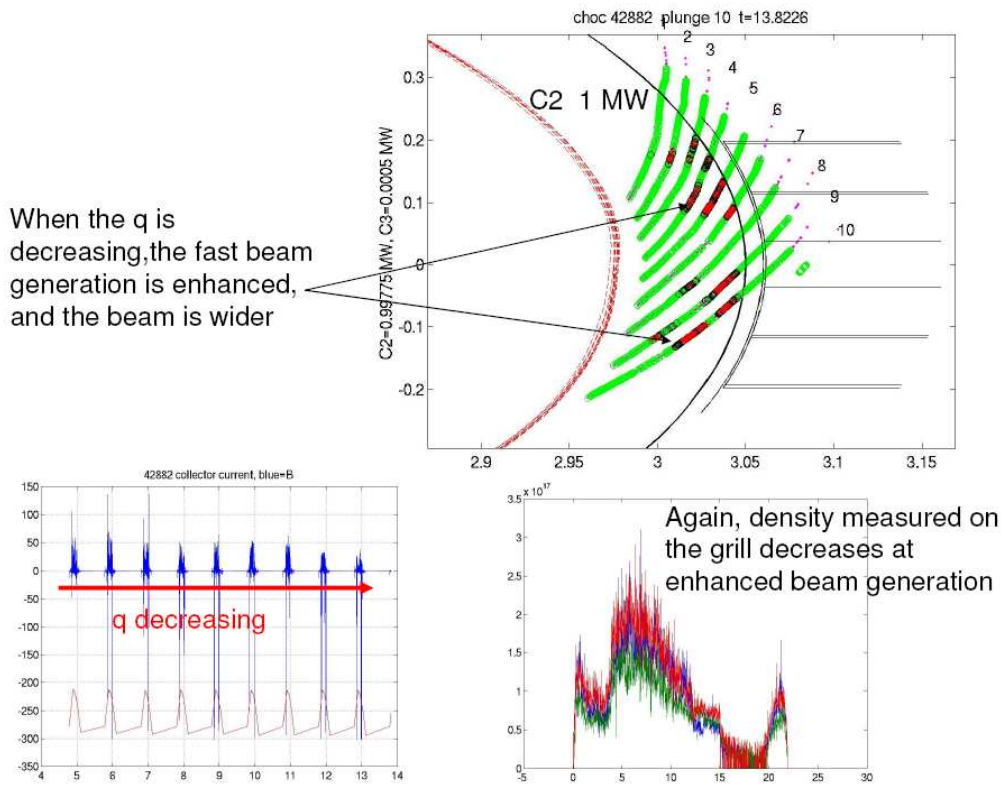


Fig. 3. The figure shows for the first time the whole radial extent of the fast beam

## Modeling of neutral beam (NB) and lower hybrid (LH) heating and current drive for COMPASS

V. Fuchs, R. Dejarnac, M. Komm, M. Stránský, J. Urban

In collaboration with:

Y. Peysson, J. Decker, Association EURATOM-CEA Cadarache, France

R. A. Cairns, University of St Andrews, UK

I. Voitsekhovitch, Association EURATOM/UKAEA Culham, UK

*Results of our Lower Hybrid Current Drive (LHCD) simulations with the ACCOME and C3PO/LUKE ray tracing and Fokker-Planck codes were reported at the 2008 EPS conference [1]. Due to problems including broad  $n_{\parallel}$  spectrum and poor accessibility at low magnetic fields, we decided to apply methods of stationary phase to wave propagation in inhomogeneous plasma. At the moment some preliminary work has been done, expecting results next year. Intensive simulations have been performed to simulate NBI behavior in COMPASS using the FAFNER Monte-Carlo code. They indicate that the orbit losses can be as high as 40 % for the counter-injection scenario, making it considerably less efficient than co-injection. The so-called beam-halo effect causes significant charge-exchange losses for the dual-beam setup. These losses can be decreased by increasing the plasma density. Standalone results of the LH and NBI heating were used to simulate heat transport in COMPASS using the transport code ASTRA. The results were presented at the 2008 SPPT conference in Prague [2].*

We concentrated on the planned COMPASS operational range  $B=1.2-2.1$  Tesla and  $I=170-250$  kA. Because of the relatively low LH source frequency (1.3 GHz), low magnetic field and high density, the study was of great interest to the understanding of LHCD under poor LH slow wave accessibility conditions. The LH antenna power spectrum is also non-typical having at  $\pi/3$  waveguide phasing a broad main peak situated at  $n_{\parallel}=2.1$  with a width  $\Delta n_{\parallel} \approx 2$ . LH power deposition and current was determined in 9 iterations between the ACCOME equilibrium and LHCD modules, and was verified using the ray-tracing and 3-D Fokker-Planck package LUKE. The principal difference between the LH ACCOME and LUKE codes is in ray tracing: ACCOME uses multiple rays, LUKE just one ray. This was the first time that the ACCOME LH module, conceived for computational speed is tested against a module devised for determining an accurate distribution function suitable for interpreting hard X-ray diagnostics. An important result was that even in the worst-accessibility regime the LH-driven current makes a considerable 25-30% of the 170 kA of feedback controlled plasma current with 110 kW of deposited LH power.

There is ongoing discussion between our and the Tore Supra LH groups concerning the applicability of ray tracing to the COMPASS configuration. The issues are:

- 1) The large LH spectrum width  $\Delta n_{\parallel} \approx 2$  comparable in size to the injected  $n_{\parallel} = 3.3$ .
- 2) Closely related to issue 1) is the question of applicability of the Tore Supra LUKE package, which should be used with one ray only, to COMPASS.

We decided to study these outstanding problems by application of stationary phase methods to wave propagation in inhomogeneous plasma. Specifically, radiation launched from a lower hybrid antenna in a tokamak generally follows a complicated path around the torus before being absorbed. If the radiation is very well collimated then using a single ray may be valid, but if there is a larger spectral width then the problem arises of just how to recreate the wave

pattern from tracing of multiple rays. We shall show by means of a simple example with a homogeneous system, where the full wave solution can be constructed in the form of an integral, that a stationary phase approximation gives very accurate results for the far field and can be interpreted as propagation along a ray modified by a factor taking account of interference with adjacent rays. Essentially, the important contributions to the amplitude at any point only come from the spectral component corresponding to the ray travelling from the centre of the antenna to that point and closely adjacent components. Other parts of the spectrum give contributions of rapidly varying phase which cancel each other out.

In the tokamak problem there is, of course, no explicit solution in the form of an integral and no simple expression for the phase. However, we develop a procedure by which the factor modifying simple propagation of the wave amplitude along the ray can be calculated without explicit knowledge of the wave phase. It requires only knowledge of the local dispersion relation and its derivatives, most of which are already needed in a ray tracing calculation.

To validate this procedure we look at another example in which the system is inhomogeneous so that the ray paths are curved. A linear gradient allows an exact solution in terms of Airy functions, but also produces a situation in which the general procedure can be implemented in a non-trivial way along lines following exactly those proposed for a tokamak. It can be demonstrated that the method does in fact give the correct phase properties and good agreement with the exact solution.

In a tokamak the procedure will require following enough rays to cover the important parts of the launched spectrum. However, ray tracing is a fairly simple and computationally efficient procedure and we anticipate that our method may allow us to reproduce the field amplitude variation around the torus in a much easier way than doing a full wave calculation. This work is to be presented at the 2009 EPS Conference in Sofia [3].

Intensive simulations have been performed to simulate NBI behaviour in COMPASS using the FAFNER Monte-Carlo code. Results indicate that the orbit losses can be as high as 40 % for the counter-injection scenario, making it considerably less efficient than co-injection. The so-called beam-halo effect causes significant charge-exchange losses for the dual-beam setup. These losses can be decreased by increasing the plasma density. Simulations for alternative particle energies show that the nominal selected 40 keV is a rather good choice. In the last quarter of 2008 we started to work on incorporation of the FAFNER code into the transport code ASTRA. We were quite satisfied with the standalone FAFNER results, so we decided to include this one instead of NUBEAM package as was originally planned.

## References

- [1] V. Fuchs, O. Bilyková, R. Pánek, M. Stránský, J. Stöckel, J. Urban, F. Žáček, Y. Peysson, J. Decker, I. Voitsekhovitch, and M. Valovič, *Heating and current drive modeling for the IPP Prague COMPASS tokamak*, 35<sup>th</sup> EPS Conf.on Plasma Phys. and Control. Fusion, 2008, Hersonnisos, Greece
- [2] Stránský M., Bilyková O., Fuchs V., Havlíčková E., Pánek R., Stöckel J., Urban J., Voitsekhovitch I., Valovič M.: *Transport simulations for the COMPASS tokamak with NBI and LH heating and current drive systems*. 23rd Symposium on Plasma Physics and Technology, June 2008, Prague, Czech Republic poster presentation
- [3] R. A. Cairns and V. Fuchs, *Recreation of lower hybrid radiation pattern from ray tracing*, submitted to 36<sup>th</sup> EPS Conf.on Plasma Phys. and Control. Fusion, 2009, Hersonnisos, Greece

## Application of the Minimum Fisher Information inverse methods in the JET neutron cameras and compact spectrometers data analyses

*J. Mlynář, V. Svoboda*

In collaboration with:

*G. Bonheure*, Association EURATOM-Etat Belge, ERM/KMS, Brussels, Belgium

*A. Murari*, Association EURATOM-ENEA, Consorzio RFX, Padova, Italy

*M. Tsalas*, Association EURATOM-Hellenic Republic, N.C.S.R. "Demokritos", Greece and JET EFDA contributors

*The inversion method based on Minimum Fisher Regularisation (MFR) [1] contributed to data analyses and, in particular, to tritium transport studies at JET in 2008. This method - implemented at JET in collaboration with the Association EURATOM/IPP.CR in previous years - was validated as a robust and rapid tool to analyse sparse data. Works in 2008 concentrated on extension and exploitation of the algorithm in spatial analyses of plasma neutron emissivities measured by the JET profile monitor (MFR tomography). Some efforts were also invested into preparation of an automated tool that would systematically analyse spectra of neutrons detected by the NE213 compact spectrometer and unfolded by the MFR.*

In early 2008, the subroutine computing the reconstruction matrix in the MFR tomography was extended with a rapid method to deal with the real widths of the viewing chords, see fig. 1. The upgrade was validated both in test runs and on experimental data. The results were presented in [2]. Second, transmission of errors via Monte Carlo simulations was studied both directly in tomography (published in a bachelor's thesis [3]) and globally in transport studies [4]. The errors show to preserve their distribution and do not display any critical behaviour in the inversion calculation. Also it is worth noting that the error studies proved that it is possible to derive new important results from the MFR reconstructions, in particular previous results of the novel ratio method [5] were confirmed. The ratio method in combination with the MFR tomography led to new and significant results of fuel transport studies using poloidally averaged (1D) and full 2D ratios of D-D and D-T neutron emissivities. The 1D analyses were presented at the EPS conference [4] and later submitted to Nuclear Fusion journal [6], the 2D results are still under internal discussion at JET. Indeed, conclusions of these articles triggered broad discussion that led to a definition of future milestones of this project.

Let us mention here some key results of the submitted article. The tritium particle thermal transport was studied for a set of JET discharges with tritium gas puff (from the JET Trace Tritium Experiments) and the particle transport coefficients were derived for the first time using the ratio technique based on MFR tomography of 14.1 MeV (D-T fusion) and 2.5 MeV (D-D fusion) neutrons. The ratio directly corresponds to the tritium concentration, and from the knowledge of spatial and temporal evolution of the tritium concentration its transport coefficients, i.e. the diffusion coefficient and pinch velocity, can be directly derived, see Fig. 2. The transport coefficients obtained are comparable within uncertainty to the values obtained in previous work. Comparison with the neoclassical values shows that tritium

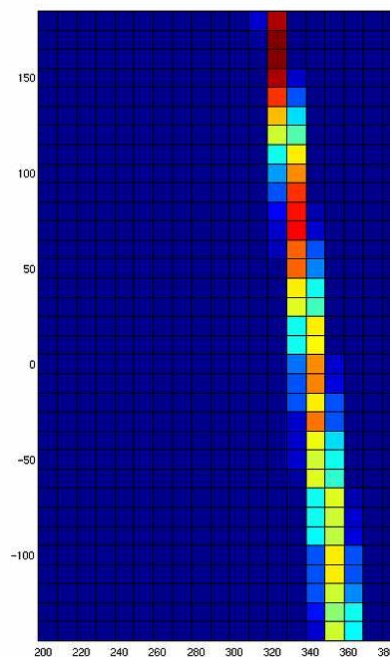


*Fig. 1. Chord 17 of the JET Neutron profile monitor with real width on standard mesh of pixels 10x10cm.*

diffusion in the core can be as low as neoclassical level. Within uncertainty, tritium particle confinement was also found to follow the ITER IPB98(y,2) global particle scaling confinement for the set of ELMy H-mode plasmas studied.

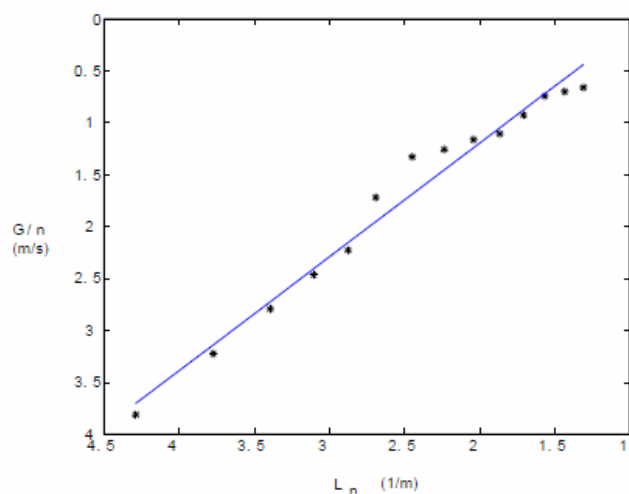


Fig. 2. Tritium concentration flux normalised to the tritium concentration is plotted as a function of the inverse gradient length of the tritium concentration. Diffusion coefficient and pinch velocity are derived from the linear interpolation.

tested both on data from neutron important past campaigns (e.g. the TTE campaign) and the current 2008 campaign. This work is an important part of the pursued implementation to automate the routine for post-pulse analyses, which is delayed due to uncertainties linked to the MatLab replacement at JET computer system.

Last, but not least, both tomography and unfolding routines were applied to data analyses of the 2008 JET campaigns (C20 – C25). Preliminary results present the expected properties of neutron emissivity due to the new ICRH heating, in particular, high energy neutrons have been identified in the NE 213 neutron spectra. However, the corresponding data suffer from low intensity of neutron emission.

## References:

- [1] M. Anton et al., *Plasma Phys. Control. Fusion* 38 (1996) 1849
- [2] J. Mlynar, G. Bonheure et al., 23<sup>rd</sup> Symposium on Plasma Physics and Technology, June 2008, Prague
- [3] M. Imrisek, Bachelor's thesis, Faculty of Nuclear Sciences and Physical Engineering, Czech Technical University in Prague, September 2008
- [4] G. Bonheure, J. Mlynar et al., 35th EPS Plasma Physics Conference, June 2008, P-4.084
- [5] G. Bonheure et al. *Nucl Fusion* 46 (2006) 725
- [6] G. Bonheure, J. Mlynar et al., A novel method for trace tritium transport studies, submitted to *Nucl. Fusion*
- [7] J. Mlynar et al., *Fusion Eng. Design* 74(2005)781
- [8] J. Mlynar et al., TFD Technical Meeting on Unfolding and Tomographic Techniques for Fusion Applications, July 2008, EFDA JET, Culham Science Centre

In the unfolding applications, work has been focused in particular on enhancing systematic JET data analysis from JET NE213 neutron scintillation detectors and their coherent integration with basic and other plasma diagnostics. The developed system of data analyses exhibits, among others, easy cooperation with existing globally used tools, like jetdsp, with individual user routines created in various systems including matlab, mathematica, idl, maple, fortran, c++, octave, root, science lab etc. It has an intuitive setup interface and output is produced in a hypertext oriented format for web-like presentation of results. The MFR unfolding algorithm [7,8] was modified and integrated into the system. It was

## 2. Development of plasma auxiliary systems

### COMPASS NBI System Design

*J. Preinhaelter, V. Fuchs, J. Urban, J. Zajac*

*A flexible neutral beam injection (NBI) system is planned for COMPASS, consisting of two injectors with particle energy 40 keV and 300 kW output power, delivering a total of 600 kW to the plasma. A complex design of the beam ducts is required to avoid beam blocking. The injectors will be connected to tangential ports, with the possibility of switching one of the injectors from co-current direction to counter-current direction with the aim of enabling non-rotating, NBI-heated plasmas. Intensive computations have been performed to simulate NBI behaviour on COMPASS using the FAFNER Monte-Carlo code.*

The planned COMPASS NBI system will consist of two beam injectors, each delivering 300 kW in 40 keV neutrals [1]. A complex design of the beam ducts is required to avoid beam blocking. The design has not been finalized yet; however, calculations for a realistic engineering project indicate that the risk of the beam blocking can be sufficiently minimized.

Intensive computations have been performed to simulate NBI behaviour on COMPASS using the FAFNER Monte-Carlo code [2]. The SND and SNT equilibria, calculated by ACCOME, with low and high magnetic fields, are applied for the FAFNER simulations. Energy balance results are shown in Fig. 1 for 1.2 T and 2.1 T SND equilibria and various injection scenarios. The shine-through is acceptable for both lower and higher density cases. Very important are orbit losses, which become very pronounced for counter-injection, where they can be as high as 40 %. As a consequence, counter-injection is considerably less efficient than co-injection.

In the previous studies [1] we considered only a single 300 kW injector and presumed that the results can be simply doubled to obtain realistic estimates for the whole NBI system performance. This is actually not true because of the so-called beam-halo effect. 40 keV neutrals will be dominantly ionized by the charge-exchange mechanism, thus creating neutrals along the beam path. These neutrals can again interact with the fast beam ions. Another charge-exchange collision may occur, after which a fast ion becomes a fast neutral and can escape the plasma. This non-linear effect is studied with the Monte-Carlo technique described in [3] and implemented in FAFNER. The beam-halo density  $n_0^h$  obviously grows with the number of the injected neutrals. The fast ions slowing down time constant is proportional to  $T_e^{3/2}/n_e$  [4] while the charge-exchange collision frequency is proportional to  $\sigma_{ch} n_0^h$ , where  $\sigma_{ch}$  is the relevant charge-exchange cross section. It is therefore the ratio  $n_0^h/n_e$ , which determines the severity of the charge-exchange losses caused by the beam-halo neutrals. This dependence also indicates that higher electron temperatures, predicted for the 2.1 T equilibria with 250 kA plasma current, cause higher charge-exchange losses, as can be seen in Fig. 1. On the other hand, higher electron temperature induces higher critical energy, at which the fast ions begin to deposit most of their energy to ions during the slowing down process. This is favourable for attaining plasmas with  $T_e \cong T_i$ . Higher density positively acts on NBI performance, except the current drive efficiency, by decreasing shine-through and charge-exchange losses.

A possible way of further optimizing the NBI performance is different particle energy. Results obtained with FAFNER for various energies, 1.2 T and 2.1 T SND equilibria and  $n_e = 5 \times 10^{19} \text{ m}^{-3}$  are presented in Fig. 2. Increasing the energy to 60 eV leads generally to

higher losses because of the higher shine-through and the longer thermalization time. Moreover, larger portion of the power is deposited on electrons. For the same reasons, the overall performance is slightly better for 30 keV compared to 40 keV. The deposition profiles are very similar for central electron densities up to  $8 \times 10^{19} \text{ m}^{-3}$ . Larger densities cause 30 keV beams to deposit the power closer to the plasma edge. A disadvantage of the 30 keV would be 1.3 times higher particle current necessary to obtain 300 kW power. This represents a higher risk of the beam duct blocking. So in fact it follows that the nominal selected 40 keV is a rather good choice.

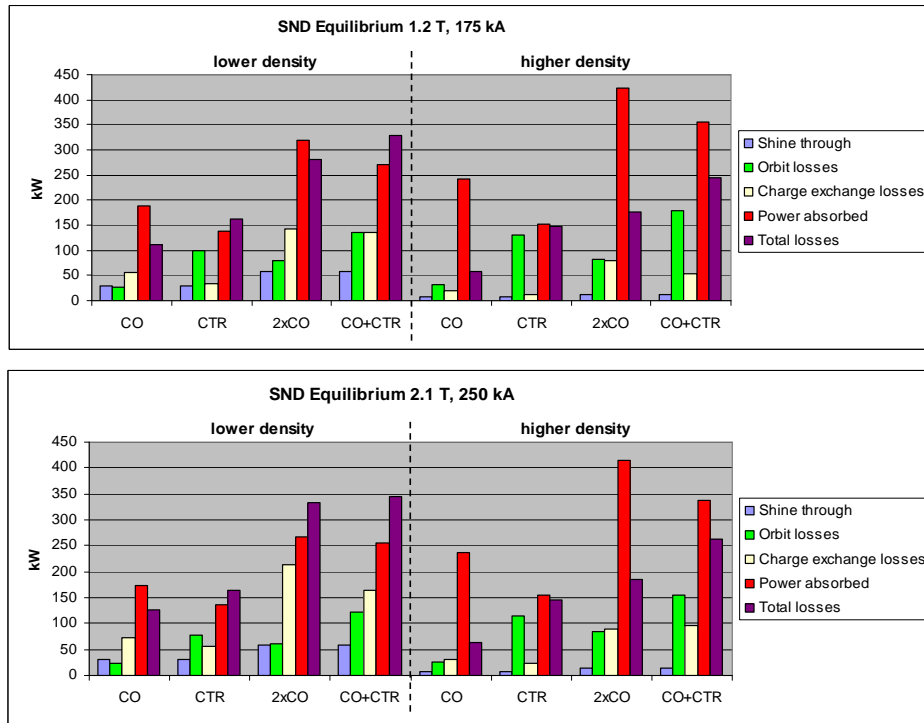


Fig. 4. NBI performance of the studied NBI scenarios, simulated with SND 1.2 T (top) and 2.1 T (bottom) COMPASS equilibria. Plotted are configurations with lower (L) and higher (H) central electron densities,  $n_e^L = 3 \times 10^{19} \text{ m}^{-3}$  for 1.2 T equilibrium and  $n_e^L = 3.5 \times 10^{19} \text{ m}^{-3}$  for 2.1 T equilibrium,  $n_e^H = 5 \times 10^{19} \text{ m}^{-3}$  for both equilibria.

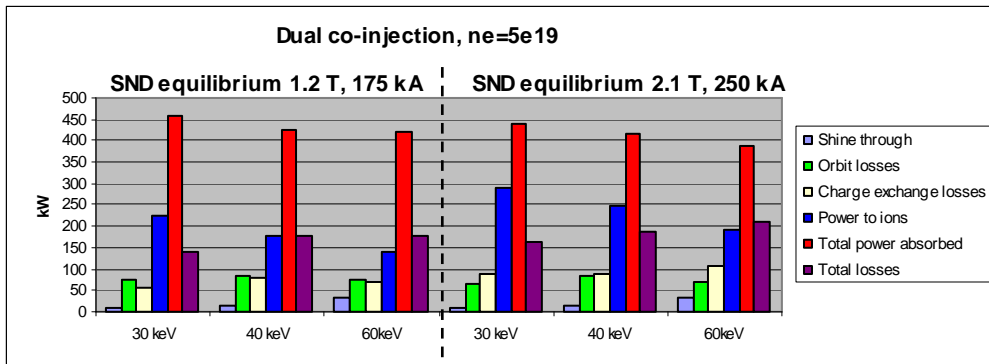


Fig. 2. NBI performance for 30, 40 and 60 eV particle energies, SND equilibria,  $n_e = 5 \times 10^{19} \text{ m}^{-3}$ .

**References:**

- [1] J. Urban et al., *Czech. J. Phys.* 56 (2006) B176
- [2] G. G. Lister, *IPP Report 4/222* (1985)
- [3] S. Succi, and G. G. Lister, *3<sup>rd</sup> Joint Varenna-Grenoble Int. Symp. on Heating in Toroidal Plasmas* (1982)
- [4] E. Speth, *Reports on Progress in Physics* 52 (1989) 57

## Direct measurements of the plasma potential and electron temperature in ELMy H-mode plasma with ball-pen probes on ASDEX Upgrade tokamak

*J. Adamek, J. Stöckel, J. Horacek, J. Brotankova*

In collaboration with:

*V. Rohde, H. W. Müller, A. Herrmann, MPI für Plasmaphysik, EURATOM Association, Garching, Germany;*

*C. Ionita, R. Schrittwieser, F. Mehlmann, Association EURATOM/ÖAW, Innsbruck, Austria*

*Experimental investigations of the plasma potential and electron temperature were performed for ELMy H-mode plasmas in the vicinity of the limiter shadow of ASDEX Upgrade. A fast reciprocating probe manipulator with ball-pen probes (BPPs) [J. Adamek et al., Czech. J. Phys. 54 (2004)] was used.*

### 1. Experimental arrangement

The fast reciprocating probe manipulator located at the midplane on ASDEX Upgrade was used to insert a probe head containing four BPPs with different retraction depth of  $h = -0.5$  mm (BPP0),  $-1$  mm (BPP1),  $-2$  mm (BPP2) and  $-3$  mm (BPP3) of its collectors and two Langmuir probes (LP1 and LP2). The data were taken during the shot #23413 with plasma parameters  $B_T=2.5$  T,  $I_p=0.8$  MA,  $n_e=4.6 \cdot 10^{19}$  m<sup>-3</sup> and  $P_{NBI}=5$  MW.

### 2. Radial profile of the plasma end floating potential

Figure 1 shows two different types of the radial profiles. Note, the frequencies higher than 250 Hz were filtered out from the raw signal to eliminate the contribution of turbulent plasma and ELM structures. The first profile (blue colour) is a mixture of all values of the plasma potential of BPP0, BPP1 and BPP2 in order to provide the total radial profile of the plasma potential obtained during one stroke.

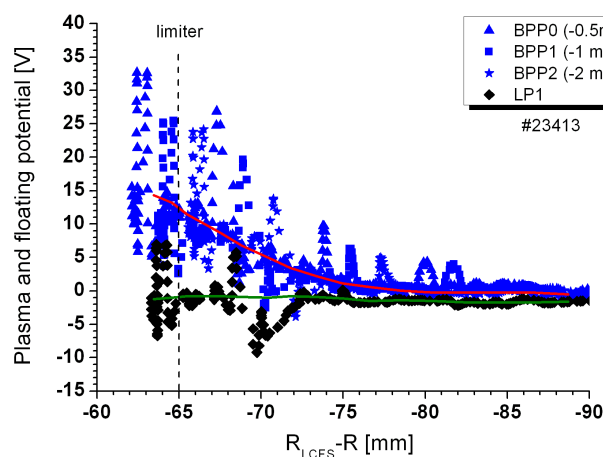


**Fig. 1:** Radial profiles of the plasma potential of BPP0, BPP1 and BPP2 (blue color). Higher frequencies than 250 Hz were filtered out from the raw signal. The floating potential of the Langmuir tip LP1 is plotted by black color.

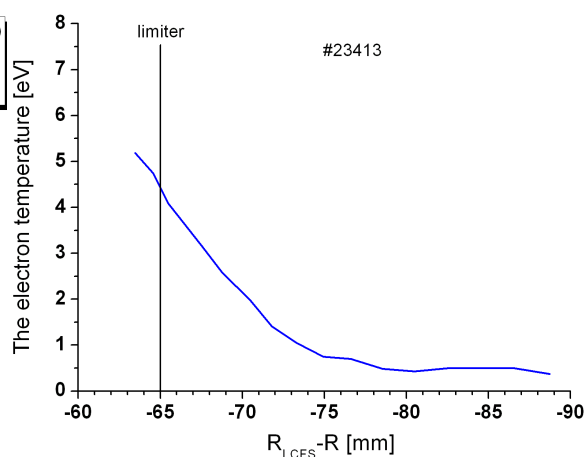


**Fig. 2:** Radial profile of the electron temperature estimated from the difference of the plasma and floating potential of the fitting curves as seen in Fig.1.

The second radial profile (black colour) represents the values of the floating potential measured by standard Landmuir tip (LP1). It is a first time, when both values, the plasma and floating potential, are measured simultaneously. Unfortunately, the values are still affected by

peaks of each ELMs even after strong filtering. Therefore, the fitting curves of each profiles are plotted in the figure (red and green line) as well.

### 3. Radial profile of the electron temperature

It is hard to calculate the electron temperature as a difference of the plasma and floating potential divided by proper constant due to the above mentioned data scattering. However, if we take the fitting curves in figure 1 as the raw estimation of the plasma and floating potential (red and green line) then the electron temperature is obtained as a difference of both potentials divided by factor 3 (roughly for hydrogen plasma), as seen in Fig. 2.

### 4. Temporal evolution of the difference of the plasma and floating potential during ELMs

The analysis of the temporal evolution of the plasma and floating potentials during the ELM events is not yet completed. The different space location of BPPs with respect to Langmuir tips causes the time shift between the corresponding signals, because of motion of the plasma itself during the ELM and even during each filament. This is partially suppressed by using a cross-correlation function of all signals, which provides the information of the time shift between all signals. It is not clear how each filament affects the probes separated in space. Moreover, the power spectra of the BPP signal is limited. The same feature has been observed also in the period in between ELMs [1].

However, the unique information of the temporal evolution of the electron temperature,  $(V_{pl} - V_{fl})/3$ , during ELM events can be still obtained as seen in the Fig. 3.

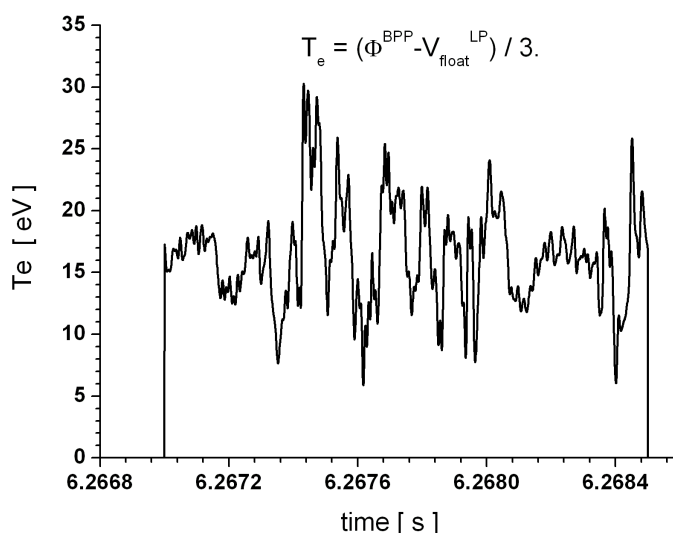


Fig. 3: Temporal evolution of the difference of the plasma and floating potential during ELM.

### References:

- [1] J. Adamek, V. Rohde, H.W. Müller, A. Herrmann, C. Ionita, R. Schrittwieser, F. Mehlmann, J. Stöckel, J. Horacek, J. Brotankova, Journal of Nuclear Materials 390-391 (2009) 1114

## Divertor probes on the COMPASS tokamak - commissioning and first results

*J Stockel, R Dejarnac*

In collaboration with:

*Ts. Popov*, Association EURATOM-INRNE/Faculty of Physics, Sofia, Bulgaria

*J. Gunn*, Association EURATOM-CEA Cadarache, France

*The COMPASS tokamak is equipped by an array of Langmuir probes embedded to a divertor plate. In the year 2008, the probes were tested and equipped by corresponding measuring circuits. First measurements indicate a proper performance of the system. Furthermore, a new power supply unit is designed and tested in collaboration with Association EURATOM-INRNE. The probe voltage is of a triangular shape, but it is applied in steps. This novel approach allows better treatment of plasma fluctuations in processing of the IV characteristics and more precise determination of the electron distribution function.*

The set of Langmuir probes (39 pins) embedded in the divertor tiles of the COMPASS tokamak was prepared for commissioning.

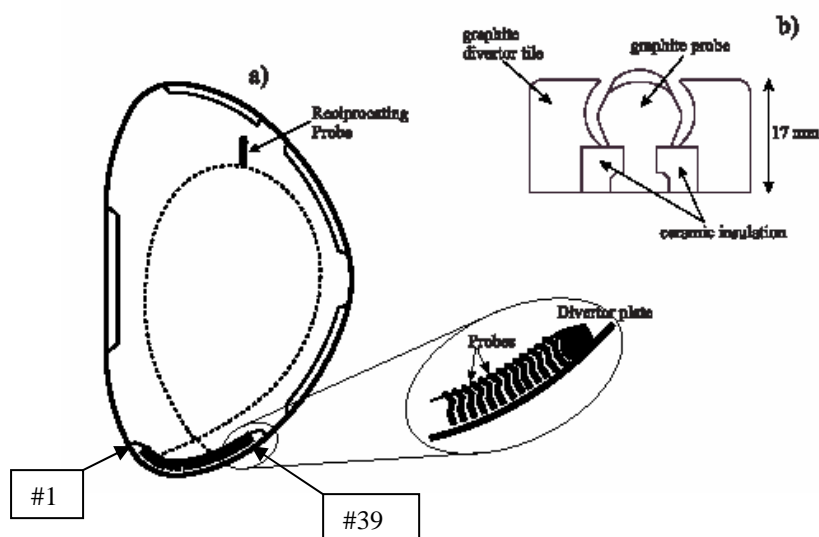


Fig. 1. Poloidal cross-section of COMPASS with the array of probes embedded to a divertor plate

The electrical connection between the individual probes, corresponding feedthrough and coaxial cables was checked. It was found that all probes are in a good status except one (#23), which is short circuited to the vessel. The electronics, which allows operation of all probes simultaneously either in the floating potential or ion saturation current, is available. Therefore, the divertor probes were ready for first measurements from the first day of tokamak operation.

An advance power supply for probes was developed in collaboration with the Association EURATOM-INRNE, Bulgaria. This system allows applying a step-like voltage waveform to probes and to record their current in eight channels. The duration and amplitude of the steps is computer controlled. The test bed measurements have shown that the minimum duration of the steps is about 100 microseconds. Such a system will reduce an impact of plasma fluctuations on the shape of the I-V characteristics and thereby allows determination the electron distribution function more precisely [1,2].

For first experiment, a simplified electric circuit for measurements of the floating potential and probe current is used, see fig 2. Eight channels are available.

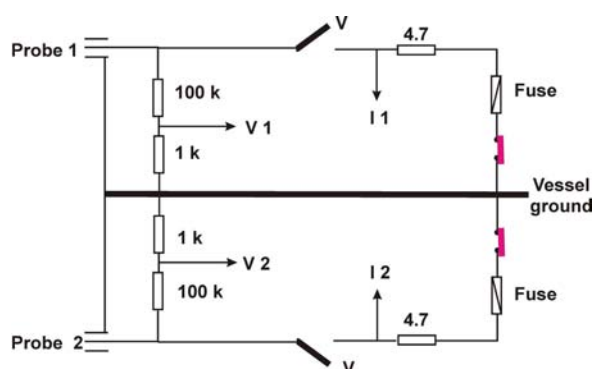


Fig. 2. A simple circuit to measure the floating potential and the probe current used in first shots.

First results are shown in Fig. 3

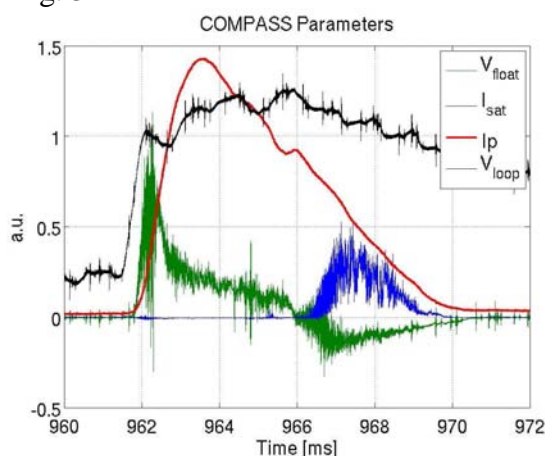


Fig. 3. Temporal evolution of the loop voltage (black) and the plasma current (red) during the start-up phase of the COMPASS discharge 227. Two signals of divertor probes are plotted as well. The floating potential of the probe No 1 is shown by green line and the probe current of the probe 19 is marked by blue line.

It is seen, that the floating potential is positive during the ramp-up of the plasma current (at 962-966 ms), which is a signature that the probe is effectively in the scrape-off layer. Later on at 966 ms, the polarity is changing to negative one. At the same time, the probe measures the current, which indicates that the plasma column is shifted downward to the probe array, probably because of a stray horizontal magnetic field, which is not compensated.

This result shows that the divertor probes can be a useful tool to study the start-up phase of the COMPASS plasma.

### References:

- [1] Popov Tsv. K., Ivanova P., Benova E., Dias F. M., Stöckel J., Dejarnac R.: On the Interpretation of the Electron Part of the Langmuir Probe Characteristics in Tokamak Edge Plasma. *35th EPS Conference on Plasma Physics, Hersinissos, Crete, June 9-13, 2008* Poster presentation, P-4.081
- [2] Tsv. K. Popov, P. Ivanova, J. Stöckel, R. Dejarnac, Electron energy distribution function, plasma potential and electron density measured by Langmuir probe in tokamak edge plasma, submitted to PPCF

## Development of advanced probe for edge tokamak plasmas - Emissive and tunnel probes

M. Tichý; P. Kudrna, I. Picková, R. Hrach, J. Šimek, Z. Pekárek

In collaboration with:

R. Schrittwieser, Petru Balan, Association EURATOM-ÖAW Innsbruck, Austria

J. Gunn, Association EURATOM-CEA Cadarache, France

E. Martines, Association EURATOM-ENEA, Padova, Italy

In accord with the forecast in the recent report we decided to study the discharge plasma in the cylindrical magnetron in pulsed regime. For this purpose we constructed a high-voltage dc switch based on power IGBT transistors, and a capacitor bank that powered the discharge during the active pulse. Time-resolved radial dependences of discharge current, plasma density, electron temperature and floating and plasma potential measured both during the on time and in the afterglow phase were evaluated from cylindrical probe data. The pressure range was changed from 1 to 10 Pa while the homogeneous magnetic field strength was kept at 10 mT where the pulsed discharge is stable. Pulses with amplitude about 700 V, duty cycle of 100 and 200  $\mu$ s and repetition period of 1 ms were applied.

A schematic of the used experimental system is shown in Fig. 1. The cylindrical magnetron consists of stainless steel cylindrical vacuum chamber with internal radius  $r_A$  of 60 mm which serves as anode and coaxially mounted water cooled cathode with the diameter of 10 mm. The discharge volume is limited by two disc-shaped electrodes (“limiters”) which are connected with the cathode to the length of 120 mm. Constant

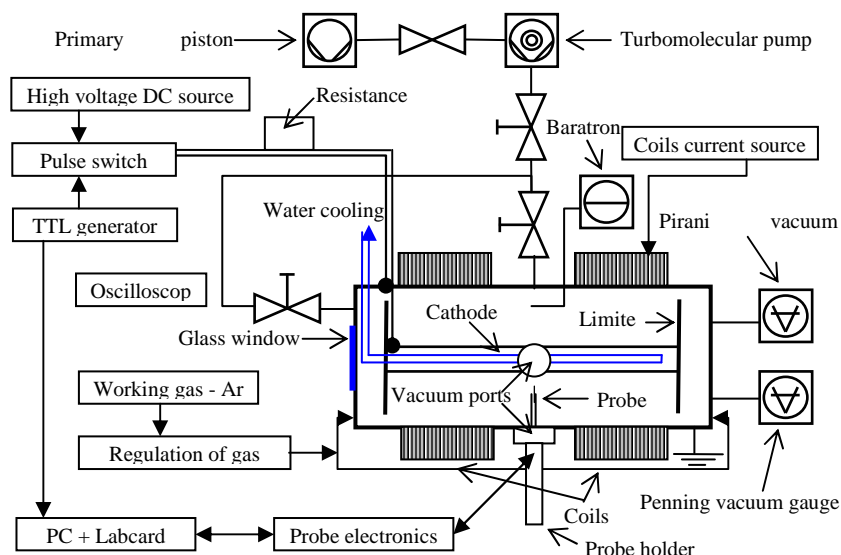


Figure 1: The scheme of pulsed cylindrical magnetron

and homogeneous magnetic field has axial direction and is created by couple of water cooled coils powered by stabilized power supply. The high-vacuum chamber is pumped by oil-free pumping system down to the ultimate pressure in the order of  $10^{-3}$  Pa. During the discharge operation the argon continuously flowed through the system with the flow rate of about 1 sccm. The pulsed discharge was operated at the pressures from 1 to 10 Pa. The magnetic field was kept at 10 mT where the fluctuations mentioned in [i] and studied in [ii,iii] were negligible and the discharge is stable. The pulse voltage ranged from 600 to 1000 V with the duty cycle 10 to 20% and the repetition period of 1 ms.

Measurements were performed using the cylindrical Langmuir probe 0.1 mm in diameter and 3 mm in length mounted on radially movable feedthrough and positioned axially in the centre of the system. The probe orientation was perpendicular to the magnetic field and together with its low value of 10mT it ensured negligible effect on electron probe current collection. Probe characteristics were acquired using PC labcard with the A/D converter sampling rate of 2 MS/s and resolution of 14 bits using the galvanically isolated and battery powered

electronics. The measurement of the probe current was performed using the current-voltage converter. During the probe measurements the probe voltage was changed gradually in small steps and for each value the time dependence of the probe current was recorded synchronously with the voltage pulses on the cathode. Consecutively the current-voltage characteristics in dependency on the time from the start of the voltage pulse had been obtained. Typically 2000 of probe characteristics with the time spacing of  $0.5 \mu\text{s}$  were collected. Therefore not only the probe data acquisition but also the evaluation of plasma parameters had to be performed automatically. Software written in Agilent VEE at first determined the floating and plasma potentials from the zero cross and zero cross of the second derivative of the probe characteristics respectively. The electron density  $n_e$  was calculated from the saturated electron current using the OML theory. The electron temperature was evaluated from the slope of electron retarding current.

The observed electron densities at the end of the pulse were greater than  $1 \times 10^{17} \text{ m}^{-3}$  what exceeded the values obtained in continuous regime by more than one order of magnitude, see Fig.2. A very rapid rise of electron temperature during the first  $10 \mu\text{s}$  up to the values  $T_e = 3 \text{ eV}$  was followed by approximately exponential decay in the remainder of the pulse. Plasma potential was measured by Langmuir probe technique as well as directly by strongly emitting emissive probe technique and the results were compared. The results were presented in the SPPT conference in Prague [iv], in ICPP conference in Fukuoka, Japan and in the International Balkan Workshop of Applied Physics in Constanta, Romania. The latter presentation was submitted as a manuscript to Journal of Optoelectronic and Advanced materials [v]. No intellectual property has been generated.

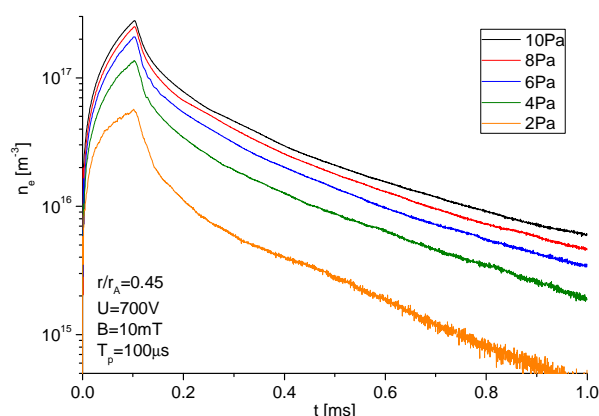


Figure 2: Time dependence of electron density at argon pressure from 2 Pa (bottom) to 10 Pa (top line).

During 2008 there appeared also the publication concerning the emissive probe mentioned in the last report [vi]. In this work among others the effect of overestimation of the plasma potential by a strongly emitting probe was discussed and the experimental data obtained in cylindrical magnetron were compared with a theoretical model.

### References :

- [i] E. Passoth, et al., J. Phys. D: Appl. Phys. 30 (1997) 1763.
- [ii] O. Bilyk, et al., Vacuum 76 (2004) 437.
- [iii] O. Bilyk, et al., Contrib. Plasma Phys. 46 (2006) 361.
- [iv] J. Klusoň, P. Kudrna, I. Picková, M. Tichý, Langmuir Probe Diagnostic of Pulsed Cylindrical Magnetron, Proc. 23rd Symposium on Plasma Physics and Technology, June 16-19, 2008, Prague, Czech Republic, J. Khun, V. Kříha, J. Píchal, M. Píchal, Eds., ISBN 978-80-01-04030-0, page 155.
- [v] P. Kudrna, J. Klusoň, I. Picková, M. Tichý, A Diagnostic Study of DC Discharge In Cylindrical Magnetron in Pulsed Regime, Journal of Optoelectronic and Advanced Materials, submitted.
- [vi] A. Marek, M. Jílek, I. Picková, P. Kudrna, M. Tichý, R. Schrittwieser, C. Ionita, Emissive Probe Diagnostics in Low Temperature Plasma - Effect of the Space Charge and Variations of Electron Saturation Current, Contrib. Plasma Phys. No 5-7 48(2008)491-496.

## **Development of millimeter-wave reflectometry methods for the measurement of edge pedestal plasma in tokamak COMPASS-D**

*J.Zajac, F.Zacek, J. Vlcek*

In collaboration with:

*M. Manso, A. Silva, P. Varela, L. Cupido*, Association EURATOM- Instituto Superior Technico / Centro de Fusão Nuclear, Lisbon

*V. Kiseliiov*, Institute of Radiophysics and Electronics-Dep. of Quasioptics, Kharkov, Ukraine

*The IST/CFN Lisbon was agreed in 2006 to be the main supplier of the reflectometry system with the technical support of IPP Prague [1]. The reflectometry system for Compass was mainly designed to perform the relevant plasma density profile measurements in the pedestal region. Five individual reflectometers are supposed to measure the plasma density profile which corresponds to the frequency range 18-90 GHz. The additional requirement is using of the reflectometers as well as an experimental diagnostics for studies of the plasma turbulence.*

The realization of the reflectometry system was supposed in a close collaboration with IST/CFN during 2006 – 2009 [1]. Problems with the manpower in IST/CFN as well as with the financing of the project have not allowed us to keep the workplan so far. Therefore the primary achievement in 2008 was the solving of the financial support of the project.

IPP and CFN/IST decided in July 2008 to propose to the subvention in the frame of the EFDA task WP08-TGS-01-06: Role of turbulence and long-range correlations during the development of edge transport barriers. This is the important extension of the physical program for the reflectometry system which will result in the increased complexity of the system.

The reflectometry for the turbulence studies require to be based on the microwave synthesizers while the density profile measurement is based on fast sweeping homodyne reflectometers. Both microwave sources should operate in fast alternating regime during the plasma discharge. The new block scheme of transmitting and receiving part is in Fig. 1.

The reflectometry system consists of two parts. First part are the microwave electronics and data acquisition which will be provided by IST/CFN. The second part are band-combiners and quasi-optical antennas which are necessary to transmit and receive all five microwave channels (O-mode K, Ka, U and E frequency bands and one X-mode Ka frequency band). A band-combiner combines quasioptically the four O-mode beams and on X-mode beam into the one transmitting beam in the frequency range 18-90 GHz. The same combiner splits the fundamental beams from the receiving beam. Such a technique has been usual only in mm and submm wavebands so far, e.g. the new millimeter-wave access system has been proposed for the JET reflectometry system [3] in the frequency range 60-190 GHz.

In 2008 a possible provider of the band-combiners and the quasi-optical antennas was found in the Institute of Radiophysics and Electronics NAS of Ukraine (IRE NASU). They offered to develop the quasioptical part of the reflectometry system based on the metal-dielectric waveguides (MDW) [4]. During 2008 all the technical aspects of the combiners and antennas were clarified between IPP and IRE so as to be sure that the MDW devices fulfill the requirements.

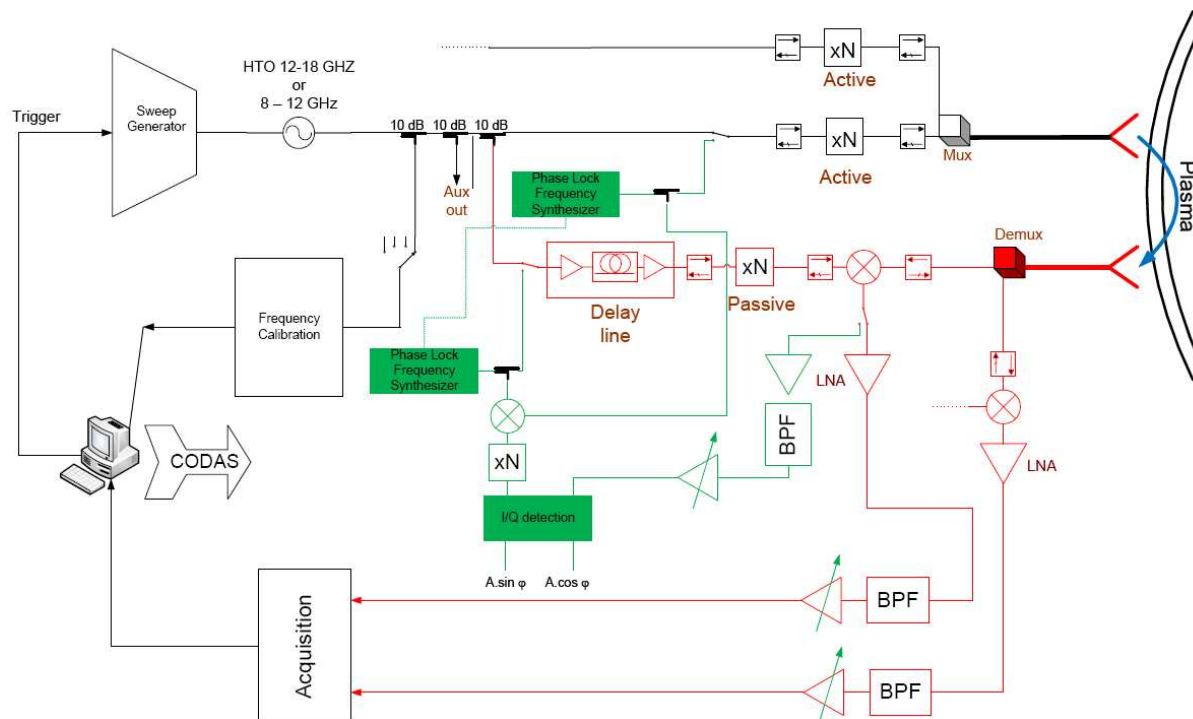


Fig. 1. New block scheme of transmitter and receiver

### References:

- [1] Framework Agreement for Scientific Collaboration between Institute of Plasma Physics - Association Euratom/IPP.CR and Centro de Fusão Nuclear, Instituto Superior Técnico - Association Euratom/IST
- [2] A.Silva et al., Ultrafast broadband FM-CW reflectometry system to measure density profiles on Asdex-U, *Review of Sci. Instr.*, 67 (12), 1996
- [3] L.Cupido et al., New millimeter-wave access for JET reflectometry and ECE, *Fusion Engineering and Design* 74 (2005) 707–713
- [4] V.I.Bezborodov, V.K.Kiseliov, B.N.Knyaz'kov, Ye.M.Kuleshov, M.S.Yanovsky, An Ultra-Broadband Quasioptical Polarization Attenuator for Metal-Dielectric Waveguides, *Telecommunications and Radio Engineering*, 51(2–3), 1997

## Beam Emission Spectroscopy system for COMPASS

V. Weinzettl

In collaboration with:

G. Anda, D. Dunai, D. Nagy, M. Berta, S. Zoletnik, Association EURATOM – HAS

A new Beam Emission Spectroscopy (BES) diagnostic for the COMPASS tokamak is under development by the Association EURATOM – HAS in a framework of the agreement between IPP Prague and KFKI RMKI. The BES system will consist of the beam injector with exchangeable ion source and the detection part based on an array of avalanche photo diodes.

Beam Emission Spectroscopy using accelerated neutral particle beams (Fig.1) became a routine technique for the determination of electron density profiles in fusion plasmas. The method is based on the fact that light emission from the neutral beam penetrating the plasma depends on plasma parameters. In the case of certain beam species, e.g. Li, Na, sensitivity on the electron temperature is small, thus the electron density profile primarily determines the beam light emission. Although the light intensity is not a local function of the electron density, numerical techniques were developed, which can determine the electron density distribution along the beam, if the light emission distribution is detected with appropriate spatial resolution.

BES techniques could be also used for the measurement of electron density fluctuations, which are connected to anomalous plasma transport. Investigations in the scrape-off layer (SOL) and edge plasma indicated strong radially dependent poloidal flows. A quasi-two-dimensional beam diagnostics was demonstrated on Wendelstein 7 – AS by rapidly scanning the beam poloidally, thus avoiding the need for a tangential observation system.

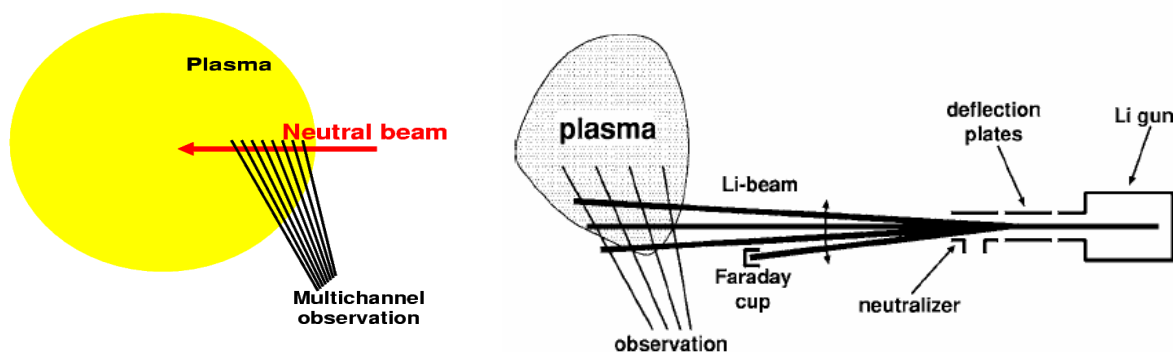


Fig. 1. Principle of BES (left) and quasi-2D BES diagnostic tool

BES allows:

- Measurement of radial profile of plasma density with  $\sim$ cm spatial and  $\sim$ 10 microsecond temporal resolution (standard density diagnostic tool).
- Characterization of density fluctuations in radial – poloidal plane on time scale characteristic for plasma turbulence (advanced BES diagnostic tool)
- Measuring poloidal flow velocities in the plasma.
- Studying the interaction between the complex system of turbulence, flows, mezo - scale structures and plasma profiles.

The BES system proposed for COMPASS would utilize all the available options developed during the past 10 years:

- Li or Na beam injection, BES observation for profile measurement with ~10 microsecond time resolution.
- quasi - 2D density fluctuation measurement with fast poloidally scanning beam.

Conceptual design of the gun was clarified and finished at the end of 2008. The BES system will be provided with an exchangeable ion source (Li, Na). Beam current will be about 5 – 10 mA. Beam simulations (CPO, Charged Particle Optics) show that an ionic beam with this current value can be focused to about 2 – 3 cm beam spot (diameter), see Fig.2. Detailed calculations for beam penetration depth were done by our own simulation code. Maximum energy of the beam will be 120 keV. The system will be able to reach a confined region of COMPASS plasmas also in H – mode.

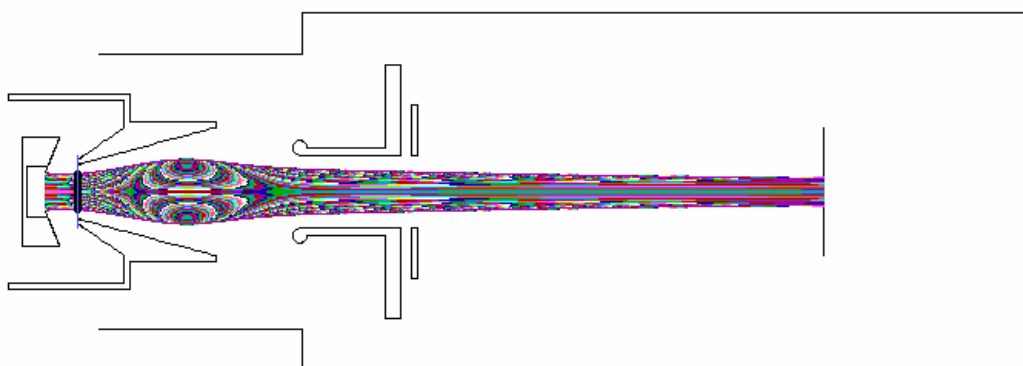


Fig. 2. Beam simulation with CPO code shows, diameter of the planned beam is 2 – 3 cm.

The observation system for the BES diagnostic on COMPASS is planning to be based on an array of avalanche photo diodes (APD), see Fig.3.

Parameters of the APD detector system follow:

- 85% quantum efficiency on wavelength 650 nm
- S8664-55 type APD with 5x5 mm<sup>2</sup> active surface
- 40 MHz cut – off frequency
- gain ~50 on 360V
- amplifier developed at RMKI – KFKI
- 1% rms noise in case of 10<sup>10</sup> total detected photons/sec
- thermally stabilized house

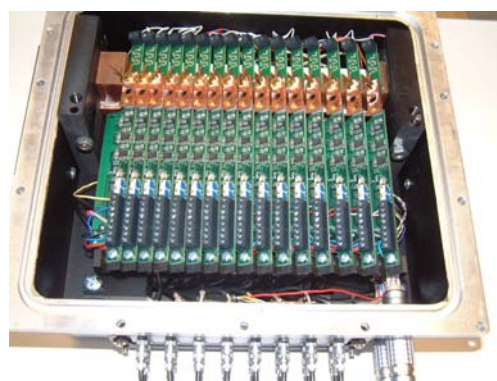


Fig. 3. APD detector system developed at RMKI – KFKI.

### References:

- [1] K. McCormick, et al., *Fusion Eng. Des.* 125 (1997) 34-35
- [2] S. Zoletnik, *Rev. Sci. Instrum.* 76 (2005) 073504
- [3] G. Anda, et al., *Fusion Eng. Des.* 74 (2005) 715–719

## Design and construction of fast tomography systems based on fast bolometric and SXR arrays for COMPASS

*V. Weinzettl, D. Naydenkova, D. Šesták, J. Vlček, R. Melich, D. Jareš, M. Vácha*

In collaboration with:

*V. Igochine*, Association EURATOM-IPP, IPP Garching, Germany

*D. Sarychev*, NFI RRC "Kurchatov Institute", Moscow, Russia

*Multi-channel spectroscopic diagnostics on the COMPASS tokamak comprising AXUV-based bolometers, soft X-ray (SXR) and visible light detectors will cover a wide spectral range of the core and edge plasma emission aiming to realize a fast tomography at microsecond time scales. The design of the special complex port plug combining all detection systems taken into account a strongly limited available space, a heat protection and a shielding during a cleaning glow discharge was finalized. All in-vessel components needed for bolometric and SXR measurements were manufactured, new electronic amplifiers were constructed and their connection with the data acquisition system was realized.*

A future application of two neutral beam injection heating systems on the COMPASS tokamak and expected local modifications of plasma parameters constricted a selection of the poloidal cross-section suitable for tomographic studies of the plasma radiation to the sector 6/7 of the diagnostic ports. There, four observation places are situated in nearly vertically symmetric manner. A small size of the corresponding ports, requirements for cooling during a vessel baking and a necessity of the shutter placement led to an optimization in a choice of the detectors and to a complex port plug design.

A fast time response of order of microseconds in combination with a good spatial resolution about 1-2 cm over the whole plasma cross-section will be reached by use of many-channels semiconductor detector arrays of the AXUV20 type (IRD Inc.) as bolometers, the LD35-5T (Centronic Ltd.) type as soft X-ray detectors, and the S4114 (Hamamatsu Photonics) type as visible light detectors, respectively. Furthermore, both the AXUV array of 20 channels and the LD35 array of 35 channels are small enough to fit well into the diagnostic ports.

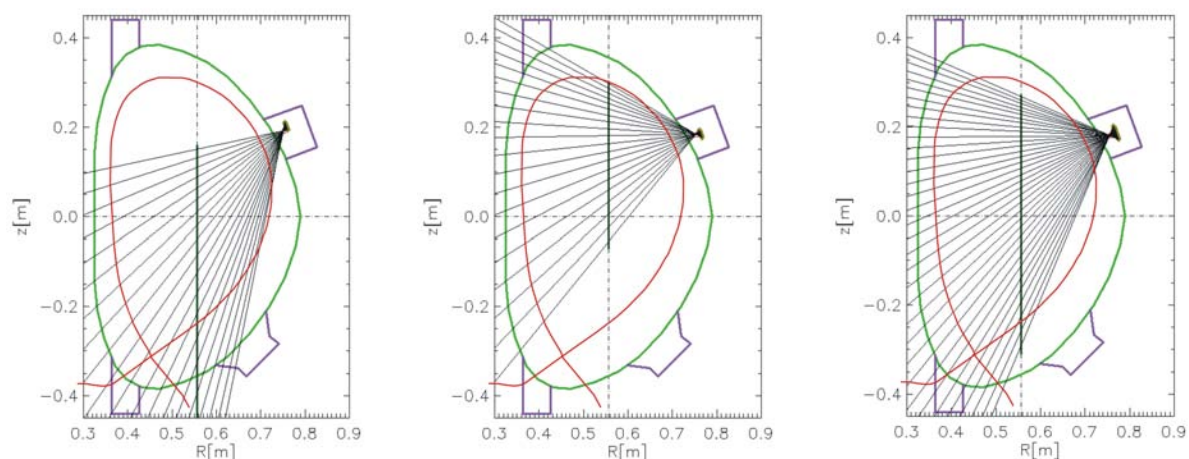


*Fig. 1: A coverage of the poloidal cross-section of the COMPASS tokamak by chords of the detectors of AXUV 1 (left), AXUV 2 (middle) and SXR (right). The violet rectangles indicate the diagnostic ports, the green oval shows the vacuum chamber and the red curve visualizes a probable plasma shape.*

A port plug design [1] was developed from a placement scheme of the detectors taking into account required observation angles (Fig. 1), and retaining an alternative of easy assemblage. The port plug (Fig.2) consists of two pieces. The first one is an inset which holds detectors, air slits, shutter, and also includes a cooling channel. The second piece is the NW100 flange containing two electrical feedthroughs, each equipped with 41 pins, one hole

for a rotary feedthrough (NW16 flange) intended as a shutter manipulator, and a hole for the NW35 viewport serving for visible light observations. Because of lack of space inside the inset, electrical signals measured by both the AXUV and SXR detectors will be guided out of vacuum, where they are amplified. From amplifiers, the signals are carried out by shielded cables (4 twisted-pair wires) to the data acquisition system.

The many-channel amplifier was designed and constructed (Fig.2) reaching a time constant about 1ms. A matching procedure of the gain of all channels was carried out giving its precision better than 1%. Afterwards, a relative calibration of the amplifier-detector complex was done using a halogen lamp. A sensitivity of the AXUV array differs from channel to channel by only 2%, except the edge ones deviating by about 50%. Similarly, all channels of the SXR detector differ by less than 10% with a wide plateau of nearly the same sensitivity for inner channels.

The above-mentioned observation locations will be shared with a visible light detection system [2] based on a registration of the light from a wide solid angle using a collimation system, located inside the diagnostic port, connected to a linear set of optical fibers. The second end of the fibers will be connected either to the HR2000+ spectrometer (Ocean Optics Inc.) with a low temporal resolution of few milliseconds covering a spectral range of 460-660 nm with a resolution better than 0.1 nm or to the 35-channel semiconductor detector array allowing fast spatially resolved measurements of the light restricted by interference filters.



Fig. 2: Design of the port plug (top): vacuum side (left) with cooling channel (1) and mounting hole (2), atmospheric side (right). Partially assembled manufactured parts of the port plug and amplifiers (bottom).

### References:

- [1] Šesták D., et al., 25th Symposium on Fusion Technology, Rostock, Germany, 15-19 September 2008, accepted for print in *Fusion Eng. Des.* (2009)
- [2] Naydenkova D.I., et al., WDS 2008, Prague, Czech Republic, 3th June - 6th June, 2008, *Proceedings of Contributed Papers Proceedings of the 17th Annual Conference of Doctoral Students - WDS 2008, Part II*, pp.100-104

## Development of fast digital video camera system for machine control, plasma overview and turbulence measurements

V. Weinzettl, M. Hron

In collaboration with:

M. Berta, G. Veres, T. Szilveszter, A. Szappanos, S. Zoletnik, Association EURATOM – HAS

*A new visible range video diagnostic has been developed by the Association EURATOM – HAS in a framework of the agreement between IPP Prague and KFKI RMKI and installed on the COMPASS tokamak. The system contains mechanical engineering parts like a port plug, a cooling, a camera holder and appropriate optics with variable scaling and focusing possibilities, and a fast visible range camera of the EDICAM (Event Detection Intelligent Camera – produced by the Hungarian Association) type with advanced features, adapted to locale conditions and requirements. The diagnostic system is equipped by a modular software package with graphical user interface and own database system for data storage.*

EDICAM [1] is a fast video camera system developed for a use with plasma physical experiments, considering triggering and frame rate requirements of such measurements, see Fig.1. The ‘fast’ epithet means up to 100 kHz temporal resolution with a reduced frame size. A built in image processing and an adaptive sensing functionality were also taken into considerations during the development.

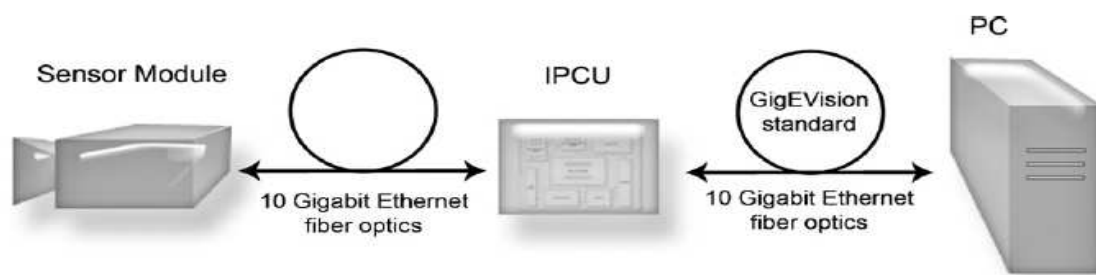


Fig. 1. Concept of the EDICAM system

In current state, the camera is capable to reach a speed that can be found in the built in LUPA 1.3 Megapixel monochrome CMOS sensors specification [2]. The fast analogue and digital hardware components are being installed and tested right after some debugging period. The raw data is 12 bit sampled, and digitalized with appropriate ultra fast data acquisition cards [3] developed by an external company. The data is stored with DMA access and collected right after every shot. The raw data and the compressed well formed jpeg formats are stored at the data acquisition PCs locale MySQL database, and are available for post processing. The data access scripts will be written for MATLAB and accompanied with advanced image processing tools.

A new software interface have been designed and tested for providing all camera features in a user friendly graphical interface. The software package contains the updated Linux driver for the data acquisition card and for the DMA drivers. Both of them are adapted for most up to date 2.6.27 Linux kernels. A C library is available for communicating with the driver. All user interactions are mediated by an HTTP based WEB Server. At the highest level a Java Spring framework based server application answers for all the incoming requests. This server has a built in a Real-Time Streaming Protocol based live video motion layer, a modular and extendable image processing toolset, a Java Native Interface for communicating with the

internal C library, to being able to pass on the requests for the camera hardware and the database access layer.

A fully functional prototype of the camera mounted with especially designed optics on a newly constructed holder (Fig.2) has been operating on the COMPASS tokamak since December 2008 (Fig.3).

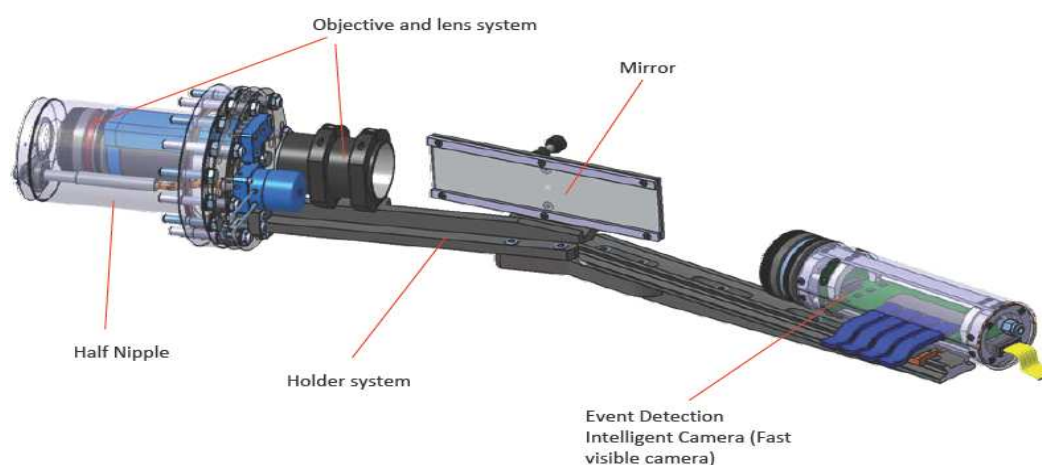


Fig. 2. Mechanical design of the Fast Camera System

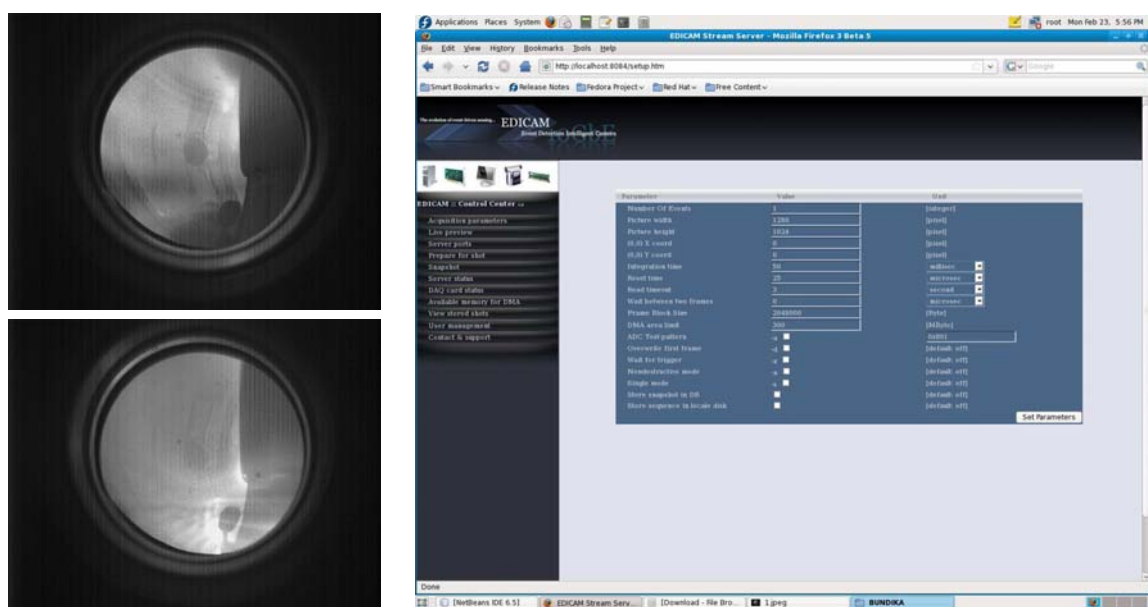


Fig. 3. Frames taken by the Fast Camera System during COMPASS tokamak discharges (left). WEB based software for a remote control of the Fast Camera System (right).

### References:

- [1] A. Szappanos, et al., *Fusion Eng. Des.* 83 (2008) 370-374
- [2] Cypress Semiconductor Corporation; *LUPA-1300 1.3MPxl High Speed CMOS Image Sensor*, Document Number: 38-05711, 2007
- [3] <http://alice-proj-ddl.web.cern.ch/alice-proj-ddl/>

## Thomson scattering diagnostic development on COMPASS

*P. Bílková, M. Aftanas, P. Böhm, V. Weinzettl, R. Melich, D. Šesták, J. Stöckel*

In collaboration with:

*M. Walsh, R. Scannell, G. Naylor, M. Dunstan* Association EURATOM-UKAEA, Culham Science Centre, MAST, Electron Kinetics Group

*Thomson scattering diagnostic (TS) will play an important role on COMPASS since it provides electron temperature ( $T_e$ ) and electron density ( $n_e$ ) profiles. Measurements of profiles will be performed in two regions – the first focusing on core plasma with spatial resolution of 10 mm and viewing 24 cm along the laser beam, the second focusing on the edge plasma region with high spatial resolution of 3 mm and viewing 10 cm along the beam line. For both regions, one common laser beam in vertical direction will be used. Scattered light will be collected using optics located inside one horizontal port for the core plasma region and one edge port for the pedestal region.*

The feasibility study is based on requirements for TS diagnostics to fulfil the scientific programme of COMPASS. Several feasible options have been identified and compared, taking into account risks, manpower and budget limits and the required temporal resolution [1,2,3]. Advanced systems and possible upgrades have been discussed and price estimates together with timescale for different options have been worked up [2].

Later on, main decisions have been made. According to access it has been decided to fire laser vertically. We based our system on Nd:YAG (1064nm)/APD technology. Scattered signal is collected by collection optics (two separate objectives, one for core and one for edge plasma region) and transmitted via optical fibers to polychromators. Due to budget limits, each polychromator detects signals from two spatial points by means of duplexing (using delay between signals by different length of optical fibers). The design of polychromator is based on polychromators used for TS diagnostic on MAST [4]. Scattered light follows zig-zag path (Fig.1). Spectral decomposition is done by means of set of spectral filters designed particularly for given temperature range and accepted error bars. Data acquisition is performed by using fast analog digital convertors (ADCs). Recently, however, a complementary option is being explored for the core plasma TS diagnostic – integration of signal. This considerably cheaper solution would allow us to use spared funds for developing a higher number of polychromators and thus not to use the duplex solution.

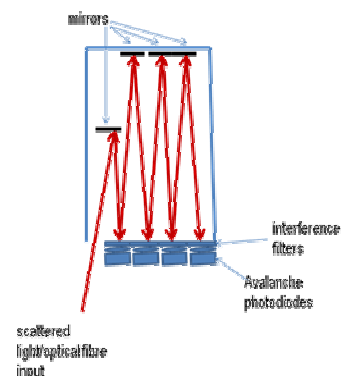


Fig. 1. Schema of polychromator

Designs of both laser beam path and mimic laser beam path have been proposed (see Fig.2). Laser is placed outside the tokamak hall, the laser beam path is 20 m long and has to be properly designed to ensure good beam parameters in the region of TS measurements and safety of the system. Most convenient path was chosen, beam is led under the floor, avoiding collisions with devices around tokamak. The beam is focused by a lens and enters the tokamak vessel from bottom, beam dump consisting of steel blades is placed on the top of the tokamak vessel. In the laser room outside the tokamak hall, laser beam mimic path is designed. It represents the actual beam path, the beam parameters can be adjusted and verified before the TS measurements in a convenient and safe way, from point of view of maintenance and protection of optical components.

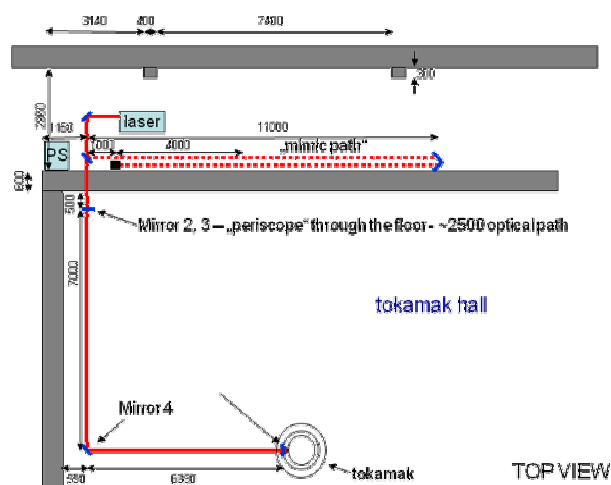


Fig. 2. Laser path design proposal

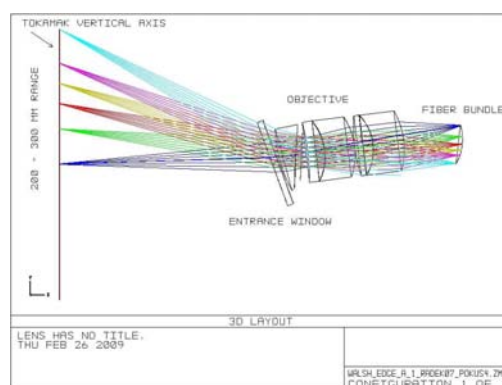


Fig. 3. ZEMAX simulation, collection optics for edge TS

The size of plasma region covered by TS diagnostic has been decided and is based on knowledge of plasma shapes on COMPASS-D tokamak in Culham (Compass-D Technical Specification, UKAEA). The edge TS will cover 200-300 mm above the midplane in the vertical direction with spatial resolution of 3mm. The core TS will look at plasma region starting from 30 mm below the midplane up to 210 mm above it and with spatial resolution of 10 mm. The design of collection TS optics is under development by ZEMAX software (see proposal of edge TS collection optics design in Fig. 3). The edge plasma is observed through the port with maximal width of 100 mm. The observed range lies at vertical axis in height of 200-300 mm above the midplane. Because the port is inclined by  $20^\circ$  with respect to a horizontal axis of the tokamak, the field of view of the objective needs to be approximately  $66^\circ$  in order to see the desired range of plasma. The design of collection optics, optical fiber arrangement and the laser beam size are connected and each item has to match others. Optical fibers are arranged in a hexagonal package, with rectangular shape of cross section on the machine side and circular shape on the polychromator side. All items are being designed to use optimally etendue of original MAST polychromators  $1,81 \text{ mm}^2\text{sr}$  [5]. The proper selection of spectral filters (the bandwidth and the central wavelength) is under development now as well as relevant error calculations (Fig. 4).

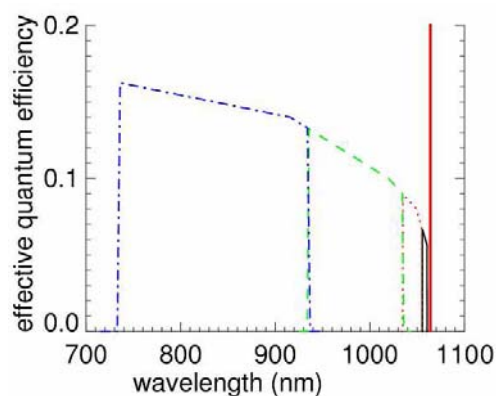


Fig. 4. Spectral filter choice proposal

## References:

- [1] P. Bílková et al., *17<sup>th</sup> HTPD, New Mexico*, May 11-15, (2008), 88 (abstract)
- [2] P. Bílková, Report Mobility, EURATOM, June 2008
- [3] D. Šesták et al., *Fusion Engineering and design* (2009), article in press
- [4] R. Scannell et al., *Review of Scientific Instruments Vol. 79, Issue 10*, (2008), 10E730
- [5] R. Scannell, thesis, UKAEA (2007)
- [6] P. Bílková, Report Mobility, EURATOM, November 2008

## Atomic Beam Probe system for COMPASS

*J. Havlíček, V. Weinzettl*

In collaboration with:

*M. Berta, A. Bencze, G. Veres, G. Anda, S. Zoletnik, Association EURATOM – HAS*

*A new method for the measurement of magnetic field fluctuations and the poloidal magnetic field in the outer regions of COMPASS tokamak plasmas is introduced as an extension of the Beam Emission Spectroscopy (BES) system by collecting the ions stemming from beam ionization. Therefore we call it Atomic Beam Probe diagnostic (ABP). The BES system is already being manufactured by KFKI RMKI and it is planned to be operated by Li and Na beams. The extension will require operating it with somewhat heavier ions and/or at higher energies.*

Heavy Ion Beam Probes (HIBP) have been used to measure density and potential fluctuations in many devices to understand fluctuation – driven transport [1, 2, 3]. Another capability of HIBP is its sensitivity to magnetic field [4, 5]. Therefore it is an exceptional method to access local information on magnetic field directly in the interior of high temperature plasmas. An idea of the ABP system is to overcome the most serious difficulty of HIBP systems, namely the difficulty in accessing the plasma by an ion beam. In our scheme neutral atoms are injected, therefore they can easily be lead along a straight horizontal diagnostic port. After ionization ions will be collected in a vertical diagnostic port located at the same poloidal cross-section. Using alkali atoms the second ionization potential is much higher than the first one; therefore ionization of the ion beam should be negligible. The typical current of an alkali diagnostic beam [6, 7] is about 3 orders of magnitude higher than the conveniently measurable ion currents; therefore we see no difficulty in detecting the ions.

The ABP system on COMPASS will operate similarly to HIBP and its aims can be following:

- measurement of magnetic field fluctuations in order to assess the relevance of electromagnetic turbulence.
- get information on the plasma current profile.
- measurement of density profile

BES and ABP system for COMPASS - D

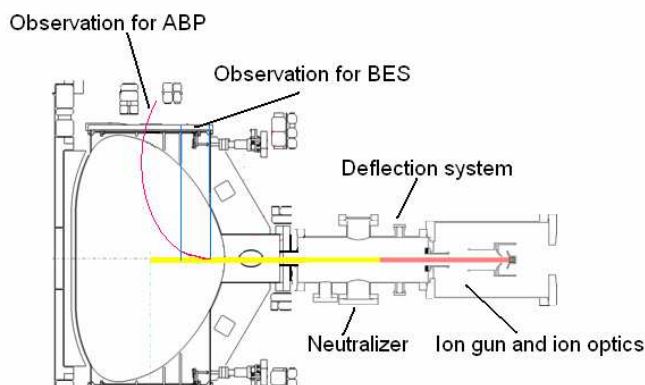


*Fig. 1. Conceptual design of the BES and ABP systems for the COMPASS tokamak.*

Atoms ionized at different radii along the beam arrive at different positions in the exit port, where, at the first approximation, the ion current is proportional to the local plasma density at the point of ionization. The poloidal magnetic field moves the ion beam toroidally, therefore the two-dimensional measurement of the ion current in the exit port can theoretically reveal information on both the density and magnetic field profiles. Additionally, the density profile can also be determined from the standard BES measurement [6, 7].

Figure 1 shows a conceptual design of the ABP system. An ion beam is accelerated by an ion optic system and neutralized in a gas cell. The neutral beam enters the plasma and subsequently it becomes ionized. A representative ion trajectory is depicted in the figure showing ions arriving in the vertical port.

Motion of charged particles in a magnetic field cannot be calculated in a general case analytically. Therefore an appropriate numerical scheme has to be chosen to solve the problem. Here the Runge – Kutta method is used, and seems to be precise enough for our initial calculations. Figure 2 shows a result of the calculation where 53 keV Rb ions are started from one radial location at the plasma edge and followed into the upper port.

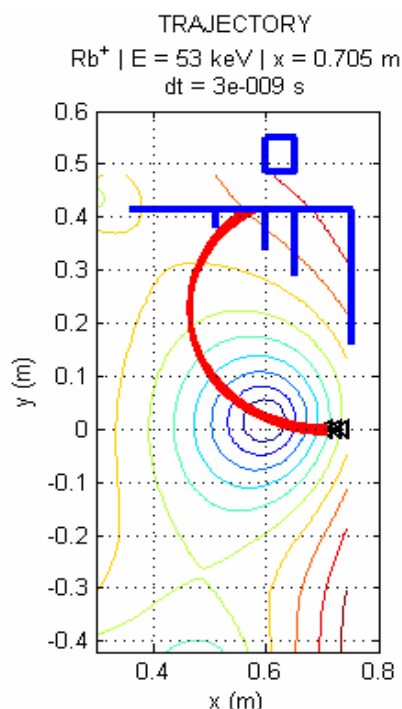


Fig. 1. Trajectories of test particles of Rb<sup>+</sup> with initial energy 53 keV. The ionization is supposed to take place at  $x=0.705$  m, near to the separatrix in typical discharges in COMPASS. Time discretization step has been chosen 3 ns, toroidal magnetic field is 1.2 T and the plasma current is 170 kA. Magnetic field shape was calculated by the EFIT code.

## References

- [1] T.S. Green, G.A.Proca, *Rev. Sci. Instrum.* 10 (1970) 41.
- [2] Y. Hamada et al., *Nuclear Fusion* 4 (1996) 36.
- [3] A.A. Chmuga et al., 28th EPS Conf. on Contr. Fusion and Plasma Physics, Funchal 2001, ECA Vol, 25A, 2157.
- [4] A. Shimizu, A. Fujisawa et al., *Rev. Sci. Instrum.* 76, (2005) 043504.
- [5] A. Fujisawa et al., *Plasma Phys. Control. Fusion* 49 (2007) 845.
- [6] K. McCormick, et al., *Fus. Eng. Des.* 125 (1997) 34-35.
- [7] S. Zoletnik, et al., *Rev. Sci. Instrum.* 76 (2005) 073504.

### 3. Development of concept improvements and advances in fundamental understanding of fusion plasmas

#### Contributions to study of interaction of magnetic perturbations with rotating plasmas

*P. Cahyna, R. Pánek, L. Krlín*

In collaboration with:

*M. Bécoulet, G. Huysmans*, Association EURATOM-CEA Cadarache, France

*E. Nardon*, EURATOM/UKAEA Fusion Association, Culham Science Centre, UK

*K. Shaing*, University of Wisconsin, Madison, USA; National Cheng Kung University, Tainan, Republic of China

*Resonant magnetic perturbations (RMPs) are currently in the focus of interest because of their potential to control Type I ELMs, as demonstrated on the DIII-D tokamak. Using those perturbations, the team working on DIII-D was able to produce ELM-free H-mode discharges. This result is important for the design of ITER, because of the negative impact of type I ELMs on the material of plasma-facing components.*

The design of RMP coils for ELM suppression on ITER [1] has been relying on the vacuum field approach where the magnetic field is taken as a superposition of the equilibrium tokamak field and the vacuum field by the perturbation coils and the effect on ELMs is supposed to be caused by the field line stochastization following from the vacuum perturbation field. The coil design is then optimized to produce the same relative extent of the stochastic region as predicted by the modeling for the successful DIII-D experiments. The vacuum approach is however only a first approximation to the true perturbation field in the plasma. It is expected that the plasma response may modify the perturbation field and vice-versa, the perturbation may modify plasma parameters, mainly by braking its toroidal rotation. Both effects are due to generation of “eddy currents” on resonant surfaces which oppose the perturbation and brake the plasma [2]. In addition, the perturbation may brake the plasma rotation globally by the mechanism of Neoclassical Toroidal Viscosity (NTV) [3]. This effect is caused mainly by non-resonant components of the perturbation field. Toroidal rotation braking might be an issue for ITER if RMP coils are used to suppress ELMs, as toroidal rotation has stabilizing effects.

The COMPASS tokamak is equipped with a set of perturbation coils which are able to produce RMPs similar to those used to suppress ELMs on DIII-D. We are planning experiments to help clarifying the mechanism of this promising, yet still poorly understood ELM control method, using the existing COMPASS coils. As a first step, we used the code ERGOS to perform the modelling of the vacuum field in a similar manner as it was done for the DIII-D and JET experiments and the design of ITER coils. Our goal was to verify if the existing COMPASS coils are able to satisfy the criterion of stochastization by the vacuum field which was derived from the DIII-D experiments, and thus if they are suitable for such research. The coils are very flexible because of the many possible wirings of the circuits and because some coil segments have adjustable positions, so our goal was also to determine the optimal coil configuration for ELM mitigation experiments. We did the vacuum modeling for several predicted COMPASS equilibria, which differ by geometry (SND or SNT) and magnetic field (2.1 or 1.2 T). We showed that for all the equilibria considered the existing RMP coils are able to satisfy the required criterion with realistic currents. We determined the optimal coil configurations and showed that for all the equilibria the coil positions can remain

the same. This result is of practical importance for the future experiments, as it will not be necessary to adjust the coils between shots [4].

As explained above, the vacuum approach is incomplete and shall be complemented by a self-consistent model of interactions between plasma and perturbation field, which is significantly more complex and require a MHD treatment of the plasma. One possible approach is using the reduced MHD equations, which are a simplification of the full MHD equations using the fact that the plasma is strongly magnetized in the toroidal direction. In CEA Cadarache a code for solving reduced MHD equations was developed by Guido Huysmans, Marina Bécoulet and Eric Nardon. It approximates the tokamak plasma as a straight cylinder with circular cross-section (cylindrical approximation) to simplify the computation by using the Fourier transform in poloidal and toroidal angles. The code includes toroidal plasma rotation and the neoclassical toroidal viscosity, which is calculated separately and given as an input. We applied this code to the predicted COMPASS equilibria. As a result we obtain the perturbation field modified by the plasma response. The simulations showed that rotation has a strong influence on islands near the plasma center which are nearly totally suppressed, and much weaker for edge islands, where we can still expect island overlap and field line stochastization. The comparison of Poincaré plots showing the islands for a case without and with toroidal rotation is shown on fig. 1.

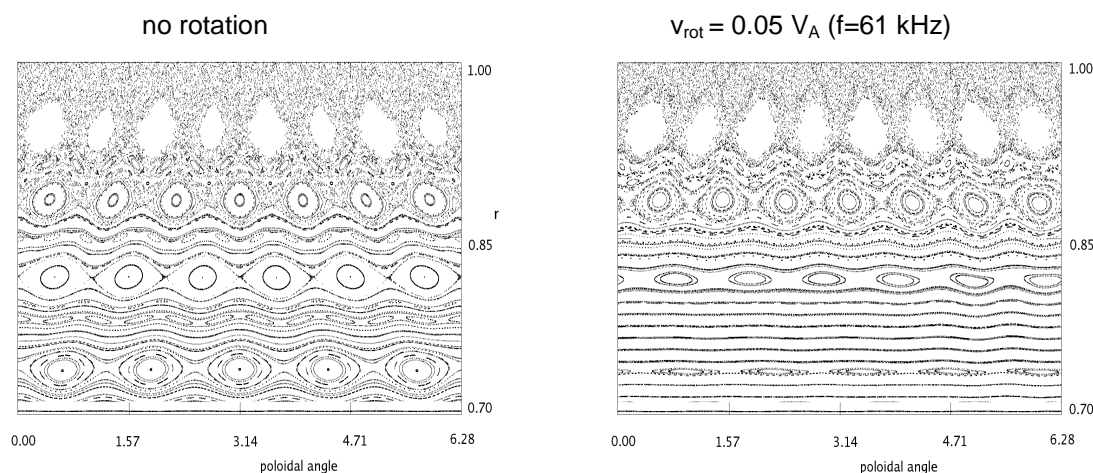


Fig. 1 Comparison of Poincaré plots of field lines without and with toroidal plasma rotation

We have also participated in the studies of RMP-plasma interaction in general and the modeling for ITER [5]. Our most important result is the proof of divergence of a formula for the neoclassical toroidal viscosity given in [3] for the so-called  $\nu$  regime. It is a consequence of neglecting collisions in the trapped-circulating particle boundary. This result was published in [6,7] together with the corrected formula derived by K. Shaing.

Our future work will be aimed at improving the reduced MHD simulations with more precise plasma profiles obtained from modelling and eventually from the experiments on COMPASS. We will also include realistic plasma rotation, which has been so far an unknown.

### References:

- [1] M. Bécoulet et al., *Nucl. Fusion* **48** (2008) 024003.
- [2] R. Fitzpatrick, *Nucl. Fusion*, **5** (1998) 3325.
- [3] K. Shaing et al., *Phys. Plasmas* **10** (2003) 1443.
- [4] P. Cahyna et al., *Proc. 22nd IAEA Fusion Energy Conference* (2008), paper TH/P9-7.
- [5] M. Bécoulet et al., *Proc. 22nd IAEA Fusion Energy Conference* (2008), paper TH/2-1Ra.
- [6] K. Shaing et al., *Phys. Plasmas* **15** (2008) 082506.
- [7] K. Shaing et al., *Phys. Plasmas* **15** (2008) 082505.

## EBW Power Deposition and Current Drive in WEGA Comparison of Simulation with Experiment

*J. Preinhaelter, J. Urban*

In collaboration with:

*H.P. Laqua*, Max-Planck-Institut für Plasmaphysik, EURATOM Ass. Greifswald, Germany

*L. Vahala*, Old Dominion University, Norfolk, VA 23529, USA

*G. Vahala*, College of William & Mary, Williamsburg, VA 23185, USA

*Electrostatic electron Bernstein waves (EBW) are studied numerically and compared to experimental results on the WEGA stellarator. Using the WEGA antenna, the two O-/X-mode radiation lobes are modelled by sets of rays with intensity proportional to the measured radiation pattern. After projecting these rays onto the plasma periphery, a full wave adaptive mesh solver of the cold plasma equations determines the O-X-EBW mode conversion efficiency around the upper hybrid resonance. From the roots of the EBW dispersion relation, ray tracing is performed to determine the power absorption on the 1<sup>st</sup> or 2<sup>nd</sup> cyclotron harmonic and current drive, assuming the Fisch-Boozer mechanism. Detailed simulations are performed on specific WEGA equilibria and its antenna launch of 2.45 GHz waves, with excellent agreement with experiment. In particular, the off-axis power deposition and the outward shift of the absorption maximum produced by increasing the magnetic field can only be explained by the presence of a hot electron component, which permits wave absorption at the 2<sup>nd</sup> harmonic near the plasma periphery. Moreover, the simulations also reproduce the current density reversal at the plasma centre for low magnetic fields and that this reversal is destroyed when larger magnetic fields are employed.*

WEGA is a medium-sized classical  $\ell = 2$ ,  $m = 5$  stellarator, with major radius 72 cm and maximum minor plasma radius 11.5 cm [1]. It consists of five identical sections, each spanning  $72^\circ$  in the toroidal direction. The plasma is generated by using up to 26 kW of 2.45 GHz ECRH. A standard steady state discharge lasts to 30 s using either a Hydrogen, Helium or Argon plasma [1]. A  $\varnothing = 83$  mm waveguide antenna with two slots in the sidewall has shown the best heating performance. Typically, for WEGA plasmas generated by the 2.45 GHz ECRH, there are two electron components—cold bulk electrons and hot tail electrons. The antenna is positioned outside the LCFS where the plasma density is below the cutoff density. This is consistent with the O-X-EBW conversion mechanism, which requires that

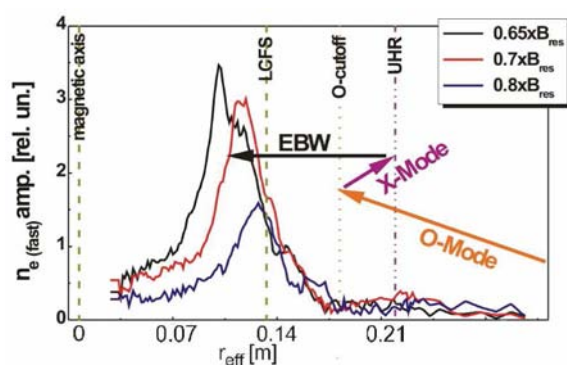


*Fig. 1: Experimental power deposition profiles for different magnetic field strength, as determined from probe measurement.*

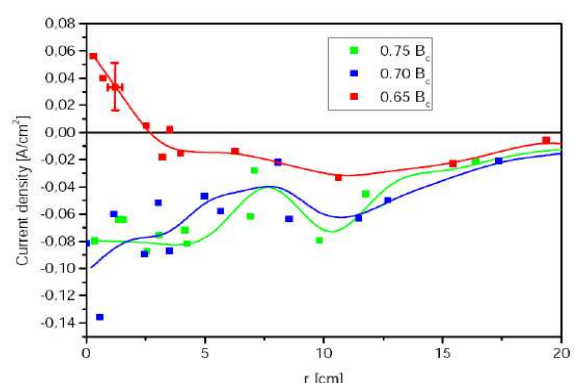


*Fig. 2: Experimental current density profiles measured by a movable Rogowski coil for 6 kW injected modulated power.*

waves are incident from an underdense region to the UHR and plasma resonance region. EBW current drive, which was first predicted by our simulations [2], was successfully detected on the WEGA. With 6 kW of constant power and 6 kW of modulated power

( $\sim 70\text{Hz}$ ), a counter (opposite to the direction of the toroidal magnetic field) current  $I_\phi \sim -50\text{ A}$  was detected.

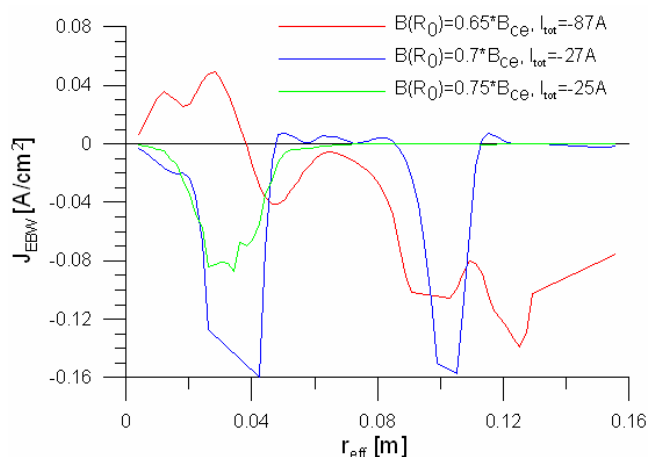
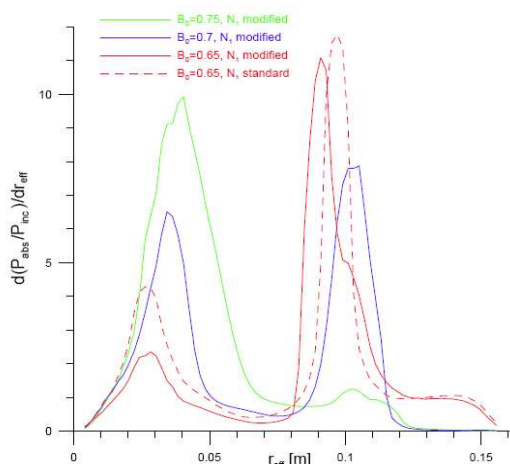


Fig. 3:  $B_0$  scan of the deposited power.  $Z_{\text{eff}} = 1$ , Fig. 4: Profiles of current density -  $B_0$  scan. 10% Ar neutrals.

In the WEGA experiment, the off-axis heating on the 2<sup>nd</sup> harmonic was prominent and the deposited power was clearly related to the existence of hot electrons. In our first simulations, we assumed a hot density profile independent of  $B_0$  and with a broad peak coinciding approximately with the detected experimental power deposition peaks. However, this did not yield a good agreement with experiment. To reach a better agreement, the  $n_1$  profiles were iteratively modified to be consistent with the simulation results. As the fast electrons are generated by the ECRH itself, the  $n_1$  peak must coincide with the power deposition peak for a particular  $B_0$ . The simulations also show a significant central deposition caused by the absorption on the 1<sup>st</sup> harmonic. However, the central deposition was not investigated in the experimental results shown in Fig. 1.

Very interestingly, a current reversal at the plasma centre was observed for  $B_0 = 0.65B_{ce}$ . Our simulations recovered the same current reversal behaviour at the plasma centre for this field (see Fig. 4). The peaked character of the current profiles results from the peaked power deposition (i.e., the generated current is localized to those positions at which the power is absorbed). The experimental profiles are smoother than those from our simulations—but this smoothing is probably caused by the finite size of the probe and the time averaging.

### References:

- [1] Otte M. et al., AIP Conference Proceedings, 2008. **993**: p. 3-10.
- [2] Preinhaelter, J., Urban et al., AIP Conference Proceedings, 2007. **933**: p. 343-346.

## Coupling of the AMR and the LUKE codes

*J. Urban, J. Preinhaelter*

In collaboration with:

*J. Decker*, Association EURATOM-CEA Cadarache, France

*Electron Bernstein wave (EBW) physics can be simulated with a linear code capable of ray-tracing and mode-conversion calculation as far as low power applications, i.e. emission or low-power heating and current drive, are concerned. AMR (antenna—mode-conversion—ray-tracing) has been created at our institute for these calculations. However; higher-power applications necessitate quasi-linear approach to solve the Fokker-Planck equation. For this reason, it was decided to couple AMR with the LUKE code to create a state-of-the-art EBW simulation suite. Presently, a basic coupling of the two codes is working. AMR can provide necessary inputs for LUKE (in data files), which LUKE can conveniently read. Test cases were successfully simulated validating the consistency of the transferred data and proving the functionality. More integrated interface is foreseen. LUKE is also running on IPP Prague computer systems.*

Our goal was primarily to enable coupled antenna, mode conversion, ray-tracing and Fokker-Planck simulations of electron Bernstein waves (EBWs). Our AMR code (Antenna—Mode-conversion—Ray-tracing) [1, 2] is capable to simulate the receiving/emitting antennas used for EBWs, the efficiency of the mode conversion between the vacuum/cold-plasma O- and X-modes and the EBWs as well as the propagation of the EBWs through a plasma using the ray-tracing method. This code is appropriate for emission and low-power regimes when linear damping is valid. However, to model high power EBW heating and current drive, quasi-linear treatment via a Fokker-Planck code is necessary. It was proposed by CEA and IPP Prague to couple the LUKE Fokker-Planck code [3] and the AMR code. Such coupling is beneficial for both sides involved as AMR provides a mode-conversion calculation, which is presently lacking in the LUKE/C3PO wave modelling suite developed at CEA.

To run LUKE with AMR data, several inputs have to be provided—the plasma configuration, i.e. the magnetic equilibrium and the electron density and temperature profiles, and the rays' data, consisting of frequency, power, trajectory and wave vector development, and also the beam parameters. It was decided to provide these data in files, which is the easiest option to implement yet it provides enough performance and flexibility. Several functions have been created in AMR for creating these data files in a suitable format for LUKE (which is implemented in Matlab; therefore, a Matlab-friendly format was chosen). Options specifying whether to output these files along with some parameters (e.g. the number of data points) have been added to the AMR main input (configuration) file. As a result, there exist a transparent way how AMR create the inputs for LUKE.

At the LUKE side, functions for data import with similar functionality were already present and thus the reading of the input files could be implemented straightforwardly. Careful checks were performed, e.g. by independently solving the dispersion relation, to guarantee that the plasma configurations and the ray-tracing data are all consistent. Particularly difficult was to unify the equilibria. AMR uses 2D splines of the poloidal flux function  $\psi$  in Cartesian ( $R, Z$ ) coordinates ( $R, \varphi, Z$  being cylindrical coordinates), while LUKE uses  $\psi, \theta$  coordinates ( $\theta$  being the poloidal angle). In order to keep consistent the second derivatives of  $\psi$ , which are needed in ray-tracing, a large number of data points must be exported.

After several test cases, particularly with COMPASS configuration, could be successfully simulated. AMR provided all necessary inputs for LUKE, which then calculated the quasi-linear damping and the driven current. This version of LUKE has been installed at IPP Prague computers, where it is maintained using the CVS system.

**References:**

- [1] J. Preinhaelter, et al., *AIP Conference Proceedings* 933 (2007) 343
- [2] J. Urban, J. Preinhaelter, *J. Plas. Phys.* 72 (2006) 1041
- [3] J. Decker, A. K. Ram, Y. Peysson, *17th Topical Conference on Radio Frequency Power in Plasmas* (Clearwater, FL, USA, 2007)

## Implementation of the induced currents model in efit++ code

*J. Havlíček, J. Urban*

In collaboration with:

*L.C. Appel, D.G. Muir*

Euratom-UKAEA Fusion Association, Culham, UK

*The main goal is to implement, within efit++, a computational model to represent induced currents that are not measured in tokamaks. These may be present particularly in coil cases and in vessel or other structural elements. All data structures necessary for actual computation of the induced currents (matrices of self and mutual inductances) were prepared, computed and tested on a simplified testing example. The coding of a C++ method began but has not been finished. This method is still in a testing phase of development; it is supposed that the induced currents model implementation will be finished in 2009.*

### Theoretical background

The induced currents model is based on the model described in the article of G.J. McArdle and D. Taylor: Adaptation of the MAST passive current simulation model for real-time plasma control [1]. The induced currents model is supposed to compute currents in passive structures, i.e. toroidal conductive structures, where current is not measured. Passive structures can be vacuum vessel or short-circuited loops or casings of poloidal field (PF) coils. The model consists of solving the induction equation:

$$(V=)0 = R_{ps} \cdot I_{ps} + L_{ps2ps} \cdot \dot{I}_{ps} + L_{ps2pf} \cdot \dot{I}_{pf} + L_{ps2g} \cdot \dot{I}_{pl} \quad (1)$$

where  $R_{ps}$  is diagonal matrix of passive structure resistances,  $I_{ps}$  is vector of passive structure currents,  $L_{ps2ps}$  is matrix of self-inductances and mutual inductances of passive structures,  $\dot{I}_{ps}$  is vector of time derivatives of currents in passive structures,  $L_{ps2pf}$  is matrix of mutual inductances between passive structures and PF coils,  $\dot{I}_{pf}$  is time derivative of currents in the PF coils,  $L_{ps2g}$  is three dimensional matrix of mutual inductances between passive structures and computational grid and  $\dot{I}_{pl}$  is two dimensional matrix of derivations of plasma currents in computational grid.

The equation (1) differs in notation from the induction equation in [1]. The notation used in this text is more compatible with efit++ internal structure. The article [1] describes the principles of rewriting equation (1) to form:

$$\frac{dx_e}{dt} = \Lambda \cdot x_e + W^{-1} \cdot B \cdot u + W^{-1} \cdot C \cdot v \quad (2)$$

$$y = D \cdot W \cdot x_e + E \cdot u + F \cdot v \quad (3)$$

where  $\Lambda$  is diagonal matrix of eigenvalues of matrix  $A = W \cdot \Lambda \cdot W^{-1} = -L_{ps2ps}^{-1} \cdot R_{ps}$ ,  $W$  is full matrix whose columns are eigenvectors of  $A$ ,  $x_e = W^{-1} \cdot x$  is state vector of eigenmodes, state vector is defined by equation  $I_{ps} = x - L_{ps2ps}^{-1} \cdot (L_{ps2pf} \cdot I_{pf} + L_{ps2g} \cdot I_{pl})$ ,  $u$  is vector  $u = I_{pf}$ ,  $B = L_{ps2ps}^{-1} \cdot R_{ps} \cdot L_{ps2ps}^{-1} \cdot L_{ps2pf}$ ,  $v$  is vector  $v = I_{pl}$ ,  $C = L_{ps2ps}^{-1} \cdot R_{ps} \cdot L_{ps2ps}^{-1} \cdot L_{ps2g}$ ,  $y = I_{ps}$ ,  $D$  is identity matrix,  $E = -L_{ps2ps}^{-1} \cdot L_{ps2pf}$  and  $F = -L_{ps2ps}^{-1} \cdot L_{ps2g}$ .

The rewriting of equation (1) to equations (2) and (3) offers several advantages for computing of induced currents. The matrix  $\Lambda$  is diagonal which allows solution the set of equations (2) as set of independent equations. This feature allows truncation of the induced currents model by setting terms of vector  $x_e$  with large negative corresponding terms of  $\Lambda$  to zero (details are explained in [1]).

The equations (2) and (3) in discrete representation are:

$$x_e(n+1) = A_d \cdot x_e(n) + B_d \cdot u(n) + C_d \cdot v(n) \quad (4)$$

$$y(n+1) = W \cdot x_e(n+1) + E_d \cdot u(n+1) + F_d \cdot v(n+1) \quad (5)$$

where matrices  $A_d$ ,  $B_d$ ,  $C_d$ ,  $E_d$  and  $F_d$  have form depending on chosen method of solving of differential equations, i.e. the matrices differ for forward Euler method and Runge-Kutta method.

### Status of implementation

The efit++ code is written in the C++ with computational core of the code in the Fortran 95. Only C++ part of the code was changed. Following methods were programmed:

- New class *InductanceBaseClass* was created, methods *mutualInductance* and *selfInductance* were added inside. These methods compute mutual and self inductance of thin wire(s).
- Method for computation of selfinductance of one passive structure *computeSelfInductance* was added into *passiveStructure* class.
- Methods for computation of matrix of mutual and selfinductances of passive structures *computePS2PSMutualInductances*, for computation of mutual inductances between passive structures and computational grid *computePS2GmutualInductances* were added into *passiveStructures* class. Matrix *mutualInductancePS2GArray* has three indices (dimensions): index of passive structure, r index of computational grid and z index of computational grid.
- Method for computation of matrix of mutual inductances between passive structures and poloidal field coils *computePS2PFMutualInductances* was added into *pfSystems* class.

These methods covers computation of matrices  $L_{ps2ps}$ ,  $L_{ps2g}$  and  $L_{ps2pf}$ . Appropriate methods necessary to retrieve computed matrices were also added.

- Method *constructCurrentDistribution* was added into *profiles2D* class. This method creates artificial plasma current distribution in the ellipse shape at defined location. It is used to compute first estimation of induced currents before equilibria (real plasma shape) are computed.
- New variables *lambdaMatrix*, *wMatrix*, *adMatrix*, *bdMatrix*, *cdMatrix*, *edMatrix* and *fdMatrix* were added into *passiveStructures* class to store data necessary to perform computation of induced currents according equations (4) and (5) in Theoretical background section of this text. The *lambdaMatrix* will be necessary for truncation of the model, which is not implemented yet.
- Method *fillAd\_fdMatricesWithEuler* was added to fill these variables (including *wMatrix* and *lambdaMatrix*). Forward Euler method of solving of differential equations was used. Variable *timeStepInAdToFd* was also added to be used when matrices are read from response functions file to check correct usage (not yet implemented).

The status of implementation of induced currents model into efit++ is as follows. All data structures necessary for actual computation of induced currents (matrices  $A_d$ , ... $F_d$ ,  $W$ ) were prepared, computed and tested on simplified testing example. The coding of method *computeInducedCurrents* in the class *passiveStructures* began but wasn't finished. This method is still in testing phase of development – induced currents were computed only for testing example of 2 passive structures, one coil and plasma current computational grid with consisting of 4 points.

### References:

- [1] G.J. McArdle et al., *Fusion Engineering and Design*, 188 (2008) 83

## Test electron and Landau damping calculations of the radial extent of lower hybrid power - edge plasma interaction

*V. Fuchs, V. Petržílka*

In collaboration with:

*J. P. Gunn, A. Ekedahl, M. Goniche, J. Hillairet*, Assoc. EURATOM-CEA, CEA/DSM/DRFC, Cadarache, 13108 Saint Paul-lez-Durance, France

In this report we analyze the radial extent of interaction of tokamak edge plasma with the lower hybrid (LH) antenna (henceforth termed “grill”) electric field. An example of the Tore Supra grill  $E_z$ -field and its spectrum calculated at the grill mouth by a coupling code are shown in Figs 1 and 2, respectively. The antenna field interacts with the plasma by means of electron Landau damping [1,2]. The electron acceleration associated with the power absorption results in high power-flows along magnetic field lines toward tokamak vessel components causing their possible damage. It is therefore of some practical importance to understand the radial extent of the LH-generated fast electron population. The standard present understanding of the radial fast electron – grill electric field interaction zone is based on the self-consistent antenna calculations of Jacquet et al [3] which include the LH-generated hot electrons, and on linear Landau damping results from 2-D simulations of Rantamäki et al. [4]. Results from [3,4] indicate a radial interaction zone of the order of a few millimeters adjacent to the grill mouth. However, recent experimental results from RFA (retarding field analyzer) measurements on Tore Supra have shown the existence of fast electrons as far as few centimeters from the grill mouth [5]. The LH-generated fast electrons causing hot spots on tokamak edge components can be divided into two quite distinct classes. To the first class belong fast electrons generated very near the grill, so we refer to these as “near-field” electrons. The “near-field” population is characterized by electric probe signals, which persist for the duration of LH power. The second class of electrons causing spots on target components stream along magnetic field lines further away from the grill mouth - of the order of cm - and are therefore referred to here as the “far-field” group. Importantly, this second class of electrons exhibits temporal intermittency at a rate comparable with the detachment rate of relatively hot and dense plasma “blobs” from the main body of the plasma [5]. In general, the probe measurements indicate the presence of two electron components: the “cold” background plus a “hot” contribution [5]. Details aside, the two groups of fast electrons appear to form one single fast electron beam extending radially over a few cm from the grill mouth toward towards the separatrix. In the present contribution we aim to explain the observed [5] substantial width of the LH-generated fast electron beam on the basis of linear electron Landau damping, thereby extending our previous [1-4] understanding of the interaction. An alternate non-linear route [6] to understanding the existence of fast electrons further away from the grill mouth is being undertaken by Petržílka [7].

The measured plasma temperature and density in the Tore Supra (TS) scrape-off layer (SOL) are typically inhomogeneous, an example of which is shown in Figs 3a, b for shot #39547. The indicated exponential fits are used in the LH slow wave dispersion relation (see Appendix). We note that the measured profiles are time averages of the fluctuations associated with the intermittent ( $\approx 10$  kHz) entry of plasma structures (“blobs”) from the plasma main body into the SOL. Such “blobs” ejected at the separatrix mid-plane were observed, in experiment [8] as well as in simulations [9], to move toward the plasma edge with their temperature and density gradually decreasing as they spread out in space toroidally and poloidally. Thus an imprint of the intermittency is bound to be strong near the separatrix, but weaker at the grill. Without LH power, we term this SOL plasma “cold” background with respect to the grill, to be distinguished from the situation with an LH-powered grill when interaction of the LH grill electric field with resonant cold background electrons generates a hot (alternatively termed “fast”) electron

population which mixes with the “cold” background. We assume here that, because of their very low collision frequency, the generated fast electrons remain on flux surfaces where they were born. These electrons rapidly move outwards from the grill in both orientations along the parallel direction forming the electron “beams” mentioned above. With these SOL characteristics in mind we approach in two steps the problem of determining the radial interaction zone in which the edge electrons can absorb power from the LH antenna electric field. In section 2 we analyze the interaction in the close vicinity of the grill mouth, where we can assume a cold homogeneous plasma layer ( $T_e=15$  eV and  $n_e=3 \times 10^{17}$  m<sup>-3</sup> from Fig. 3). This cold layer efficiently absorbs the high- $n_{\parallel}$  spectrum components in a very narrow interaction zone of order mm. Of interest here is the fate of the remaining, lower- $n_{\parallel}$ , spectrum components. This is discussed in section 3, which deals with the interaction in an inhomogeneous SOL plasma.

One of the conclusions of the present study is first of all the affirmation of previous results [1-4], now experimentally verified using Retarding Field Analyzer (RFA) probe techniques beyond any reasonable doubt [5]. Specifically, we re-iterate that the LH antenna - edge plasma interaction is initiated at the grill mouth by cold electrons, which are resonant with the high- $n_{\parallel}$  part of the grill spectrum. This spectral range, typically between  $100 < n_{\parallel} < 160$ , is absorbed by the cold electrons within a very thin layer of order mm adjacent to the grill mouth. Powered by the absorbed spectrum, these electrons spread throughout accessible velocity space forming a “hot” electron component.

New results here concern the remaining, lower- $n_{\parallel}$  part of the spectrum, which we show can be absorbed radially deeper in the SOL. A number of factors, not considered before, play a role. We first note that as a function of  $n_{\parallel}$ , the “hot” electron Landau damping rate is not everywhere stronger than the damping rate on the “cold” background. For conditions at the grill mouth, the “cold” damping rate dominates for  $n_{\parallel} > 70$ . The crossover value of  $n_{\parallel}$  determines, in fact, the radial width of the near-field interaction zone. Below the crossover  $n_{\parallel}$ , the “hot” component effectively screens the “cold” background from the radiation. This self-consistent reaction of the hot electron population also determines the radial extent of the interaction region deeper in the SOL in the relevant case of an inhomogeneous SOL plasma, where the plasma temperature, density and consequently also the Landau damping rate all increase toward the separatrix. Moreover, with increasing electron temperature, lower- $n_{\parallel}$  spectral components are pulled into resonance. The nature of the problem at hand suggests using as a measure of Landau damping efficiency the inverse of the perpendicular (i.e. radial) damping rate  $d_{\perp} \equiv 1/\text{Im}(k_{\perp})$ , rather than the damping rate  $\text{Im}(k_{\perp})$  itself. We term  $d_{\perp}$  the Landau “penetration depth”. We are naturally interested in establishing condition for which values of  $d_{\perp}$  are larger than about 1mm but smaller than the width of the SOL.

The LH-generated hot electron population thus self-consistently controls its own radial extent by limited access of radiated power to the “cold” background which needs to absorb power for generating hot electrons at deeper radial positions. The hot population can be characterized by two principal quantities. One is the variance of its velocity distribution function (i.e. the kinetic temperature), the other is its concentration. Test electron simulations of the following sections indicate for the C2 antenna field of Figs. 1 and 2 a temperature and concentration of the hot electron population between 600 eV and 950 eV and 2% and 8%, respectively, both quantities depending on radial position. The width of the interaction zone depends mainly on the concentration of fast electrons. For higher concentrations, a narrow interaction zone adjacent to the grill mouth is expected. For low hot electron concentrations the Landau penetration depth of the spectrum is essentially determined by the much higher concentration of the “colds”, which allows the spectrum to penetrate deeper into the “cold” background.

## Properties of the LH-generated fast electron population

In this section we concentrate on establishing properties of the fast electron distribution we shall need for the calculation of the grill spectrum Landau damping, i.e. the fast electron concentration and temperature. Without LH power, we assume here, for the sake of simplicity, a homogeneous “cold” background with  $T_e=15$  eV and  $n_e=3 \times 10^{17}$  m<sup>-3</sup>, as measured [5] at the grill mouth in Tore Supra shot #39457. Neglecting plasma inhomogeneity effects is equivalent to working at the immediate vicinity of the order of mm in front of the grill. Inhomogeneity will be considered in the next section.. With LH power there is also a fast electron component originating from power transfer via Landau damping from the field to resonant electrons. These subsequently diffuse throughout the velocity space stochastic region delimited by the Chirikov overlapping of resonant modes as seen in the diagram of Fig. 4. The fine blue lines are the separatrices of the grill spectrum Fourier modes, centered around the phase velocities  $v_m=k_m/\omega$ , for  $-7 < m < 7$ , where  $k_m=(\phi/d)*(1+4m)$ ,  $m=\text{integer}$ . For the TS C2 antenna  $d=d_{\text{guide}}+d_{\text{septum}}=10.5$  mm and  $\phi=\pi/2$  is the waveguide phasing in the multijunction modules. Figure 4 illustrates the difference in resonance conditions between 15, 45, and 150 eV electron Maxwellian distributions. So, for example, the 15 eV plasma requires the presence of the  $m < 7$ , and  $m > -7$  Fourier modes to initiate velocity space diffusion. These modes are effectively damped within a depth of about 1 mm, so that a 15 eV electron distribution is practically transparent to the spectrum deeper in the plasma. For continuing interaction hotter electrons resonant with  $|m| > 7$  modes are therefore required.

In order to determine the radial extent of the interaction zone we first carry out full-trajectory test electron simulations to obtain information about the generated fast electrons and use this to calculate the spectrum electron Landau damping from the LH slow wave dispersion relation (Appendix A). The test electron simulation code is described in detail in Ref. [10] and here works with the antenna field of Fig. 1 determined for the Tore Supra C2 LH antenna at 25 MW/m<sup>2</sup> by the antenna coupling code ALOHA [11]. In the given model, “cold” background Maxwellian electrons are initially loaded along the simulation region and during the simulation an inflow of cold background electrons into the grill region in the parallel direction along magnetic field lines is maintained. Figure 5 shows the resulting temperature and power-flow, i.e. the velocity variance and third velocity moment of the distribution function. Figure 6 gives an indication of how the electron distribution function evolves along the simulation region as the right- and left-propagating suprathermal (“hot”) electrons move through the grill. The electron temperature of Fig. 5 obviously depends on both the “cold” and “hot” electron species and therefore varies along the simulation region with the temperature  $T_h$  and the concentrations  $\eta_c$  and  $\eta_h$  of respectively the “cold” and “hot” electrons. In order to make further progress we need to determine the two principal characteristics  $T_h$  and  $\eta_h$  of the hot electron population, i.e. we need to find a way of separating the cold and hot components of the computed distribution function from each other. Moreover, for the subsequent calculations of the spectrum electron Landau damping, we aim to preferably fit the “hot” distributions by Maxwellians characterized by  $T_h$ .

The concentration  $\eta_h$  is easily obtained from the first moment of the distribution function after identifying the “cold” 15 eV bulk and the suprathermal tail, as seen, e.g., in Fig. 6. Estimating the temperature  $T_h$  is not so simple since the fast electron distribution is not strictly Maxwellian. We proceed in a few steps. First, we attempt a Maxwellian fit to the suprathermal tail at the grill edges, depicted in Fig. 7. We note in passing that at the grill

edges both the "cold" and "hot" distributions have the best chance of being near-Maxwellian, since the edge is the point of cold Maxwellian inflow, and the suprathermal distribution has had time to develop having traversed the entire grill region from the other grill extremity. Next, we show in Fig. 8 a Maxwellian fit at the grill center, clearly not as good as at the grill edge. Therefore, in order to verify the fit of Fig. 8, we employ the useful technique, well known from probe diagnostics, of estimating the temperature from the slope of the Volt-Ampere characteristic (which is a second integral of the distribution). Here, we construct the V-I characteristic at either grill edge from the computed distribution function  $f(z,u)$ :

$$I(V) = -qn_0S \int_{-\infty}^{u_v} u f(z,u) du \quad ; \quad u_v = \sqrt{2qV/m_e} \quad (1)$$

where  $n_0$  is the background density,  $S$  is the probe surface area intercepting to the fast electron beam, and  $f$  is normalized to unity. Figure 9 shows the result at conditions of Fig. 8, i.e. at the grill center for the nominal C2 antenna case of  $P_{LH} = 25 \text{ MW/m}^2$ . The temperature shown (908 eV) is the result of taking a mean over all local slope values along the characteristic. Given that we are here neglecting sheath effects at the probe, the computed "hot" temperature agrees reasonably well with estimates from measured V-I probe characteristics [5].

In order to complement the results of Figs 6-9 for the nominal conditions  $25 \text{ MW/m}^2$  of the C2 antenna, we give results for  $P_{LH}=14 \text{ MW/m}^2$  and  $40 \text{ MW/m}^2$  in Fig 10. This should provide an idea about the scaling of fast electron distribution properties with antenna power. We are now in a position to proceed with the discussion of the electron – antenna field radial interaction zone.

### Grill spectrum radial penetration depth

In this section we numerically solve the LH slow wave electrostatic dispersion relation (Appendix) for the perpendicular wavenumber  $k_{\perp}(n_{//})$ , in the entire relevant  $n_{//}$  range:  $-200 < n_{//} < 200$  (for  $T_e=15 \text{ eV}$ , the "resonant"  $n_{//}$  equals  $c/\sqrt{qT_e}/m_e \approx 180$ ). Of special interest here is the radial damping rate  $\text{Im}[k_{\perp}(n_{//})]$  and its inverse,  $d_{\perp}(n_{//})=1/\text{Im}[k_{\perp}(n_{//})]$  - the slow wave radial e-folding penetration depth, which is the depth required to reduce the wave amplitude by 67%, or equivalently the power by about 90%, (although we could have obviously used a different measure of the damping efficiency).

For the sake of illustrating the formation of an interaction region near the grill mouth, we first consider in the next Fig. 11,  $d_{\perp}(n_{//})$  at hypothetical fast electron conditions  $T_h=150 \text{ eV}$  and  $\eta_h = 10\%$ . Shown is  $d_{\perp}(n_{//})$  for the cold background (black curve), and for the mixed background + LH-generated fast electron population (red curve). The damping process is straightforward in the spectral region  $n_{//} > 70$ , where the hot damping is weaker:  $d_{\perp}^{\text{cold}} \leq d_{\perp}^{\text{hot}}$ . The spectrum is absorbed there in a very thin layer of order 0.4 mm on the cold population and an interaction zone is formed between the dashed red lines. The hot population thus generated will spread along magnetic field lines in the parallel direction forming an interaction zone adjacent to the grill mouth. In contrast, in the region  $n_{//} < 70$  where  $d_{\perp}^{\text{cold}} \geq d_{\perp}^{\text{hot}}$ , the process of forming the interaction zone may become strongly nonlinear owing to the very existence of the hot population which damps the radiation more efficiently than the cold population in that spectral range. Close to the intersection of the black and red  $d_{\perp}$  lines the interaction zone can "leak" some of the radiation, which reaches the "cold" region, new fast electrons are generated and the interaction zone is extended to about 1mm. Below  $n_{//} \approx 60$ , the radiation is again blocked by the plateau on the red  $d_{\perp}$  line and by the time the "hot" damping is weak enough to let the spectrum through, the damping on the "colds" has become far too weak for initiating more interaction within the SOL region of about 6-7 cm.. It follows that the

interaction zone is essentially limited by the generated fast electrons. Intuitively, we should expect wider interaction zones for lower fast electron concentrations.

We now proceed to calculations with fast electron parameters established in the previous section. So Fig. 12 shows the penetration depths for the three cases of  $P_{LH} = 14, 25$  and  $40 \text{ MW/m}^2$ , while Fig 13 shows the result for the nominal  $P_{LH} = 25 \text{ MW/m}^2$  at the grill edge (low  $\eta_h = 0.07$ ), and the grill center (higher  $\eta_h = 0.24$ ). These results, showing wide interaction zones are however incompatible with the assumption of a homogeneous plasma. Moreover, as the spectrum penetrates deeper into the plasma it loses its high- $n_{||}$  components which are efficiently damped close to the grill mouth. Next, we therefore attempt to analyze the inhomogeneous plasma situation.

The inhomogeneous analysis uses the plasma profiles of Fig. 3. As before in the homogeneous case, we carry out test electron simulations to establish the fast electron characteristics at a few radial positions. The antenna field to be used at a particular flux surface located at the position  $r$  is determined as follows. Let us introduce the low-pass filter  $F(r, n_{||}) = \exp[-r/d_{\perp}(n_{||})]$ , which defines a "cutoff"  $n_{||\text{cutoff}}$  at which  $r/d_{\perp}(n_{||}) = 1$ . Clearly,  $F = 1$  for  $n_{||} < n_{||\text{cutoff}}$ . The field to be then used in a test electron calculation at  $r$  is the inverse Fourier transform of  $S(n_{||}) F(r, n_{||})$ . Selected results are shown in the Table below, with the fast electron temperature  $T_h$  and concentration  $\eta_h$  calculated at the grill edges.

$r$ [cm]	$T_e$ [eV]	$n_e$ [ $10^{17} \text{ m}^{-3}$ ]	$n_{\text{cutoff}}$	$T_h$	$\eta_h$
0.10	14.5	3.15	55.4	950	0.07
1.0	17.4	3.72	41.6	750	0.045
2.0	21.0	4.78	36.3	700	0.02
3.0	25.5	6.14	32.2	600	0.01
4.0	30.8	7.88	28.8	650	0.032
5.0	37.2	10,12	25.9	700	0.08
6.0	45.0	13.0	23.3	750	0.087

Table I Fast electron  $T_h$  and  $\eta_h$  from test electron simulations at various radial positions

Figure 14 shows  $d_{\perp}(n_{||})$  calculated for this inhomogeneous case for two different value of fast electron concentration. For the value  $\eta_h = 0.07$  of Table I, we obtain an interaction width of about 2 cm. For lower concentrations we see that the width would be substantially larger.

### Conclusion.

We have shown that at edge plasma conditions of Tore Supra shot #39547 and at nominal power conditions  $P_{LH} = 25 \text{ MW/m}^2$  of the Tore Supra C2 LH antenna, the LH-generated fast electrons can exist within a radial zone of about 2 cm adjacent to the grill mouth. This is an order of magnitude larger than previously predicted by theory [3,4], but falls short of the observed 5 cm in experiment [5]. The problem we embarked upon here of establishing the interaction zone in an inhomogeneous plasma is complex and is the subject of ongoing work.

## Appendix The LH slow wave dispersion relation at the plasma edge

With  $k_{//}$  imposed by the antenna we seek the solution  $\text{Im}(k_{\perp})$  of the LH slow wave dispersion relation at the plasma edge. Since  $n^2 \gg |e_{ij}|$  for the refractive index and the dielectric tensor elements, the electrostatic approximation (see Stix [12]) can be used. Assuming  $\vec{E} = \nabla\phi$  the dispersion relation becomes

$$\varepsilon_{//} k_{//}^2 + \varepsilon_{\perp} k_{\perp}^2 = 0, \quad \varepsilon_{\perp} \cong 1 - \frac{\omega_{pi}^2}{\omega^2} + \sum_e \frac{\omega_{pe}^2}{\omega_{ce}^2}, \quad \varepsilon_{//} = 1 + \sum_{\alpha} \chi_{\alpha} \quad (\text{A1})$$

with the susceptibilities

$$\chi_{//\alpha} = \left( \frac{\omega_{p\alpha}}{k_{//} v_{T\alpha}} \right)^2 [1 + \xi_{\alpha} Z(\xi_{\alpha})] \quad (\text{A2})$$

where in (A1) we sum over the electron species and

$$\alpha = i, e_{\text{cold}}, e_{\text{hot}}, \quad \xi_{\alpha} = \frac{c}{n_{//} \sqrt{2} v_{\alpha}}, \quad v_{\alpha} = \frac{q T_{\alpha}}{m_{\alpha}} \quad (\text{A3})$$

### References:

- [1] V. Fuchs, M. Goniche, Y. Demers, et al., *Phys. Plasmas* 3 (1996) 4023
- [2] M. Goniche, D. Guilhem, P. Bibet, et al., *Nucl. Fusion* 38 (1998) 919.
- [3] P. Jacquet, Y. Demers, V. Fuchs, et al. *Phys. Plasmas* 6 (1999) 214.
- [4] K. M. Rantämäki, T. G. H. Pättikangas, S. J. Karttunen, et al., *Nucl. Fusion* 40 (2000) 1477.
- [5] J. P. Gunn, V. Petržílka, A. Ekedahl, V. Fuchs, E. Gauthier, M. Goniche, M. Kočan, J.-Y. Pascal, and F. Saint-Laurent, Measurement of lower hybrid hot spots using a retarding field analyzer in Tore Supra, *To appear in: Journal of Nuclear Materials*
- [6] V. Petržílka, *Plasma Phys. Controlled Fusion*, 33 (1991) 365.
- [7] V. Petržílka, private communication
- [8] O.E. Garcia, R.A. Pitts, J. Horacek, A.H. Nielsen, W. Fundamenski, J.P. Graves, V. Naulin, J. Juul Rasmussen, *Turbulence simulations of interchange motions and intermittent transport in TCV scrape-off layer plasmas*. *Journal of Nuclear Materials* 363-365 (2007) 575-580. Paper on-line, local.pdf
- [9] O.E. Garcia, J. Horacek, R.A. Pitts, A.H. Nielsen, W. Fundamenski, V. Naulin and J. Juul Rasmussen, *Fluctuations and transport in the TCV scrape-off layer*, *Nucl. Fusion* 47 (2007) 667–676.
- [10] V. Fuchs, J.P. Gunn, M.Goniche, V. Petržílka, *Tokamak edge electron diffusion and distribution function in the lower hybrid electric field*, *Nucl. Fusion* 43 (2003) 341.
- [11] J. Hillairet, D. Voyer, B. Frincu, O. Meneghini, A. Ekedahl, M. Goniche, *Modeling of lower hybrid antennas using the ALOHA code and comparisons with Tore Supra experiments*, *Fusion Engineering and Design*, In Press. Available online 21 January 2009, ISSN 0920-3796, DOI: 10.1016/j.fusengdes.2008.12.058.
- [12] T. H. Stix, *Waves in Plasmas*, (American Institute of Physics, New York, 1992).

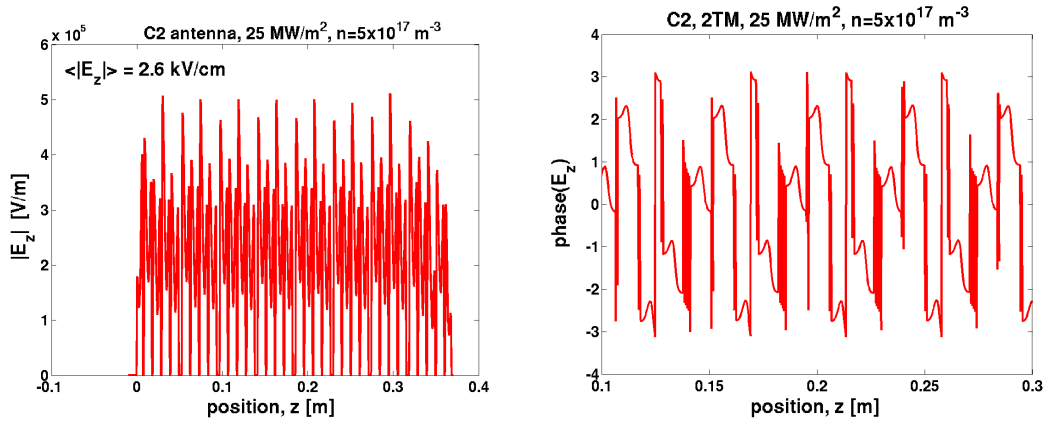


Fig. 1 (a) The absolute value and (b) the phase of the Tore Supra C2 LH antenna  $E_z$ -field calculated with the TEM and two first TM modes, from the ALOHA antenna coupling code. In Fig. 1b the phase progression in 4 of the 8 antenna modules is shown.

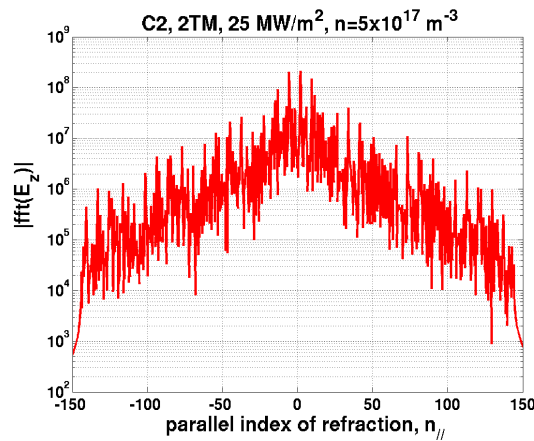


Fig. 2 Spectrum of the field of Fig. 1.

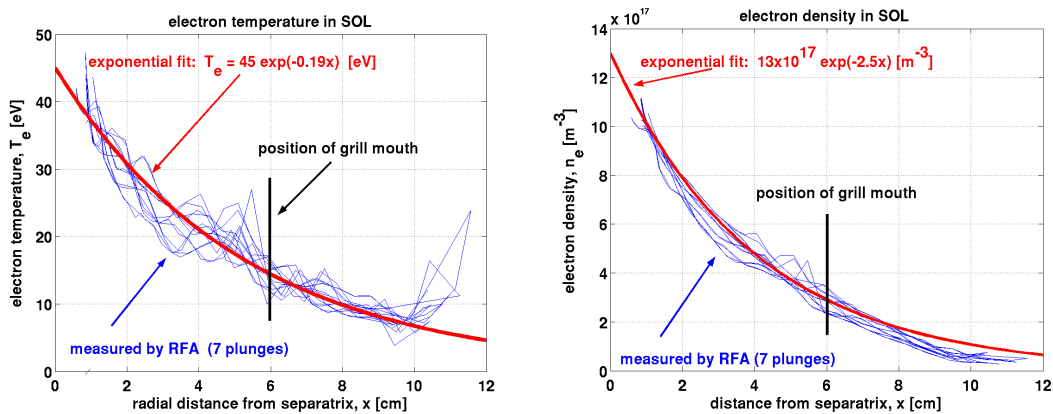


Fig. 3 Radial profiles of a) electron temperature and b) density, in the Tore Supra scrape-off layer for shot # 39000. The separatrix is at  $r=0$  cm, the grill mouth is at  $r=6$  cm. Blue lines: measurement, red line: fit between separatrix and grill mouth.

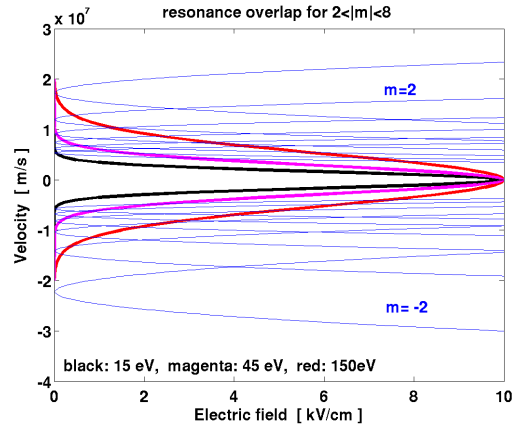


Fig. 4 Resonance overlap diagram: Fourier mode separatrix width in velocity versus electric field strength. The modes in question are the principal components of the spectrum shown in Fig. 2, with phase velocities  $v_m = k_m c / \omega$ , where  $k_m = (\pi/2d)(1+4m)$ .

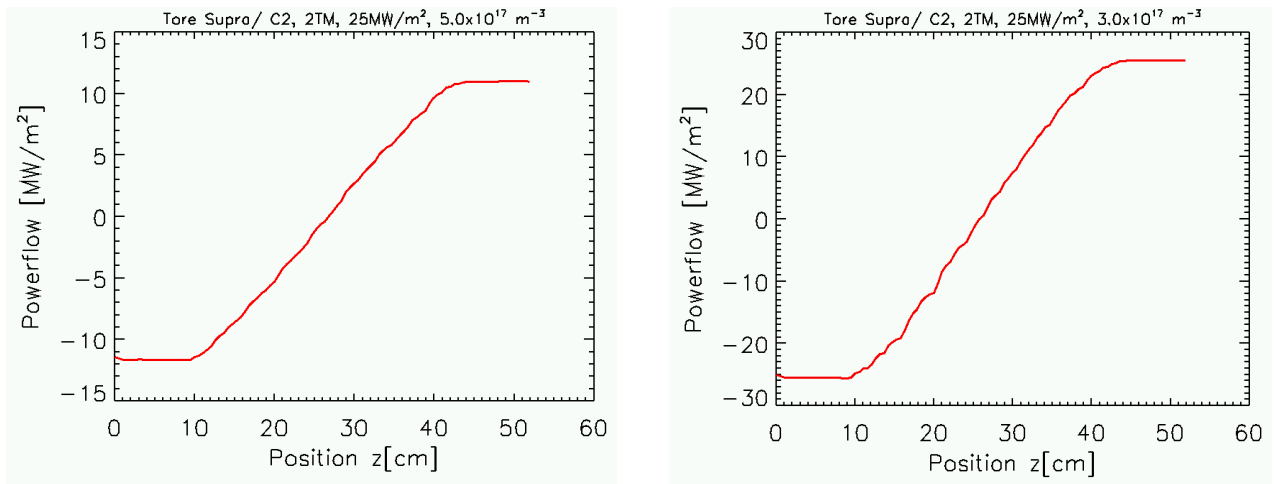


Fig. 5 Selected results from a test electron simulation of a 15 eV Maxwellian population in interaction with the field of Fig. 1: a) temperature versus position along simulation region, b) powerflow versus position.

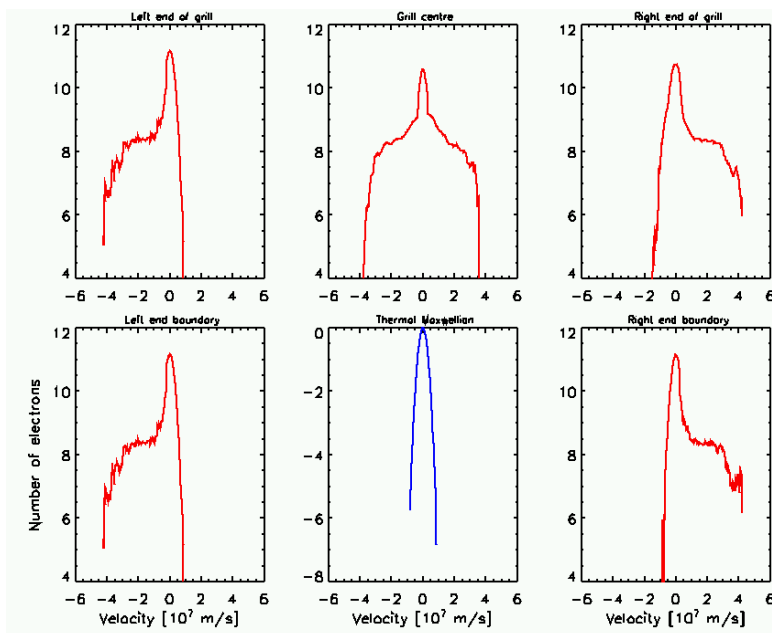


Fig. 6 Electron velocity distribution function for six positions along simulation region.

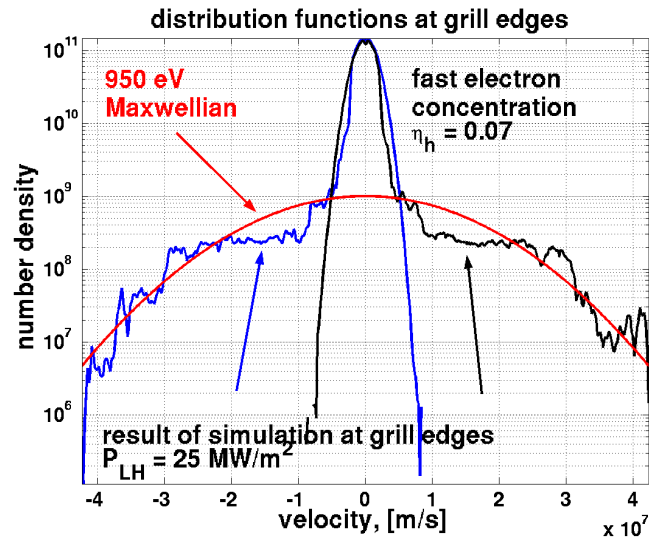


Fig. 7 Electron distribution function at the grill edges, from test electron simulation. Also shown is a Maxwellian fit.

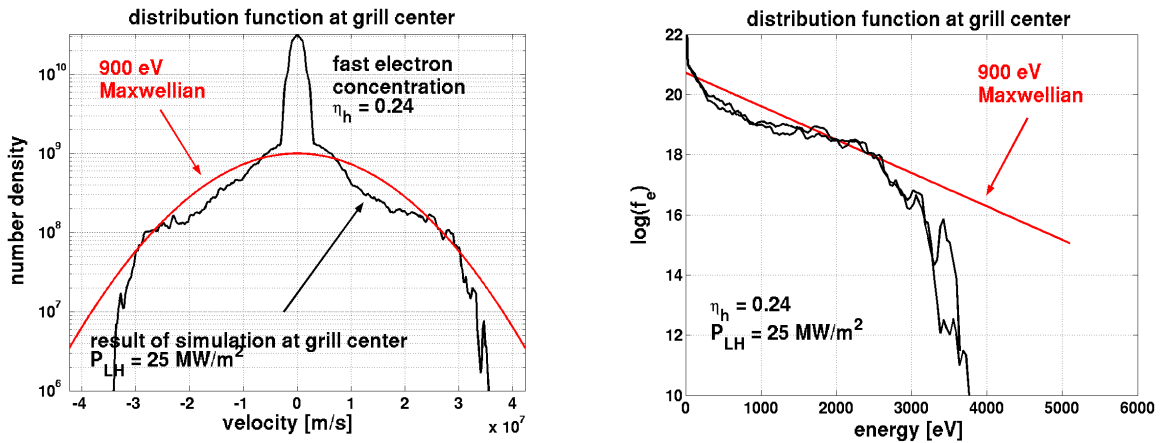


Fig. 8 Electron distribution function at the grill center, from test electron simulation. Also shown is a Maxwellian fit.

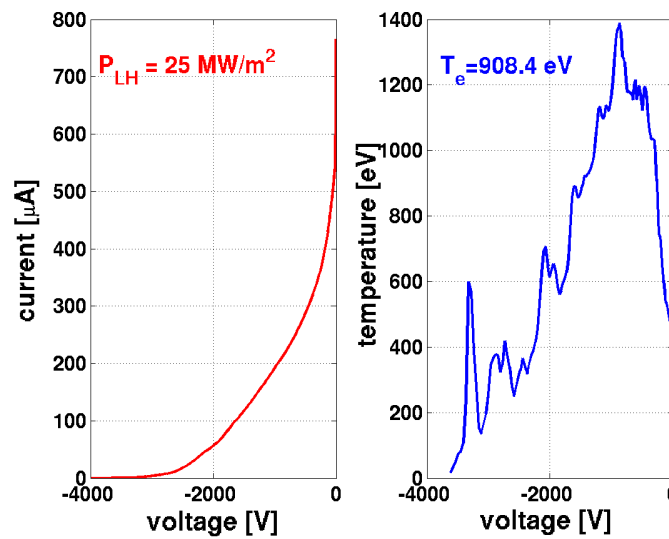


Fig. 9 V-I characteristic and the electron temperature derived from its slope, for the case of Fig. 8.

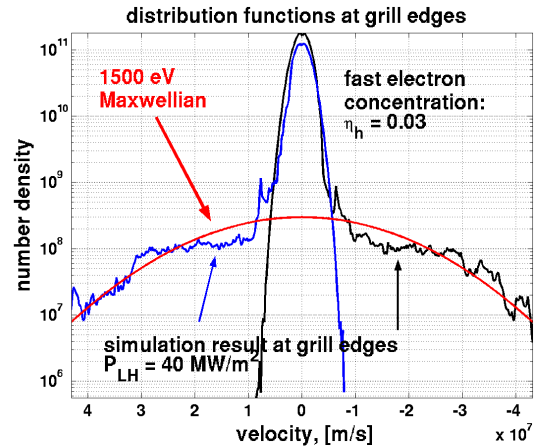
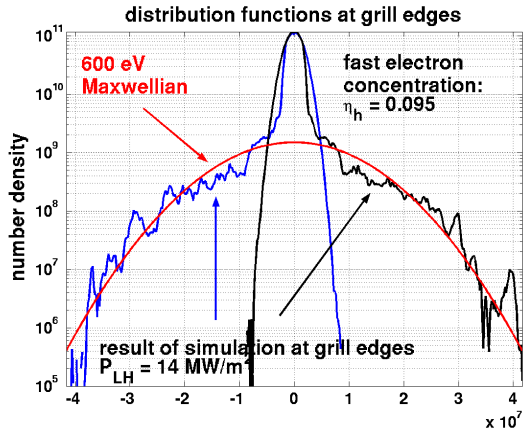


Fig. 10 Electron distribution function at the grill edges from a test electron simulation for two different values of antenna power density.

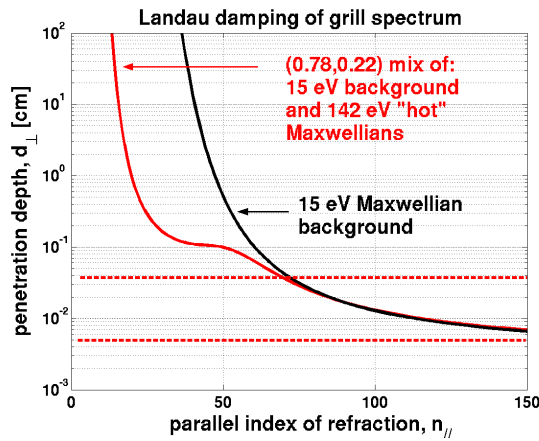


Fig. 11 LH slow wave radial penetration depth  $d_{\perp}=1/\text{Im}(k_{\perp})$  versus  $n_{\parallel}$ , computed from the electrostatic dispersion relation, for a homogeneous plasma region near the grill.

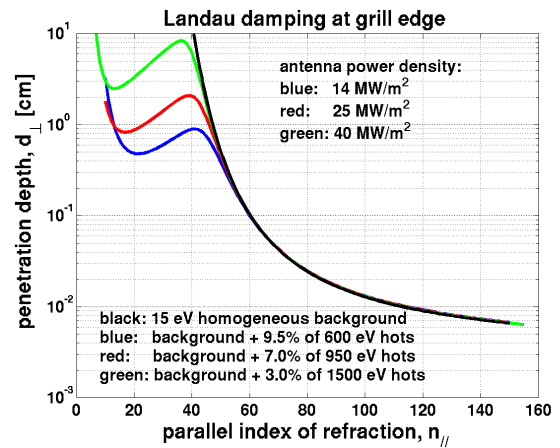


Fig. 12 LH slow wave radial penetration depth  $d_{\perp}=1/\text{Im}(k_{\perp})$  versus  $n_{\parallel}$ , computed from the electrostatic dispersion relation, for three different antenna power densities.

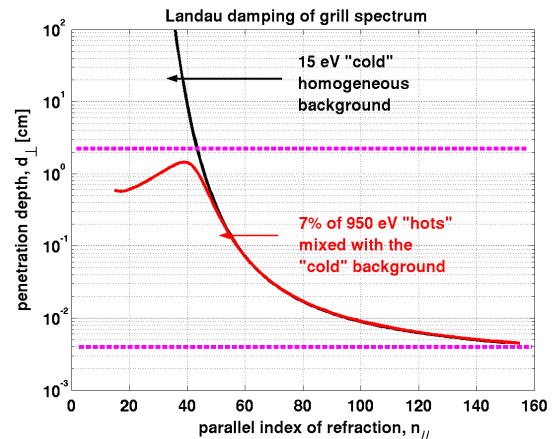
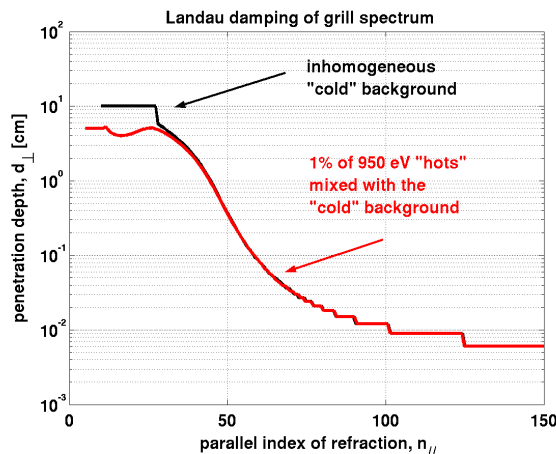


Fig. 14 LH slow wave radial penetration depth  $d_{\perp}=1/\text{Im}(k_{\perp})$  versus  $n_{\parallel}$ , computed from the electrostatic dispersion relation, for the inhomogeneous plasma of Fig. 3 and a) for  $\eta_h=0.01$ , and b) for  $\eta_h=0.07$  of Table I.

## A 2D PIC code for tunnel probe simulations

R.Dejarnac, M. Komm

In collaboration with:

J.P. Gunn, Association EURATOM-CEA, Centre de Cadarache, France.

*The aim of this project was to develop a two-dimensional numerical (kinetic) code to calibrate a new kind of Langmuir probe, the tunnel probe (TP). Development and benchmarking of our in-house code have been performed for the cylindrical version needed for this purpose.*

The equations for the potential and electric field calculations, as well as for the particles motion in cylindrical co-ordinates being already implemented in our 2D code (2007), we need to focus our efforts on the injection of particles. In cylindrical geometry the cell volumes (needed to calculate the density) increases with the radial co-ordinate. We need therefore to inject more particles in the outer cells than in the inner ones to keep the density constant. The method we have chosen consists of injecting particles in a homogeneous way from the injection plane but including a geometrical weighting proportional to the radius of the particle,  $r / L_r$ ,  $L_r$  being the length of the box in the radial direction (= tunnel radius). This way, particles close to the axis  $r = 0$  have less weight than particles far from the axis for density calculation in each cell. The advantage of launching the particle homogeneously along the injection plane guarantees to have the same number of particles per cell (typically 100 in PIC codes) in order to have a good statistic.

The geometrical weighting needs to be taken into account when calculating the charge and the current densities. Indeed, errors in the interpolation scheme within the cells are generated (especially at the borders) and corrections need to be done. Let's first calculate the number of particles located in the  $i^{th}$  grid point,  $\rho_i$ , as a function of the density in this same cell,  $n_p$ . Using a first-order weighting, or bilinear interpolation, for the charge density [1] we can write:

$$\rho_i = \int_0^{2\pi} d\theta \int_{z_i - \Delta z/2}^{z_i + \Delta z/2} dz \left( \int_{r_i - \Delta r}^{r_i} n_p \frac{r}{L_r} \frac{r + \Delta r - r_i}{\Delta r} dr + \int_{r_i}^{r_i + \Delta r} n_p \frac{r}{L_r} \frac{r_i - r + \Delta r}{\Delta r} dr \right) \quad (1)$$

with  $r$  and  $z$  the position of the particle in polar (cylindrical) co-ordinates,  $\Delta r$  and  $\Delta z$  the size of the cell in the radial and toroidal directions, respectively,  $\theta$  being the polar angle in the 3<sup>rd</sup> co-ordinate.

After simplification, we find:

$$\rho_i = \frac{n_p}{L_r} 2\pi r_i \Delta r \Delta z \quad (2)$$

where the volume of a cell centred on  $r_i$  ( $V = 2\pi r_i \Delta r \Delta z$ ) is correctly seen, therefore no correction are needed.

Now, if we calculate the number of particles in a cell at the axis  $r = 0$ , we have:

$$\rho_i = \int_0^{2\pi} d\theta \int_{z_i - \Delta z/2}^{z_i + \Delta z/2} dz \int_{r_1}^{r_2} n_p \frac{r}{L_r} \frac{\Delta r - r}{\Delta r} dr \quad (3)$$

which gives after simplification:

$$\rho_i = \frac{n_p}{L_r} 2\pi \frac{\Delta r^2}{6} \Delta z \quad (4)$$

where we can see that the volume calculated here differs from the volume of the first (half-) cell,

$V_1 = \pi \left( \frac{\Delta r}{2} \right)^2 \Delta z$ . Therefore, a correction factor of 4/3 should be taken into account.

For the cells at a border parallel to the  $r = 0$  axis, the volumes are also reduced and we have:

$$\rho_i = \int_0^{2\pi} d\theta \int_{z_i - \Delta z/2}^{z_i + \Delta z/2} dz \int_{r_{i-1}}^{r_i} n_p \frac{r}{L_r} \frac{r - r_i + \Delta r}{\Delta r} dr \quad (5)$$

which gives:

$$\rho_i = \frac{\pi n_p}{L_r} \left( r_i \Delta r - \frac{\Delta r^2}{3} \right) \quad (6)$$

The calculation of the density by the code can be checked with a simple model. Let us assume monoenergetic ions in the toroidal direction with Maxwellian distribution in the perpendicular direction, without electric field in order to focus only on the trajectories without forces. We want to calculate the radial density profile at the backplate of the tunnel. First, we have to calculate the position of the guiding-center with respect to the phase  $\varphi$  on its orbit, then check if the orbit intersects the inner surface of the tunnel and finally integrating over all initial positions gives the following formula:

$$n = \frac{1}{2} \int \left( 1 - e^{-\frac{(1-r^2)^2}{4(r \cos \varphi + 1)^2 r_L^2}} \right) d\varphi \quad (7)$$

where  $r_L$  is the ion Larmor radius.

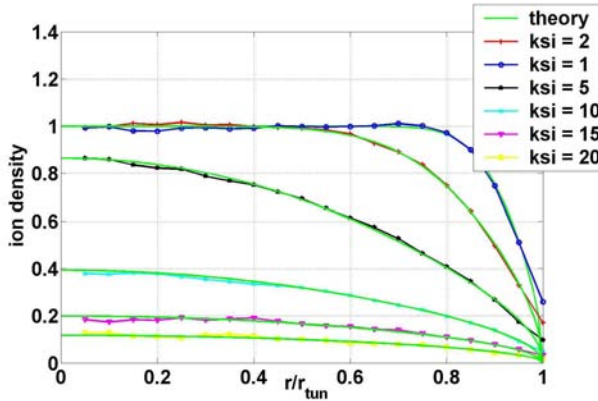


**Figure 1:** Normalized radial density profiles at the back plate of the TP for different Larmor radii calculated by SPICE (lines with symbols) compared with analytical model (theory – green line).

small ( $\xi \ll 1$ ), which means that  $r_L$  is small compared to the radius of the tunnel, the normalised density is close to 1 mainly everywhere in the tunnel; a decrease of the density appears only close to the wall due to losses of the particles to the absorbing wall. Increasing  $r_L$  leads to decreasing the number of particles entering the tunnel and for the extreme case  $\xi = 20 = L_r$  we can see that very few plasma enters the tunnel.

Now, in the presence of electric field, the potential calculated by the code can be compared with the analytical solution for cylindrical geometry [3]. Figure 2 shows the difference between the numerical and the analytical potential. We can observe a general good agreement between the two. The peaks at the wall are only due to corner effects.

For a more realistic modeling of the plasma-wall interaction at the bottom of the TP, secondary electron emission has to be taken into account. An algorithm has been written but not yet implemented into the code for technical reasons and lack of time.

### References:

- [1] C.K. Birdsall and A.B. Langdon, "Plasma Physics via Computer Simulation", McGraw-Hill Book Company.
- [2] J.P. Gunn, Phys. Plasmas **4** (1997) 4435.
- [3] H.S. Carslaw and J.C. Jaeger, "Conduction of heat in solids", Oxford Science Publications.

We now vary the Larmor radius of the particles and observe the dependence of the radial density profiles. In the code, this variation is done via the

parameter  $\xi = \frac{r_L}{\lambda_D}$ , with  $\lambda_D$  the Debye

length, which parametrise the magnetic sheath in our model [2]. We have taken a tunnel radius  $L_r = 20 \lambda_D$  and we vary  $r_L$  from 1 to 20. Figure 1 presents the comparison for the different runs with equation (7) which is labelled as "theory" in the legend. We can see that we obtain a good agreement for all cases. When  $\xi$  is

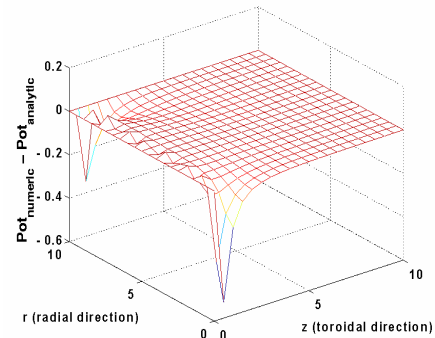


**Figure 2:** Difference of analytic and numeric electric potential in a squared simulation box.

## 4. Emerging Technologies

### **Influence of neutron irradiation on the properties of candidate fusion materials**

*J. Matějčík*

In collaboration with:

*L. Viererbl, J. Zmitkova, Nuclear Research Institute, Rez, Czech Republic*

*G. Pintsuk, Forschungszentrum Juelich, Germany*

*J. Sedlacek, Czech Technical University, Prague, Czech Republic*

IPP participates in a broader project "Materials and Components for Nuclear Reactors", led by the Nuclear Research Institute, Řež.

The goal is to investigate the changes in candidate fusion materials properties after neutron irradiation. Particular focus is placed on plasma sprayed coatings (tungsten, copper, stainless steel, alumina) and other bulk materials with potential application in ITER, DEMO or other fusion devices. The material features studied include structural changes, thermal and electrical properties and behavior under heat flux.

#### **Studied samples**

Samples for the basic characterization of material properties were prepared by plasma spraying at IPP. Bulk material samples included CuCrZr alloy from Ansaldo Ricerche, various steel grades from Ciemat and LAM glasses and CFC compounds from Politecnico Torino. Additionally, compound samples and mock-ups for high heat flux testing were prepared both by plasma spraying and brazing of bulk materials (Fig. 1).

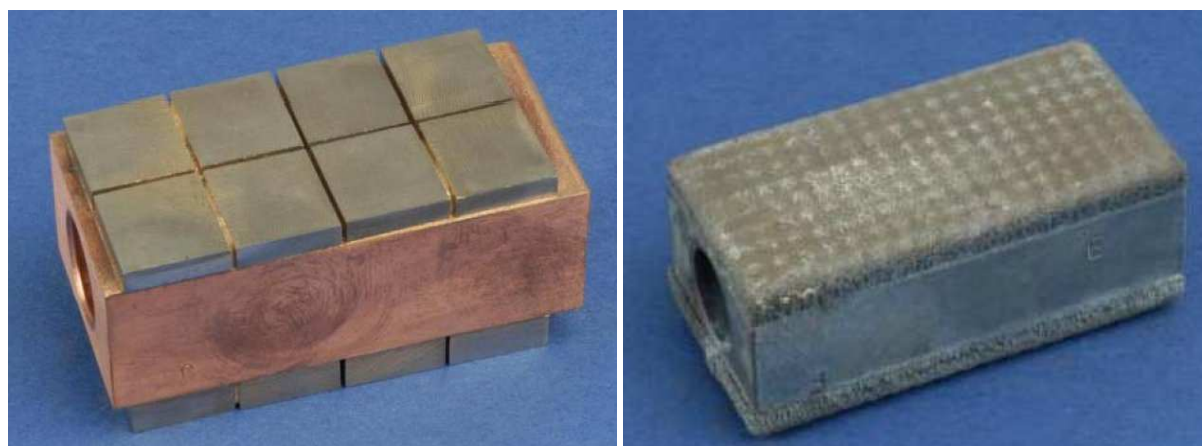


**Fig. 1.** Mock-ups of plasma facing components for high heat flux testing: left - brazed bulk W tiles, right - plasma sprayed W, both on CuCrZr cooling block.

#### **Preparation phase**

In the preparation phase, samples of powder materials used in plasma spraying were irradiated in one short term cycle and their activity was determined. As some samples were to be irradiated at higher temperature, and active temperature control in an irradiation capsule

would be difficult, a concept of a heating block, where heat would be generated by the neutron irradiation itself, was introduced. FEM calculations were performed, taking into account the heat transfer in a capsule, and a steady-state temperature and corresponding heating block dimensions were determined. Irradiation capsules for different sample dimensions were designed and manufactured and their water-tightness was tested prior to insertion in the reactor (Fig. 2). Neutron fluence monitors were included in the capsules as well.



**Fig. 2.** L: Irradiation capsule inserts containing small samples for structural studies and measurement of thermal and electrical properties, R: capsules containing the mock-ups shown in Fig. 1. for high heat flux testing.

### **Pre-irradiation characterization**

Thermal diffusivity and conductivity were determined by the flash method at IPP at FZJ, in a 100 – 400 C range. High heat flux testing was performed on the JUDITH facility at FZJ. Electric resistivity was measured at CTU, according to the DIN/ IEC 468 (metallic materials) and ASTM D257-66 (ceramic materials) standards. Results are summarized in IPP's research report no. 2/2008. The obtained values will be compared to those after irradiation.

### **Irradiation campaign**

The irradiation campaign started in May 2008, when six capsules were inserted in the LVR-15 reactor at NRI. For most samples, the irradiation is targeted at 1 dpa total fluence. Steel samples from Ciemat include also 0.05 dpa and 0.5 dpa series. The 0.05 dpa samples were already extracted and the neutron fluence received was measured. The remaining capsules were rearranged in the irradiation channel, in order to approximately balance out the spatial variation of the neutron flux.

## 5. Areas covered by EFDA tasks (technology)

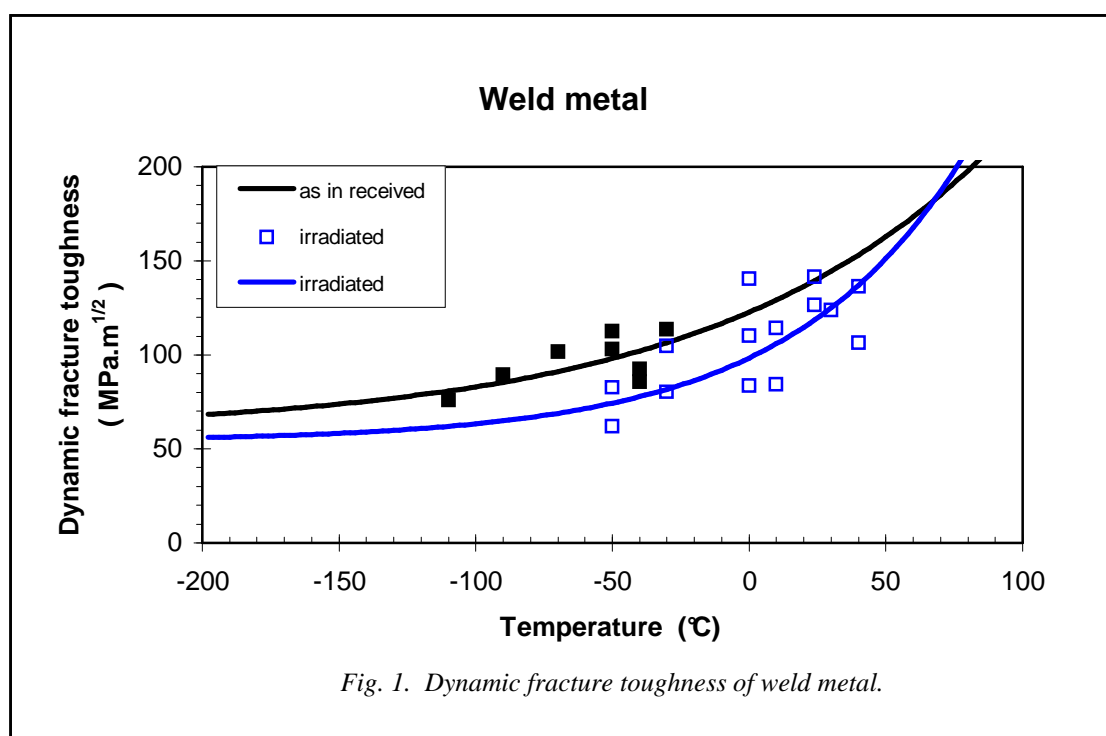
### Static and dynamic fracture toughness of plates and weldments at the transition irradiated up to 2.5 dpa at 200°C – 250°C

TW2-TTMS-001b, D3

Novosad, K. Splichal P.M. Falcnik M. Kytka,

*Reduced activation ferritic and martensitic (RAFM) steels are considered as structural materials for the fusion reactor applications. At the present time experimental studies are focused on effects of neutron irradiation at lower temperatures 230° C on fractural properties of martensitic steel EUROFER 97 which was developed as a structural material for the first wall TBM (Test Blanket Module). Fracture toughness testing at the transition temperature should be performed and static and dynamic fracture toughness should be evaluated in as received state and after irradiation.*

Static and dynamic toughness at the transition temperature of plates and weldments are measured at room temperature and the temperature of about 250°C with KLST sub size specimens 4 x 3 x 27 mm. Neutron irradiation was performed at the temperature of 235° C up to neutron dose of 2.5 dpa. Böhler Bleche GMBH manufactured plate IMF I-E 14 of EUROFER 97 steel from Heat E 83698. EUROFER segment No 4/15 was cut and steel sample plate 330 x 300 x 14 mm was delivered to NRI by Forschungszentrum Karlsruhe. For dynamic fracture toughness testing, the cells have been equipped with a Tinius Olsen Model 74, Zwick RKP450 and RKP50 impact test machines, instrumented with data acquisition and analysis system. The equipment has been fitted with a resistance furnace and a cooling box working with liquid nitrogen for test temperatures from –170° C to +310° C. For fatigue pre-cracking of the specimens, Alfred J. Amsler model 421 machine of 20 kN



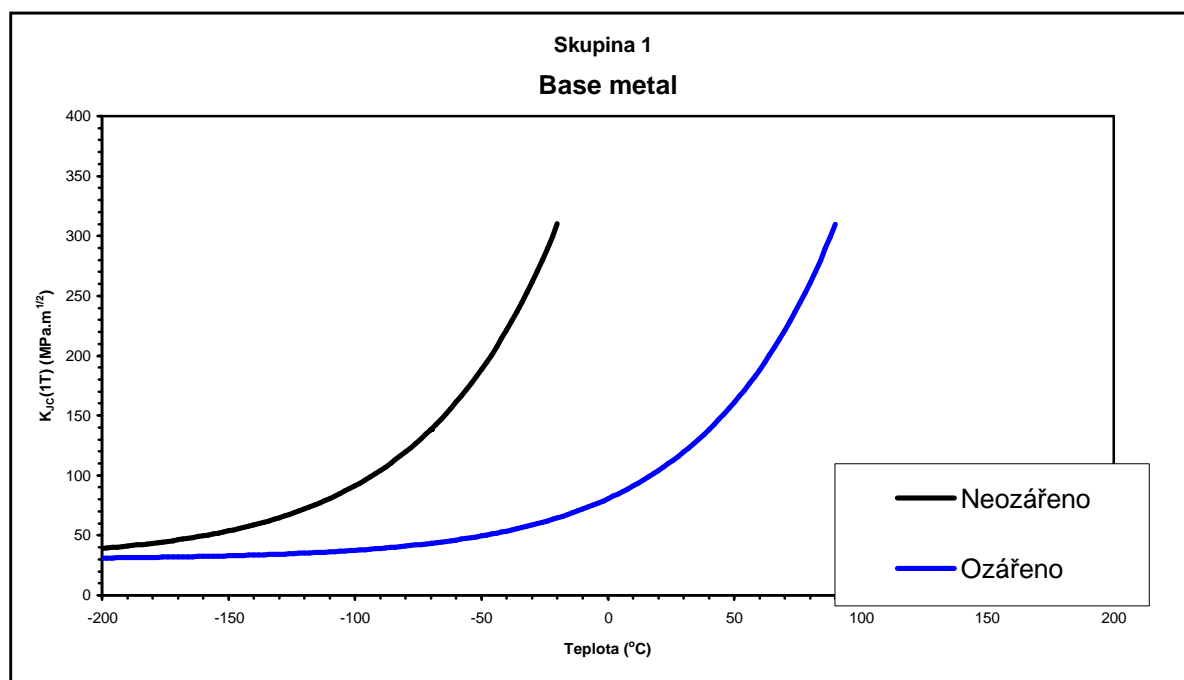


Fig. 2. Static fracture toughness of base metal. Black line: not irradiated. Blue line: irradiated.

capacity is used. Static fracture toughness samples are measured using INSTRON tensile testing machine, PC control stations using Instron's software control their function.

This standard equipment was tailored for hot-cell operation by adding stainless steel pull rods and opening furnaces and cooling boxes (operated by manipulators) of NRI's own design. The heating and cooling system covers test temperatures from -170 °C to +310 °C. During the tests, the load point displacement is measured by LVDT transducer gauges mounted on pull rods outside the furnace or cooling box. [1].

Irradiation experiment was performed in Chouca rig at the temperature of 235°C with fast neutron flux  $4.4 \cdot 10^{13} \text{ cm}^{-2} \text{ s}^{-1}$  under He atmosphere of 100 kPa. The temperature and He pressure are online monitored. Total irradiation time from the beginning of the experiment was 11,246 hours, total reactor work about 96,924 MWh and total radiation level about 2.51 dpa.

Testing of dynamic and static fracture toughness were finished and the transition temperature curves of base and weld metals in as received state and after irradiation at the temperature of 235°C were evaluated. Transition curves of dynamic fracture toughness for weld metal and static transition curves for base metals are given in Fig. 1 and 2 respectively. Our results will be compared with data from [2].

### References:

- [1] M. Falcnik, Kytka M., Laboratory Report 2007/ 37, NRI, 2007
- [2] E. Lucon, Rachid Chaoudai, M. Decreton, Mechanical properties of the European reference RAMF steel ( EUROFER 97) before and after radiation at 300°C, *J. Nucl. Mat.* 329-333 (2004) 1074 - 1082

## EUROFER and Pb-Li melts testing under higher temperature irradiation conditions

TW2-TTMS-003b

K. Šplíchal, J. Berka, J. Burda, Vl. Masarik, Z. Lahodová, L. Viererbl

*Compatibility of martensitic steel EUROFER 97 was investigated with Pb-Li eutectic melt under at temperature 500°C under irradiation condition. Effect of irradiation on Pb-Li melts properties was investigated regarding microstructure, chemical composition and radioactivity. The irradiation of eutectic melts results in the production of tritium and polonium owing to transmutation reaction and bismuth from induced reaction. The post irradiation examinations did not show any noticeable attack of martensitic steel.*

The aim of the task was to perform compatibility tests of EUROFER weld material with Pb-17Li liquid metal under neutron irradiation at 500°C [1]. In-pile corrosion testing of TBM weld metal was situated in molten Pb-Li and located in the active channel of a reactor LVR 15. The weld specimens were irradiated for 6,630 hr up to the level of 1.45 dpa. After dismantling the irradiation rig post-irradiation examinations of the specimens were performed in the hot cell.

The Pb-Li in pile rig was designed. Three mock up experiments were performed and operational parameters were measured. Computer programme COSMOS FloWorks was used for the rig design and input data were corrected according to the results of Pb-Li in pile rig mock-ups. Generated nuclear heating was used for in pile rig, an external electrical heating was not used. Nuclear heating and dedicated cooler of the rig ensured required test temperature of about 500-550°C in the hot part and about 350-400°C in the cold part. Corresponding temperature gradient is in the range of 100-150° C. Flow of the molten Pb-17Li eutectic was driven by natural convection.

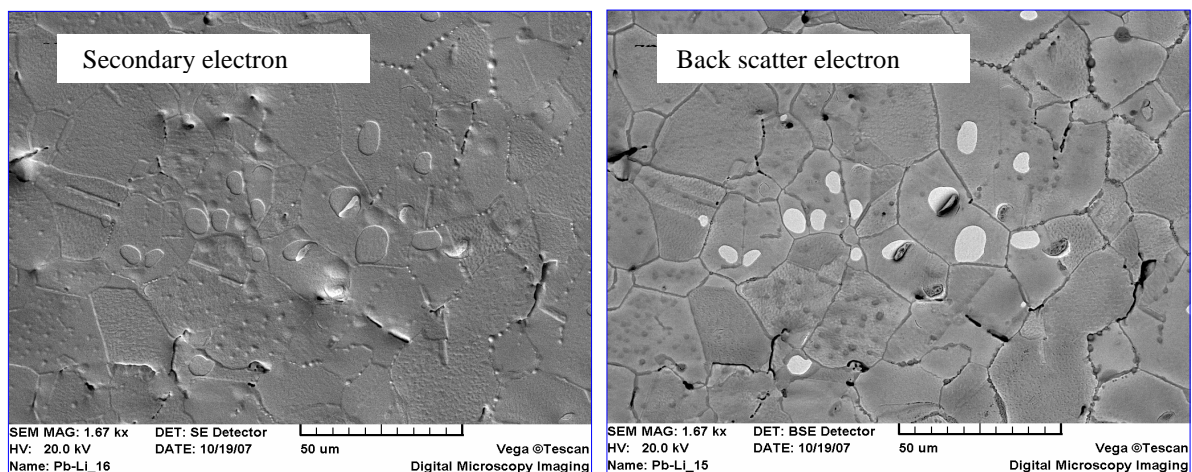
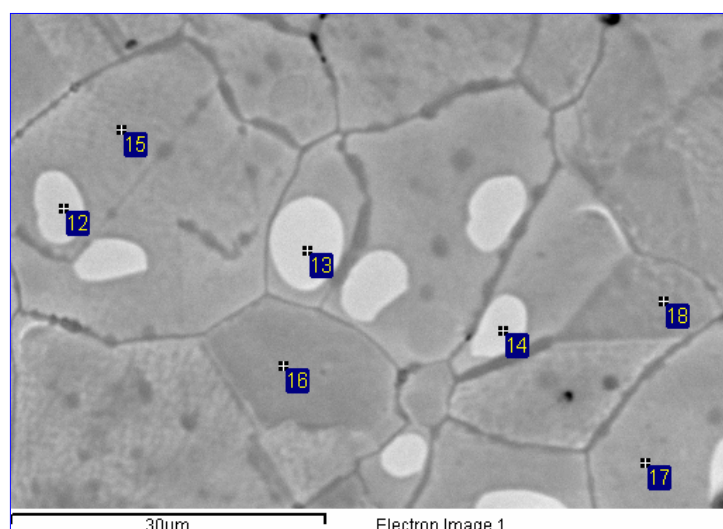


Fig. 1. Microstructure of Pb-Li melt after irradiation at 520°C.



Analýza	O	Pb
12		100,00
13		100,00
14		100,00
15	13,58	86,42
16	14,37	85,63
17	12,23	87,77
18	13,82	86,18

Fig. 2. EDX analyses of Pb-Li matrix and light oval Pb-Li areas.

Post-irradiation investigation was performed by sampling of Pb Li melt after re-melting of Pb-Li metals at 500°C in the laboratory furnace under Ar. Microstructure of Pb-Li melt did not show any eutectic structure and corresponded to one of lead without alloy elements (Fig.1). Higher content of oxygen was analysed in metal matrix. Light oval phase consist

Element	$\gamma$ -analyses [g/g Pb-Li alloy]	Calculated value [g/g Pb-Li alloy]
Tritium	$2.2 \cdot 10^{-9}$	$9.1 \cdot 10^{-6}$
Polonium 210	$7.3 \cdot 10^{-11}$	$4.5 \cdot 10^{-11}$
Bismuth 210	-	$1.5 \cdot 10^{-12}$

from relatively pure lead. Lithium content was not indicated because removing of Pb-Li metals from rig inner part was not correct. This enabled oxidation of lithium during the re-melting of eutectic alloy.

Gamma-spectrometric analyses of eutectic specimens proved tritium (H3) and polonium Po as a result of transmutation reaction, bismuth Bi as a result

of induced reaction. The comparison of gamma analyses and calculation results (Tab.) show that the measured H3 content is about two orders lower than the calculated one and the content of Po is similar for both values [2]. No increase of Cr, Fe and Mn, contents in Pb-17Li melt was observed as a results of interaction of EUROFER weld metal with in pile environments.

### References:

- [1] M. Zmitko, Y. Poitevin, R.Lässer: The European Concepts of the Blanket Module Development, EFDA, Garching, 2005
- [2] H. Morymya at all: Tritium recovery from liquid metals, *Fus. Engin. And Design* 28 (1995), 226

## Development and testing cold traps, high temperature flanges and circulation pump for the liquid metal Pb-Li loop

TW5-TTBC-005, D2

L. Kosek, J. Berka, Vl. Masarik M. Ruzickova, K. Splichal

*Operation parameters for PbLi loop was verified. Temperatures and flow speed required for purification experiments were in projected ranges. Two purification experiments with artificially added impurities were carried out. Design of sampling system was simplified from once shot to more flexible one. Efficiency of cold trap for removing corrosion products from circuit was investigated. Simple evaluation of kinetics of precipitation process was also performed. High temperature flanges was manufactured and testing is ongoing. Special loop for measurement of circulation pump characteristic was designed.*

This task is focused on development and testing of circulation pump, cold trap and high-temperature flanges<sup>1</sup> for the Pb-Li Ancillary system for HCLL Test Blanket Module. PbLi loop Meliloo with impeller type pump and cold trap (similar to Tritex phase V one)<sup>2</sup> was designed and manufactured. During test run the dependence of flowspeed on pump's

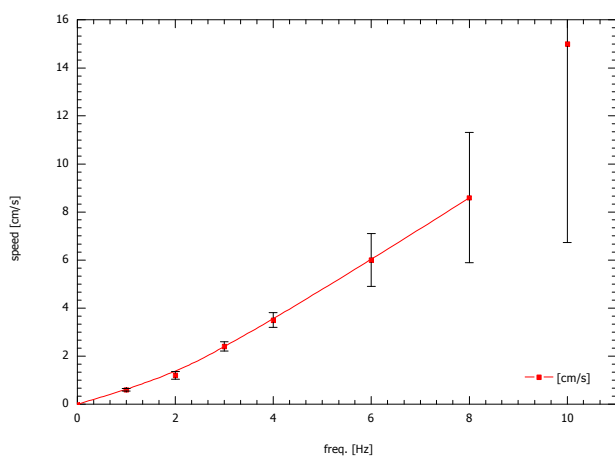


Fig. 1 Flowspeed as fuction of pump frequency.

frequency was determined and temperature gradient needed for purification experiment achieved. The highest temperature - 550°C was established in circulation pump and the test section area while the lowest temperature was maintained in the cold trap between 280°C and 300°C.

After verification of operation parameters two purification experiments were performed. For this purpose corrosion products – Fe, Cr, Mn were artificially added to circuit in form of pure metals. Dosed amount of these metals was ekvivalent to highest solubility of each metal in pure Pb17Li

<sup>3,4,5</sup> Mixture of PbLi and “impurities” was heated in argon atmosphere at 500°C for 200h to dissolve as high amount of dosed metals as possible. Then the whole loop was heated to 500°C and filled with prepared alloy. After PbLi homogenization in loop first sample was



Fig. 2. Original “once shot” sampling system and new simplified one for repeatable use. Sample of PbLi.

collected. Then cold trap was cooled to operation temperature (below 300°C) and PbLi circulated at speed 3-4cm/s for 50 hours in loop. Then alloy was sampled again. Before loop was drained, cold leg of loop was freezed and sample of PbLi solidified level in Cold trap was collected.

Second experiment was aimed to long term pump operation on high temperatures. New simplified sampling system was designed. Loop was running for 1500h with pump on 550°C. After achieving this objective, experiment for investigation kinetics of corrosion products precipitation was performed. Temperature in cold trap was increased to 450°C for 5days to dissolve its content. Then the temperature in cold trap was decreased again and samples were collected after 2h, 24h and 72h from cooling start.

### Results

Circulation pump showed reliable performace at temperatures up to 550°C. After 2500h of operation was dismantled for evaluation and there was found no vapor deposits of PbLi or any other damage in bearing area. To support design activities on PbLi Ancillary system a special loop for measuring pump characteristic is being manufactured. Measurements are foreseen in next quarter.

Chemical analyses of collected samples show similar efficiency of corrosion products removing for cold trap in both purification experiments. Concentration of Fe was reduced by 30%, Mn by 80%, Ni by 70%. Content of Cr is not reduced and shows no change in concentration at all, although on level of cold trap we have found higher concentration of Cr than in other samples. Concentration of corrosion products is significantly higher on the level of cold trap and this supports idea that corrosion products has tendency to float on level of PbLi rather than precipitate on inner surfaces.

Simple evaluation of kinetics shows that precipitation of all impurities except Mn is faster than 2hours. Mn showed slow continuous decrease of concentration for 72h. This needs to be verified by modified experimental setup, because we was unable to keep temperature of cold trap constant during rapid cooling in second experiment.

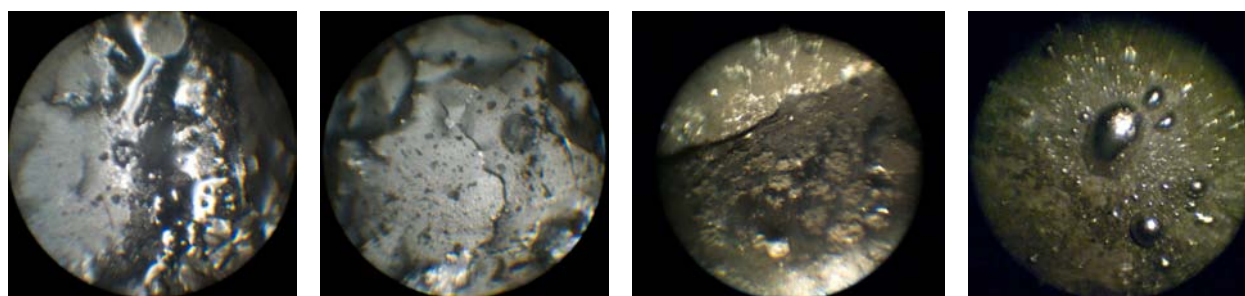


Fig. 3 Few images from cold trap: Two types of solidified surface – polish and matte. PbLi level with precipitated corrosion products. Vapour deposits on walls of the trap.

### References:

- [1] P. Hájek, V Richter, M. Zmitko, Pb-17Li Auxiliary and purification systems: Design of the auxiliary Pb-Li loop for Helium, NRI 12096, 2004
- [2] H. Feuerstein, S. Horn, G. Kieser, Tritex - A Ferritic Steel Loop with PbLi, 1999
- [3] N. Simon et al., *J. Nucl. Mater.* 254 (1998) 185
- [4] M. G. Barker, T. Sample, *Fusion Engineering and Design* 14 (1991) 219-226
- [5] H. Feuerstein et al., report FZKA 5596 (1995)

## Compatibility of EUROFER samples coated by Al and $\text{Er}_2\text{O}_3$ layers with Pb-Li melt under higher temperature conditions

TW6-TTMS-003, D5

L. Kosek, K. Šplíchal, J. Berka, M. Zmitko

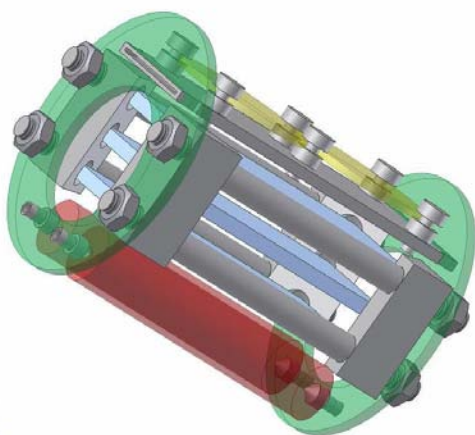
In collaboration with: W. Krauss, FZK Karlsruhe, H. Maier IPP Garching

*Under Test Blanket Module operation conditions sufficient corrosion resistance and limitation of tritium penetration through EUROFER steel are required. Several types of anti-corrosion and/or tritium anti-permeation coatings on EUROFER steel were selected. The main objective of experimental works is investigation of the coatings compatibility with Pb-Li liquid metal and their corrosion resistance. The investigation will evaluate kinetics of the coating thickness, mechanism of interaction of eutectic melt with coating layers, microstructure and chemical composition of layers and characterization coating - base metal bonding.*

The liquid metal loop available in NRI Rez will be used as a facility for corrosion and compatibility testing in real Test Blanket Module (TBM) conditions. Different types of coating layers should be investigated. They include erbium oxide, Al coating (electrochemical deposition process), W plasma spraying technique. The coatings have to ensure required properties of protective barriers under long-time exposure at higher temperatures.

The corrosion and compatibility test will be performed at 550°C in flowing Pb-15.7Li eutectic with anti-corrosion and tritium anti-permeation coatings at 550°C in flowing velocity

in the range of 1-10 cm/s in long-term exposure up to 5,000 hours. Cold trap in the loop circuit should enable to remove impurities in particular corrosion products release, from Pb-15.7 Li melts. Rectangular samples will be used and coating layers of various thicknesses will be investigated. Two types of specimens with Al coating should be prepared in FZK. The cylindrical  $\text{Ø}$  of 8 mm, length of 40 mm and flat 20 x 40 mm x 1.5 mm were suggested. The specimens of  $\text{Ø}$  20 mm and thickness 2 mm with erbium oxide will be prepared in IPP Garching. A new holder



of specimens (Fig.) was designed to improve the manipulation of specimens during the experiments in Pb-Li loops. According to TBM task changes it is foreseen that two types of coating layers will be only prepared and subsequently tested in the liquid metal loop: a) specimens with erbium oxide (IPP Garching), b) specimens with Al coating (Forschungszentrum Karlsruhe). The start up of Pb-Li operation is delayed due to defects that were indicated in weld joints of the pump and the cold trap. Damaged components were replaced. Coating investigation will start after verifications of operational parameters of the Pb-Li loop and the specimen holder in second half of this year.

## The Facility for Thermal Fatigue Tests of Be Coated First Wall Qualification Mock-ups

TW4-TVB-TFTEST2

T. Klabík, V. Masařík, O. Zlámal, P. Hájek

In collaboration with:

P. Lorenzetto, S. Wikman, Fusion for Energy, Barcelona, Spain

*In the frame of international project focused on material testing for ITER first wall the BESTH (Beryllium Sample Thermal Testing) device was constructed and operated in Nuclear Research Institute Rez, plc. Purpose for construction was based on need of having non-active testing device which is capable of providing required heat flux with data record and evaluation. The main goal of proposed tests is to validate Be-CuCrZr HIP joint endurance under high heat flux cycle load, which simulates thermal conditions in fusion reactor with respect to joint life-time. Tested mock-ups come from EU, USA, Japan, China, Korea and Russia. This paper describes realisation steps and progress in BESTH device operation.*

The objective of this task is to perform thermal fatigue tests of beryllium coated primary first wall mock-ups of dimensions 250 mm x 110 mm x 70 mm to compare the fatigue performance of different beryllium/CuCrZr alloy joints. The tests shall be performed at 0.625 MW/m<sup>2</sup> surface heat flux for a total number of 12,000 cycles of about 300 s duration. The inlet water temperature is about 100 °C with a water velocity of about 1.3 m/s as stated in [1]. Ultrasonic testing is performed on each mock-up to check the soundness of the Be/CuCrZr joints before start of the thermal fatigue testing and at the end of test campaign of 12,000 cycles.

The testing furnace chamber contains two of First Wall Qualification Mock-ups (FWQM) situated in horizontal position and is filled with Helium gas. All of FWQ mock-ups are thermal fatigue tested at 0.625 MW/m<sup>2</sup> for 12,000 cycles as requested in [1]. Electrically heated panels situated in small distance parallel to the Be surface is used to evoke required heat flux. Heat flux on the FWQM surface consists of (He) gap convection, conductivity and radiation. The FWQ mock-ups are connected in parallel and actively cooled using coolant water with inlet temperature of 100°C. Flow rate of the cooling water is controlled to achieve specified Be/CuCrZr joint temperature range and is adjusted during a mock-up test using a special regulation valve and flow rate measurement. A flow velocity of 1.3 m/s is used. Measured data are collected by a PC.

Number of tests was carried out in order of finding most efficient and reliable solution with proper technical parameters. Finding of sufficient heat flux source with requested cyclic capability needed lot of effort and technical tests. After many demanding tests of various heating sources was graphite meander-shaped heating panel chosen. It keeps low emission of impurities in surrounding gas atmosphere and provides best power and life-time characteristics.

Since we are dealing with health-hazardous Beryllium, all tests must be carried out in sealed area with exhaust ventilation system; glove box with ventilation was chosen to accommodate furnace chamber



Fig. 2: Beryllium laboratory with the BESTH glove boxes

in which cyclic heat flux tests take place. Power supply for graphite heating panel is provided from adjustable electric source with PLC. Two-circuit cooling system with cooling tower able to remove 120kW of thermal power was built in order to assure we are able to heat-up and cool down whole system as requested. Primary cooling circuit is equipped with plate heat exchanger and electric heating rods to preheat primary cooling water on 100°C before commencing heat flux tests.

BESTH device is placed in certified Beryllium-handling laboratory supported with Helium-supply system which maintains Helium pressure in furnace chamber on pre-set level. Two air-conditioning systems are available in Beryllium laboratory in order to conform to National Institute of Public Health's requirements: one ventilation circuit exhausts laboratory itself while other is connected straight to glove boxes through HEPA filters. Furnace chambers are filled with Helium atmosphere as mentioned above. Glove boxes are equipped transfer boxes allowing staff to install and manipulate with mock-ups without direct expose to Beryllium.

FWQ mock-ups are simulating internal cladding of fusion reactor's primary wall and consist of three different parts: stainless steel body, CuCrZr alloy heat sink and three Beryllium tiles which are attached to heat sink with hot isostatic pressing, non-destructive conjunctive process based on application of high temperatures and pressure on the jointed materials. BESTH's main output is measuring of temperature on each Beryllium tile which refers to development of tile detachment due to cyclic heat load. Each mock-up must undergo ultrasonic inspection before and after heat load test to determine if irreversible changes appeared on HIP joint during testing. Mock-up assembly, containing two FWQMs from different manufacturers, is cooled by forced-water circulation during testing; inlet water pipes are entering each mock-up in CuCrZr heat sink section; outlet water pipes are coming from stainless steel body. Dimensions of tested mock-ups are specified by Iter Organization in [2] and should be about 250x60x60 mm but recent experience shows it may vary a little.

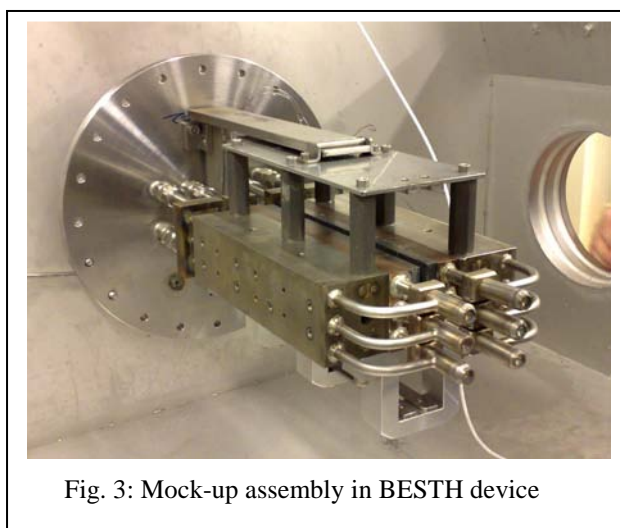


Fig. 3: Mock-up assembly in BESTH device

The main objective of FWQM testing is to evaluate life-time endurance of HIP joint between Beryllium tiles and CuCrZr alloy under conditions of cyclic heat load.

### References:

- [1] Specification – Heat Flux Test of First Wall Qualification Mock-ups, ITER\_D\_28322A, v1.2
- [2] Specification for manufacturing of First Wall qualification mock-up, ITER\_24KTBS v2.1

## Progress and results of thermal fatigue tests of Be coated First Wall Qualification Mock-ups

TW6-TVM-TFTEST

T. Klabík, O. Zlámal, V. Masařík

In collaboration with:

P. Lorenzetto, S. Wikman, Fusion for Energy, Barcelona, Spain

*The BESTH testing device operated by Reactor Services Division, NRI Řež,plc in Czech Republic, allows to carry out out-of-pile tests of Beryllium coated First Wall Qualification Mock-ups under conditions of cyclic heat load in order to evaluate soundness of Be/CuCrZr HIP joint for fusion reactors. Testing of Aluminium and Copper samples for evaluation of heat flux distribution is successfully finished as well as testing of first two FWQ mock-ups, supplied by US and EU Domestic Agencies (DA). Obtained results were evaluated and testing of four more mock-ups from different DA is foreseen during year 2009.*

In the frame of international project focused on material testing for ITER first wall the BESTH (**B**eryllium **S**ample **T**hermal Testing) device was constructed and operated in Nuclear Research Institute Rez, plc. Purpose for construction was based on need of having non-active testing device which is capable of providing required heat flux with data record and evaluation. The main goal of proposed tests is to validate Be-CuCrZr HIP joint endurance under high heat flux cycle load, which simulates thermal conditions in fusion reactor with respect to joint life-time. Tested mock-ups come from EU, USA, Japan, China, Korea and Russia. This paper describes realisation steps and progress in BESTH device operation.

The objective of this task is to perform thermal fatigue tests of beryllium coated primary first wall mock-ups of dimensions 250 mm x 110 mm x 70 mm to compare the fatigue performance of different beryllium/CuCrZr alloy joints. The tests shall be performed at 0.625 MW/m<sup>2</sup> surface heat flux for a total number of 12,000 cycles of about 300 s duration as stated in [1]. The inlet water temperature is about 100 °C with a water velocity of about 1.3 m/s. Ultrasonic testing is performed on each mock-up to check the soundness of the Be/CuCrZr joints before start of the thermal fatigue testing and at the end of test campaign of 12,000 cycles. Ultrasonic testing is performed on each mock-up to check the soundness of the Be/CuCrZr joints before start of the thermal fatigue testing and at the end of test campaign.

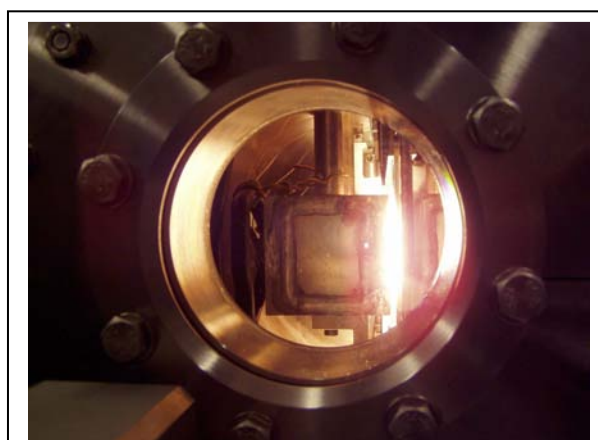


Fig. 4: BESTH device insight during pre-tests

The BESTH testing device was constructed to be able to proceed with long-time automatic unmanned operation and to allow NRI staff to safely handle Beryllium coated FWQ mock-ups. Two mock-ups can be tested at once in one of two furnace chamber, giving together four mock-ups to be tested at once.

Each mock-up represents model of Iter blanket section and consists of three different parts: stainless steel body, CuCrZr alloy heat sink and three Beryllium tiles. Tiles are attached to heat sink with hot isostatic pressing procedure and during operation are cooled by forced water circulation.

The BESTH device includes two glove boxes with furnace chamber inside. Each furnace chamber can accommodate mock-up assembly (made of two mock-ups) and heating

panel. In order to prolong life-time of graphite heating panels there is Helium atmosphere in each furnace chamber. The whole BESTH device is placed in Beryllium laboratory which is equipped with two air-conditioning systems, electric power supply source and two cooling circuits. Normal operation of BESTH device is controlled by Honeywell PLC with automatic data record.

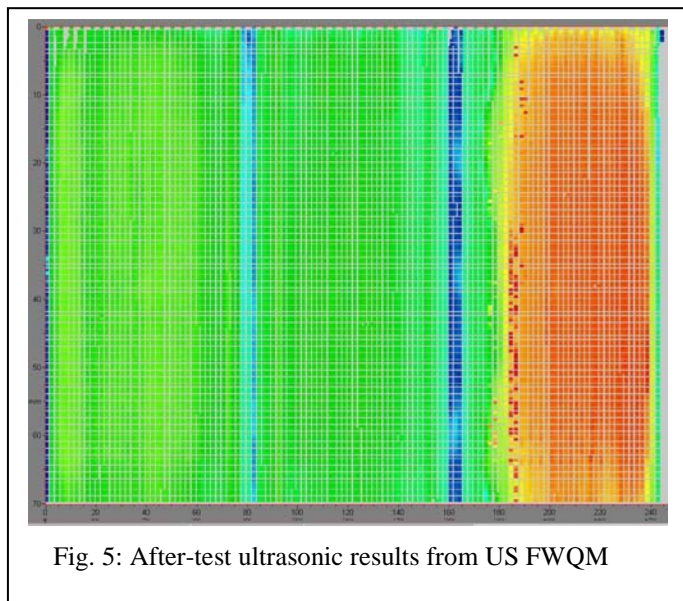


Fig. 5: After-test ultrasonic results from US FWQM

Before commencing tests with Beryllium coated mock-ups the BESTH device was tested with different samples, made of stainless steel, aluminium and copper, to prove basic heat transfer characteristics such as generated heat flux and flatness of heat distribution. All pre-tests proved BESTH device and its personnel are

able to assure all safety requirements related to handling of Beryllium and tests were considered successfully finished.

At the end of year 2008 two FWQ mock-ups were tested in BESTH device: one was supplied from EU, made by AREVA, France; the other one came from Sandia National Laboratory, USA. Both mock-ups underwent ultrasonic inspection and after receiving approval from Iter Organization, thermal fatigue tests were commenced. Mock-ups reached 12000 cycles after approximately 70 days of testing and after automatic shut-down and dismantling of furnace chamber both mock-ups again underwent ultrasonic (UT) inspection. As long as first UT inspection showed no detachments between Beryllium tiles and CuCrZr heat sink, all deviations mentioned in report from second UT inspections were considered as thermal fatigue origin. After-test UT proved flawless state of Be/CuCrZr joint on EU FWQM and small detachment under third Beryllium tile on US FWQM which was observed even during testing in BESTH device by Beryllium temperature rising due to decline in heat removal. Testing itself was with no major problems and it was interrupted only twice. Heating panel was changed approximately after 8700 cycles to prevent its failure due to graphite deterioration. Further details are available in [2].

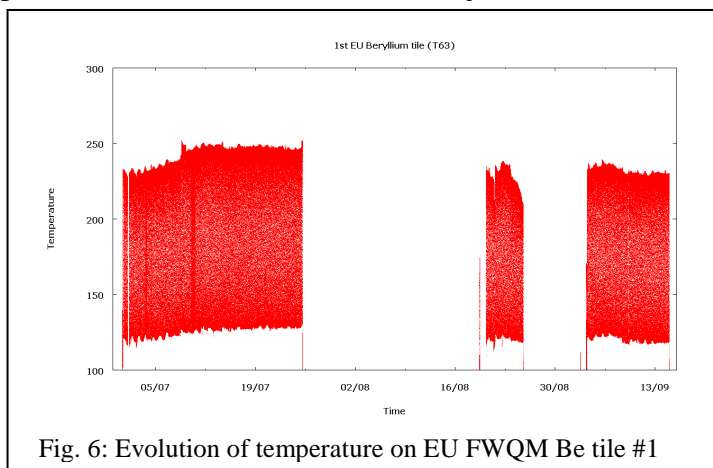


Fig. 6: Evolution of temperature on EU FWQM Be tile #1

### References:

- [1] Specification – Heat Flux Test of First Wall Qualification Mock-ups, ITER\_D\_28322A, v1.2
- [2] Test report, Mock-up ID: FWQM-1NM-US2, Mock-up ID: PH/S-75QB, ÚJV-13072T

## **In-pile thermal fatigue testing device for Primary First Wall Mock-ups with Beryllium cladding**

TW3-TVB-INPILE

T. Klabík, V. Masařík, O. Zlámal, P. Hájek

In collaboration with:

P. Lorenzetto, S. Wikman, Fusion for Energy, Barcelona, Spain

*The objective of this task is to perform in-pile thermal fatigue testing of actively cooled Primary First Wall (PFW) mock-ups to check the effect of neutron irradiation on the Be/CuCrZr heterogeneous joints under representative PFW operation conditions. Two PFW mock-ups will be irradiated at 0.6 dpa with parallel thermal fatigue testing at 0.6 MW/m<sup>2</sup> for 20,000 cycles. Investigation is focused on design, manufacturing and verifications on thermal fatigue equipments and qualification testing without irradiation.*

In-pile testing device was constructed to determine and evaluate steadiness and life-time of tested joint between CuCrZr alloy and Beryllium tiles on PFW mock-ups under more demanding conditions than non-active testing. Aside of long-term cyclic heat load each mock-up will be facing neutron flux provided from LVR-15 research reactor, which is operated by Reactor Services Division of Nuclear Research Institute Řež, plc.

Significant efforts and funds were invested in order to chose and verify best heat source available, capable to provide long-term cyclic heat load and transfer requested heat flux on Beryllium surface without direct contact. Time-consuming test were carried out, including using of Thermocoax electric heating wire, kanthal wire, induction heating, heating by hot gas and IR heating. None of previously mentioned heat sources proved reliable and sufficient time-life, requested heat flux generation or simple technical solution.

The most efficient heat source was found in plate meander-shaped graphite panel, which is able to withstand cyclic high heat flux generation in conditions of super-clear gas surroundings. To find the less deteriorating type of graphite three following grades were tested: isostatic R 4340 grade, composite CC 1001 G grade and isostatic R 8710 grade. Last mentioned graphite grade showed most promising results and was selected for further tests.

Testing loop for two PFW mock-ups will be placed in E1 and E2 positions in LVR-15 core, both mock-ups are jointed together by stainless steel cooling water pipe. Heating of PFW mock-ups is supplied by



Fig. 7: Central part of testing loop

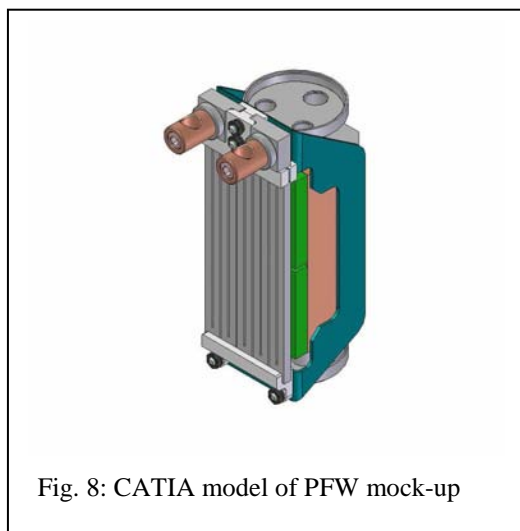


Fig. 8: CATIA model of PFW mock-up

graphite resistance-heating panel and gamma heating from core. The central part of loop, accommodating both mock-ups and prepared for irradiation, is made of 4 mm thick metal plate. Bottom lock is profiled to fit in lower reactor lattice. According to Iter Organization's documentations  $50 \text{ W/cm}^2$  heat flux is requested on Beryllium surface and each of 20,000 cycles shall take 7 minutes.

The programmable logic controller HC 900, supplied by Honeywell company, is used for regulation and control of proposed testing loop. Control application is written under Hybrid Control Designer, communication and

visualisation of PLC output is directed on PC with SpecView32 user interface.

Recent status of project progress is that testing loop body is manufactured and computations are carried out to assess heat load on internal loop components due to small inner volume. Selection of construction material in central loop part and their cooling shall be verified by computation codes. Computations shall also verify if proposed solution with graphite heating panel is feasible at all.

Non-active testing must be carried out to validate all computations with heat transfer, regulation, control and other design features before starting tests in reactor core. Results from non-active tests shall be also used as a basis for documentation submitted to State Office for Nuclear Safety. To obtain applicable results from non-active testing NRI staff will come up with non-active test as similar as in-pile test, only without presence of neutron flux. Same testing loop, same control system and same heating panel will be employed in order to get best estimate results for further evaluation.

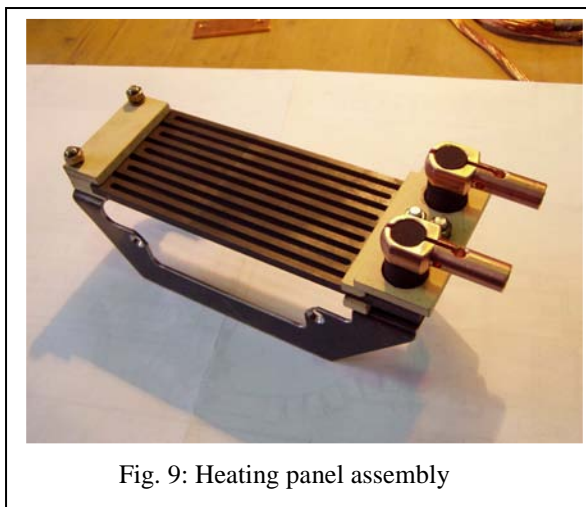


Fig. 9: Heating panel assembly

## Experiments for the validation of Bi cross-sections up to 35 MeV in a quasi-monoenergetic neutron spectrum

TW6-TTMN-002, D6

*P. Bém, V. Burjan, M. Gotz, M. Honisek, V. Kroha, J. Novák and E. Šimečková*  
*Association IPP.CR-Euroatom, Nuclear Physics Institute Rez, CR*

In collaboration with:

*U. Fischer and S.P. Simakov, Association FZK-Euratom, Forschungszentrum Karlsruhe, D-76021 Karlsruhe, Germany*

*The task is a part of a program for developing an off-line method for the neutron spectrum determination in the IFMIF Test Cell Modules. The  $D_2O(p,xn)$  neutron source reaction at 37 MeV proton energy of the U-120M cyclotron facility was utilized leading to the white neutron spectrum with IFMIF-relevant energies). For the determination of the neutron spectra from the  $\gamma$ -activities induced on Al, Ti, Fe, Co, Nb, Rh, In, Tm and Au set of DF foils, the modified code SAND-II was used. In the neutron energy range 10 to 25 MeV (21 dosimetry reactions included), the uncertainties of the spectrum assessed as a mean square deviation of  $A_{cal}/A_{exp}$  ratios from unity amount of 3%. Above 25 MeV, only  $^{59}Co(n,3n)^{57}Co$  and  $^{197}Au(n,4n)^{194}Au$  reactions were used in adjustment procedure, for which the cross section uncertainty could be estimated at level of 20 - 30% (mean deviations of EAF-2005 cross sections from measured ones). For the further suitable reactions in the high-energy region -  $^{209}Bi(n,3-6n)^{207-204}Bi$  - only two independent measurements of cross sections above 20 MeV neutron energies were reported up to now with data uncertainties of about 30%. No preference could be done for evaluated  $^{209}Bi(n,xn)$  reactions cross sections for the libraries EAF-2005, ENDF-VI.8 or IAEA-2001 within such uncertainties. New cross section measurements are therefore needed.*

The experimental investigation of  $^{209}Bi(n,3-5n)^{207-204}Bi$  reaction cross-sections was carried out utilizing the quasi-monoenergetic neutrons from the NPI p- $^7Li$  source in neutron energy range from 19 to 35 MeV (neutron peak energy). Measured data of specific activities of reaction products will be analyzed in terms of EASY-2007 system under close collaboration with the team of FZ Karlsruhe (TW6-TTMN-002B, D7)

The target station of quasi-monoenergetic neutron source based on  $^7Li(p,n)$  reaction was presented in previous work [1]. The proton beam from NPI isochronous cyclotron U120M strikes the  $^7Li$  foil. The carbon backing of  $^7Li$  target serves as a beam stopper. Samples of Bi, Al and Au foils were irradiated in the p- $^7Li$  neutron field generated by protons of 22.1, 27.1, 32.1 and 36.5 MeV energies (neutron spectra peaked at 19.6, 24.3, 29.6 and 34.3 MeV, respectively). Two distances (48 and 88 mm) of foils from the Li target was utilized to test the effect of the flux-density gradient in the vicinity of neutron source. The typical proton beam current was about 3-5  $\mu A$ . The time profile of the neutron source strength during the irradiation was monitored by the proton beam current on the neutron-source target, recorded by a calibrated current-to-frequency converter on PC. The dimensions of Bi samples together with irradiation parameters of experiment are given in Tab.1. Irradiated samples were investigated by means of gamma-spectroscopy method. Two calibrated HPGe detectors of 23 and 50 % efficiency and FWHM of 1.8 keV at 1.3 MeV were used. Activated isotopes were identified on the basis of  $T_{1/2}$ ,  $\gamma$ -ray energies and intensities. Cooling times of gamma measurement ranged from minutes to approx. 100 day. (Each sample was measured at approx. 5 cooling times) To evaluate the neutron spectral flux at sample positions the spectral yield of source reaction p+ $^7Li$ (C backing) were taken from Fig. 2 of paper published by Uwamino et al. [2]. In this work, the spectral yield data were measured by TOF technique at proton energies of 20, 25, 30, 35 and 45 MeV. The spectra consist of quasi-monoenergetic part corresponding to the reactions to g.s. and 0.429 MeV states in  $^7Be$ , and of the low-energy

tail generated a) by reactions on  $^7\text{Li}$  leading to further excited states in  $^7\text{Be}$  and b) by reactions of protons on carbon stopper.

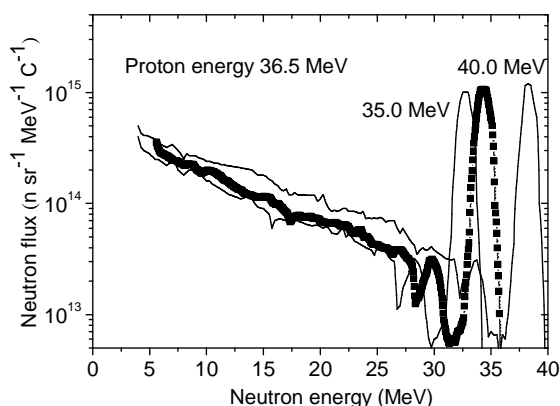


**Fig. 1.** The neutron spectrum at the proton energy of 36.5 MeV resulting from interpolation of data at 35 and 40 MeV, given in Ref. 2

The neutron flux and spectra at proton energies of present experiment were determined by an interpolation procedure. The total uncertainty of 12% in absolute neutron intensity is composed from claimed 10% error of initial data and from difference (up to 5%) of integrals on derived data and only available tabulated values of flux intensity of peak and the peak-to total flux ratio (Table 1 of Ref. 2). In present work, the effect on an integration of spectral yield over acceptance angles of samples at different distances from the target was approximately taken into account using angular distribution data (Fig. 4 of Ref. 2). The integration effect comes out as the attenuation of neutron

peaks due to strong angular dependence of forward directed quasi-monoenergetic neutrons while the neutrons contributing to the tail of spectrum reveal nearly isotropic angular distribution (see Ref. 3) and their dependence of intensity on the target-to-sample distance follows  $r^2$ -law. These statements are well illustrate by detail investigation of data measured at two distances from the target.

Run No	1		2		3		4	
Ep(MeV)	22.1		27.1		32.1		36.5	
Reaction	$A_{sp}(\text{Bq/kg})$				$\Delta(\%)$			
	Source-to-sample distance $S = 48.1$ mm							
<b>Bi-209(n,3n) Bi-207</b>	2,215E+04	1	5,786E+04	3	5,208E+04	4	6,001E+04	3
<b>Bi-209(n,4n) Bi-206</b>			8,997E+04	5	3,778E+07	4	1,142E+08	4
<b>Bi-209(n,5n) Bi-205</b>							4,066E+05	6
	Source-to-sample distance $S = 88.1$ mm							
<b>Bi-209(n,3n) Bi-207</b>	7,315E+03	2	2,067E+04	2	1,895E+04	3	1,910E+04	4
<b>Bi-209(n,4n) Bi-206</b>			3,267E+04	1	1,349E+07	1	3,953E+07	1
<b>Bi-209(n,5n) Bi-205</b>							1,553E+05	2

**Tab. 2.** Specific activities (calculated to the end of irradiation) of reaction products  $A_{sp}(\text{Bq/kg})$  from reactions on Bi foils. Errors shown correspond to the mean square values from the analysis of gamma spectra.

## References:

- [1] P.Bém, V.Burjan, U.Fischer, M.Götz, M.Honusek, V.Kroha, J.Novák, S.P.Simakov, E.Šimečková, The NPI Cyclotron-based Fast neutron Facility ND-2007, International Conference on Nuclear Data for Science and technology,
- [2] Y.Uwamino et al., NIM A389 (1997) 463.
- [3] R. Nolte, priv. comm

## Determination of reflection properties of hydrocarbon radicals for ITER-like divertor conditions

TW6-TPP-CNDMSTICK

Z. Herman, J. Žabka, A. Pysanenko

*J. Heyrovsky Institute of Physical Chemistry, Academy of Sciences of the CR*

In collaboration with:

*T. D. Märk and his research group (Institute for Ion and Applied Physics, University of Innsbruck, Innsbruck), Association EURATOM-ÖAW, Austria*

*The subject of this project is obtaining data on interactions of slow ions (incident energies between a few eV up to about 100 eV) with surfaces of materials relevant to plasma-wall interactions in fusion devices. The objective is - on the one hand - to obtain data on the survival of slow ions in surface collisions, product ion energy losses in ion-surface interactions, dissociative and chemical processes at surfaces, and information on collision kinematics, using the special ion-surface scattering apparatus available in Prague*

### 1. Collisions of selected slow hydrocarbon ions $CD_4^{*+}$ , $CD_5^+$ , $C_2D_4^{*+}$ , and $C_2H_5^+$ with room temperature and heated tungsten surfaces [1].

The interaction of the title hydrocarbon ions with room temperature and heated (600°C) tungsten surfaces was investigated at incident energies of 15-45 eV and at incident angles 60° and 45° with respect to the surface normal. The results were compared with earlier published analogous studies on carbon surfaces.

Ion survival probability of the investigated ions for both room-temperature and heated W-surfaces was in general 2-15 times smaller than on carbon (HOPG) surfaces. The ion survival probability tended to be smaller for radical cations ( $CD_4^{*+}$ ,  $C_2D_4^{*+}$ ) than for closed-shell ions ( $CD_5^+$ ,  $C_2H_5^+$ ). For the incident angle of 60° (to the surface normal) the values of  $S_a(W)$  were 0.03% for  $CD_4^{*+}$ , 0.2 % for  $C_2D_4^{*+}$ , 0.5 – 4 % for  $CD_5^+$ , and 0.2 – 2 % for  $C_2H_5^+$ .

Product ion mass spectra from collisions of radical cations  $CD_4^{*+}$ ,  $C_2D_4^{*+}$  on room temperature W-surfaces, suggested both the occurrence of simple projectile ion fragmentation and reactions with hydrocarbons adsorbed on the room temperature surface. These observations are similar to those for collisions with room temperature carbon (HOPG) surfaces. Reactions with adsorbed hydrocarbons were namely H-atom transfer leading to the formation of  $CD_4H^+$  ( $C_2D_4H^+$ ) and their fragmentation products, and carbon chain build-up reactions (formation of  $C_2X_3^+$  and  $C_3X_3^+$ , X=H,D, in reactions with terminal  $CH_3$ - groups of the surface hydrocarbons). Closed-shell ions ( $CD_5^+$ ,  $C_2H_5^+$ ) exhibited only fragmentation processes. On heated surfaces, only fragmentation of the incident projectile ions was observed.

Translational energy and angular distributions of product ions from collisions with W-surfaces were very similar to data obtained earlier for carbon (HOPG) surfaces. Translational energy distributions (at the maximum of the angular distribution) peaked at 30-50% of incident energy; the peak shifted somewhat to higher energies with increasing incident energy. In collisions with W-surfaces heated to 600°C the maximum of the translational energy distributions was 5 – 30% higher than with room-temperature W-surfaces (Fig. 1).

The similarity of results on heated tungsten and HOPG surfaces may be caused by substantial coverage of W-surfaces by tungsten carbide, originating from cracked surface hydrocarbons.

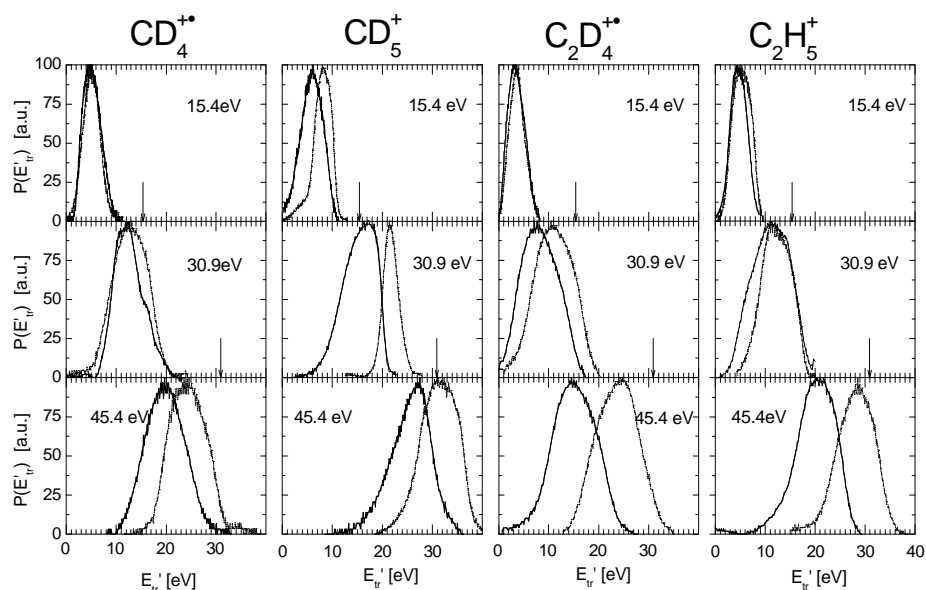


Fig. 1: Translational energy distributions of products from collisions of incident ions with room-temperature (full line) and heated (dashed) tungsten surfaces

## 2. Collisions of very low energy (5-12 eV) $C_2D_4^{+}$ ions with room-temperature carbon surfaces [2,4,6].

The scattering of the hydrocarbon radical cation  $C_2D_4^{+}$  from room-temperature carbon (highly oriented pyrolytic graphite, HOPG) surface was investigated at low incident energies of 6- 12 eV. Mass spectra, angular and translational energy distributions of product ions were measured. From these data, information on processes at surfaces, absolute ion survival probability, and kinematics of the collision was obtained. The projectile ion showed both inelastic, dissociative and reactive scattering, namely the occurrence of H-atom transfer reaction with hydrocarbons present on the room-temperature carbon surface. The absolute survival probability of the ions for the incident angle of  $60^\circ$  (with respect to the surface normal) decreased from about 1.0 % (16 eV) towards zero at incident energies below 10 eV. Estimation of the effective surface mass involved in the collision process led to  $m(S)_{\text{eff}}$  of about 57 a.m.u. for inelastic non-dissociative collisions of  $C_2D_4^{+}$  and of about 115 a.m.u. for fragment ions ( $C_2D_3^{+}$ ,  $C_2D_2^{+}$ ) and ions formed in reactive surface collisions ( $C_2D_4H^{+}$ ,  $C_2D_2H^{+}$ , contributions to  $C_2D_3^{+}$  and  $C_2D_2^{+}$ ). This suggested a rather complex interaction between the projectile ion and the hydrocarbon-covered surface during the collision.

## 3. Collisions of dications and cations $SF_4^{2+/+}$ with hydrocarbon-covered steel surface [3,5]

In joint experiments with the Innsbruck group of Prof. T. D. Märk the projectile ions were mass selected by a 2-sector-field mass spectrometer and decelerated to incident energies of 60 to a few eV. Product ions were measured with the use of a time-of-flight spectrometer and their relative abundances determined as a function of the incident energy of the projectile ions (collision-energy-resolved mass spectra, CERMS curves). The mass spectra of product ions were dominated by fragment ions  $SF_3^{+}$ ,  $SF_2^{+}$ , and  $SF^{+}$  at incident energies below 40 eV, while sputtering of contaminant adsorbates prevailed at higher energies. The results indicate that the likely major reaction sequence responsible for the observed CERMS curves of product ions from  $SF_4^{2+}$  collisions is charge exchange to form singly-charged projectile ions followed by

subsequent unimolecular fragmentation. In addition, chemical reactions between projectile ions and hydrocarbon adsorbates were observed leading to  $\text{SF}_2\text{CH}_3^+$ ,  $\text{SFCH}_2^+$ , and  $\text{SCH}^+$  ions. The paper has been accepted for publication [3].

**References:**

- [1] A. Pysanenko, J. Žabka, T.D. Märk, Z. Herman, *Int. J. Mass Spectrom.* **277**, 229-235, 2008.
- [2] A. Pysanenko, J. Žabka, Z. Herman: *Collection Czech. Chem. Commun.* **73**, 755-770 (2008).
- [3] L. Feketeová, V. Grill, F. Zappa, N. Endstrasser, B. Rasul, Z. Herman, P. Scheier, T.D. Märk, *Int. J. Mass Spectrom.* (accepted)
- [4] A. Pysanenko, J. Žabka, Z. Herman, *XVI Symposium on Atomic, Cluster, and Surface Physics (SASP 2008), Les Diablerets, (CH) Contributions, R.D. Beck, M. Drabels, T.R. Rizzo, Eds. Innsbruck University Press, 2008, p. 130.*
- [5] B. Rasul, F. Zappa, N. Endstrasser, W. Schustereder, J. D. Skalny, Z. Herman, P. Scheier, T.D. Märk, *18th International Conference on Plasma-Surface Interactions, Toledo (E), 2008 (Abstract)*
- [6] A. Kendl, K. Becker, S. Denifl, O. Echt, N. Endstrasser, B. Farizon, M. Farizon, S. Feil, L. Feketeová, V. Grill, Z. Herman, T.D. Märk, S. Matejčík, S. Matt-Leubner, M. Probst, B. Rasul, P. Scheier, W. Schustereder, J.D. Skalny, P. Sulzer, M. Winkler, F. Zappa, *Proceedings of the 22nd IAEA Fusion Research Conference, Geneva, 2008*

## Transport and Deposition of First Wall Impurities SEWG Chemical Erosion and Material Transport

WP08-PWI-06

### Reactive Interaction of Molecular Ions with Surfaces

PWI-08-TA-06

Z. Herman, J. Žabka, A. Pysanenko

J. Heyrovsky Institute of Physical Chemistry, Academy of Sciences of the CR

In collaboration with:

T. D. Märk and his research group (Institute for Ion and Applied Physics, University of Innsbruck, Innsbruck), Association EURATOM-ÖAW, Austria

The aim of this research are dedicated ion-surface scattering experiments with low-energy beams of ions on carbon surfaces to determine energy transfer, surface processes and ion survival probability as a function of impact energy using special ion-surface beam machines. Notice that due to the task management this work has been also reported under Part III.1.

#### 1. Collisions of slow ions $C_3H_n^+$ and $C_3D_n^+$ ( $n=2-8$ ) with room temperature carbon surfaces: mass spectra of product ions and the ion survival probability. [1]

Mass spectra of product ions from collisions of  $C_3H_n^+$  ( $n=2-8$ ) ions and some of their per-deuterated analogues with room temperature carbon (HOPG) surfaces (hydrocarbon-covered at room temperature) were measured at incident energies of 16, 31, and 46 eV and main fragmentation paths of the incident projectile ions, energized by the surface collision, were determined. The extent of fragmentation increased with increasing incident energy. Mass spectra of even-electron ions  $C_3H_7^+$  and  $C_3H_5^+$  showed only fragmentations of the incident projectile ions, mass spectra of radical cations  $C_3H_8^{*+}$  and  $C_3H_6^{*+}$  showed both simple fragmentations of the incident projectile and formation of products (protonated projectile and its fragmentation products) of a surface reaction of H-atom transfer between the projectile ion and hydrocarbons on the surface. No indication of carbon-chain build-up reactions (formation of C4 hydrocarbons) was detected.

The survival probability of the incident ions was found to be usually about 1 - 2% for radical cation projectile ions ( $C_3H_8^{*+}$ ,  $C_3H_6^{*+}$ ,  $C_3H_4^{*+}$ , and  $C_3H_2^{*+}$ ) and several % up to about 20% for even-electron C3 projectile ions ( $C_3H_7^+$ ,  $C_3H_5^+$ ,  $C_3H_3^+$ ). There was no systematic change with incident energy. The main process in ion-surface collisions is tralization of the incident ion projectile.

A simple correlation between survival probability of the hydrocarbon species C1, C2, C3, C7 and ionization energy of the species in question (instead of the unknown recombination energy) was found. It showed a decrease from more than 10% to less than 1% in between IE 8.5 - 9.5 eV (Fig. 1a) and a further decrease at higher IE. A semi-logarithmic plot  $\log S_a - IE$  showed that the decrease of  $S_a$  was approximately linear over the entire range of IEs of the investigated species (Fig. 1b) and the data could be fitted with an empirical relation

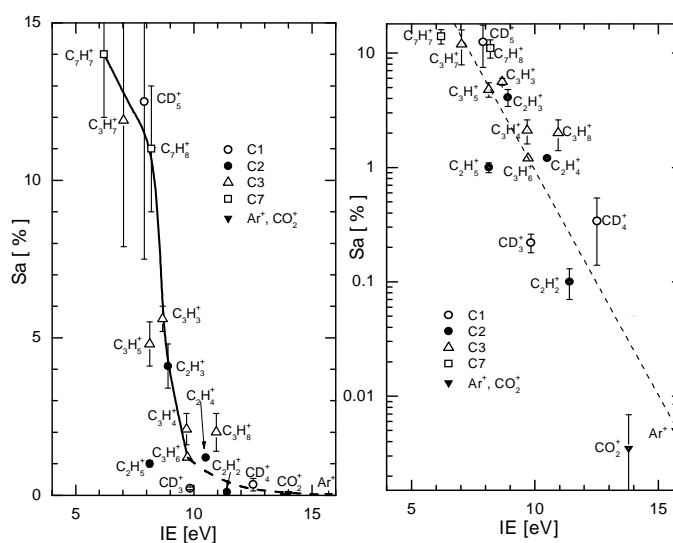


Fig 1a,b: Dependence of  $S_a$  on IE.

$$\log S_a = (3.9 \pm 0.5) - (0.39 \pm 0.04) IE.$$

## 2. Collisions of low energy $C_2D_4^+$ and $Ar^+$ ions with stainless steel, carbon (HOPG), and two different diamond surfaces: Surface-induced dissociation and chemical reactions. [2]

The subject of this research was to find out, how different material of a surface at room-temperature, underlying a hydrocarbon coverage, influences surface processes, namely to compare the behaviour of hydrocarbon-covered H-terminated diamond (hydrophobic), O-terminated diamond (hydrophilic) with two standard surfaces (carbon and stainless steel).

Mass spectra of the product ions were measured over the range of incident energies from a few eV up to about 50 eV and the respective CERMS (collision-energy resolved mass spectra) curves of the product ions were determined. The product ions observed with projectile ions  $C_2D_4^+$  indicated both fragmentation of the projectile ion  $C_2D_4^+$ , chemical reactions of H-atom transfer with the surface hydrocarbons, chemical reactions of carbon chain build up (C3 hydrocarbon ion formation), and a small contribution of hydrocarbon ions sputtered from the surface. Sputtering by  $Ar^+$  ions showed the presence of hydrocarbons on all investigated surfaces.

The CERMS curves of the product ions were analyzed to provide the CERMS curves for product ions coming from direct surface-induced dissociation of the projectile ion and those coming from chemical reactions of H-atom transfer. The CERMS curves for direct dissociation of the projectile were (after a correction of the data for the DH surface) very similar for all studied surfaces and thus indicated a similar translational-to-internal energy transfer in the surface collisions. No substantial difference was found between the two room-temperature (hydrocarbon covered) substances of diamond (DO and DH). The product ion distributions over the studied incident energy range could be fitted by an energy transfer distribution function that included the initial internal energy of the projectile ion and assumed a conversion of 10% of the incident energy of the projectile ion in the surface translation-to-internal energy transfer. The CERMS curve for reactive processes (formation and fragmentation of  $C_2D_4H^+$ ) on DO and DH surfaces were very similar. The only observed difference between the two diamond surfaces at room temperature was the ratio of probabilities of reactive vs. reactive and dissociative processes,  $P_R/(P_R+P_D)$ , as a function of incident energy (Fig. 2). This ratio increased from a threshold at 6-7 eV to about 70% for the SS, HOPG, and DO surfaces, but only to about 45% for the DH surface.

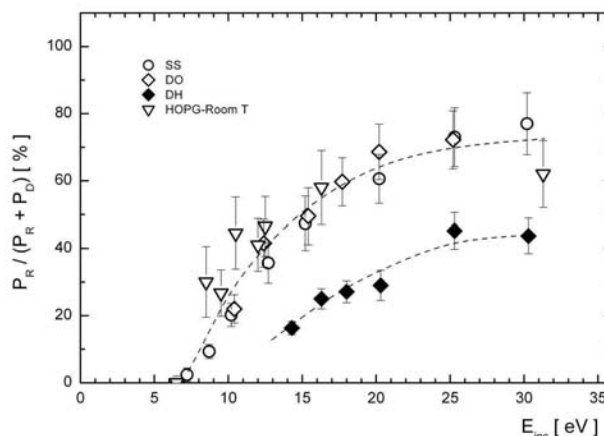


Fig. 2: The ratio  $P_R/(P_R+P_D)$  as a function of the incident energy of  $C_2D_4^+$ .

## References

1. A. Pysanenko, J. Žabka, L. Feketeová, T.D. Märk, Z. Herman, *Eur. J. Mass Spectrom.* **14**, 335-343 (2008).
2. L. Feketeová, J. Žabka, F. Zappa, V. Grill, P. Scheier, T. D. Märk, Z. Herman, *J. Am. Soc. Mass Spectrom.* (accepted)

## Study of the micro-mechanisms of cleavage fracture of 14% Cr and 18% Cr ODS ferritic steels

H. Hadraba, Institute of Physics of materials AS CR, v.v.i.  
Association EURATOM-IPP.CR

In collaboration with:  
B. Fournier, CEA Saclay, France

*The distinctive degradation of fracture properties of ODS variant of the Cr-W steels had been observed [1]. In these materials reinforced with phases of a few nanometers, larger  $Y_2O_3$  oxides are also present. They might act as carbides in 9%Cr ODS steels, and lead to a degradation of impact properties [2]. The influence of the production way (powder metallurgy and hot extrusion) is also of major interest regarding impact properties. In contrast to the carbide containing steels, there is no comprehensive idea of the role of nanometric oxide particles in cleavage fracture micromechanism. Possible microstructural changes connected with operation temperatures (considered in range of about 550 - 650°C) such as precipitation, grain coarsening and grain boundary embrittlement could also occur [3]. Synergy of the effects of the oxide particles with the influence of long term thermal ageing on cleavage fracture remains unexplained as well. Detailed understanding of failure mechanism of these steels in thermally unaffected and affected state is critical for their proposed future applications.*

A bar of 14%Cr ( $\varnothing 12$  mm) and a plate of 18%Cr (35×5.85 mm) ODS ferritic steels containing 1%W, 0.3%Ti and 0.3% $Y_2O_3$  were prepared by hot extrusion from mechanically alloyed powders. The powders were produced by atomisation of the prealloyed powder (Aubert & Duval) and subsequent mechanical alloying of the powder by  $Y_2O_3$  (Plansee). Mini-Charpy (KLST) specimens of 3 × 4 mm cross section and length of 27 mm were then machined from the semifinished bars. The “V” notch of 1 mm depth was machined in tensile side of the specimens. The length of the specimens was oriented along the length of the bar, which means that the crack propagated perpendicularly to the extrusion direction (Fig 1). An impact testing of specimen prepared was conducted by means of instrumented pendulum impact tester.

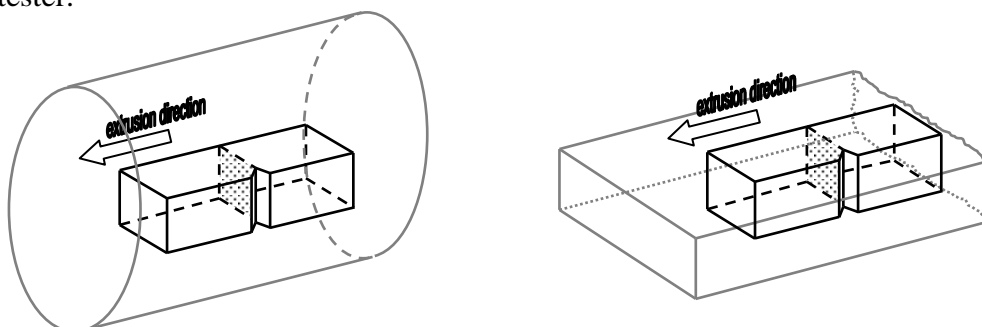


Fig. 1. Orientation of specimens inside the 14%Cr steel (left) and 18%Cr steel (right) steel bar. The arrows indicate the direction of material flow during extrusion.

The macrostructure of both steels presented grains elongated parallel to the extrusion direction of the bars (14%Cr steel) and also perpendicularly along the width of the plate (18%Cr steel). The EBSD examination revealed grains (or agglomerates of grains) elongated in the extrusion direction with aspect ratio about 10:1 (Fig. 2).

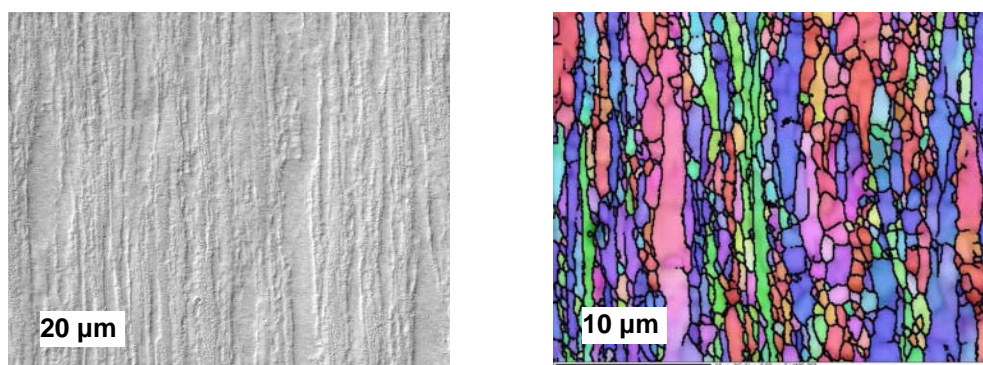


Fig. 2. Texture of the 14%Cr steel bar in direction parallel to the extrusion direction (optical (left) and EBSD scanning electron (right) microscopy).

The upper shelf energy level of the 14%Cr steel was about four times higher (about 11 J) than in the case of 18%Cr steel (2.25 J) and could be just estimated due to not ruptured specimens of 14%Cr steel at higher temperatures. The observation of fracture surfaces for both 14%Cr and 18%Cr ODS steel highlighted the strong influence of morphological texture (elongated grains) on the brittle fracture process (Fig. 3). Numerous secondary cracks were observed. Unstable portion of crack was formed by cleavage fracture and the perpendicular crack of grain (or grain agglomerations) boundaries were found. Also marks of deep cracking of material in the perpendicular direction were found in the fracture surface. Because of elongated grains along the extrusion direction the secondary cracks observed on fracture surfaces might correspond to intergranular cracking along this elongated direction. The fracture spread inside the sample along the steps formed by intersection of fracture plane and planes coming from microstructure orientation given by the extrusion process.

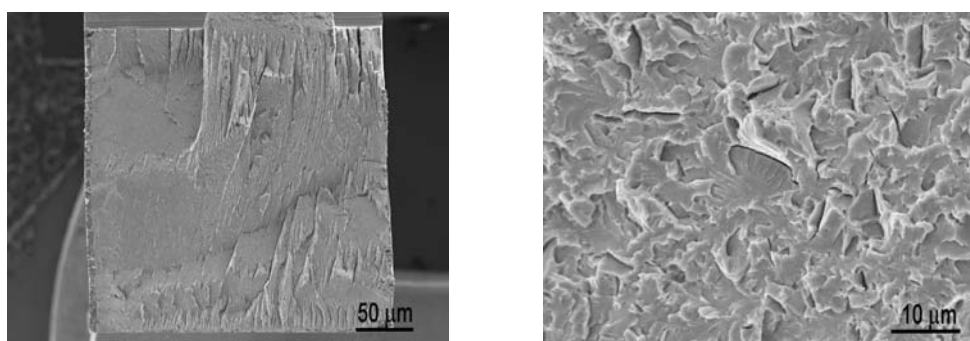


Fig. 3. Fracture surface of 18%Cr (left-overall picture) and 14%Cr (right-detailed picture) steel.

Charpy testing along the other directions of the 18%Cr ODS steel will be carried out next year to discuss this assumption. In addition EBSD mapping started this year will be completed and fully next year in order to discuss the link between morphological and crystallographic textures.

#### References:

- [1] R. Lindau et al, *J. Nucl. Mater.* 307-311 (2002) 769
- [2] D. Preininger, *J. Nucl. Mater.* 307-311 (2002) 514
- [3] P. Fernandez et al.: *J. Nucl. Mater.* 329-333 (2004) 273

## Development of functional gradient materials using powder laser deposition.

*J. Matějček, H. Boldryeva*

In collaboration with:

*P. Ambrož, Czech Technical University in Prague (ČVUT), Prague, Czech Republic*

*In this study, processing of tungsten-steel functionally graded materials (FGMs) from W powder on steel substrate by laser spraying technique is described. Morphological characteristics and content analysis are observed by scanning electron microscopy (SEM). Thermal properties depending on different composition and microstructure are briefly discussed.*

Tungsten-based functional gradient materials have potential application in tokamak nuclear fusion reactor components as an intermediate layer between tungsten parts, directly exposed to plasma, and steel or copper construction or heat sink parts. Therefore, thermal, as well as mechanical properties are of crucial importance for this kind of materials. There are various methods for producing FGMs, such as: powder metallurgy [1], plasma spraying [2], laser sintering [3, 4], HIPing [5], etc. The method described in this work is laser spraying (also called laser cladding or laser sintering) and has several potential advantages in comparison to other techniques. As commonly known, tungsten is a metal with the highest melting point in pure form (3422°C), nevertheless, employing laser with proper conditions gives enough energy for tungsten micro-powder to be processed, i.e. partly or totally melted. Another advantage lies in the surface nature of this technique, which involves no significant thermal effects on the whole part. Also, since it consists of local deposition and scanning, substrate with almost any shape could be treated. Potentially problematic disadvantage of this method is the porosity of prepared samples, which hopefully might be minimized with further research.

The experiments were performed on laser facility (JK701H, Lumonics) in collaboration with Czech Technical University in Prague. Working parameters of that facility is listed in Table 1.

Laser type	solid state laser, Nd:YAG
Wavelength	1064 nm
Energy output	550 W
Pulse energy	0.1-70 J
Pulse width	0.5-20 ms
Frequency	0.2-500 Hz
Focal distance	50, 120, 200 mm

*Table 1. Technical parameters of laser facility JK701H (Lumonics).*

Tungsten powder used for laser spraying was pre-treated by water-stabilized plasma jet torch; therefore it had spherical shape (Fig. 1), with average diameter of 60-80 μm. As schematically shown in Fig. 2, tungsten powder is carried by Ar gas through the pipe into the facility's head, which is connected to the scan system and laser. Then, during the scanning, the powder is blown down from the bottom of the head onto the steel substrate while simultaneously melted by the laser beam. Two different speeds of scanning (200 mm/min and 400 mm/min) were employed, whereas the feed rate of tungsten powder and supplying Ar gas pressure (1 bar) were kept stable. When applying lower scanning speed, increased thickness of single sprayed layer was observed.

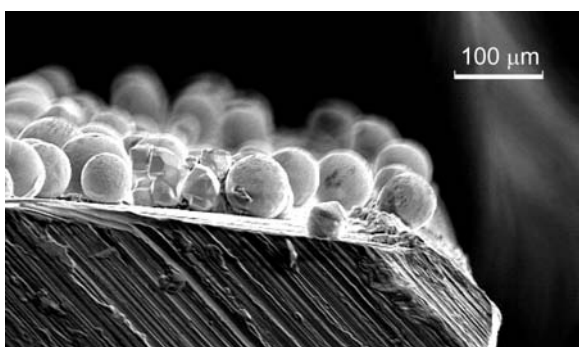


Fig. 1. SEM image of initial tungsten powder.

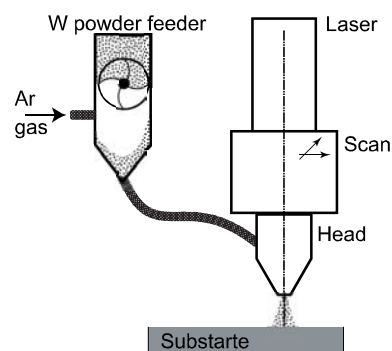
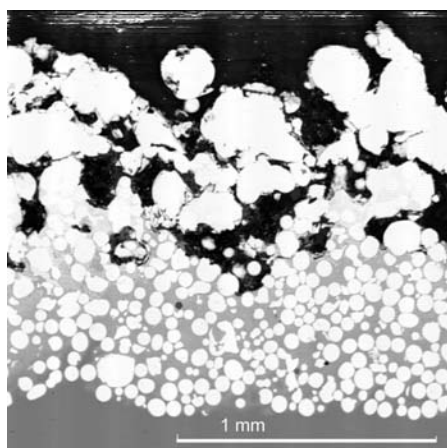
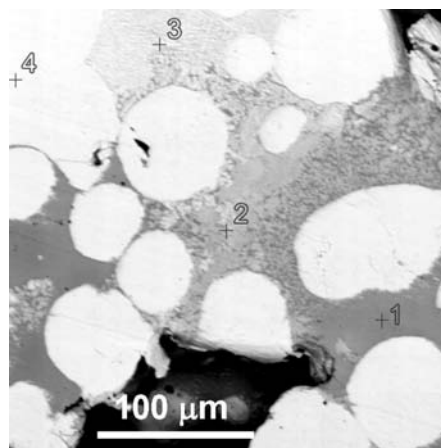


Fig. 2. Scheme of laser spray experiment.

Cross-sectional SEM image of sample which was scanned for three times subsequently, so that it consisted of three layers, is shown in Fig.3 (a). The first laser-sprayed layer consists of slightly melted tungsten microgranules immersed in a melted steel substrate. The height of the single layer reaches up to 0.75 mm and can be varied by applying different laser-spraying conditions: feeding rate, scanning speed or regime of scanning. Average diameter of tungsten microgranules estimated from cross-sectional SEM images (65  $\mu\text{m}$ ) is comparable with the size of the initial powder. The top layer has a microporous structure and consists of melted tungsten. Content analysis in the points 1, 2, 3 and 4 (see Fig. 3 (b)) between pure W microgranules shows a certain amount of tungsten, which increases toward the surface. This gradient of tungsten concentration in steel matrix is due to partial melting of tungsten during the spraying and its diffusion in melted steel and it could significantly influence mechanical properties. Further measurement and investigation in this direction are necessary. Thermal diffusivity of sample similar to the one presented in Fig. 3 (a) is 0.039  $\text{cm}^2/\text{s}$ . We believe that this value is highly influenced by porous structure of our materials and it might be improved reduction of the porosity.



(a)



(b)

Fig. 3. Cross-sectional SEM image of laser sprayed sample..

### References:

- [1] F. Delannay, Ch. Colin, *Materials Science and Engineering A* 495 (2008) 236
- [2] J. Matějčiek, F. Zahálka, J. Bensch, W. Chi, J. Sedláček, *J. Thermal Spray Technology* 17 (2008) 177
- [3] G. Pintsuk, S.E. Brunings, J.-E. Doring, et al, *Fusion Eng.Design* 66-68 (2003) 237
- [4] A. Viswanathan, D. Sastikumar, H. Kumar, A.K. Nath, *Surface & Coatings Technology* 203 (2009) 1618
- [5] S. Saito, K. Fukaya, S. Ishiyama, K. Sato, *J. Nuclear Mat.* 307–311 (2002) 1542

## 6. Training and career development

### **Collaboration of IPP Prague with Universities in fusion training**

*J. Mlynář, I. Ďuran, J. Stöckel*

*Although the tokamak department of IPP had no experimental facility in 2008, it attracted increasing number students from Universities who got extended training support. Ten postgraduate (doctoral) students have been preparing their dissertation here. Number of undergraduate students looking for a fusion-oriented topic also increased. The tokamak department tried hard to find suitable research topics and an expert supervisor for all of them. In 2008 the tokamak department of IPP Prague led practical works of 7 MSc level students and 7 BSc level students from both Czech Technical University and Charles University.*

In total, 12 doctoral students and 18 undergraduate students were involved in the work of the IPP tokamak department in 2008. Two students of the FNSPE (Martin Kubič and Pavel Háček) obtained their BSc diploma with their research work based at IPP. Dr Jakub Urban finished his work on "Electron Bernstein Wave Emission Simulations for Spherical Tokamaks", supervised by IPP Prague, and received a PhD diploma from the Faculty of Mathematics and Physics in June 2008.

Research scientists from the institute also participated in teaching at several universities in the framework of both regular and irregular courses. The major teaching load was linked to the collaboration with the Faculty of Nuclear Sciences and Physical Engineering, Czech Technical University in Prague (FNSPE) which runs from 2006 a masters curriculum "Physics and Technology of Thermonuclear Fusion". In the summer term, our staff was responsible for 3 courses: Introduction to thermonuclear fusion, Technology of thermonuclear facilities and Topics from magnetic confinement fusion. We also participated with several lectures in the course Plasma diagnostics and organised practica in which several labs from Prague participate. In the winter term, our staff was responsible for the course Tokamak physics and for organising joint FNSPE – IPP seminars. In the framework of these seminars, we had lectures given by, among others, Prof. Guido van Oost from the Ghent University or Dr. Ivo Furno from CRPP EPFL.

## Training and education

*J. Stockel, J Mlynář, M. Hron, R. Dejarnac, M. Řípa, V. Svoboda, D. Břeň*

In collaboration with:

*G. Veres, M. Berta, A. Bencze*, Association EURATOM-HAS, Hungary

*G. van Oost*, Association EURATOM/Etat Belge, Belgium

*Training and education effort was focused on-co organization of the **Summer Training Course (SUMTRAIC)** together with the Association EURATOM/HAS, the organization of semester course **Physics and Technology of Thermonuclear Fusion** for master and PhD students of the Faculty of Nuclear Science and Physical Engineering (FNSPE) of the Czech Technical University. In addition, a new Curriculum with the same title continued for the second year at FNSPE (for the students in the third year of their studies).*

The 6th Summer Training Course (SUMTRAIC 2008) was organized by the Association EURATOM/HAS in Budapest in the period 26.6.08 - 4.7.2008. The SUMTRAIC took place at Budapest University of Technology and Economics, Budapest. Before practical training, several lectures have been presented to participants:

- The road to fusion (S. Zoletnik)
- The theory of glow discharges (G. Veres)
- Engineering Challenges in ITER (O. Bede)
- Signal processing basics (G. Por)
- Data access and data acquisition (D. Dunai)
- Langmuir probe theory and applications (M. Hron)
- Langmuir probe measurements on CASTOR and other tokamaks (J. Stockel)
- Inertial Confinement Fusion (K. Gal)

The Czech Association contributed the Course by two lectures.

Trainees participated in three experiments:

- Langmuir probe characteristics in a glow discharge
- Spectroscopy of different light sources
- Fluctuations in fluids

M Hron participated in the experimental part of the Course by supervising experiments on probe measurements in a glow discharge.

The Course was attended by 11 students from 6 countries: Yuriy Petrov, Oleksandr Yeryomin (Ukraine), Ioana Luciu (Romania), Erik Olofsson (Sweden), Mohamed Mokhtar (Egypt), Diana Naydenkova (Czech Rep), Lampert Mate, Boross Peter, Szabó Attila, Vasvari Gyula, Csajbok Viktoria (Hungary). The next SIMTRAIC 2009 will be organized at IPP Prague on the COMPASS tokamak again in close collaboration with Association EURATOM/HAS.

IPP.CR experts also traditionally participated in the 7<sup>th</sup> Summer School in Kudowa Zdroj, Poland in June 2008 and agreed on chaining this school to SUMTRAIC in 2009. This cooperation may also become formalised in near future.

The MSc curriculum “Physics and Technology of the Thermonuclear Fusion” started its 3<sup>rd</sup> academic year at Faculty of Nuclear Sciences and Physical Engineering in 2008. Consequently, it opened for the first time the final (diploma) winter term. Several new subjects were opened in 2008 for the first time, in particular, Diagnostics of fusion plasmas, Technology of thermonuclear fusion, Modelling of fusion plasmas and Fusion seminars. Importantly, on 17th November FNSPE CTU hosted international kick-off meeting of the FUSENET consortium, which is responsible for the EURATOM Coordination and Support Activity (CSA) in fusion education.

## 7. Other activities contributing to the EURATOM fusion programme

### Outreach and Public Information Activities

Milan Řípa, Jan Mlynář

Without any question the main event in public information last year was the official unveiling of the COMPASS tokamak in Prague. Its program had been prepared well in advance and attracted many VIPs of Europe and Czech Republic: HM ambassador Ms Linda Joy Duffield, chairman of the Consultative Committee EURATOM-Fusion Sir Chris Llewellyn Smith, Director of EURATOM Mr Octavio Quintana Triaz, Minister of industry of the Czech republic Mr Martin Říman, President of the Czech Academy of Sciences prof Václav Pačes, chairman of International Board of Advisors of the Association EURATOM-IPP.CR prof Hardo Bruhns, Mr Vladimír Remek MEP, and others.



The extraordinary interest of media was proved by 17 newspaper and magazine reports, 12 internet reports, four broadcastings and three Czech press office reports.

PI activities of Association were presented in the 8th Public Information Group meeting in Lisboa on May 8 to 10, 2008.

We believe the year for this even was well chosen: Indeed, 2008 was full interesting fusion anniversaries for the fusion PI (80 years of word „plasma“, 50 years of tokamak, 50 years of the 2nd Conf. „Atoms for Peace“, 40 years of the tokamak breakthrough, 25 years from the first JET discharge, and the year when the ITER construction began). Tokamak COMPASS hosted well above 20 visits from schools, universities, governmental institutes and industries in 2008. Quite naturally, all these visits involved rather detailed information on the ITER project and its status. A list of other ITER and COMPASS relevant PI events and activities in 2008 follows.

#### LIST OF PUBLIC ACTIVITIES

##### *Event of the year*

Official inauguration (unveiling) of the COMPASS tokamak, IPP AS CR v.v.i., Praha, April 1st, 2008

##### **TV and Radio broadcast**

- Václav Pačes & Pavel Chráska interview (Bohumil Klepetko, Edita Horáková): The research reactor was transported into Czech Republic, Czech State TV ČT 1 Události, April 1, 2008, 19:00
- Jiří Petrovič & Edita Horáková: Czech scientists presented tokamak reactor COMPASS, Czech State TV ČT 1, News (Zprávy), April 1, 2008, 12:00
- Michel Chatelier and Pavel Chráska interview on ITER in the „Millenium“ series, Czech state News Channel ČT24, May 22, 2008, 11:35 (and online)

- Martin Hron and Jan Mlynář interview on COMPASS in the „Millenium“ series, , Czech state News Channel ČT24, May 26, 2008, 11:35 (and online)
- Václav Pačes interview (Pavel Prouza): The fusion will be tested in Czech Republic, Radiožurnál, April 1, 2008, 12:00
- Václav Pačes interview (Jan Pokorný): You can see reactor COMPASS tokamak in Prague, Radiožurnál, April 1, 2008, 8:50
- Pavel Chráska and Jan Mlynář guests of the „Third dimension“, digital radio broadcast Leonardo on April 4th, 2008 at 14:00 (and online)
- Pavel Chráska interview on fusion in „Science“ of the Vltava radio broadcast on May, 25
- Milan Řípa: Interview about fusion for ČTK, Faculty of Nuclear Sciences and Physical Engineering, Czech Technical University in Prague, December 3
- Milan Řípa: Tokamak, On line interview for Radiožurnál, December 3 , 2:37 p.m.

### Selected e-news

- Jiří Kokmotos: The Czech scientists presented today a special reactor – COMPASS Tokamak, <http://www.rozhlas.cz/izurnal/cesko/zprava/439906>
- Josef Tuček: The apparatus was unveiled which will search the energy of the future, [http://aktualne.centrum.cz/veda/clanek.phtml?id=601198&tro5341\\_1\\_0](http://aktualne.centrum.cz/veda/clanek.phtml?id=601198&tro5341_1_0)
- Pavel Chráska IPP director responded questions on fusion online April 4th in the news server Aktualne.cz <http://aktualne.centrum.cz/veda/clanek.phtml?id=601513>
- Jan Mlynář, Viktor Velek: Star Power, Compass reactor gives nuclear fusion research new bearing, The Prague Post, (in English) <http://www.praguepost.com/articles/2008/04/16/star-power.php>
- ČTK: The reactor for thermonuclear fusion in Prague, [http://vat.pravda.sk/cesi-slavnostne-odhalili-tokamak-compass-f14-sk\\_vtech.asp?c=A080401\\_173704\\_sk\\_vtech\\_p09](http://vat.pravda.sk/cesi-slavnostne-odhalili-tokamak-compass-f14-sk_vtech.asp?c=A080401_173704_sk_vtech_p09)
- ČTK Thermonuclear fusion – the energy of the future will be tested in Prague, [http://technet.idnes.cz/v-cesku-se-bude-testovat-termojaderna-fuze-8722-energie-budoucnosti-1cz-/tec\\_technika.asp?c=A080401\\_102643\\_tec\\_technika\\_vse](http://technet.idnes.cz/v-cesku-se-bude-testovat-termojaderna-fuze-8722-energie-budoucnosti-1cz-/tec_technika.asp?c=A080401_102643_tec_technika_vse)
- ČTK: Czech scientists unveil tokamak Compass [http://www.praguemonitor.com/en/306/czech\\_national\\_news/20778/](http://www.praguemonitor.com/en/306/czech_national_news/20778/)

### PI Articles

- Vladimír Weinzettl: Thermonuclear fire in a continuity, CHEMmagazín, 13 (2008), No.1, pp. 6 to 7
- Milan Řípa: Great Britain (did not) managed nuclear fusion 50 years ago., Lidové noviny, 18 (2008), January 25, 2008, p. 18
- Milan Řípa: The second tokamak for the Czech Republic, Lidové noviny, 18 (2008), April 2, 2008, p. 17
- Jan Mlynář, Viktor Velek: Star Power, COMPASS reactor gives nuclear fusion research new bearing, The Prague Post, April 16
- Milan Řípa: Compass, Vesmír, 87 (2008), No 5, p. 274
- Milan Řípa: Tokamak COMPASS was festive unveiled, Technický týdeník, 56 (2008), No 11, May 27, 2008, p. 11
- Milan Řípa: The smuggled tokamak, Lidové noviny, 18 (2008), June 5, 2008, p. 16
- Milan Řípa: Hollywood and fusion, Technický týdeník, 56 (2008), No 12, June 10, 2008, p. 4
- Milan Řípa: Energetic safety against environmentalism?, EKO (Ekologie a společnost), 19, 2008, No 3, pp. 31– 34

- Milan Řípa: Fusion energy, hydro energy, biophysical energy, Technický týdeník, 56 (2008), No 13, June 24, 2008, p. 15
- Milan Řípa: 25 years of the first plasma in JET tokamak, Technický týdeník, 56 (2008), No 15, August 5, 2008, p. 4
- Milan Řípa, Radomír Pánek, Jan Mlynář: Tokamak COMPASS installation in Prague, Československý časopis pro fyziku, 58 (2008), No 4, pp. 200 – 207
- Milan Řípa: Tokamak history in the world and in our country, Československý časopis pro fyziku, 58 (2008), No 4, pp. 208 – 211
- Pavel Chráska, Jan Mlynář: Let us present Institute of Plasma Physics of ASCR, v. v. i. and COMPASS tokamak, Jemná mechanika a optika, 2008, No 4, p.99
- Milan Řípa: Unexpected relationship or what steel for towers and fusion reactors, Technický týdeník, 56 (2008), No 20, September 30, 2008, p. 22
- Milan Řípa: How the steel melted, Lidové noviny, 18 (2008), September 24, 2008, p. 17
- Jan Mlynář, Radomír Pánek: “Tracking ITER with COMPASS”, Physics World supplement for the IAEA Fusion Energy Conference, October 13
- Milan Řípa: Big nuclear fusion anniversary, Lidové noviny, 18 (2008), October 17, 2008, p. 17
- Milan Řípa: Magnets for ITER, Technický týdeník, 56 (2008), No 23, November 11, 2008, p. 16
- Milan Řípa: ITER project in the year zero, Energetika, 58(2008), No 11, pp. 360 – 361
- Milan Řípa: Inertial Electrostatic Confinement, Energetika, 58(2008), No 11, pp. 362 – 364
- Milan Řípa: The second way to fusion, Lidové noviny, December 3, 2008, p. 17
- Milan Řípa: The world heard the word of TOKAMAK fifty years ago, Technický týdeník, 56 (2008), No 26, December 23, 2008, p. 30
- Milan Řípa: Igor Janovský: Research reactors and radiating technology in Czech countries, review, Technický týdeník, 56 (2008), No 26, December 23, 2008, p. 25
- Milan Řípa: 50 years of tokamak, 3pol, <http://www.tretipol.cz/index.asp?clanek&show&744>
- Jan Mlynář a Milan Řípa: 50 years of tokamaks, Fusion News, EFDA Close Support Unit Garching, Germany, Volume 2, December

### Lectures

- Jan Mlynář: Controlled thermonuclear fusion, University of the third age, Faculty of Nuclear Sciences and Physical Engineering, CTU Pratur, May 5
- Jan Mlynář: Light from terrestrial stars, Open science for regions, Nový Jičín, May 5
- Milan Řípa: ITER is the way, Gymnasium Liberec, Liberec, May 22
- Jan Mlynář: Will scientists be able to build a Sun? Playing with science, June 2
- Milan Řípa: The stars are directed on Earth, Festival Fantasy, Chotěboř, July 3
- Milan Řípa: ITER is the way, Gymnasium Vítězslava Nováka Jindřichův Hradec, Jindřichův Hradec, September 18
- Milan Řípa: ITER is the way, Gymnasium Luďka Pika Plzeň, FJFI, Praha, October 13 2008
- Milan Řípa: ITER is the way, Faculty of environment, J.E. Purkyně University, Most, October 20& 21
- Jan Mlynář: Will ITER help to build thermonuclear power plants? Lectures from modern physics, Faculty of Mathematics and Physics, Prague, October 30
- Milan Řípa: Plasma is helping to humans, The week of science and technology, Muzeum policie Praha, November 6

- Milan Řípa: 50 years of tokamak, public workshop of Physics and technology of thermonuclear fusion, Faculty of Nuclear Sciences and Physical Engineering, Czech Technical University in Prague, December 3
- Jan Mlynář: Tokamaks COMPASS and ITER, Faculty of Electrotechnics, University of West Bohemia, Pilsen, December 9, 2009
- Milan Řípa: 50 years of tokamak, Department of optic diagnostics, IPP ASCR, v.v.i., Turnov, December 19
- Milan Řípa: ITER is a way, Department of optic diagnostics, IPP ASCR, v.v.i., Turnov, December 19

### **Posters**

- Milan Řípa, Jan Mlynář: Public Information Activities On Controlled Thermonuclear Fusion Research In The Czech Republic, poster and other materials on Int. Conference on Public Information Materials Exchange (PIME), Praha, February 11 to 12
- Milan Řípa, Jan Mlynář: Compass in Prague, The week of science and technology, ASCR, Praha 1, Národní 3, November 3 to 9

### **Open days of the Institute of Plasma Physics AS CR, v.v.i.**

November 7 and 8

## 8. Coordination, in the context of a keep-in-touch activity, of the Member State's civil research activities on Inertial Fusion Energy

### Experiments on interaction of focused high-power laser beams with multilayer high-Z targets

*Jiří Ullschmied, Eduard Krouský, Karel Mašek, Jiří Skála*

In collaboration with:

*A. Kasperczuk, T. Pisarczyk, S. Borodziuk, D. Baran, J. Wolowski, J. Badziak*, Association EURATOM-IPPPM, Warsaw, Poland

*Ph. Nicolai, V. T. Tikhonchuk, C. Stenz*, CELIA, Université Bordeaux 1, Talence, France

*J. Kravárik, D. Klír*, FEE Czech Technical University in Prague, Prague, CR

*M. Káral, M. Martínková*, FNSPE Czech Technical University in Prague, Prague, CR

*Plasma production by long-pulse (ns-duration) laser ablation of solid targets is a complex process at which the laser beam interacts in a non-linear way with the plasma it creates itself. The process of plasma production is influenced not only by the laser characteristics (energy, colour, pulse duration, intensity profile, etc.), and target irradiation geometry (size of the focal spot and position of the focus), but also by the target material. By a proper choice of all these parameters optimum conditions can be found either for launching plasma jets, or for ablative acceleration of flyers, and efficient laser acceleration of plasma ions. For formation of a convergent narrow jet an annular structure of the laser focal spot proved to be indispensable, however the annular target irradiation can be created spontaneously during the laser beam – plasma interaction, providing that the focal point of a focusing lens is situated inside the target [1, 2].*

Our earlier experiments at the PALS iodine laser facility have shown that well formed supersonic plasma jets can be launched by a slightly defocused laser beam of a modest energy of  $\sim 100$  J, but on targets made of high-Z metals ( $Z > 29$ ) only (Cu, Ta, Pb). The aim of the experiments on laser ablation performed in 2008 was to elucidate the relative role of two different mechanisms responsible for formation of plasma jets at interaction of a flat-profile pulsed high-power iodine laser beam with flat solid-state targets, namely the radiation cooling and the cumulative hydrodynamic effects. For that purpose we used double targets consisting of a massive high-Z substrate covered by a thin layer of lighter material (Cu-plastic, Ta-plastic, Cu-Al, Ta-Al) and, on the contrary, Al and plastic targets covered with thin high-Z layers. It turned out that even a very thin layer of high-Z material makes it possible to generate plasma jets on low-Z materials such as plastic, and, vice versa, low-Z surface layer inhibits jet formation on high-Z targets [3, 4], as illustrated by Fig.1.

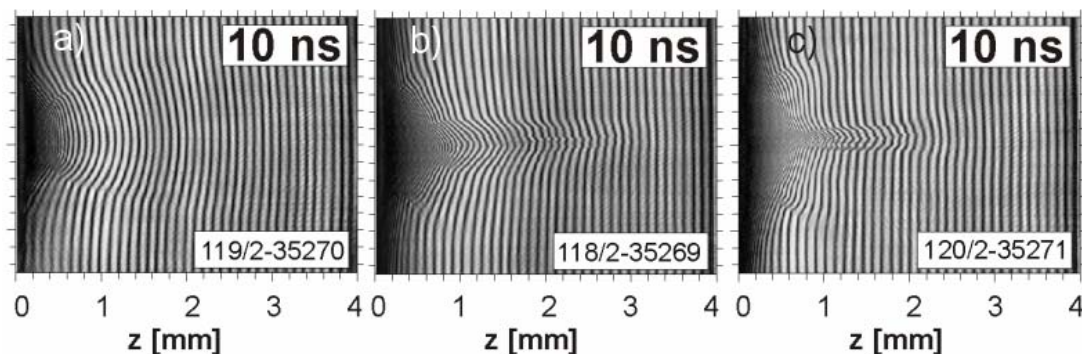


*Fig. 1. Interferograms of the plasma jets launched on a) CH plastic target – no jet, b) CH target covered by 28-nm Cu layer, c) Cu target at 10 ns after the laser pulse. Laser: 30 J, 438 nm, 250 ps. Focus inside the target, focal spot radius 400  $\mu\text{m}$ . (Picture by T. Pisarczyk, IPPLM Warsaw)*

The above result speaks in favour of a decisive role of the cumulative effects caused by strong target irradiation inhomogeneities resulting from non-linear laser beam - plasma interaction at the very beginning of the laser pulse. Radiation losses are negligible in the case of the plasma created of light elements and, thus, cannot be responsible for the jet formation. Nevertheless, in high-Z plasmas, radiation cooling becomes important at later stages of the jet formation. The demonstrated possibility to create plasma jets on low-Z targets is here of primary importance, as it would open the way for producing plasma jets e.g. on IFE-relevant frozen D-T targets.

The laser interferometry/shadowgraphy used in the experiments with plasma jets was exploited also for determination of the amount of energy transferred to the ablative plasma, by watching the motion of a plasma-driven flyer target [5]. The same diagnostics proved to be useful in experiments on laser-driven acceleration of macroparticles [6]. Macroparticles accelerated to high velocities are being concerned in the impact schemes of fast ignition, can test materials of the first wall of thermonuclear reactors or simulate impacts of micrometeorites.

At the PALS facility an original acceleration concept, the reversed acceleration scheme, has been tested [7]. The macroparticle represented by a thin circular metallic foil is not accelerated directly by reactive ablation pressure, but by the hot plasma produced on the surface of an auxiliary massive copper target, located at a short distance behind it. The laser beam passes through a small hole in the foil to be accelerated – see Fig. 2. The new laser acceleration concept is much more efficient than a standard one, as the laser energy is not wasted on evaporation and ablation of the accelerated particle the mass which, in addition, does not change during the acceleration. Velocities of hundreds of km/s have been achieved in this way at laser energy of 130 J, ICF-relevant velocities being expected at higher energy and under optimised irradiation conditions.

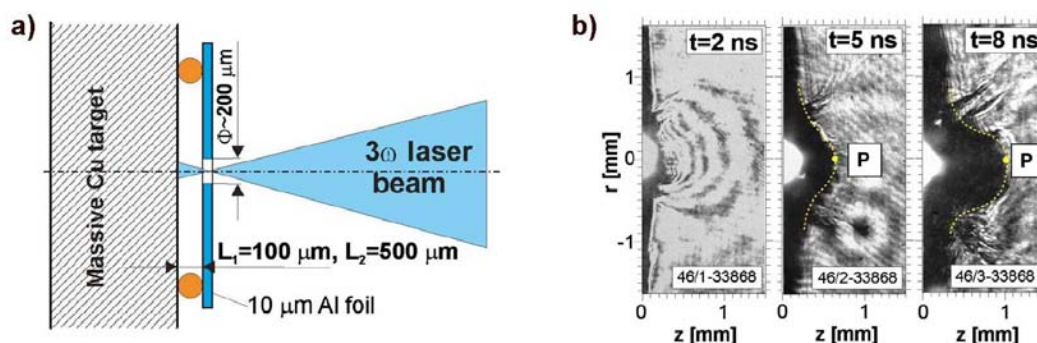


Fig. 2. a) Experimental arrangement. b) Laser shadowgrams showing the foil deformation at 2, 5, and 8 ns after the laser pulse. Central velocity of the accelerated foil can be determined from the shift of the point P. (Pictures by T. Pisarczyk and A. Kasperczuk, IPPLM Warsaw)

## References:

- [1] A. Kasperczuk, T. Pisarczyk, M. Kalal et. al., *Laser & Part. Beams* 26(2008) 189-196
- [2] A. Kasperczuk, T. Pisarczyk, J. Badziak et al., *J. Phys. Conf. Ser.* 112 (2008) 022047
- [3] A. Kasperczuk, T. Pisarczyk, M. Kalal et al., *ECA* Vol.32 (2008) P-1.118
- [4] A. Kasperczuk, T. Pisarczyk, N.N. Demchenko et al., *subm. to LPB* (2009)
- [5] A. Kasperczuk, T. Pisarczyk, S.Yu. Gus'kov et al., *Rad. Effects & Def. in Solids* 163 (2008), 519-533
- [6] J. Wolowski, J. Badziak, A. Borrielli et al., *J. Phys.: Conf. Ser.* 112 (2008) 022072
- [7] S. Borodziuk, A. Kasperczuk, T. Pisarczyk et al., *Appl. Phys. Lett.* 93 (2008) 101502

## Laser generated plasma jets for ICF and astrophysics

Jiří Ullschmied, Eduard Krouský, Karel Mašek, Jiří Skála

In collaboration with:

A. Kasperczuk, T. Pisarczyk, D. Baran, Association EURATOM-IPPPM, Warsaw, Poland

Ph. Nicolai, V. T. Tikhonchuk, C. Stenz, CELIA, Université Bordeaux 1, Talence, France

P. Velarde, M. Gonzales, C. G. Fernandez, DENIM, Madrid, Spain

J. Kravárik, D. Klír, M. Káral, Czech Technical University in Prague, Prague, CR

*Collimated plasma outflows - plasma jets - are a subject of interest both in ICF research and in astrophysics. Plasma jets are observed at contact surfaces of different materials at laser interaction with multi-shell targets, highly supersonic plasma jets may find its use in some impact fast ignition schemes. They can propagate over considerable distances, so that their interaction with surrounding media can be used for laboratory simulation of some astrophysical phenomena, such as Herbig-Haro objects. In the collaborative experiments performed at the PALS facility the jet like structures have been created in several ways by using a modest energy ( $\sim 100$ -J) 250-ps laser beam at the 1<sup>st</sup> and 3<sup>rd</sup> harmonics of the iodine laser (1315 nm) [1,2]. The direct method of plasma jet generation consisted in irradiation of a massive planar target, made of a relatively heavy material (atomic number at least 29), by a partly defocused laser beam. The other two indirect methods employed either the impact of an ablatively accelerated flyer, or a cumulative compression of a conically shaped foil target. The optimised directly generated highly supersonic plasma jets were used for detailed investigations of jet interaction with gas-puff plasmas [3].*

Directly generated plasma jets evolve from the annular plasma structure spontaneously formed during laser interaction with high-Z solid targets, which collides at the central axis of symmetry. Under optimum conditions stable narrow plasma jets with the Mach number above 10 can be generated in this way. The directly generated jets were exploited in experiments on jet interaction with ambient gas [3]. Jet parameters remain similar both at normal and oblique (30°) incidences of the laser beam, the latter being used to avoid disturbances caused by gas preionization in the interaction region. The interaction of jets with He and Ar gas-puff targets was studied by means of a three-frame laser interferometer, framing pinhole CCD x-ray camera, x-ray streak camera and XUV spectrometer [4], and interpreted by using a semi-analytical model [5,6]. 2D numerical modelling [3,7,8] simulates qualitatively well particular phases of jet forming and interaction, for instance the bow shock generation in Ar gas (Fig. 1).

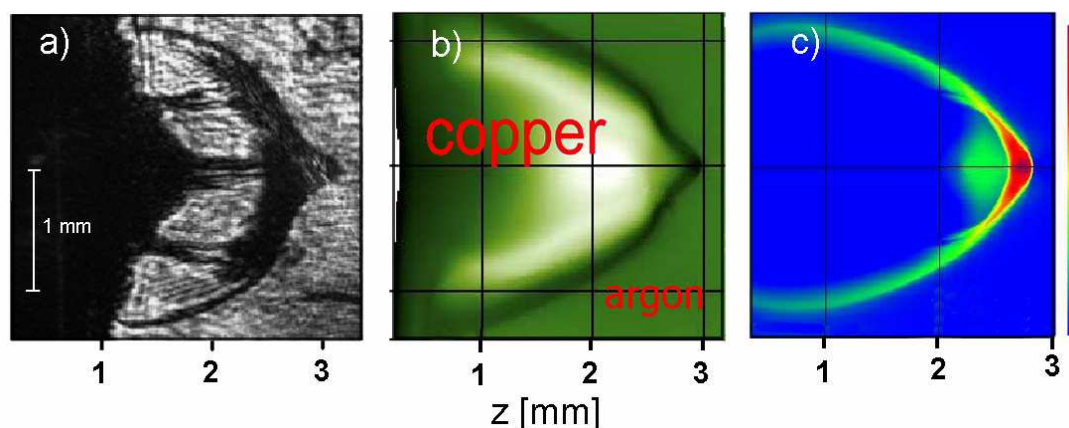


Fig. 1. a) Bow shock produced in Ar by Cu-plasma jet. a) Shadowgram, b) Simulated density map, c) Density map of a simulated bow shock (Ar pressure: 10 bar, time: 7 ns after the laser pulse). (Shadowgraphy: T. Pisarczyk, IPPLM, 2D simulations: Ph. Nicolai, V. Tikhonchuk, CELIA.)

Our experiments at PALS have shown that plasma jets can be effectively produced also in an indirect way [1], by using an ablatively accelerated flyer disk, which impacts a massive solid target. The impact occurs  $\sim 23$  ns after the laser pulse. Special target construction made it possible to visualize jet development in the period 0-17 ns after the impact. Velocity of the observed axial narrow ( $\sim 250$   $\mu\text{m}$  in diameter) plasma stream with a maximum density of  $3 \times 10^{19} \text{ cm}^{-3}$  exceeded  $10^7$  cm/s.

In another series of experiments the jets were produced due to cumulative effects, which occur at laser beam interaction with cone-shaped targets. The cones with an apex angle of  $90^\circ$  and height  $250$   $\mu\text{m}$  were made of Al foil  $9$   $\mu\text{m}$  thick. In the reversed cone configuration shown in Fig 2a plasma jets of a velocity higher than  $0.8 \times 10^8$  cm/s were observed. They had a relatively high electron density, considerably above  $10^{19} \text{ cm}^{-3}$ , and a steep plasma front, as illustrated by equidensitograms in Fig. 2b.

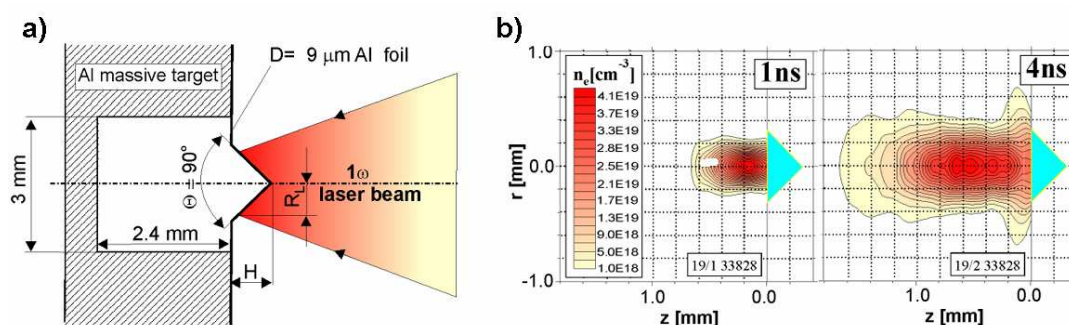


Fig. 2. a) Laser target and b) Equidensitograms of a cumulative plasma jet at 1 ns and 4 ns after the laser pulse. Laser: 550 J, 1315 nm, 250 ps. (Interferometry by T. Pisarczyk, IPPLM Warsaw.)

All the three methods of plasma jet production described above are simple and easy to use at single-beam laser facilities of modest laser energy of the order of 100 J only.

### References:

- [1] A. Kasperczuk, T. Pisarczyk, M. Kalal et al., *ECA* Vol. 32 (2008) P-1.117
- [2] A. Kasperczuk, T. Pisarczyk, M. Kalal et al., *ECA* Vol.32 (2008) P-1.118
- [3] V. T. Tikhonchuk., Ph. Nicolai, X. Ribeyre et al., *Plasma Phys. Contr. Fus.* 50 (2008) Art. 124056
- [4] A. Kasperczuk, T. Pisarczyk, Ph. Nicolai et al., *30th ECLIM*, Darmstadt, Germany, Aug. 31 – Sep. 5, 2008
- [5] A. Kasperczuk, T. Pisarczyk, N. N. Demchenko et al., *Laser & Particle Beams* 2009 (submitted)
- [6] P. Velarde, M. Gonzalez, C. G. Fernandez et al., *J. Phys.: Conf. Ser.* 112 (2008) Art. 042010
- [7] Ph. Nicolai, C. Stenz, A. Kasperczuk et al., *Phys. Plasmas* 15 (2008) 082701